



NTNU – Trondheim
Norwegian University of
Science and Technology

Fischer-Tropsch Catalysts for Jet Fuel Production

**Mario Ernesto Casalegno
Garduño**

Chemical Engineering

Submission date: June 2014

Supervisor: Magnus Rønning, IKP

Co-supervisor: Erling Rytter, Statoil research centre, Rotvoll

Norwegian University of Science and Technology
Department of Chemical Engineering



NTNU – Trondheim
Norwegian University of
Science and Technology

Fischer-Tropsch Catalysts for Jet Fuel Production

Mario Ernesto Casalegno Garduño

Submission date: June 2014
Supervisor: Prof. Magnus Rønning
Co-Supervisor: Adj. Prof. Erling Rytter

Norwegian University of Science and Technology
Department of Chemical Engineering

Abstract

Diverse β -zeolite and β -zeolite/Fischer Tropsch catalysts were prepared under hydrothermal conditions to obtain a tailored jet fuel catalyst. The Fischer Tropsch catalyst that was employed is cobalt-based and it was provided by Statoil Research Center at Rotvoll. A sample of pure β -zeolite was synthesized to obtain a reference product.

The hydrothermal synthesis of the β -zeolite and β -zeolite/Fischer catalyst was performed at 155 °C. It was decided to elaborate the bifunctional catalyst to obtain jet fuel products with β -zeolite because this zeolite type possesses larger micropores than other zeolites. The initial chemical components of the β -zeolite/Fischer catalyst were: silicon source, aluminum source, organic template, water, and Fischer Tropsch cobalt based catalyst.

Especially attention was paid to the silicon source because it is well known that a few ppm's of sodium could affect negatively the performance of the Fischer Tropsch cobalt-based catalyst. It was concluded that fumed silica possesses the best trade-off qualities between purity and price to perform large a number of hydrothermal synthesis.

Different procedures were used to modify the final hydrothermal β -zeolite/Fischer catalyst. The most successful was the impregnation of the internal pores of the Fischer Tropsch cobalt-based catalyst alumina support with the organic template.

Prior to the Fischer Tropsch synthesis test, all the produced β -zeolite/Fischer catalyst were characterized. The BET method was utilized to measure the surface area, pore volume, and pore size. XRD powder patterns were used to verify the presence of the β -zeolite and also to prove that the calcination at 550°C did not damage the Fischer Tropsch cobalt based catalyst. SEM was employed as a qualitative technique to confirm the presence of the β -zeolite in the Fischer Tropsch catalyst surface. Chemisorption was used to determine the metal dispersion and the cobalt crystal size.

Several bifunctional catalyst were tested in the Fischer Tropsch synthesis. The results show that a higher quantity of β -zeolite in the β -zeolite/Fischer Tropsch catalyst produces elevated amounts of methane and decreases the production of C_{5+} products. Comparing the resulting products of the pure Fischer Tropsch catalyst with the ones of the β -zeolite/Fischer catalyst, the final amount of C_3 to C_6 products remain in the same values. However, the remarkable change is the olefin/paraffin ratio; which is affected by the β -zeolite presence, decreasing the olefin percentage. A linear correlation between methane and C_{5+} was found.

Acknowledgements

I would like to thank the staff at SINTEF in Oslo who received me in their facilities during the summer and provided me with materials. They also patiently guided me when I started synthesizing zeolites and helped me with the characterizations. I specially thank Ornulv V., Jasmina H.C., Ruth S., Aud S., and Anna L.

I would also like to thank Statoil Research Center in Rotvoll for providing me with the Fischer-Tropsch cobalt-based catalyst sample, the γ -alumina sample, and the Parr autoclave reactor to perform the β -zeolite/Fischer Tropsch catalyst synthesis.

My thanks to the Nanolab technical staff at NTNU for the training in the use of the S(T)EM.

I personally acknowledge the financial support from the Mexican National Council of Science and Technology (CONACyT) to pursue my master studies.

I appreciate the help and support of Rune Myrstad during the Fischer-Tropsch test of my β -zeolite/Fischer-Tropsch catalyst.

To my lovely family in Mexico.

Finally, I specially thank Magnus Rønning and Erling Rytter, my supervisor and co-supervisor, for their continuous guidance and valuable feedback.

A ti Adriana R., amorosamente agradezco tu invaluable apoyo e incondicional soporte durante la elaboración de este proyecto.

I declare that this is an independent work according to the exam regulations of the Norwegian University of Science and Technology (NTNU).

Place and date: Trondheim, 16th of June, 2014

Signature:



Mario Ernesto Casalegno Garduño

List of symbols and abbreviations

All variables, symbols and abbreviations used in the present work are listed below.

Symbols

- #	Sequential series of numbers
°C	Degrees Celsius
C ₁	Hydrocarbons with one carbon
C ₂	Hydrocarbons with two carbons
C ₂ =/C ₂ -	Ethene/Ethane ratio
C ₃	Hydrocarbons with three carbons
C ₃ =/C ₃ -	Propene/Propane
C ₄	Hydrocarbons with four carbons
C ₄ =/C ₄ -	1-Butene/n-Butane
C ₅	Hydrocarbons with five carbons
C ₅ =/C ₅ -	1-Pentene/n-Pentane
C ₆	Hydrocarbons with six carbons
C ₆ =/C ₆ -	1-Hexene/n-Hexane
g	Grams
h	Hour
K	Degrees Kelvin
kton	1x10 ⁺³ tone
l	Liter
min	Minutes
p	Pressure, [bar]
p ₀	Saturation pressure, [bar]
ppm	Parts per million
rpm	Revolutions per minute
T	Temperature, [°C]
vol%	Volume percentage

wt%	Mass percentage
α	Chain growth probability
β	Beta
β-zeolite	Beta zeolite
γ	Gamma
Θ	Angle, [°]
μ	Micro, 1×10^{-6}
μS	Micro-Siemens

Abbreviations

1D-	1-dimension
2D-	2-dimensions
3D-	3-dimensions
Ads	Adsorption
ASME	American Society of Mechanical Engineers
avg	Average
BBU	Basic building unit
BEA	Beta zeolite
BET	Brunauer-Emmett-Teller
BJH	Barret-Joyner-Halenda
BTL	Biomass to liquid
CAS	Chemical Abstracts Service
CBU	Composite building units
CHA	Chabazite
CTL	Coal to liquid
Des	Desorption
ERI	Erionite
FAU	Faujasite
FBR	Fixed-bed reactor
FER	Ferrierite
FT	Fischer-Tropsch
FTc	Fischer-Tropsch catalyst
FTS	Fischer-Tropsch synthesis
GHSV	Gas Hourly Space Velocity
GTL	Gas to liquid
HC	Hydrocarbons
HTFT	High temperature Fischer-Tropsch
IUPAC	International Union of Pure and Applied Chemistry

IUPAC	International Union of Pure and Applied Chemistry
IZA	International Zeolite Association
Jet A	Civil jet fuel grade, freezing point -40°C
Jet A-1	Civil jet fuel grade, freezing point -47°C
JP-5	Military jet fuel grade, used to aircraft carriers
LTFT	Low-temperature Fischer-Tropsch
LTL	Zeolite L (Linde Type L)
MAOP	Maximum allowable operating pressure
MFI	ZSM-5 (Zeolite Socony Mobil - five)
MOR	Mordenite
MTW	ZSM-12 (Zeolite Socony Mobil - twelve)
MWW	MCM-22 (Mobil Composition of Matter-twenty-two)
rHC	Rate of Hydrocarbons
S(T)EM	Scanning transmission electron microscope
S-5	Syntroleum process
SBCR	Slurry bubble column reactors
SEM	Scanning electron microscope
SSPD	Sasol slurry phase distillate process
syngas	Synthesis gas
TEA-OH	Tetraethylammonium hydroxide
TEOS	Tetraethyl orthosilicate
TOS	Time of Synthesis in hours
WOC	Without calcination
XRPD	X-ray powder diffraction

List of Figures

Fig. 1-1 Fischer-Tropsch product distribution as function of chain growth probability [4].....	3
Fig. 1-2 Support effect on FTS over cobalt-based catalysts in FBR and SBCR [9]	5
Fig. 1-3 Effect of particle size of cobalt on C ₅₊ selectivity [15].....	6
Fig. 1-4 Frequency of new natural (a) [18] and synthetic (b) [1] zeolites from 1800 to 2010 ...	7
Fig. 1-5 Pore size distribution of zeolites, carbon and alumina materials [22]	8
Fig. 1-6 The standard framework view represents BBU (a and b) and CBU (c) [24]	9
Fig. 1-7 Schematic representation of the dimensional channels of: (a) LTL-1D, (b) MWW-2D, (c) CHA-3D [1]	9
Fig. 1-8 The free pore diameters and structures of synthetic zeolites [17].....	11
Fig. 1-9 Schematic representation of template sited in the cages of zeolite [17].....	12
Fig. 1-10 Schematic representation of main steps of the zeolite synthesis [20]	13
Fig. 1-11 Pore dimensions of zeolites and critical dimensions of hydrocarbons [23]	16
Fig. 1-12 Some examples of hydrocarbon molecular diameter [25].....	16
Fig. 1-13 Effect of alkali loading in the selectivity of: heavy hydrocarbons (a), methane (b) and CO ₂ (c) [6].....	19
Fig. 1-14 Possible pathways for naphthalene hydrogenation [20]	21
Fig. 1-15 Schematic representation for the in situ up-grading of primary FTS products into high-octane gasoline components [20]	22
Fig. 1-16 Different modes of deactivation by carbonaceous deposits in zeolites [23]	22
Fig. 1-17 Relationship between total catalyst acidity and deposited coke content [32].....	23
Fig. 1-18 Schematic representation of a core-shell hybrid FT-acid catalyst configuration [20]	23
Fig. 1-19 Fractional distribution of hydrocarbons for Fischer-Tropsch iron-based and cobalt-based catalysts [33].....	24
Fig. 1-20 Examples of how zeolites can be used to increase selectivity for a reaction [34]	26
Fig. 1-21 The reactant pathway from bulk to active site encompasses diffusion processes on a broad length scale in common catalytic processes [20]	27

Fig. 1-22 Concentration and temperature changes from the bulk phase through a stagnant film of thickness δ to a particle surface and then through the porous catalyst particle, assuming an exothermic reaction occurs [35].....	27
Fig. 1-23 Schematic representation of a typical catalyst pellet comprised of small porous particles [35]	28
Fig. 2-1 Parr Autoclave, Series 4560 Mini Reactors, 100-600 mL with Modular Controller model 4848 [40]	34
Fig. 2-2 General autoclave configuration, internal view of the main components	35
Fig. 2-3 Plot of pressure vs. time during nano BEA synthesis for an (A) unvented reactor, (B) a reactor [41]	36
Fig. 2-4 Fischer Tropsch setup schematic representation [15]	47
Fig. 2-5 Brunauer classification, Types of sorption isotherms [22].....	52
Fig. 2-6 Schematic representation of Bragg's Law [43].....	55
Fig. 2-7 Interaction of the primary electron beam with the sample [22].....	57
Fig. 2-8 Adsorption isotherms for Pt dispersed on Al_2O_3 : 1) H_2 adsorption on Al_2O_3 in Henry's law region, 2) H chemisorption on Pt, 3) Total H_2 chemisorption on Pt/ Al_2O_3 catalyst [35]	58
Fig. 3-1 β -zeolite/FT catalyst BET surface area comparison, long pressure range	64
Fig. 3-2 β -zeolite/FT catalyst BET BJH pore size comparison	64
Fig. 3-3 β -zeolite/FT catalyst BET surface area between long pressure range and short pressure range.....	65
Fig. 3-4 β -zeolite/FT catalyst BET surface area short pressure range	66
Fig. 3-5 XRD powder pattern for pure β -zeolite sample BEA-14AUT, white calcined sample	67
Fig. 3-6 Comparison of XRD patterns of γ -alumina and FT catalyst	68
Fig. 3-7 XRD powder pattern for β -zeolite/FT catalyst sample BEA-14AUT, black sample..	69
Fig. 3-8 XRD powder pattern for β -zeolites collection. Greek letter β represents the main peaks of pure β -zeolite reference pattern from IZA [21]. Dotted gray lines are spatial reference lines	70

Fig. 3-9 XRD powder pattern for β -zeolites/FT catalyst collection. Greek letter β represents the main characteristic peaks of β -zeolite reference pattern from IZA [21], Co represents the main characteristic peaks for cobalt oxide [15] and Greek letter γ represents the main characteristic peaks of γ -alumina. Dotted gray lines are spatial references71

Fig. 3-10 XRD powder pattern for β -zeolites/FT catalysts that were tested in the FT reactor. Greek letter β represents the main characteristic peaks of β -zeolite reference pattern from IZA [21], Co represents the main characteristic peaks for cobalt oxide [15] and Greek letter γ represents the main characteristic peaks of γ -alumina. Dotted gray lines are spatial references72

Fig. 3-11 SEM images of BEA-11 AUT BLACK using different focus73

Fig. 3-12 β -zeolite/FT cobalt-based catalyst BEA-14AUT BLACK and FT catalyst, gold-coated.....74

Fig. 3-13 β -zeolite/FT catalyst BEA-10AUT 1 μ m, gold-coated75

Fig. 3-14 Carbon Monoxide conversion in the Fischer Tropsch reaction test.....82

Fig. 3-15 Carbon Monoxide 50% conversion in the Fischer Tropsch reaction test. Samples are sorted according to FT catalyst content83

Fig. 3-16 Methane generation of the different samples in FT reaction test. Samples are sorted according to FT catalyst content84

Fig. 3-17 C₃ to C₆ hydrocarbon products of the different samples in FT reaction test. Samples are sorted according to FT catalyst content84

Fig. 3-18 Olefin to paraffin ratio of the different samples in FT reaction test. Samples are sorted according to FT catalyst content.....85

Fig. 3-19 Methane as function of C₅₊ components. The plotted data were based in the last adjustment of gas flow to obtain approximately 50% CO conversion. Dotted line is used as reference to show the linearity of the results86

Fig. 3-20 Total percentage of C₅₊ generated during the FT tests. The data were based in the average of the last adjustment of gas flow to obtain approximately 50% CO conversion87

List of Tables

Table 1-1 Major overall reactions in Fischer-Tropsch synthesis [4].....	3
Table 1-2 Zeolite nomenclature base on IZA three-letters code.....	10
Table 1-3 Pore packing sizes of synthetic zeolites [1] [8] [22]	11
Table 1-4 Main applications of zeolites in the industriy [8] [17]	15
Table 1-5 Fischer-Tropsch synthesis of hydrocarbons at 200°C and a space velocity of 100 h ⁻¹ [27]	18
Table 1-6 Bifunctional hydrocracking catalysts [20]	21
Table 1-7 Composition decanted water of FTS [33]	25
Table 1-8 Synthetic jet fuels of LTFT syncrude from the Sasol (SSPD) and Syntroleum (S-5) processes [3].....	29
Table 2-1 Chemical liquid zeolite components A.....	32
Table 2-2 Chemical solid zeolite components B.....	32
Table 2-3 Additional chemical components	33
Table 2-4 Relative costs for selected silica raw materials [41].....	43
Table 2-5 Hydrothermal synthesis products name and general composition	44
Table 2-6 β -zeolite and β -zeolite/FTcatalyst molar composition	45
Table 2-7 β -zeolite/FTcatalyst molar composition of seed-assisted materials	45
Table 2-8 Fischer Tropsch reaction chemical components	46
Table 2-9 Fischer Tropsch tested catalyst dilution.....	48
Table 2-10 Fischer Tropsch tested catalyst dilution adjusted.....	49
Table 2-11 Type and characteristics of sorption isotherms [22].....	53
Table 3-1 Hydrogen chemisorption results for the β -zeolite/FT catalyst samples without calcination. The catalysts were sorted by high to low FT catalyst weight content	76
Table 3-2 Hydrogen chemisorption results for the β -zeolite/FT catalyst samples that were tested in the FT reactor. The catalysts were sorted by high to low FT catalyst weight content	77

Table 3-3 Hydrogen chemisorption crystal sizes for the β -zeolite/FT catalyst samples that were tested in the FT reactor. The catalysts were sorted by high to low FT catalyst weight content.....	78
Table 3-4 Silicon source for the β -zeolite/FT catalyst samples that were tested in the FT reactor	79
Table 3-5 Mass composition of the β -zeolite/FT catalyst and pure FT cobalt-based catalyst tested in the Fischer Tropsch reactor.....	81
Table 3-6 Mass composition of the β -zeolite/FT catalyst and pure FT cobalt-based catalyst, including white and black phases, seed-assisted procedure and TEA-OH pretreatment. Samples are sorted according to FT catalyst content	82

List of Equations

Eq. 1.....	53
Eq. 2.....	55
Eq. 3.....	56
Eq. 4.....	59

Contents

ABSTRACT.....	I
ACKNOWLEDGEMENTS.....	III
LIST OF SYMBOLS AND ABBREVIATIONS	V
LIST OF FIGURES.....	IX
LIST OF TABLES.....	XIII
LIST OF EQUATIONS.....	XV
1. INTRODUCTION.....	1
1.1 Fischer-Tropsch synthesis	2
1.2 Biomass to liquid process	4
1.3 γ -Alumina support influence in Fischer-Tropsch	5
1.4 Zeolites background	7
1.5 Zeolite synthesis.....	12
1.6 Zeolites as a catalyst.....	15
1.7 Alkali promoters in Fischer-Tropsch synthesis	18
1.8 Bifunctional Fischer-Tropsch zeolite catalyst	21
1.9 Mass and heat transfer limitations in bifunctional zeolite/Fischer-Tropsch catalysts.	26
1.10 Jet fuel background	29
2. METHODS.....	31
2.1 Zeolite/FT catalyst synthesis	31
2.1.1 Chemical components	32
2.1.2 Synthesis and treatment equipments	34
2.1.3 Synthesis and treatment conditions.....	36
2.1.4 Synthesis and treatment procedures.....	38
2.1.5 Selection of silicon sources	43
2.1.6 Zeolites recipes	44
2.2 Fischer Tropsch reaction	46
2.2.1 Fischer Tropsch chemical components	46
2.2.2 Fischer Tropsch reaction equipments	47

2.2.3	Fischer Tropsch reaction	48
2.3	Characterization methods	51
2.3.1	Brunauer-Emmett-Teller (BET)	52
2.3.2	X-ray diffraction (XDR).....	55
2.3.3	Scanning electron microscope (SEM).....	57
2.3.4	Chemisorption.....	58
3.	RESULTS AND DISCUSSION	61
3.1	β -zeolite/Fischer Tropsch catalyst	61
3.1.1	Brunauer-Emmett-Teller (BET)	63
3.1.2	X-ray diffraction (XDR).....	67
3.1.3	Scanning electron microscope (SEM).....	73
3.1.4	Chemisorption.....	76
3.1.5	Silicon source	79
3.2	Fischer Tropsch reaction test	80
4.	CONCLUSIONS	89
5.	FURTHER WORK	93
6.	BIBLIOGRAPHY	95
7.	APPENDIXES	99
	Appendix A.....	99
	Appendix B.....	109
	Appendix C.....	113
	Appendix D.....	151
	Appendix E.....	161
	Appendix F.....	183
	Appendix G.....	197
	Appendix H.....	207
	Appendix I.....	209
	Appendix J.....	211

1. Introduction

In the past couple of decades, a large effort has been made to optimize, increase, and tailor the selectivity and activity of the catalysts. This has been achieved using diverse kinds of metals as active material and support materials as dispersed material.

The introduction of zeolites as catalysts in the petrochemical field was originated in the last years of the 1950's, when Union Carbide developed a zeolite as an isomerization catalyst. This represents the first major bulk separation process using true molecular sieving selectivity [1]. After Union Carbide, also other companies as Mobil Oil, Grace, and Henkel, to mention some of them, worked extensively developing a wide range of zeolites for different processes. Nowadays the use of zeolites is part of the common life. For example, in 2008, 367 kton of zeolite Y were used in catalytic cracking to produce gasoline [1].

Fischer-Tropsch Synthesis (FTS) allows the production of liquid hydrocarbons using synthesis gas as raw material. FTS is a technology that has been deeply studied since its discovery. The first industrial application of FTS started in Germany in 1938 [2]. In the last 20 years, remarkable progress has been made in terms of materials of the reactor, reactor design, catalyst attrition resistance, increased selectivity and activity. These advances let FTS to start competing with the standard gasoline sources as petroleum in a very convenient and economical way.

Extensive work has been performed to optimize also product distributions. Positive results have been obtained with the use of promoters that improve the concentration some components in the product. However, regardless of the use of promoters, FTS remains with the same very high selectivity for two products that depends of the process conditions: methane or hard waxes. The use of low-temperature Fischer-Tropsch (LTFT) provides an excellent source of hard waxes. The LTFT product requires further process to break the large hydrocarbon chains, in order to obtain gasoline (C_5 - C_{12}), jet fuel (C_{11} - C_{13}), and diesel (C_{13} - C_{17}).

The purpose of the present work is to create the bases to develop a future tailored catalyst, which can increase the concentration of medium sized hydrocarbons (C_5 - C_{17}) under the LTFT process conditions, using cobalt-based catalyst and zeolites in a single catalyst and reactor.

1.1 Fischer-Tropsch synthesis

It has been more than 80 years since the study of Fischer-Tropsch synthesis (FTS) started. Three countries stand out in the developing of FTS: Germany, United States, and South Africa, all of them with industrial scale plants. Many of the oil major companies have invested in Fischer-Tropsch research to improve the activity and selectivity of FTS [3].

The main principle of FTS is based on the conversion of carbon monoxide (CO) and hydrogen (H₂), also called syngas (CO + H₂), into hydrocarbons. The main sources of syngas for FTS are: coal, natural gas, and in the last years, biomass.

Based on the process that generates syngas to produce FTS products different names are used. The syngas produced via coal is called *coal to liquid* (CTL) with a H₂/CO ratio circa 0.7-1.0 [4]. For natural gas it is called *gas to liquid* (GTL) with a H₂/CO ratio circa 1.6-2.5 via auto thermal reforming [5]. The most attractive source, biomass, is called *biomass to liquid* (BTL) with a variable H₂/CO ratio lower than natural gas reforming but higher than coal gasification [6].

As mentioned previously each of these alternatives generates different ratios between H₂/CO. This ratio is an important parameter to keep in mind during the selection of the catalyst and process conditions for FTS because it enables the value of the chain growth probability (α) to be shifted [4]. There is no single number of the syngas ratio, but for cobalt-based FTS very often the number is between 2.10 to 2.15.

Mainly three different technologies emerge in the FTS for the industrial scale sizes.

- High temperature Fischer-Tropsch (HTFT) iron-based
- Low temperature Fischer-Tropsch (LTFT) iron-based
- Low temperature Fischer-Tropsch (LTFT) cobalt-based.

The selection of technology is based on the source of syngas and the final products that are expected. For gasoline production with syngas generated via coal gasification, HTFT iron-based is preferred despite the methane generation. The LTFT is more suitable to produce hard waxes, as the major product is rich in linear alkanes. The difference in the selection of the catalyst metal is based also in the source of the syngas. For natural gas and biomass cobalt-based catalyst is selected, while for coal gasification iron-based is the best option [2] [3].

Whatever the source of the syngas, FTS process conditions, and the catalyst; further treatment is always required to upgrade the products into more valuable products such as gasoline, jet fuel, diesel and chemicals.

As chemical process, FTS involves several reactions that give origin to main products such as alkanes, alkenes and side products as CO, CO₂ and water. The reactions that have large contribution during FTS are shown in Table 1-1:

Table 1-1 Major overall reactions in Fischer-Tropsch synthesis [4]

<i>Main reactions</i>	
Alkanes	$n\text{CO} + (2n + 1)\text{H}_2 \longrightarrow \text{C}_n\text{H}_{2n+2} + n\text{H}_2\text{O}$
Alkenes	$n\text{CO} + 2n\text{H}_2 \longrightarrow \text{C}_n\text{H}_{2n} + n\text{H}_2\text{O}$
<i>Side reactions</i>	
Water-gas shift	$\text{CO} + \text{H}_2\text{O} \rightleftharpoons \text{CO}_2 + \text{H}_2$
Alcohols	$n\text{CO} + 2n\text{H}_2 \longrightarrow \text{H}(\text{CH}_2)_n\text{OH} + (n - 1)\text{H}_2\text{O}$
Boudouard reaction	$2\text{CO} \longrightarrow \text{C} + \text{CO}_2$

Product distribution plays an important role in the final FTS products. With selected catalyst and process conditions for that catalyst, the factors that can change product distribution are syngas composition, partial pressures and the promoters in the catalyst. A typical product distribution is shown in Fig. 1-1.

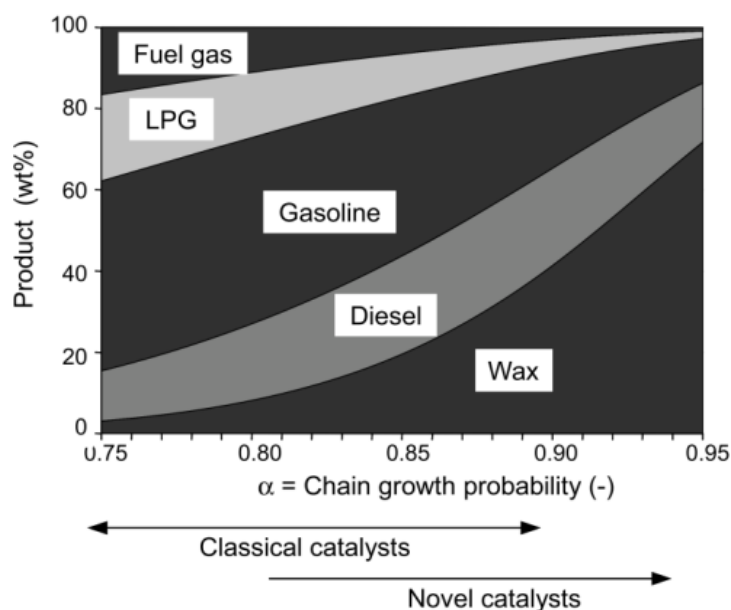


Fig. 1-1 Fischer-Tropsch product distribution as function of chain growth probability [4]

1.2 Biomass to liquid process

Environmental policies today drive the innovation to find new ways to utilize the available resources around us such as biomass or carbon-rich waste. The most promising way of make profitable the biomass to liquid (BTL) process is process intensification, cutting down production costs of synthesis gas derived from biomass [3] [7].

A convenient definition of biomass is “the material that contains woody and herbaceous components as main resources”. Some specifications need to be fulfilled to consider the biomass as an excellent source of syngas. The most relevant specifications are: origin of biomass, water content, chips’ size, and impurities [8].

A wide number of processes and products utilize the biomass as a feedstock. Biomass treated via fermentation, extraction, and hydrolysis produces base chemicals; via combustion produces power; and via pyrolysis or gasification produces liquid fuels. Under the consideration that biomass is an abundant and renewable resource, it is an excellent source of syngas for FTS. The main interest on the production of syngas from biomass is that it contains an important amount of carbon and hydrogen to produce high quality fuels compared to coal and it is a material that is not linked with the oil and gas industry [4].

BTL can deal with the problem of transportation related to the low energy density of biomass. FTS offers a promising energy upgrading technology for gasified biomass, in terms of increased lower heating value (LHV) of the final products [3]. Biomass in FTS could produce diesel and hard waxes, as well as gasoline.

It is convenient to clarify the difference between biodiesel and diesel from FTS. Biodiesel is a blend of methyl or ethyl esters of fatty acids, while diesel is a product of FTS after biomass gasification, conversion and treatment. The fuels produced via FTS are considered hydrocarbons with ultraclean environmental specifications: very low content of sulfur and nitrogen compounds.

Due to the importance nowadays of the alternative sources of energy, BTL is an attractive route to take into account in the near future. The hydrocarbons produced via FTS can be converted mainly into fuels but also into other base chemicals, e.g. alcohols are used to produce biodegradable detergents [2].

1.3 γ -Alumina support influence in Fischer-Tropsch

Different metals have been used to produce FTS catalyst, but only Fe, Co, Ni, Ru have the required characteristics for industrial scale up. Nickel has high selectivity to produce methane that is not a desirable product in FTS. Ru's price is high due to the scarcity in nature, limiting the use of this element in the industrial applications. This ends with only two possible candidates: iron and cobalt. Whereas iron is abundant in nature, the price is very low compared with cobalt; in fact, to be more precise the price is about 1000 times lower [2].

Both metals are used as catalyst for FTS; the selection of one or other is based principally in the source of syngas and the final products.

Based on cobalt prices, the methods to use it as catalyst must be improved. The most employed method to maximize the use of cobalt is impregnating the metal over a support, that can influence or not the final products. The use of the supports increases enormously the dispersion area reducing the amount of required active metal. Common support materials are alumina (Al_2O_3), silica (SiO_2), and titania (TiO_2) with 10 to 30% in weight of loading metal [8] [2].

Titania as a FTS cobalt-based support catalyst is not a reasonable option. Titania has very low surface area as a support (10-15 m^2/g), cobalt titanate (CoTiO_3) formation and non-uniform dispersion of the particles in the reactor. These factors influence the final catalyst, affecting the amount of cobalt loading [9].

Silica and alumina supports are considered the most adequate for FTS with surface areas of about 150-250 m^2/g . The selection of the most appropriate support depends on the catalytic activity and selectivity. Alumina-supported cobalt exhibits high performance in terms of selectivity and activity under the same process conditions [9]. Fig. 1-2 shows the activity of the different supports in two different reactor types.

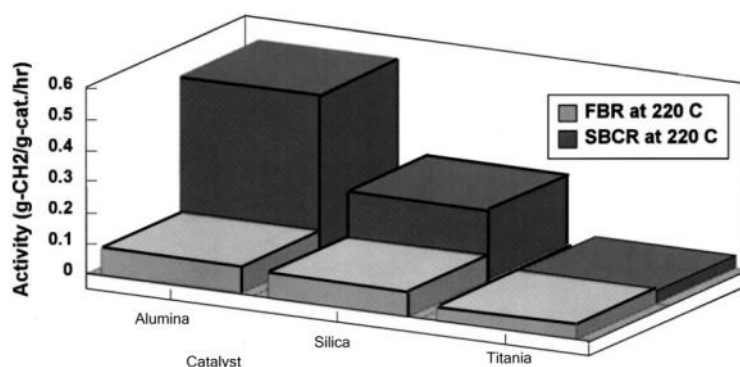


Fig. 1-2 Support effect on FTS over cobalt-based catalysts in FBR and SBCR [9]

Based on the performance of alumina in FTS, it is considered the best support for cobalt metal. This support has different phases: α , χ , η , δ , κ , θ , γ , ρ -alumina. The phase is controlled via heat treatment of the alumina precursor. The α -alumina phase is the most stable thermodynamically and the most suitable for high temperature applications but this high resistance decreases the available area ending in an alumina with a very low surface compared to the other phases [10] [11]. In general, alumina with low surface area ($15 \text{ m}^2/\text{g}$) results in low metal dispersion reducing the activity of FTS catalyst [12].

The most relevant phase in terms of catalysis for FTS is γ -alumina due to its high surface area, allowing high loading of metals to disperse over the surface. Diverse studies prove that the size of the pores in the support plays an important role in the selectivity and activity of the catalyst in the FTS. The dependence between the size of the distributed particles of the cobalt metal and the pore size and is high; the smaller the pores, the smaller the metal particles dispersed in the support and vice versa [13][14].

In addition, the product distribution has significant dependency on the cobalt particle size. The product selectivity, measured at the same process conditions shows that the smaller cobalt particles increase the production of light hydrocarbons ($\text{C}_1\text{-C}_4$) and the larger cobalt particles increase the selectivity towards heavy hydrocarbons (C_{5+}). Fig. 1-3 shows the effect of particle size of cobalt in product selectivity [15][16].

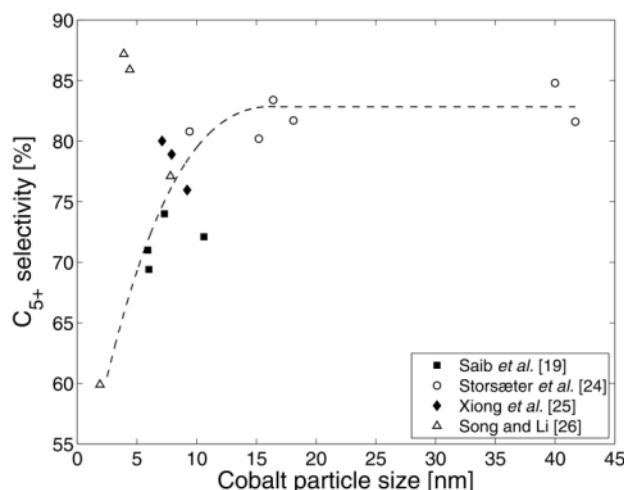


Fig. 1-3 Effect of particle size of cobalt on C_{5+} selectivity [15]

Alumina as support for cobalt in FTS catalysts has a remarkable influence in the final products. Different vendors supply commercial γ -alumina; the most appropriate for FTS is a modified Puralox® high purity activated alumina produced by Sasol.

1.4 Zeolites background

Zeolites are natural minerals result of volcanic activity. Volcanic dust deposited in saline lakes creates zeolites over the world. Natural zeolites in are used as a building material, water treatment adsorbent, odor control agent, gas separation agent, desiccants, agriculture, and animal feed supplements [8] [17].

Due to the importance of the natural zeolites in our lives and the requirements of new industrial applications, synthetic zeolites were developed. The first step had the purpose of reproducing natural structures. Then development of new and fascinating unknown structures started, with specific applications as: process extraction, process purification, and heterogeneous catalysis. Fig. 1-4 shows how the use of natural and synthetic zeolites increased in number along two centuries.

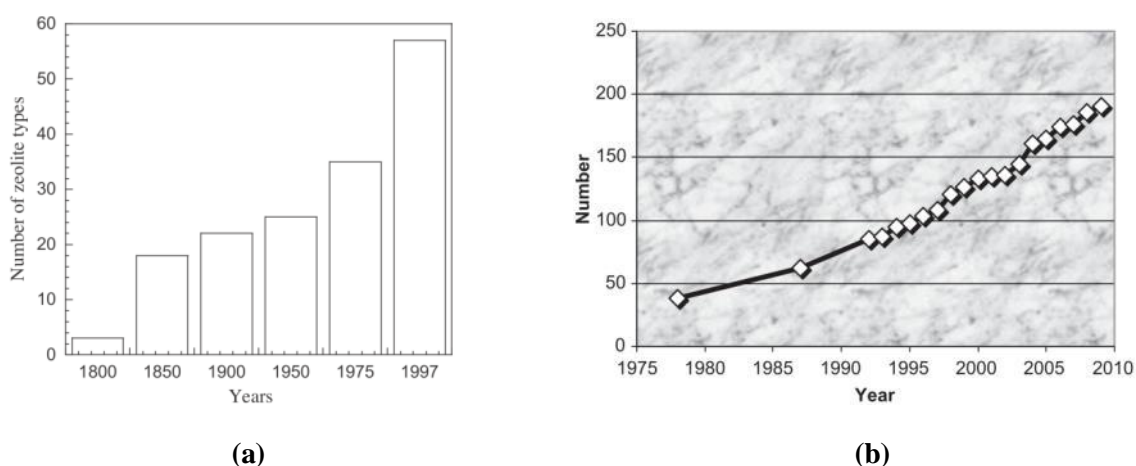


Fig. 1-4 Frequency of new natural (a) [18] and synthetic (b) [1] zeolites from 1800 to 2010

Until 1997, around 60 new zeolites had been synthesized and by 2010 this number had reached 190. The synthesis of new zeolite structures is still growing every year [19] [20]. According to the International Zeolite Association web page the most updated number of zeotype structures is 213 framework type codes in July 2013 [21]. As a growing field of science, a new association was organized in 1973. The International Zeolite Association (IZA) was created to promote and encourage the development of all aspects of zeolite science and technology [21].

A single definition of zeolites does not exist. *Buschow et al.* defined zeolites as aluminosilicates possessing three-dimensional frameworks of linked silicon-aluminum-oxygen tetrahedral. Another definition describes zeolites as crystalline aluminosilicates with a

three-dimensional framework of linked tetrahedra structure that forms uniformly sized pores of molecular dimensions consisting of four O atoms surrounding a cation [18] [22].

The extensive use of synthetic zeolites promotes a breakthrough in industrial process applications. Synthetic zeolites allow tailoring desirable microstructures with an ultra regular and well defined pore size and cavities, Fig. 1-5. The structures are unique in that they incorporate pores as part of the regular crystalline structures. The pores act as molecular sieves, allowing only the passage of the molecules for which it was designed, imposing a constrain for it due to their narrow and well organized structure, enhancing molecules with a predicted structure [23] [22].

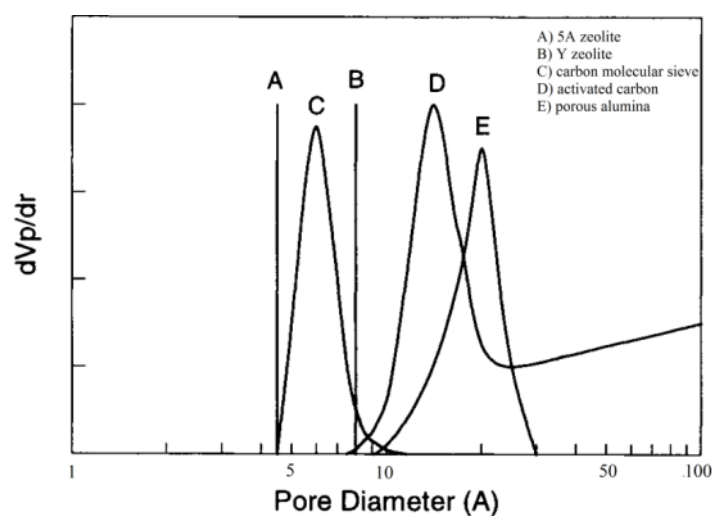


Fig. 1-5 Pore size distribution of zeolites, carbon and alumina materials [22]

The pores and cavities normally host water molecules and cations. Both can be removed easily via evaporation and ion exchange respectively. The synthetic zeolites are represented by the chemical empirical formula $M_{2/n}O \cdot Al_2O_3 \cdot ySiO_2 \cdot wH_2O$, where y is 2-200, n is the cation valence and w represents the water contained in the voids of the zeolite [1]. Aluminum has a valence of three positive charges originating a negative charge into the zeolite structure. To balance the charges a counter ion is required. The counter ions are part of group IA and IIA elements, such as sodium, potassium, magnesium and calcium [8].

Zeolites are composed of primary structural units called basic building unit (BBU) as TO_4 ($T=Al$ or Si) tetrahedron as Fig. 1-6 (a), assembled in secondary ones such as cubes, hexagonal prisms. The union of many BBU gives origin to chain structures as in Fig. 1-6 (b). The three-dimensional framework structure formed by linking BBUs in a continuous repeating lattice is called composite building units (CBU) as is illustrated in Fig. 1-6 (c) [1].

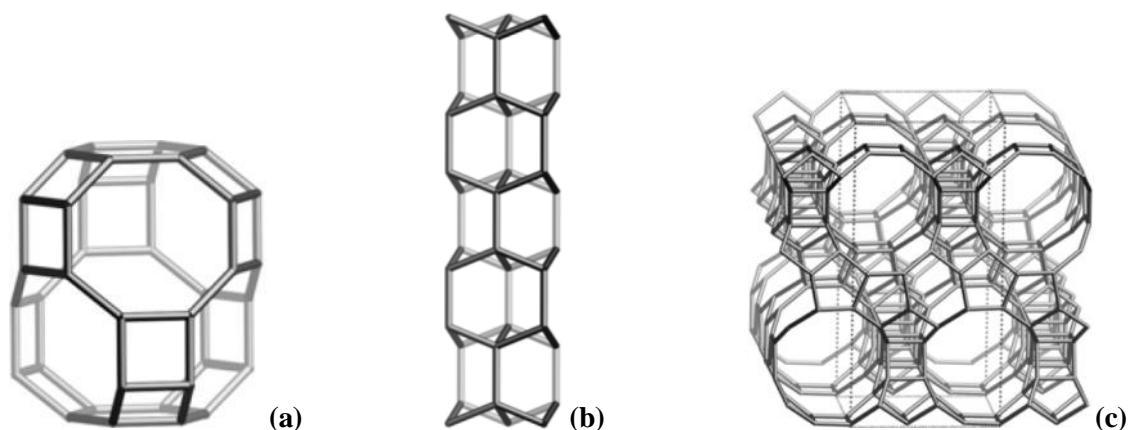


Fig. 1-6 The standard framework view represents BBU (a and b) and CBU (c) [24]

Every zeolite has a defined composition in terms of Si and Al linked with O and a counter ion to balance the charges, e.g. beta zeolite the crystal chemical data is $[\text{Na}_7][\text{Al}_7\text{Si}_{57}\text{O}_{128}]$.

The internal volume of zeolites consists of framework systems, which are uniform channels interconnected on different dimensions. The classification of these systems is one-dimensional channel (1D) Fig. 1-7 (a), two-dimensional channel (2D) Fig. 1-7 (b) or three-dimensional channel (3D) Fig. 1-7 (c). The channels or pores connect. All pores and cavities represent 50% of the crystal volume. The selected dimensions are two or three-dimensional channels, because these allow efficient and fast diffusion of the molecules into the pores, representing an advantage for catalyst applications.

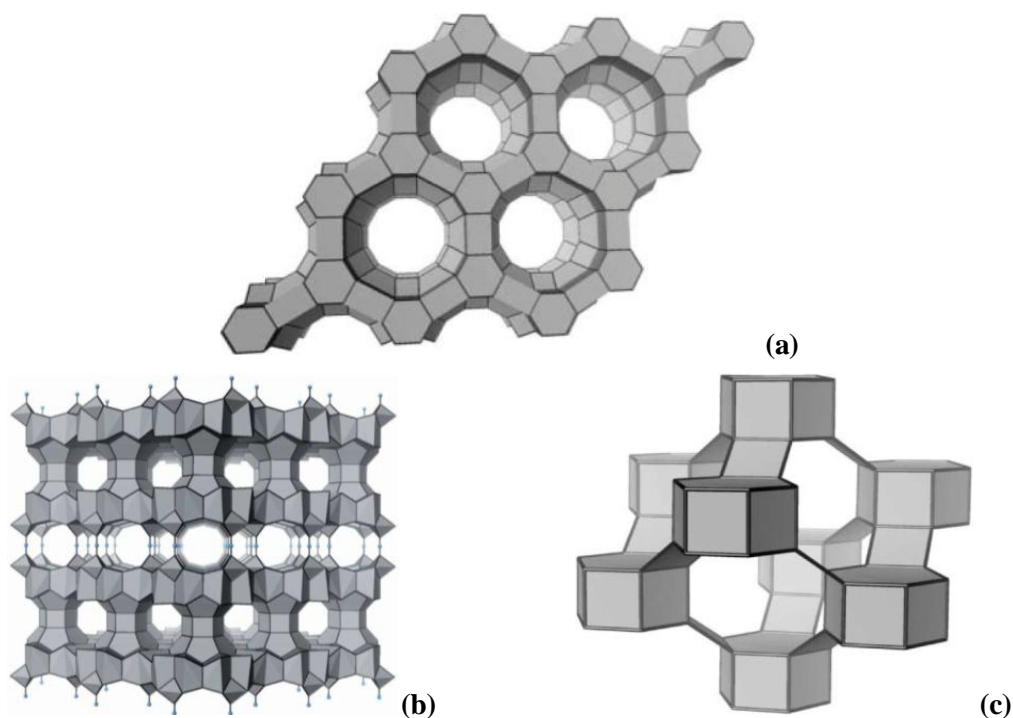


Fig. 1-7 Schematic representation of the dimensional channels of: (a) LTL-1D, (b) MWW-2D, (c) CHA-3D [1]

As for each chemical component, zeolites nomenclature was established. The organization that is responsible of naming natural and synthetic zeolites is the IZA structure commission. The name of synthetic zeolites consists of a three letters code, which describes the zeolite framework type regardless of composition. The rules for framework type assignment are described in the *Atlas of Zeolite Framework Types* [24] [18].

Several zeolites could also have an alternative name that is directly related to the developer of the structure or the composition of the zeolite or the mineral name. Some examples of the different names are: ZSM-# family, that means Zeolite Socony Mobil developed by Mobil company; SAPO-# family, that means Silico-aluminophosphate and Chabazite, which is the name of the natural zeolite mineral. The most accepted and standardized method to call zeolites is the IZA structure commission method. Table 1-2 includes some zeolites' names and their corresponding common or commercial name.

Table 1-2 Zeolite nomenclature base on IZA three-letters code

IZA code	Zeolite Name
BEA	Beta Zeolite
CHA	Chabazite/SAPO-34
MFI	ZSM-5
MTW	ZSM-12

Dense phase frameworks with a regular structure are not considered zeolites or zeotype materials; these contain very low size pores that limit the porosity. Zeolites must contain voids with volumes larger than 0.25 nm diameter, sphere and pore sizes from 2.8 to 20 Å. Fig. 1-8 shows several well-known zeotype materials.

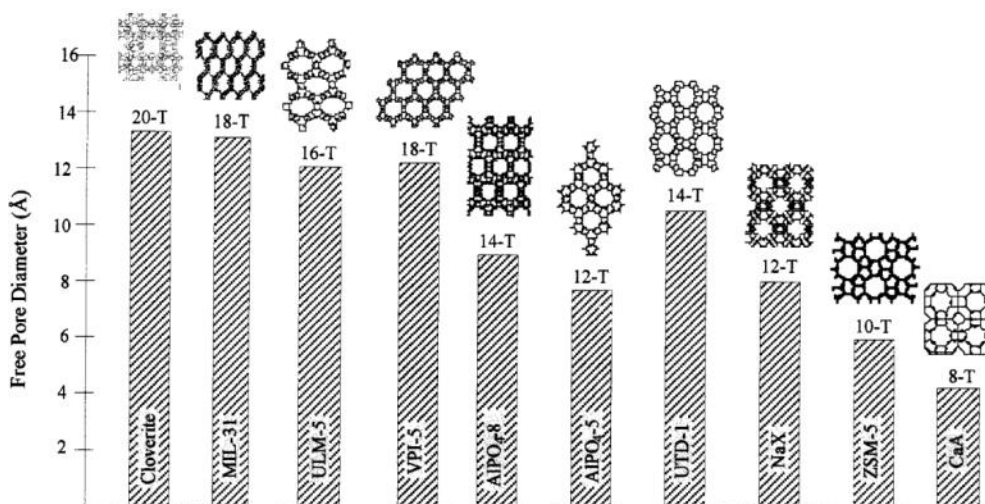


Fig. 1-8 The free pore diameters and structures of synthetic zeolites [17]

Pore size is defined by the structure of the oxygen-packing with Si or Al. Zeolites have different pore size structure based on the number of oxygen-packing form the n -ring. Table 1-3 describes the pore size and an example of a zeotype material.

Table 1-3 Pore packing sizes of synthetic zeolites [1] [8] [22]

Packing	Size	Maximum free aperture, [Å]	Pore diameter [Å]	Zeolite
4-ring	very small	1.6	-	Sodalite
6-ring	very small	2.8	-	Afghanite
8-ring	small	4.3	3.0-4.5	Zeolite A
10-ring	medium	6.3	4.5-6.0	ZSM-5
12-ring	large	8.0	6.0-8.0	Zeolite X
14-ring	extra-large	10.0	7.0-10.0	UTD-1
20-ring	Ultra-large	14.0	10.0-14.0	Cloverlite

The classification of the pore size is given by IUPAC. Under this classification, zeolites are considered micropore materials (pores smaller than 20\AA). The control of the pore in zeolites is crucial for the final application because the size determines the selectivity at molecular scale, which is the reason why zeolites are known as molecular sieves.

1.5 Zeolite synthesis

Zeolites are synthesized via hydrothermal conditions using: a source of aluminum and silica, an organic molecule as a template, and water under highly acidic or alkaline conditions with temperatures typically between 100-200°C, at equilibrium pressure conditions. Hydrothermal synthesis is defined as the heterogeneous reaction of materials in aqueous solvent. The advantage of using water as solvent is that it is cheap compared to other solvents, very abundant in the nature and very easy to treat for further disposal [1] [17].

Synthesis conditions for hydrothermal zeolite processes are: reaction temperature, reaction homogeneity, pressure, time, pH medium condition, water and reactants purity, reactant concentration, agitation. The time to form the zeolite crystals is in the range of a few hours to several days and in exceptional cases a couple of weeks [8].

The water solution contains the crystalline structures that are balancing with the charge in the cations in the resulting product. The microporosity of the zeolite is an outcome of the organic template that is used to fill the void spaces that originate the pore sizes and cavities. Water amount is an important parameter to take in account to produce the expected phase and control the crystal size and product morphology.

The template is an organic component that is encapsulated by aluminum and silica sources to produce a solid material around it; the concept is illustrated in Fig. 1-9. The size of the targeted pore mimics the size of the template; by varying the template structure and sizes also, the final pore varies.

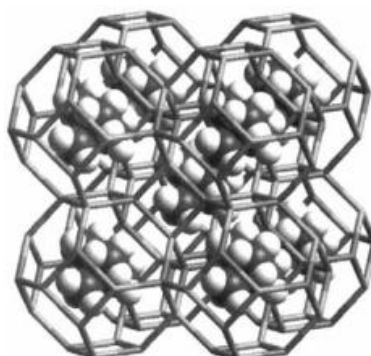


Fig. 1-9 Schematic representation of template sited in the cages of zeolite [17]

According to Čejka *et al.* a typical zeolite synthesis will involve the following steps:

1. Formation of the primary amorphous phase. This is a mixture of amorphous reactants such as Si, Al in a basic or acidic medium.
2. Heating the solution in metal autoclaves at the desired temperature.
3. Formation of the secondary amorphous phase with a solution phase.

4. Formation on nuclei giving origin to the quasi-steady state amorphous solid.
5. Growth of the zeolite at the expense solid formed in the previous step.

The nucleation step is only a part of the first moments of the synthesis, and then all nuclei forming at expenses of amorphous phase are converted in crystals phase. The crystal size increases linearly as a function of time in most of the crystallization process as is shown in Fig. 1-10.

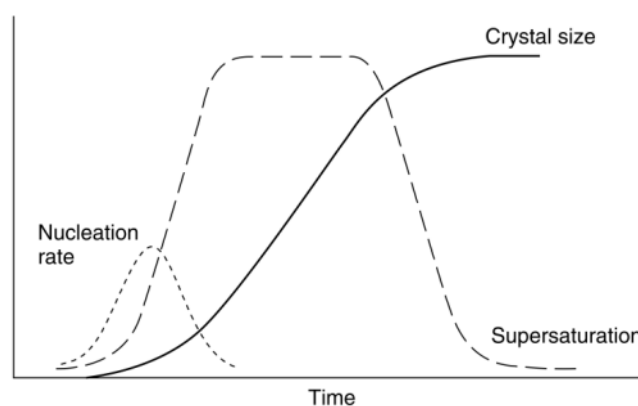


Fig. 1-10 Schematic representation of main steps of the zeolite synthesis [20]

The device that is commonly used to perform zeolites hydrothermal synthesis is a stainless steel autoclave to withstand the pressures. Autoclaves include an internal Teflon liner that works as inert container to avoid reactions or degradation between the metal and the components due to the high acidic or alkaline conditions.

During zeolite synthesis, stirring or rotating equipments is also required for some products to increase the dispersion and facilitate crystal formation. It is necessary to keep homogeneity in the solution in terms of heat and composition to have the same nucleation rate and avoid unwanted products with different morphology or particle sizes.

Besides temperature and aging, pH plays a central role in the final zeolite composition, it is mandatory to maintain the pH of the solution below 3.5 to avoid precipitation of aluminum species. The precipitation makes difficult the incorporation of the aluminum in the zeolite structure, resulting in a final material with a different composition than expected.

After the reaction time, the zeolite product must be recovered. The used procedure is dewatering via decantation of the clear solution, extraction, filtration and washing of the zeolite. If the filtration step is too slow, centrifugation is the alternative procedure that is recommended to sediment the fine powder contained in the solution.

The washing step is a critical factor to maintain the integrity of the powder and zeolite structure. Powder forms some aggregates that are stable under certain pH conditions, if the water amount is too generous, pH changes and the aggregates are broken resulting in a loss of material into the mother liquor. Over-washing also creates a problem with the cationic balance; this process, known as decationization, is reversible with an alkali solutions post-treatment [1].

After washing, the zeolite is ready to dry under stagnant conditions from 60-90°C. The most recommendable temperature is 60°C, to avoid the trapped water molecules from escaping too fast from the internal structure zeolite and cause damage to the zeolite structure. Once zeolites are dry, calcination is used to remove the organic template to create the void spaces that originate the ultra regular and well-defined pores and cavities. Alternative procedures to remove the template without destroying it via calcination can be used, but these are only applicable when the template is very complex to synthesize and its destruction incurs in very high costs; otherwise, calcination still the best.

At industrial scale, adding binders in zeolites is common. Binders increase particle size to minimize pressure loss and increase mechanical strength to reduce the attrition in moving-bed reactors [1].

Regarding the acid or basic behavior of zeolites, some of them are considered as solid Brønsted acids and others as solid Lewis bases. The acidity strength of zeolites is conditioned to the Si:Al ratio: at high Si ratios compared to Al, the result is a stronger acid and more hydrophobic zeolite. Zeolite acidity can be manipulated with the modification of the counterion, substituting it for an ammonium group via ionic exchange. The basicity of zeolite is less well documented [8].

The surface area of zeolites is considered to be very high, some of them have an area of circa 400 m²/g. This converts the zeolites in a perfect option as support material. Likewise, zeolites contain extremely regular and structural channels that increase the dispersed area for metal loadings.

1.6 Zeolites as a catalyst

There are uncountable examples of the use of zeolites as a catalyst from the first generation of synthetic zeolites. All these efforts in the use of zeolites as a catalyst brought a remarkable number of them with tailored shape selectivity and structural diversity.

The introduction of zeolites as catalyst started in the petrochemical industry to optimize and enhance the gasoline production, and this is still the most dominant process in the zeolites utilization for more than 60 years. Table 1-4 shows the most remarkable applications of zeolites in the petrochemical industry.

Table 1-4 Main applications of zeolites in the industry [8] [17]

Application	Zeolite	Notes
Catalytic Cracking	HY-high silica zeolite	Selectivity and high conversion rate
	REY	Medium pore zeolites
Hydrocracking	H-ZSM-5, FAU(X, Y), USY, Co, Mo, W, Ni on MOR	Conversion rate high
Dewaxing	Pt-MOR, ZSM-5, silicalite, FER	Low pour and cloud points
Hydroisomerisation	Pt-MOR	Low octane pentanes and hexanes converted to high octane yields
Aromatization	Pt, K, Ba silicalite, Pt, Ga, Zn-ZSM-5	Aromatization of C3–C8 cuts, aromatization of LPG
Benzene alkylation	ZSM-5	Production of ethylbenzene and styrene (minimizing by-products)
Xylene isomerization	ZSM-5	High selectivity to para yield
Toluene disproportionation	ZSM-5, MOR	Production of xylenes and benzene
Methanol to petroleum	ZSM-5, ERI	High olefin yields and high petroleum yield
Fischer-Tropsch	Co or Fe-ZSM-5	Natural gas to petroleum

Despite the high selectivity of zeolites and the perfect tailored structure, only a dozen of them have an industrial application, and only those with medium pore sizes. Thermal and mechanical stability are the most concerning issues that limit the use of zeolites in industrial massive scale. In addition, many zeolites have high costs related to synthesis and recovery time and expensive chemical components [19].

The industrial use of zeolites in the petrochemical sector is strongly affected by coke formation over the surface, causing a quick deactivation of the catalyst. Zeolites compete to replace other processes. Many times the original process, free of zeolites, is apparently less

expensive. However, with increased ecological consciousness and more restrictive environmental policies regarding toxic wastes, zeolites look better from the environmental point of view. Regarding coke formation, zeolites produced less than the synthetic silica/alumina catalysts [25].

Zeolites play a role as sieves in a molecular scale, providing a very high selectivity in the final selected product. The molecular sieve property is a result of the regular and controlled structure of the pores and cavities, allowing zeolite synthesis to be tailored a regular and well-known pore size for a specific molecular size. Fig. 1-11 shows the zeolite and the corresponding hydrocarbon dimension and Fig. 1-12 shows the sizes of some hydrocarbons.

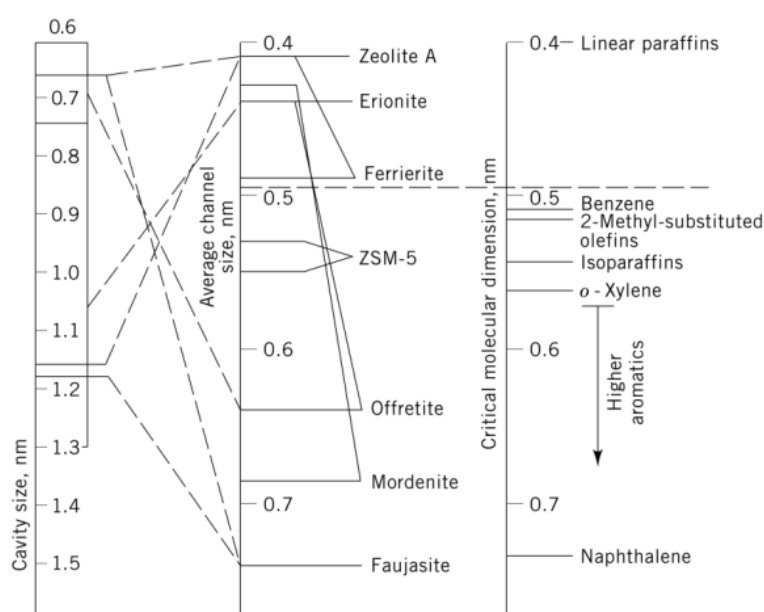


Fig. 1-11 Pore dimensions of zeolites and critical dimensions of hydrocarbons [23]

Hydrocarbon	Size (nm)
<i>n</i> -Paraffins	0.45
Methyl paraffins	0.57
Dimethyl paraffins	0.63
Benzene	0.63
Toluene	0.63
Cyclohexane	0.65
1,2,4-trimethyl benzene	0.69
1,2,4,5-tetramethyl benzene	0.69
1,3,5-trimethyl benzene	0.78
Pentamethyl benzene	0.78

Fig. 1-12 Some examples of hydrocarbon molecular diameter [25]

These regular structures make zeolites an ideal catalyst in terms of ultrahigh selectivity, providing high amounts of the desirable product.

The inclusion of zeolites in the petrochemical industry decreased enormously the production cost of many fuels and refining products. As *Weitkamp* states that “the cost of petroleum refining worldwide would be higher by at least 10 billion US dollars per year, if zeolites were not be available today” [26].

1.7 Alkali promoters in Fischer-Tropsch synthesis

During many decades, there have been promising advances on FTS catalyst providing new developments in activity and selectivity. In addition, innovative ways in the way to obtain syngas, bring exciting and new challenges due to the incorporation of new chemical elements in syngas compositions. Some of these elements are considered as poisons while others have a benefic effect in the FTS selectivity.

Alkali and alkaline earth elements were studied to compare the activity and selectivity among them in FTS, with a blank reference catalyst without any promoter addition. Moreover, important information was found during the inclusion of promoters in the catalyst. The effect of the promoter is strongly linked to the catalyst preparation method during the dispersion; changes in the preparation method also vary the final products despite the promoter amount. Comparing catalyst with the same dispersed amount of promoter results in different CO conversions. Additionally, the sequence of dispersion alters CO conversion.

As a base line, unpromoted catalyst is used to compare CO conversion between the different preparation methods. The results show that dispersed metal and promoter with only one solution demerits the activity instead of sequential dispersed steps of different solutions [27]. Table 1-5 shows the effect of method preparation in the CO conversion.

Table 1-5 Fischer-Tropsch synthesis of hydrocarbons at 200°C and a space velocity of 100 h⁻¹ [27]

Entry	Sample	Conversion of CO, %	Selectivity for CO, mol %				Probability of chain growth α
			CO ₂	C ₁	C ₂ -C ₄	C ₅₊	
1	Co/Al ₂ O ₃	72*	4	12	9	75	0.86
2	Co/Al ₂ O ₃	94	15	29	15	41	0.68
3	(0.01K,Co)	67	1	4	3	92	0.91
4	(Co,0.01K)	59	2	9	8	81	0.84
5	(Co + 0.01K)	41	2	5	2	91	0.85

At a synthesis temperature of 190°C.

The use of promoter in the FTS catalyst increases the C₅₊ hydrocarbons selectivity at expenses of decreasing CO conversion. A positive effect is also the significant decrease of generation of methane [28].

Several promoters were included and tested in the FTS catalyst, either iron or cobalt-based. The promoters that have been already tested are K, Cs, Rb, Na, Li, and Ca; in a wide range compositions from 25 ppm to 20000 ppm. These experiments were performed to quantify the effect of alkalis in the metal dispersion and activity and selectivity of products.

The results of including alkali promoters show clear evidence regarding effect of the different components and concentrations on the final products. The positive effects are the increase of the selectivity of heavy hydrocarbons (C_{5+}) depicted in Fig. 1-13 (a), and the decrease of the methane generation depicted in Fig. 1-13 (b). In contrast the activity decreases and the CO_2 generation increases slightly, as depicted in Fig. 1-13 (c) [6].

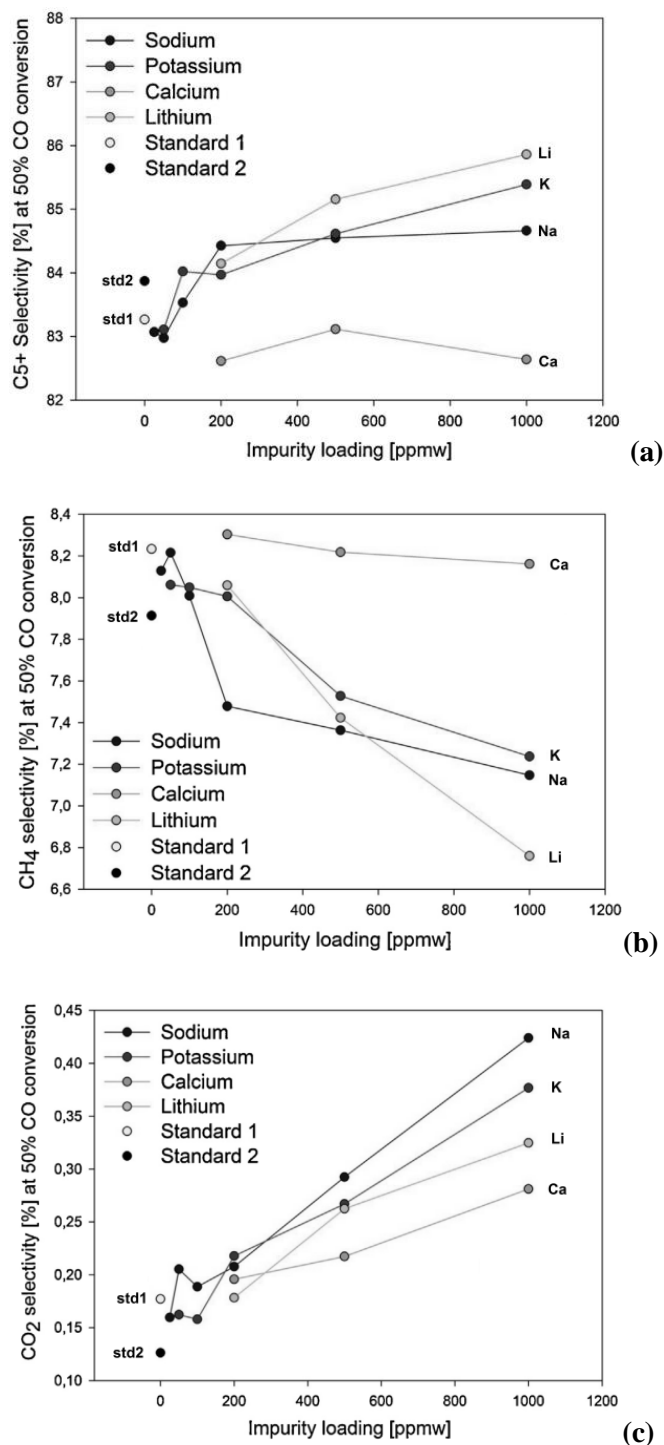


Fig. 1-13 Effect of alkali loading in the selectivity of: heavy hydrocarbons (a), methane (b) and CO_2 (c) [6]

The study of the effect of alkali and alkaline earth components in FTS is relevant because syngas from biomass sources contains a considerable amount of additional compounds that poison the FT catalyst. These compounds are chemical elements of the group I and II of the periodic table, that are considered as impurities contained in the biomass syngas produced via gasification [6] [29].

In general, cobalt-based FTS catalysts are more sensitive to promoters such as alkalis, than iron-based catalyst. The alkali addition in the FTS catalyst decreases the active metal surface resulting in a positive and negative effect because selectivity increases but at expense of CO conversion. Other positive effect at molecular scale is that promoters influence the CO bond strength and enhance the insertion properties of CO. Alkalis increase the olefin and oxygenate production, in the iron-based catalyst, enhancing the water gas shift reaction [30].

Among all alkali compounds that have been tested the one with strong negative effects in FTS is the sodium element. The consequences of using Na as a FTS catalyst promoter are: decline of the catalyst activity and increase of the CO₂ selectivity [29]. These two effects are opposite to the general objective of catalyst improvements, which is to increase *activity* to maximize production rates and *selectivity* to promote the desirable products.

A remarkable fact to clarify, based on an experiment performed by *Khodakov et al.* is the effect of ions as a solution. They tested the FTS performance with the injection into the reactor of water solution containing Na, K, or Cl ions as a poison together with the syngas stream. The general performance of FTS did not represent any significant changes in the activity or selectivity for FTS iron-based catalyst, but the direct dispersion of some of this elements during the catalyst preparation did [31].

1.8 Bifunctional Fischer-Tropsch zeolite catalyst

Zeolites are the ideal candidate to use as a bifunctional catalyst due to the possibility of controlling pore sizes, metal distribution and strength of the acidity. The engineered design of zeolites allows manipulating the zeolite structure in order to control the final products. In the future, zeolites could control complex reactions as shown in Fig. 1-14 to select the final chemical product as closed ring or completely open ring.

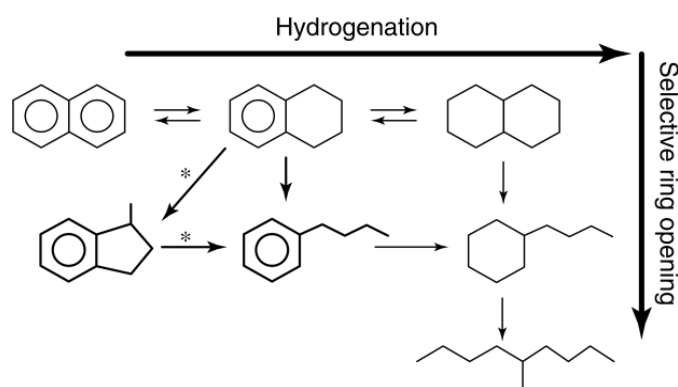


Fig. 1-14 Possible pathways for naphthalene hydrogenation [20]

Zeolites are used as bifunctional catalyst due to their intrinsic Brønsted acidity for different applications. Table 1-6 shows how the use of zeolites as bifunctional catalyst increases the acidic function of the support. Some processes that use bifunctional catalyst are hydrocracking of heavy naphtha, catalytic reforming of naphtha, alkylation of isoparaffins and CO hydrogenation to mention a few regular industrial applications today [23] [20].

Table 1-6 Bifunctional hydrocracking catalysts [20]

	Hydrogenation function	Acidic function (support)	
Increasing	↓ Ni/Mo	Al ₂ O ₃	↓ Increasing
Hydrogenation Power	Ni/W Pt/Pd	Al ₂ O ₃ /halogen SiO ₂ /Al ₂ O ₃ Zeolites	Acidity
	(low-S conditions)		

A specific example of the bifunctionality property of zeolites is gasoline octane enhancement by changing linear hydrocarbons into branched ones. This occurs via isomerization of linear alkanes over acid sites. Typically, the bifunctional catalysts for the platforming process include Pt supported on alumina-zeolite [17].

Including zeolite in FTS iron-based catalyst improves selectivity against gasoline range products (Fig. 1-15). Zeolites increase the aromatic content of the FTS products. The natural cracking property of some zeolites and well defined structure limits the molecular length of the hydrocarbons.

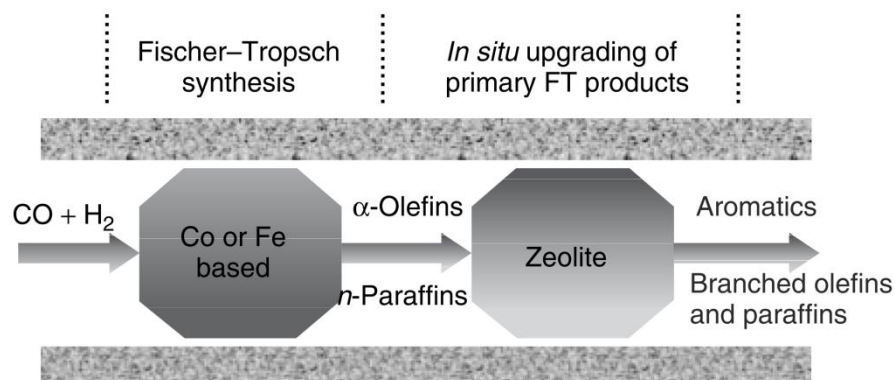


Fig. 1-15 Schematic representation for the in situ up-grading of primary FTS products into high-octane gasoline components [20]

The limitation of the use of zeolites in FTS under gasoline production process conditions is the rapid formation of carbon (coking) over the acid sites and pores (Fig. 1-16), resulting in a decrement of the zeolite acidity (Fig. 1-17). The loss of acid sites impacts directly in the aromatic selectivity; olefins are not converted to aromatic compounds. Moreover, the alkali promoters used in the FTS catalyst migrate to the acid sites [32].

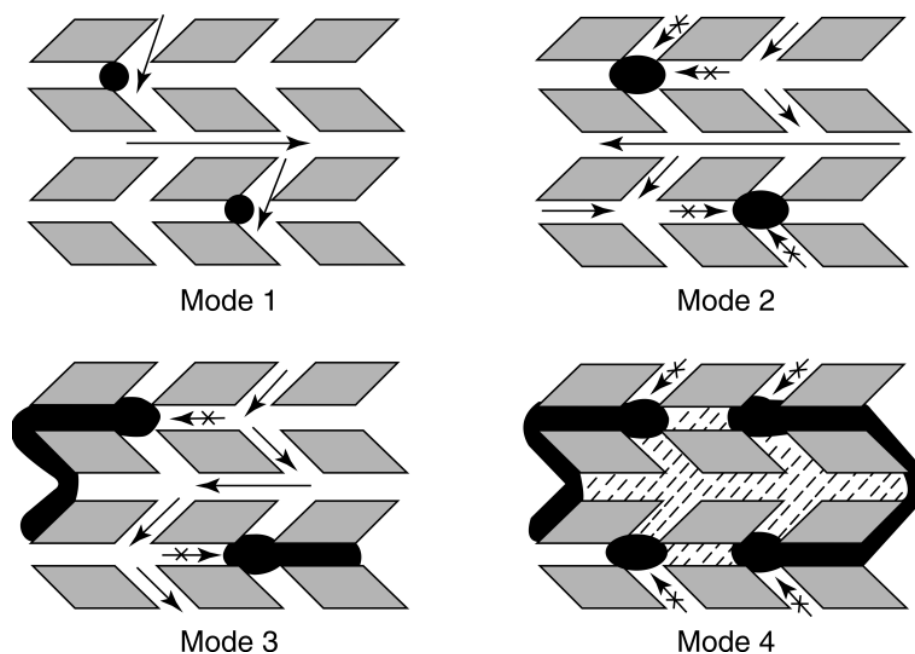


Fig. 1-16 Different modes of deactivation by carbonaceous deposits in zeolites [23]

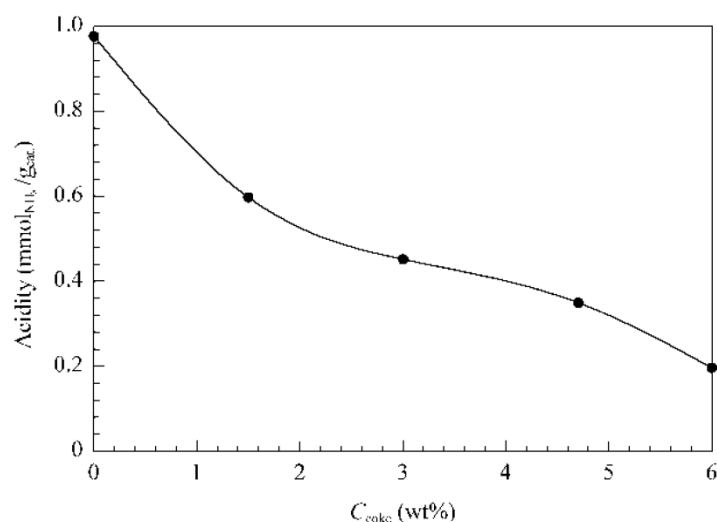


Fig. 1-17 Relationship between total catalyst acidity and deposited coke content
[32]

Advances in synthesis techniques of catalyst preparation include structures known as core-shell structure, where the core is one component and the shell is another different component. This method of preparation was applied to FTS catalyst to obtain a catalyst with a core of cobalt-based catalyst supported in alumina with zeolite shell formed via hydrothermal synthesis [20]. Fig. 1-18 represents core and shell structure of FTS zeolite catalyst.

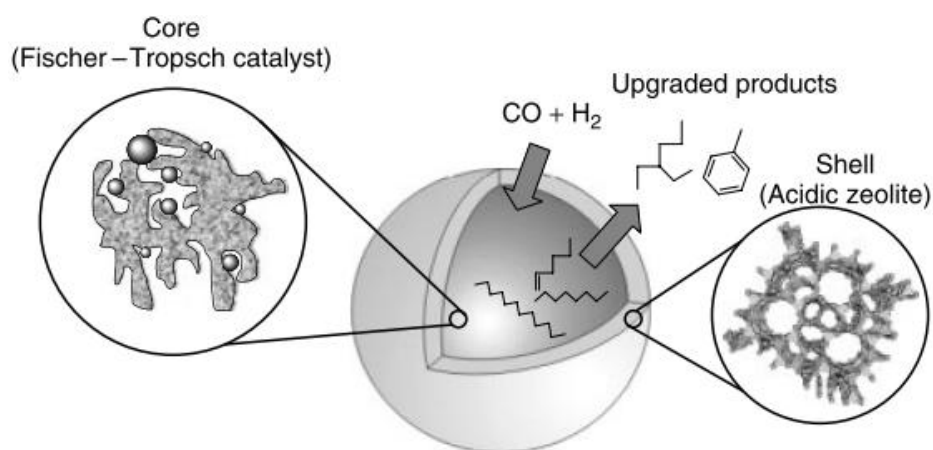
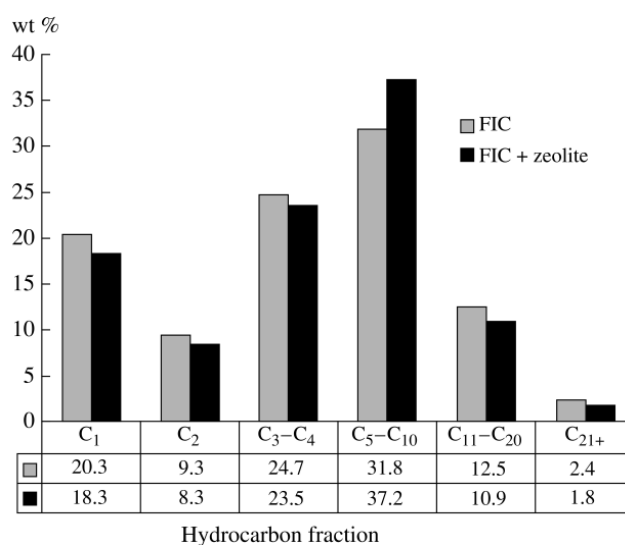


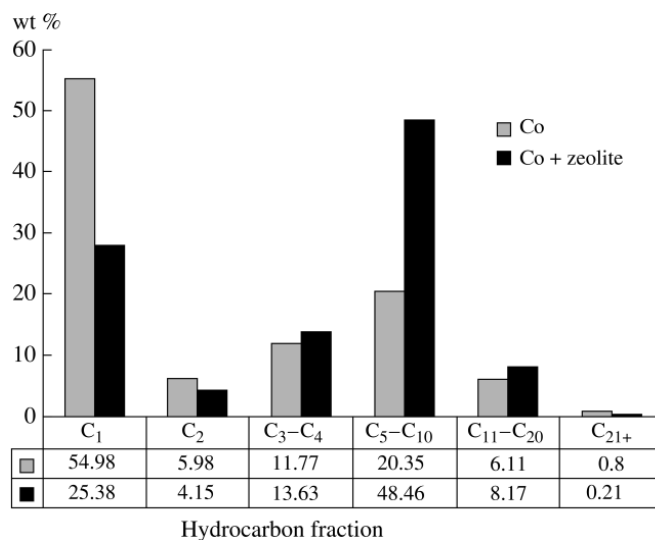
Fig. 1-18 Schematic representation of a core-shell hybrid FT-acid catalyst configuration [20]

During the FTS reaction, the hydrocarbon chains form in the core cobalt-based catalyst. Before leaving the particle, the long chains pass through the zeolite shell where the acid sites transform the linear products in branching and lighter products compared to the standard FTS catalyst cobalt-based.

Another outstanding application of zeolites is to use them as diluents of active FTS cobalt-based catalyst to avoid hot spots in the reactor and control the temperature gradient along the reactor. The introduction of zeolites as diluents in the reactor contributes in terms of selectivity of the products due to their natural acid behavior. A benefit of using zeolites is the balance of heat, the thermodynamic effects of exothermic FTS with the endothermic zeolite reaction in a single process, improving stability, selectivity and activity [33]. These were tested in both iron-based and cobalt-based catalysts. Fig. 1-19 (a) and (b) shows the contribution in selectivity using zeolites as diluents for FTS catalyst.



(a) Iron-based catalyst



(b) Cobalt-based catalyst

Fig. 1-19 Fractional distribution of hydrocarbons for Fischer-Tropsch iron-based and cobalt-based catalysts [33]

Vytnova *et al* report the decanted water composition of FTS using different catalyst and zeolites as diluents. The effect of zeolites was the decrease of alcohols, acetone and hydrocarbons. The best result was in the cobalt-based catalyst diluted zeolite as shown in Table 1-7.

Table 1-7 Composition decanted water of FTS [33]

Run no.	Catalyst	T, °C	x _{CO} , %	Amount in reaction water, wt %				
				methanol	ethanol	acetone	C ₃₊	Σ
1	FIC ₁	245–269	52	1.55	9.0	0.4	3.73	14.68
2	FIC ₁	260–293	75	0.99	8.68	0.56	3.2	13.43
3	FIC ₁ + zeolite	230	74	0.7	1.81	0.22	0.53	3.26
4	FIC ₂	290	80	1.33	6.08	0.8	4.2	12.41
5	FIC ₂ + Al ₂ O ₃	270–275	84	0.49	4.48	0.8	3.12	8.89
6	FIC ₂ + zeolite	280	98	0.49	1.88	0.56	0.79	3.72
7	FIC ₃	294–320	89	0.87	3.07	0.88	1.54	6.36
8	FIC ₃ + zeolite	270	98	0.32	0.36	0.34	0.19	1.21
9	FIC ₃ + zeolite	261	98	0.34	0.32	0.32	0.08	1.06
10	Co catalyst*	203–234	96	0.32	0.5	0.02	0.5	1.34
11	Co catalyst + zeolite two-component	206–241	72	0.11	0.05	0.03	0.11	0.3
12	Co catalyst + zeolite one-component	206–207	91	0.33	0.14	none	0.01	0.5

1.9 Mass and heat transfer limitations in bifunctional zeolite/Fischer-Tropsch catalysts.

The relevant fact that must be taken under consideration using zeolites as bifunctional catalyst is mass and heat transfer limitations due to internal or external diffusion problems.

In general terms, zeolites are excellent materials due to their intrinsically well-defined structure. This property confers zeolites high selectivity of chemical reactions, because geometrical limitations in the zeolite pores and structure. Zeolites offering three different selectivity mechanisms as depicted in Fig. 1-20.

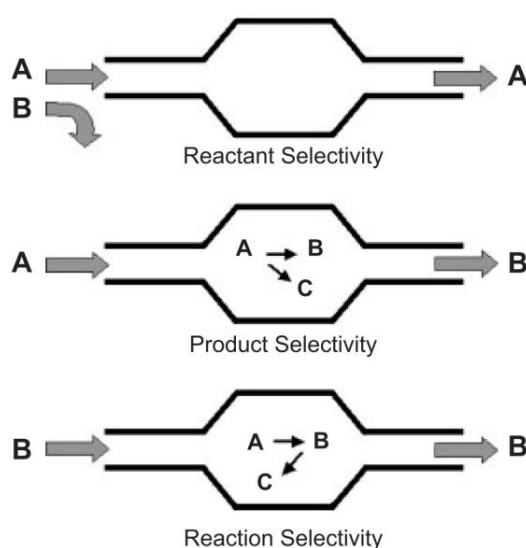


Fig. 1-20 Examples of how zeolites can be used to increase selectivity for a reaction [34]

The zeolite selectivity mechanisms are:

- *Reactant selectivity:* avoiding bulky reactants from entering the active sites to react.
- *Product selectivity:* promoting the formation of desirable products.
- *Transition state or reaction selectivity:* prohibiting the transition products because narrow pores and caves inside the catalyst. [34]

The well define structures in zeolites that helps to control selectivity of reactants or products cause also mass and heat transfer limitations, because the narrow pores and cages limiting. The diffusion limitations in zeolites are important, because to accomplish the reaction steps, reactants need to reach the active sites in catalyst and leave the same active site as product (Fig. 1-21).

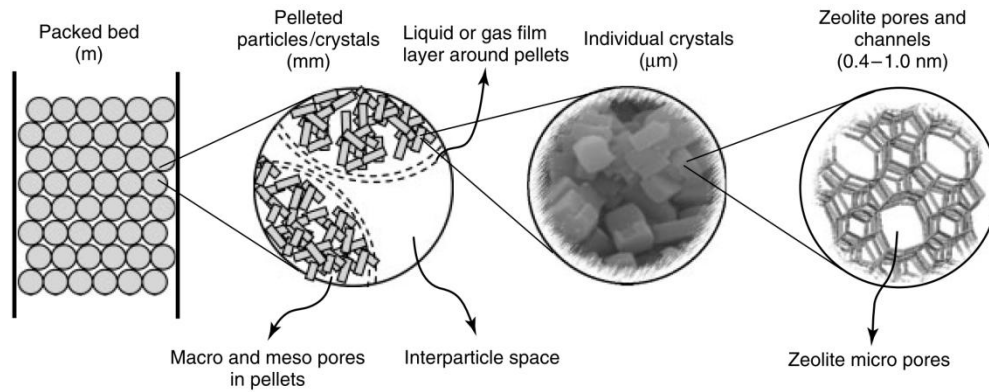


Fig. 1-21 The reactant pathway from bulk to active site encompasses diffusion processes on a broad length scale in common catalytic processes [20]

In a catalytic reaction, the reactant molecule reaches the catalyst surface in sequential steps [35]:

- Transportation of the reactant molecules from the bulk phase to the catalyst surface.
- Diffusion of the reactant molecules in the catalyst pores.
- Adsorption of the reactants.
- Reaction over the surface of the catalyst.
- Desorption of products from the surface to the pore system.
- Diffusion of products out of the pore system.
- Transportation of products from the catalyst surface to the bulk phase.

Interphase gradients originate diffusion and convection. Intraphase gradients occurred inside the pores in the active site, consequently pore diffusion come at the same time of the reaction (Fig. 1-22).

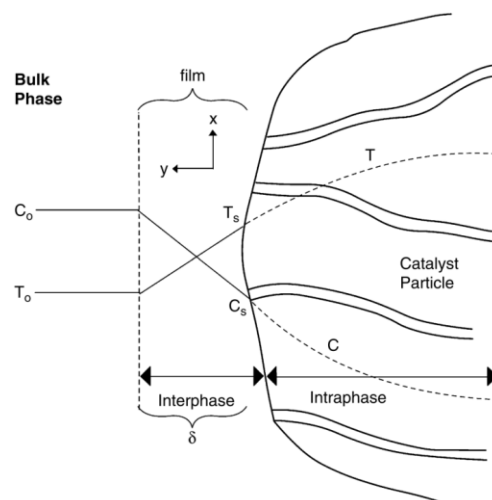


Fig. 1-22 Concentration and temperature changes from the bulk phase through a stagnant film of thickness δ to a particle surface and then through the porous catalyst particle, assuming an exothermic reaction occurs [35]

In the standard catalyst, commonly the pore size is designed in the macropores range ($d_{\text{pore}} > 50 \text{ nm}$) to minimize the heat and mass transfer limitations. In terms of handling the catalyst in the reactors and avoiding losses, the small particles (powder) are pelletized in big agglomerates called pellets (Fig. 1-23). This pelletizing process is also performed in zeolite crystals (powder) creating big agglomerates that are easy to handle but the pore size remain in the mesopores ($2 < d_{\text{pore}} < 50 \text{ nm}$) or even in the worst case in terms of mass and heat transfer limitations in the micropores range ($d_{\text{pore}} < 2 \text{ nm}$) [20].

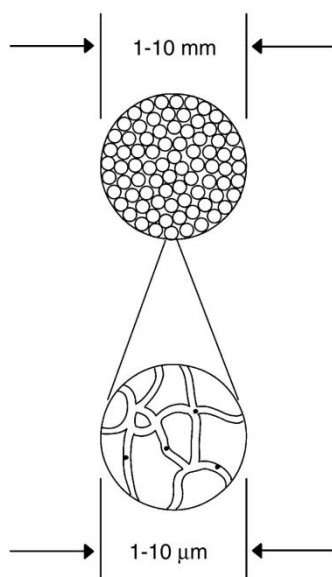


Fig. 1-23 Schematic representation of a typical catalyst pellet comprised of small porous particles [35]

The mass and heat transfer limitations could be split in two different types, one related with the external surroundings of the particle like a film layer and the other one related with the internal structure of the particle like the size or path configuration of the internal cages and size or tortuosity of the pores in the catalyst. In addition, the pelletized particles are agglomerates that have deficient heat transfer properties.

Because zeolites possess very small pore size, internal diffusion limitations are a predominant issue to take in account when zeolites are combined with a common catalyst to create bifunctional catalysts. Diffusion in micropores structures is different from mesopores and macropores materials. There are successful industrial applications of zeolites despite of slow transport and diffusion limitations increase the selectivity of the process against desirable products [34].

1.10 Jet fuel background

Jet fuel is an aviation turbine fuel that is strictly regulated in the aromatic content. These regulations obey the fact that the aromatics components affect the combustion via soot formation, causing turbine damage. The maximum allowable content is up to 25 vol% and less than 3 vol% naphthalenes. Jet fuel could be produced via FTS but the aromatic content specifications are even more stringent allowing a content range 8-22 vol% [3].

Today a clean fuel is measured in terms of sulfur content. For jet fuel, it is a critical parameter to keep as low as possible because during combustion sulfur oxides are formed in the turbine. These oxides are corrosive to the metal parts in the turbine body. The specification of sulfur content in jet fuel from conventional oil extraction varies between 0.3 to 0.4 wt%. The FTS process offers ultralow sulfur content products with a range 0.01 to 0.0001 wt%; this range is based on the supplier technology [3].

The rest of the hydrocarbon components in the fuel mixture is not completely regulated as a composition parameter. It is indirectly established with the thermal stability requirements for low temperature conditions during high altitude. For example, for Jet A-1 fuel the freezing point specification is -47°C and for Jet A is -40°C . These values ensure that the fuel is still liquid to move in the internal fuel system in the aircraft. The difference between freezing point temperatures in jet fuels is based on the duration of flights: short distance flights allow slightly high freezing point compared to long distance flights that demand lower freezing points [36]. Table 1-8 shows a comparison between different kinds of jet fuels from different industrial competitors.

Table 1-8 Synthetic jet fuels of LTFT syncrude from the Sasol (SSPD) and Syntroleum (S-5) processes [3]

Property	Synthetic		Semi-synthetic		Specifications	
	SSPD	S-5	SSPD/Merox ^a	SSPD/DHC ^b	Jet A-1	JP-5
Density at 15 °C (kg m ⁻³)	747	764	776	784	775–840	788–845
Flash point (°C)	45	64	48	53	<38	<60
Freezing point (°C)	-48	-51	-51	-50	<-47	<-46
Viscosity at -20 °C (mPa s)	4.2	6.1	4.4	4.6	<8.0	<8.5
Smoke point (mm)	>50	>43	36	37	>25	>19
Net combustion heat (MJ kg ⁻¹)	44.1	44.1	–	–	>42.8	>42.6
<i>Composition</i>						
Aromatics (vol.%)	0	0.4	9.9	6.5	8–25	<25
Sulfur (mass%)	<0.01	<0.0001	0.07	<0.01	<0.3	<0.4
Thiol content (mass%)	0.0002	<0.0001	0.0004	0.0003	<0.003	<0.002
Acidity (mg KOH g ⁻¹)	0.009	0.0014	0.009	0.01	<0.015	<0.015
<i>Distillation (°C)</i>						
IBP	154	183	152	156		Report ^c
T10	168	194	169	179	<205	<206
FBP	267	267	267	278	<300	Report ^c

^aBlend of SSPD material and Merox-sweetened crude oil-derived kerosene in a 1:1 ratio.

^bBlend of SSPD material and crude oil-derived kerosene from distillate hydrocracking (DHC) in a 1:1 ratio.

^cValue must be stated on the jet fuel analysis, but the value is not subject to regulation.

Further information about specific requirements of jet fuels is deeply detailed in the ASME standards. Jet fuel from conventional sources is regulated by ASME standard D1655-13 “*Standard Specification for Aviation Turbine Fuels*”, and for unconventional sources as synthetic fuels applies ASME standard D7566-13 “*Standard Specification for Aviation Turbine Fuel Containing Synthesized Hydrocarbons*” [36] [37].

Despite that FTS products are easy to refine in jet fuel, a rigorous testing program has to be performed in order to qualify the material from synthetic fuels. In addition to these testing programs the pathway must be approved. The complete acceptance of jet fuel from synthetic sources is not completely clear nowadays because it is still under development to improve every single characteristic of the actual jet fuels.

Promising and challenging studies are being conducted to improve the performance of jet fuel from synthetic sources. The use of zeolites shows an enhancement in the fuel reformation for jet fuel according to *Lee, I. C.* [38].

FTS has high selectivity for methane (C_1) and hard waxes (C_{35}). Process conditions determine the end product (preferably hard waxes). This must be cracked and distilled to obtain gasoline (C_5 - C_{12}), jet fuel (C_{11} - C_{13}), and diesel (C_{13} - C_{17}).

2. Methods

Hydrothermal zeolite synthesis that changes the amorphous phases into crystal phases after nucleation via heat, pressure and change of chemical structure was employed for the synthesis.

The methods used to characterize the zeolite were Brunauer-Emmett-Teller (BET) to measure the available surface area, X-ray powder diffraction (XRD) to match the composition with the recipe, hydrogen Chemisorption to measure the metal distribution over the catalyst surface, and scanning electron microscope (SEM) to see in detail the microstructure of the crystal micrograins.

2.1 Zeolite/FT catalyst synthesis

Zeolites/FT catalyst were prepared via hydrothermal synthesis. Several steps are involved in order to obtain the right zeolite structure. The procedure to estimate the amounts of each component in the zeolite structure during the preparation of the solution of gel is called *recipe*. Every zeolite is associated with a specific structure but there are several recipes to obtain it. These different recipes include different components; the important aspect of the recipe is the final structure product, this means the calculated ratio between aluminum and silica and the adequate pore size and crystal structure. **Appendix A** contains a reference of syntheses for different zeolite materials.

It was decided to work with beta zeolite because its structure possesses large pores that offer less resistance to the mass and heat transfer limitations resulting in high selectivity in the direction of jet fuel products.

Different catalysts were produced varying the reaction procedure, reactants and reaction steps. Detailed description of every technique will be provided in the next sections of this chapter. The procedures were:

- Standard hydrothermal synthesis.
- Seed-assisted β -zeolite followed by standard hydrothermal synthesis.
- Seed-assisted FT catalyst followed by standard hydrothermal synthesis.
- Pretreated FT catalyst with TEA-OH followed by standard hydrothermal synthesis.

Different procedures were proposed to investigate the effects of the final coated catalyst on the Fischer Tropsch synthesis products distribution and activity.

2.1.1 Chemical components

The main components involved in the hydrothermal zeolite/FT catalyst synthesis are a source of aluminum and silica, an organic molecule as a template, and water under highly alkaline conditions with temperatures typically between 100-160°C, at equilibrium pressure conditions.

For the catalyst/zeolites and zeolites synthesis the following materials were used to obtain the specific structure and reaction conditions. It was decided to divide the chemical reactants in two groups. Liquid components, such as water and template, are listed in Table 2-1. Solid components such as silicon oxides, alumina oxide, and Fischer Tropsch catalyst, are listed in Table 2-2.

Table 2-1 Chemical liquid zeolite components A

	Material	Chemical name	CAS Number
Solvent	Water	Distillate water [39]	7732-18-5
Template	40% TEA-OH 60% H ₂ O	Tetraethyl ammonium hydroxide (for hydrothermal synthesis)	77-98-5
	20% TEA-OH 80% H ₂ O	Tetraethyl ammonium hydroxide (for TEA-OH pretreatment)	77-98-5

Table 2-2 Chemical solid zeolite components B

	Material	Chemical name	CAS Number
Silica Source	40 wt% SiO ₂	Colloidal silica suspension	7631-86-9
	60 wt% H ₂ O	(LUDOX® HS-40)	
	SiO ₂	Fumed Silica powder, 0.007µm	112945-52-5
	Si(OC ₂ H ₅) ₄	Tetraethyl orthosilicate 99.0 vol% (TEOS)	78-10-4
	Si(OC ₂ H ₅) ₄	Tetraethyl orthosilicate 99.999 vol% (TEOS)	78-10-4
Aluminum source	γ-Al ₂ O ₃	Aluminum oxide gamma phase	1344-28-1
	12 wt% Co		-----
FT catalyst	0.3 wt% Re Balanced Al ₂ O ₃	Fischer-Tropsch cobalt-based catalyst	

The Fischer-Tropsch catalyst and γ -alumina materials were provided by Statoil Research Center in Rotvoll. The γ -alumina material is a modified structure with wide pores that belongs to the PURALOX® family commercialized by Sasol with a surface area of 190 m²/g. The FT catalyst has a chemical composition of 12 wt% of cobalt with 0.3 wt% of rhenium as a reduction promoter, both components are supported in modified γ -alumina. This catalyst sample is not a commercial FT catalyst, it is a material under development. The provided catalyst was a regular microspheres without sieving.

In addition, absolute ethanol was employed to soak the Fischer-Tropsch catalyst during TEA-OH procedure (section 2.1.4).

The additional material used during this test is shown in Table 2-3.

Table 2-3 Additional chemical components

	Material	Chemical name	CAS Number
Solvent	C ₂ H ₆ O	Absolute Ethanol, 100%	64-17-5

2.1.2 Synthesis and treatment equipments

To perform all zeolite/FT catalyst syntheses, autoclave equipments played an important role during the zeolite/FT catalyst synthesis. Hydrothermal conditions must prevail during the crystallization. Using an autoclave allows these conditions, supporting an environment in which high temperature is developed at the correspondent equilibrium pressure.

Parr autoclave Mini Bench Top Reactors 4560 was employed to develop all the zeolite/FT catalyst synthesis. The apparatus was equipped with a metal reactor with a MAOP of 70 barg, Teflon liner to guaranty high resistance to the chemical attack, variable speed propeller to control the agitation speed, heat mantle to heat up the reactor, temperature controller to set the reaction temperature, gauge manometer to measure the pressure along the reaction, rupture disc as safety device. Fig. 2-1 illustrates the external components of the Parr equipment.



Fig. 2-1 Parr Autoclave, Series 4560 Mini Reactors, 100-600 mL with Modular Controller model 4848 [40]

The internal autoclave components are shown in Fig. 2-2.

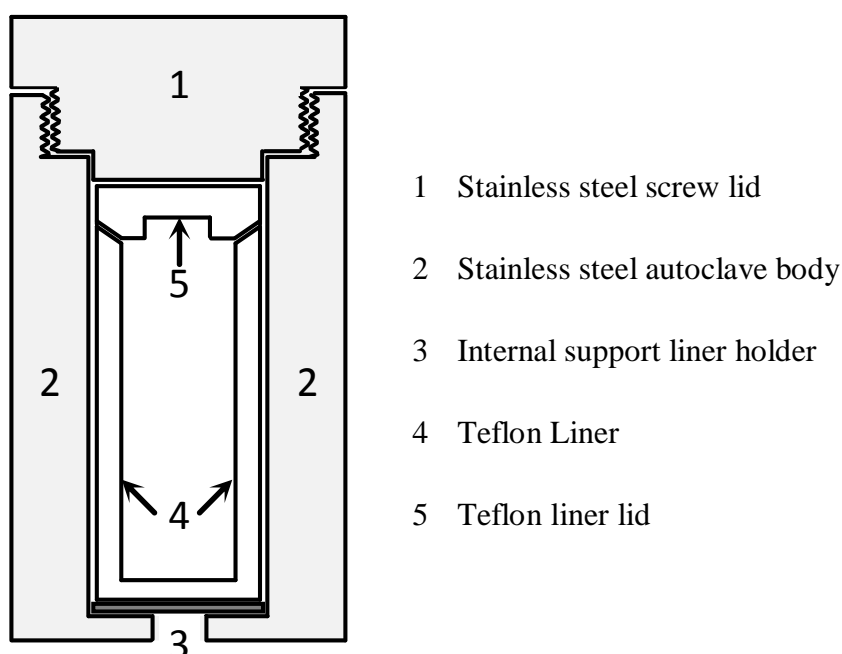


Fig. 2-2 General autoclave configuration, internal view of the main components

After the synthesis period, commonly three days, the product was recovered and washed by centrifugation. A centrifuge with 10000 rpm was used to sediment zeolites/FT catalyst, the amount of water used to washed was 0.25 l per sample.

The product was recovered by centrifugation. It was placed in a ceramic crucible to be dried and calcined. A stagnant oven with temperature program steps was employed to dry and calcined the samples.

After drying and prior to calcination, the zeolite/FT catalyst was crushed and grounded with a mortar and pestle until an uniform powder free of agglomerates or flakes was obtained. This step allows uniform heating and easy release of the template from the internal caves and pores of the zeolite of the sample during calcination. In the case of catalysts that contained zeolite/FT catalyst this step was performed carefully to avoid damaging in the micro spherical particles of the Fischer Tropsch catalyst.

The calcination was performed using an electrical muffle furnace with a sequence temperature program; the sample was carried in a crucible.

2.1.3 Synthesis and treatment conditions

Syntheses were performed using autoclave equipment. It was set with hydrothermal process conditions of 155°C and 150 rpm at equilibrium pressure of the mixed components around 6 barg. Detailed description of every procedure will be provided in the next sections of this chapter.

The synthesis process takes three to four days based on the selected synthesis procedure and the final process conditions remain the same despite the pressure that increases until 12-14 barg. The pressure raise is common during beta zeolite synthesis as is shown in Fig. 2-3, this increase is consequence of template decomposition via the Hoffman elimination reaction generates ethylene and triethylamine [41].

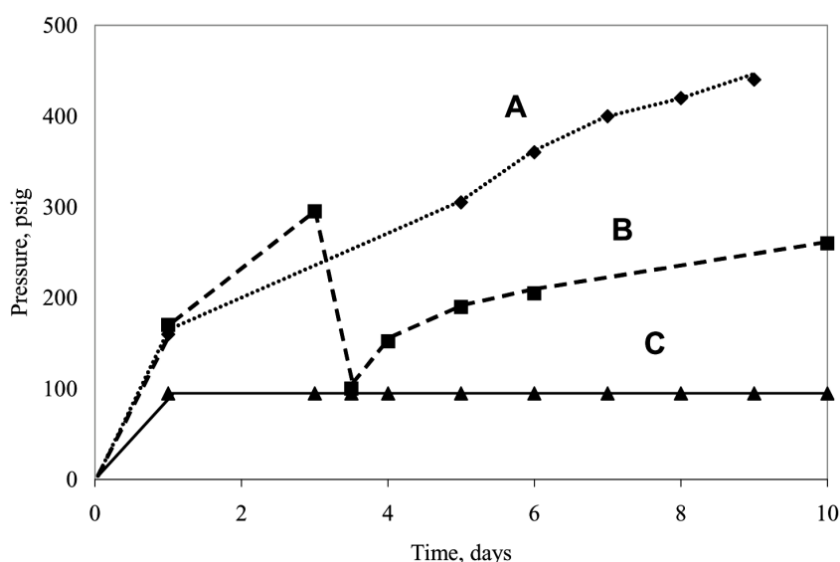


Fig. 2-3 Plot of pressure vs. time during nano BEA synthesis for an (A) unvented reactor, (B) a reactor [41]

Centrifugation was set at 10000 rpm during 10 minutes. At least every centrifugation sampler holder was centrifuged 5 to 6 times.

Drying step was performed from room temperature to 80°C for 8 hours. The heat rate was set as 5°C/min. During drying, the heat rate is not an important factor as it is in calcination but it is important to keep the temperature below 100°C to avoid steam generation that could damage the zeolite structure due to the water abundance and fast release from the zeolite particles.

During calcination, the first step was to remove traces of remaining water, with a ramp of constant heat of 5°C/min, the temperature range was from 80°C to 100°C. Once the set point was reached, the temperature was kept for three hours. Afterwards the temperature was increased from 100°C to 550 °C, with a ramp of 2 °C/min and kept at 550°C for eight hours. The temperature guarantees the complete decomposition and remotion of the organic template. During this time changes of color occurred over the catalyst, but at the end, the final color of the catalyst particle is the same as the beginning. The change of color is because during calcination the organic template in the zeolite was decomposed. Then the final step was to cool from 550 to 30°C with a ramp of 3°C/min.

2.1.4 Synthesis and treatment procedures

Prior to running hydrothermal synthesis, Risk Assessment was performed to assure the safety conditions during the operation hours of the Parr autoclave. **Appendix B** contains relevant information about operational risks of Parr autoclave used to perform hydrothermal syntheses and the safety barriers.

For the present work two different materials were prepared. The first ones that contain only β -zeolite and the second ones that contain β -zeolite and Fischer-Tropsch cobalt-based catalyst. All products were prepared under the same reaction conditions. Different procedures were employed to synthesize the different products. The four procedures are the following.

- **Procedure 1:** Standard hydrothermal synthesis

It was decided to call “standard hydrothermal synthesis” the general procedure that is involved in the full set of synthesized materials.

Zeolite synthesis involves a procedure called recipe. The main parts described in a recipe are: type of material, batch composition, source materials, batch preparation including amounts of each component, temperature conditions, synthesis time, recovery steps of the zeolite, and the expected results in the product characterization.

Reliable recipe sources are papers and books as the compendium of recipes published by the Synthesis Commission of the IZA called “*Verified Syntheses of Zeolitic Materials*” [39]. The used recipe for the pure β -zeolite and β -zeolite/FT catalyst was provided by Statoil Research Center. The amount of the added Fischer Tropsch catalyst vary from 16.5 to 90 grams.

The general steps to perform a pure β -zeolite and β -zeolite/FT catalyst synthesis are listed below:

The first step to synthesize a zeolite is to follow exactly the recipe and kept a strict respect of the amounts of each component. The amounts determine the final ratio composition in the zeolite structure. The main components for a pure β -zeolite are: a source of silica oxide (SiO_2), a source of aluminum oxide (Al_2O_3), a source of template (TEA-OH), and water (H_2O). For β -zeolite/FT catalyst are: the same components as pure β -zeolite and in addition the Fischer-Tropsch cobalt-based catalyst.

The second step is to mix all reactants in the Teflon liner. It is important to follow the right sequence to avoid agglomerates in the final solution. In the case of basic solutions it is good practice to dissolve the solids in water first, before the addition of the silica source. After the preparation of the solid-water solution and the addition of the silica source, it is relevant to stir, as much as possible to avoid flocks formation. Based on the recipe and the water content in the recipe, often the final mix of reactants looks like a very viscous whitish liquid. It is important to mix well all components, to get the same composition in the complete solution.

The Fischer-Tropsch cobalt-based catalyst was the most heavy component in the recipes. It was decided to add it as the final reactant after 1h of intense agitation to obtain complete homogenization of the rest of the components. The color of the solution changes from white to black.

The third step is the hydrothermal synthesis process in which the zeolite structure is formed. Typical syntheses crystallize between room temperature up to 200°C under autoclave equilibrium pressure; the required time ranges from hours to days. The used synthesis conditions are mentioned in the *Synthesis and treatment conditions* section. Temperature and agitation speed were set in the Parr autoclave controller.

The fourth step is autoclave cooling. When the reaction was considered as finished, the autoclave heat source was turned off. Once the heating source is turned off the reactor starts to cool down slowly. To avoid damages in the Teflon liner the heating mantle was kept during 30 min, subsequently the mantle was removed and the reactor was cooling down by natural convection, the entire process took around 2h.

The fifth step is recovery. Once cooled the sample at room temperature, there is a standard procedure followed to recover the zeolites. The solid and liquid components of the Teflon liner were transferred to centrifugation-sealed vessels to remove the water excess and the organic material. After centrifugation, the washing procedure to remove the mother liquor starts. The catalyst was washed with 0.25 l of distilled water. It is crucial not to wash in excess because it is possible that the pH varies too much in the zeolite and the flocks deagglomerate. Some of the hydrothermal products are spontaneously split in two phases identified as “black” and “white” at the end of the reaction in the Teflon liner. In this particular case, the products are washed separately to keep the composition of the original final products from the reaction.

The sixth step is drying. After the last wash, the zeolite contains large amounts of water trapped in the intraparticle structure. A crucible was used to recover and dry the hydrothermal product. This procedure was performed to remove the water retained over the β -zeolite and β -zeolite/FT catalyst surfaces. The used treatment conditions are mentioned in *Synthesis and treatment conditions* section. Black and white products are carried in individual crucibles and the drying step was performed separately.

The seventh step is calcination. Before calcination the β -zeolite was crushed and grounded with a mortar and pestle until, obtaining a uniform white powder free of agglomerates or flakes. In the case of the hydrothermal synthesis products that include β -zeolite/FT catalyst special attention is paid during the crushing because the particles of the provided Fischer-Tropsch cobalt-based catalyst were already microspheres that could be damaged if the crushing had been too intense. Calcination was performed to remove the template from the β -zeolite and β -zeolite/FT catalyst structure.

The calcination procedure for β -zeolite and β -zeolite/FT catalyst has several of steps, which are listed below:

1. The first step of the calcination is to remove completely any trace of water from the surface material but also from the internal pores. With a programmed sequence, the crucible that contains the zeolite sample was heated from 80 up to 100 °C, with a ramp of 5°C/min and kept at 100°C for 3 h.
2. Three hours elapsed; the temperature was increased from 100°C to 550 °C with a ramp of 2°C/min, and kept at 550°C for 8 h. High temperature guarantees the complete decomposition and remotion of the organic template. It is crucial heating up with a regular slow step size sequence as a ramp, the sudden increasing of heat destroy the internal structure of the zeolite due to the very fast expansion and evaporation of the water and the template.

A quick visual effect of wrong heating ramp procedure is if the resulting powder after calcination is finer than the initial one because of the destruction of the pores and cavities in the zeolite structure.

During this time, changes of powder color occurred over the pure β -zeolite and β -zeolite/FT catalyst due to decomposition of the organic compound. The initial color of the pure β -zeolite powder was white, during calcination the color changes gradually from

light color to dark and from dark to light again. The color of the β -zeolite/FT catalyst was dark gray and remains almost unchanged during the calcination.

In β -zeolite the initial change of color occurred at 250°C a light beige color was in the zeolite, at 300°C a yellow color was present, at 350°C a light brown, at 400°C a dark brown was observed. The colors were the decomposition of the organic material in the zeolite. After eight hours elapsed, the color of the powder returned to white.

3. Once accomplished the removal of the template from the β -zeolite and β -zeolite/FT catalyst structure, the muffle furnace was cooled down to 30°C with a ramp of 3°C/min. The ramp sequence is not compulsory during the cooling step because the muffle furnace remains hot for a long period, but it is a good practice to perform it as a normal procedure. The sudden cooling from 550°C to ambient temperature in a short period could lead to the damage the zeolite structure due to stress contracting forces.

The already calcined β -zeolite and β -zeolite/FT catalyst samples were collected in wide mouth glass bottles with plastic lid, labeled with a sequential sample number and stored for further characterization.

- **Procedure 2:** Seed-assisted β -zeolite/FT catalyst followed by standard hydrothermal synthesis.

The seed-assisted procedure was a pre-step to prepare a precursor of the further hydrothermal synthesis. The seed was prepared with a short time, around 24h, via hydrothermal synthesis process to obtain a seed gel. Process conditions were: temperature of 100°C at equilibrium pressure with agitation speed of 150 rpm. This gel contains very small crystals that were used as a nucleating material in the β -zeolite/FT catalyst synthesis.

Seed-assisted hydrothermal synthesis also follows a recipe but the composition was slightly different than the one used in the standard hydrothermal synthesis. The main components for a β -zeolite seed are: a source of silica oxide (SiO_2), a source of aluminum oxide (Al_2O_3), a source of template (TEA-OH), and water (H_2O).

The resulting seed gel was utilized to prepare the β -zeolite/FT catalyst via standard hydrothermal synthesis described in **Procedure 1**. The amounts of silica oxide, template, and water was included in the final recipe to balance all the components and kept the same

molar composition of the non seed-assisted synthesized materials. The rest of the reactants to equalize the molar composition were added after seed-assisted synthesis and prior to the standard hydrothermal synthesis. To the obtained seeding solution the added components were: source of silica oxide (SiO_2), Fischer Tropsch catalyst and water (H_2O).

For the pure β -zeolite synthesis the procedure that was followed is **Procedure 1**.

- **Procedure 3:** Seed-assisted FT catalyst followed by standard hydrothermal synthesis.

The modified seed-assisted FT catalyst procedure is similar to the **Procedure 2**. The singular difference is the Fisher Tropsch catalyst was added from the beginning during seed assisted hydrothermal synthesis. The main components for a β -zeolite/FT catalyst seed are: a source of silica oxide (SiO_2), a source of aluminum oxide (Al_2O_3), a source of template (TEA-OH), Fischer-Tropsch cobalt-based catalyst and water (H_2O).

The same process conditions as **Procedure 2** were used. The rest of the reactants to equalize the molar composition were added after seed-assisted synthesis and prior to the standard hydrothermal synthesis. The added components to the obtained seeding solution were: source of silica oxide (SiO_2), and water (H_2O).

- **Procedure 4:** Pretreated FT catalyst with TEA-OH followed by standard hydrothermal synthesis.

The pretreatment procedure was used to incorporate the organic template inside the pores of the catalyst support before the hydrothermal synthesis starts. This procedure consisted in soaking the Fisher-Tropsch cobalt-based catalyst at room temperature in a 20 wt% TEA-OH solution for 8 hours. The amount of liquid template that was used is one part of solution template per one part of solid catalyst. Afterwards the liquid template was removed from the solution via decantation take care of not lose any solid particle. After decanting completely the solution it was washed with absolute ethanol once; this ethanol was removed by decantation. It was then soaked in fresh absolute ethanol for 24h. This step was employed to remove the template from the surface of the catalyst particles, the main objective of this technique is the internal incorporation of the template.

The pretreated FT cobalt-based catalyst was retrieved after 24h of soaking, by decantation of the ethanol and drying for 1h at 70°C . The pretreated catalyst was used as a component in a zeolite recipe, the amount of the catalyst is based on recipe calculation.

2.1.5 Selection of silicon sources

The silicon source was a big concern for the zeolite/FT catalyst, because Fischer Tropsch cobalt-based catalysts are especially sensitive to alkaline components such as sodium. The different silicon sources contain an amount of this alkali metal that could be considered as a poison of the final zeolite/FT catalyst.

This is the prevalent reason why different silicon sources were tested to have clear evidence of how the sodium content could affect the final zeolite/Fischer Tropsch catalyst. It is also a fact that high pure reactants are often more expensive but the sodium content is extremely low (Table 2-4).

Table 2-4 Relative costs for selected silica raw materials [41]

<i>Silica source</i>	<i>Example</i>	<i>Purity</i>	<i>%Na</i>	<i>Ease of use</i>	<i>Relative cost</i>
Sodium silicate	Grade 40 Clear	Low	~ 9	Easy	0.2
Precipitated	Ultrasil VN3 SP	Moderate	~ 0.4	Moderate	1
Colloidal	Ludox AS-40	Moderate	~ 0.1	Easy	2
Fumed	Aerosil 200	High	< 1 ppm	Difficult	4
Molecular	TEOS*	High	~ 0	Moderate	10

* Tetraethylorthosilicate

The different silica sources were utilized are Ludox with 1000 ppm of sodium, fumed silica with 1 ppm of sodium and TEOS with almost 0 ppm of sodium. The final amount of the sodium in the zeolite/Fischer Tropsch catalyst is always lower than the initial sodium amount because the silicon oxide component normally represents between 10 to 18 wt% of the reactants, with an average of 15 wt%. It means that the rest of the reactants (free of sodium) in the zeolite/FT catalyst synthesis always diluted sodium concentration. Based on this consideration the maximum concentrations of sodium per silicon source were: Ludox with 180 ppm of sodium, fumed silica with 0.18 ppm of sodium and TEOS with almost 0 ppm of sodium.

The use of low content sodium components presents additional challenges. Fumed silica is extremely difficult to handle because the ultra small particles and singularly low density makes the use of it laborious. Tetraethyl orthosilicate is very easy to handle but is not a direct source of silicon oxide molecule; previously hydrolysis reaction must be done. The final products were silicon oxide molecules, water and some remaining ethanol from the hydrolyzation[42].

2.1.6 Zeolites recipes

The general code to name all the samples were: BEA-##AUT, BEA to reflect the content of β -zeolite, a progressive serial number 01 to 14 in the ## position and AUT for autoclave. Table 2-5 refers some examples of the used nomenclature. The complete nomenclature names are included in **Appendix I**.

Table 2-5 Hydrothermal synthesis products name and general composition

Name	General Composition
BEA-01AUT	Pure β -zeolite
BEA-14AUT	β -zeolite/FT catalyst
Co12Re0.3	FT cobalt-based catalyst

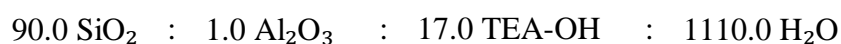
The last hydrothermal synthesis products BEA-09AUT to BEA-14AUT were split before calcination in two different samples. One of the samples remained without calcination procedure and the other one was calcined. To differentiate both samples the not calcined samples were called WOC at the end of the established nomenclature code, which means without calcination (e.g. BEA-09AUT WOC). The nomenclature names are included in **Appendix I**.

In the last reactions of the hydrothermal synthesis few products split spontaneously inside the reactor; in other words, two phases were found when the reactor was opened. The liquid and light phase was called WHITE containing almost pure β -zeolite and the solid and heavy phase in the bottom of the liner was called BLACK containing β -zeolite/FT catalyst.

Only three materials presented this case: BEA-11AUT, BEA-13AUT and BEA-14AUT. To differentiate the product from the WHITE or BLACK phases the nomenclature includes the color of the product after the AUT letters (e.g. BEA-11AUT BLACK). The nomenclature names are included in **Appendix I**.

The entire set of recipes were elaborated using the same recipe. The recipes' mass were calculated using 200g reactants amount. The differences among the hydrothermal products were: the silicon source, the employed amount of FT catalyst, the use of pretreated FT catalyst with TEA-OH and, the use of seed-assisted procedure. The complete description of the differences is included in the **Appendix J**.

The expected molar composition was:



Some small deviation from the ideal molar composition could be expected because the amount of the components during the weighting step is not always exactly the same as the recipe. The complete set of recipes is described in Table 2-6.

Table 2-6 β -zeolite and β -zeolite/FTcatalyst molar composition

	Expected molar composition				Obtained molar composition			
	Si ₂ O	Al ₂ O ₃	TEA-OH	H ₂ O	Si ₂ O	Al ₂ O ₃	TEA-OH	H ₂ O
	mol	mol	mol	mol	mol	mol	mol	mol
BEA-01AUT	100.0	1.0	35.3	1400.0	93.1	1.0	32.8	1303.7
BEA-02AUT	100.0	1.0	35.3	1400.0	*	*	*	*
BEA-03AUT	90.0	1.0	17.0	1110.0	89.9	1.0	17.0	1110.0
BEA-04AUT	90.0	1.0	17.0	1110.0	89.8	1.0	17.0	1107.4
BEA-05AUT	90.0	1.0	17.0	1110.0	89.8	1.0	17.0	1108.0
BEA-06AUT	90.0	1.0	17.0	1110.0	89.6	1.0	16.9	1104.0
BEA-07AUT	414.4	1.0	17.0	6259.1	417.8	1.0	17.0	6259.1
BEA-08AUT	90.0	1.0	17.0	1110.0	89.9	1.0	17.0	1109.8
BEA-09AUT	90.0	1.0	17.0	1110.0	89.5	1.0	17.0	1105.5
BEA-10AUT	90.0	1.0	17.0	1110.0	90.1	1.0	17.1	1111.8
BEA-11AUT	90.0	1.0	17.0	1110.0	90.7	1.0	17.0	1110.0
BEA-12AUT	90.0	1.0	17.0	1110.0	89.9	1.0	17.0	1108.7
BEA-13AUT	90.0	1.0	17.0	1110.0	90.0	1.0	17.0	1109.6
BEA-14AUT	90.0	1.0	17.0	1110.0	90.2	1.0	16.9	1104.0

* This product is not successful due to reactor failures

The molar composition of seeds is described in Table 2-7.

Table 2-7 β -zeolite/FTcatalyst molar composition of seed-assisted materials

	Expected molar composition				Obtained molar composition			
	Si ₂ O	Al ₂ O ₃	TEA-OH	H ₂ O	Si ₂ O	Al ₂ O ₃	TEA-OH	H ₂ O
	mol	mol	mol	mol	mol	mol	mol	mol
BEA-07AUT seed	50.0	1.0	17.0	1110.0	49.9	1.0	17.0	1105.8
BEA-08AUT seed	14.1	1.0	17.0	433.9	14.1	1.0	17.0	434.0
BEA-09AUT seed	14.1	1.0	17.0	433.9	14.0	1.0	17.0	433.4
BEA-13AUT seed	40.6	1.0	17.0	433.9	40.6	1.0	17.0	433.8

2.2 Fischer Tropsch reaction

The Fischer Tropsch test was conducted in a fixed-bed reactor with a constant syngas flow of 2.11 hydrogen/carbon monoxide ratio, at constant pressure of 20 barg and temperature of 210°C. Before the reaction conditions were established, several steps must be followed to get a representative test.

These steps guarantee that the obtained data from the test could be comparable to standard Fischer Tropsch catalyst tests.

From this point forward, the pure Fischer-Tropsch cobalt base catalyst will be called Co12Re0.3.

2.2.1 Fischer Tropsch chemical components

In the Fischer-Tropsch synthesis reaction, the components were used are: helium gas, hydrogen gas, syngas, silicon carbide, and beta zeolite/Fischer Tropsch Catalyst. The material used during FT test is shown in Table 2-8.

Table 2-8 Fischer Tropsch reaction chemical components

	Material	Chemical name	CAS Number
Gas	He	Helium, 99.999 vol%	7440-59-7
	H ₂	Hydrogen, 99.999 vol%	1333-74-0
	65.8 vol% H ₂		
	31.2 vol% CO 3.0 vol% N ₂	Synthesis Gas	-----
Solid	SiC	Silicon Carbide	409-21-2
	BEA##-AUT	Beta zeolite/Fischer Tropsch Catalyst	-----

2.2.2 Fischer Tropsch reaction equipments

The Fischer-Tropsch synthesis reaction was carried on the set-up reactors belonging to SINTEF Materials and Chemistry. Each reactor possess an independent heat source, flow meters of the incoming gases, independent temperatures and pressure meters hot and cold pots. The complete set of reactors is connected to only one gas chromatograph to analyzed the outcoming gases, the capacity of the equipment is analyze one sample every hour.

Hot pots were used to accumulate the reacted syngas converted in heavy hydrocarbons (C_5+). The cold pots were used to trap the carried heavy components and water in the gas sent it to the gas chromatograph.

The four used fixed-bed reactors have independent inlet of syngas flow and independent outlet for hydrocarbon gas flow. Fig. 2-4 is a schematic representation of a Fischer Tropsch setup; it does not represent the equipment that was used to perform the test but it is similar to the used one.

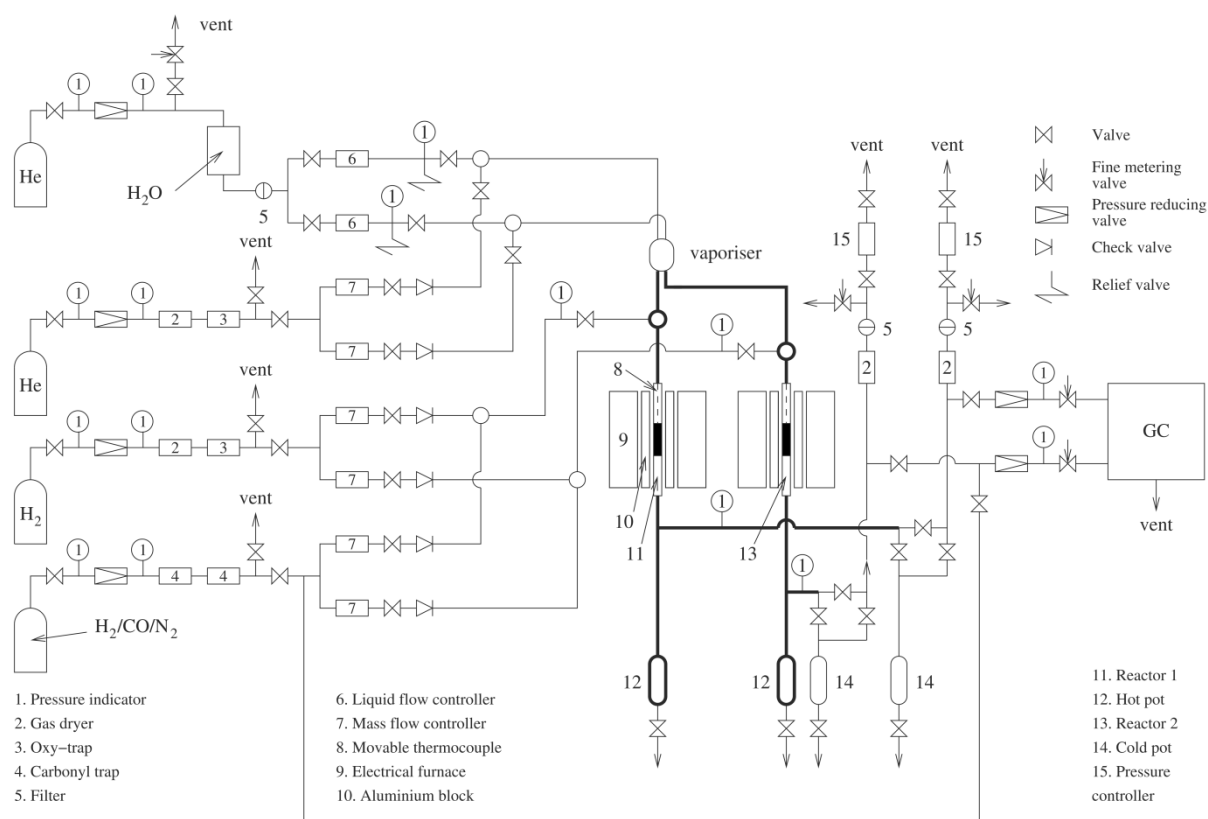


Fig. 2-4 Fischer Tropsch setup schematic representation [15]

2.2.3 Fischer Tropsch reaction

The performed Fischer Tropsch reaction generates a wide range of hydrocarbon products and water. These products were classified in gas, liquid, and solid phase. The gas phase products were ranged from methane to hexane, the liquid and solid products were collected as only one product. This mixed product is normally called waxes, and the water is collected as liquid product. In Fischer Tropsch reaction waxes are also known as C₅₊ components.

At the Fischer Tropsch conditions, 210°C and 20 barg, the products were gas and liquid. These products were split via gas phase separator (hot pot).

The gas phase was sent to a second separator to remove the remaining water and hydrocarbons larger than six carbons, the temperature of the cold pot was 25°C. After removal of the liquid components at 25°C the gas was analyzed in a gas chromatograph. The analyzed gas via gas chromatography were the hydrocarbons ranged from methane to normal hexane and from ethene to 1-hexene. This measured gas stream contains hydrocarbons with five (n-pentane and 1-pentene) and six carbons (n-hexane and 1-pentene), as a definition this components were added to the C₅₊ components percentage.

The liquid phase collected at the bottom of the gas phase separator was purged and collected. The product was separated by decantation to obtain the liquid and solid hydrocarbons and water. The liquid products solidified at 25°C.

The tested catalysts in the Fischer Tropsch reactors were diluted with Silicon Carbide (inert component at the Fischer-Tropsch conditions) to avoid heat gradients and guarantee isothermal conditions along the fixed-bed reactor (Table 2-9).

Table 2-9 Fischer Tropsch tested catalyst dilution

	FTc *¹	SiC	β-zeolite/FTc	SiC	β-zeolite/FTc
	g	g	g	wt%	wt%
Co12Re0.3	-	19.5010	1.7060	8.0	92.0
BEA-10AUT	90.0	18.0477	3.0011	14.3	85.7
BEA-11AUT	16.5	18.0107	3.0068	14.3	85.7
BEA-12AUT	31.0	18.0021	3.0005	14.3	85.7
BEA-13AUT	31.0	18.0028	3.0014	14.3	85.7
BEA-14AUT	70.0	18.0009	3.0024	14.3	85.7

*¹ Content of Fischer Tropsch cobalt-based catalyst in the hydrothermal synthesis recipe

The weight percentage of Fischer Tropsch catalyst in the mixture was recalculated based only on the mass of FT catalyst used to prepare the sample, adding the mass of the zeolite to the mass of the inert phase (silicon carbide).

Table 2-10 Fischer Tropsch tested catalyst dilution adjusted

	FTc *2	% of FTc *3	SiC/ β -zeolite	FTc*4	SiC/ β -zeolite	FTc*4
	g	wt%	g	g	wt%	wt%
Co12Re0.3	-	100	19.5010	1.7060	8.0	92.0
BEA-10AUT	90.0	87	18.4258	2.6230	12.5	87.5
BEA-11AUT	16.5	59	19.2405	1.7770	8.5	91.5
BEA-12AUT	31.0	62	19.1513	1.8513	8.8	91.2
BEA-13AUT	31.0	75	18.7592	2.2450	10.7	89.3
BEA-14AUT	70.0	86	18.4092	2.5941	12.4	87.6

*2 Content of Fischer Tropsch cobalt-based catalyst in the hydrothermal synthesis recipe

*3 Estimated weight percentage of Fischer Tropsch catalyst in the original β -zeolite/FT catalyst. The estimated FT catalyst will be described in section 3.2

*4 Calculated mass of pure Fischer Tropsch catalyst in the original β -zeolite/FT catalyst.

Once the fixed-bed reactors were loaded with the SiC/ β -zeolite/FT catalyst the reactors were installed in the set up to run the test. The first step before starting the procedure is the leak test, that was carried out at 20 barg with 250 ml/min of inert gas. After ensuring that there systems does not leak the reduction could start.

The reduction was done at 350 °C for 10h with a constant flow of hydrogen of 250 ml/min. The temperature controller kept the reactor at 170°C after reduction sequence. The hydrogen flow is closed and helium flow (250 ml/min) was used to remove the reducing atmosphere. The syngas flow was fed together with the helium flow, the helium flow was gradually closed until 0 ml/min flow and syngas was gradually increased to 250 ml/min. Then the reactor was heated up in two steps: the first from 170 to 190°C and the second from 190 to 208°C. The final temperature of the reaction is 210°C the 2 degrees difference is due to the exothermic reaction of Fischer Tropsch catalyst.

The first chromatograph analysis of reactor one was performed during the first hour, and the second reactor in the hour two and so on to reactor four. The adjustments of the syngas flow started after three complete cycles of the chromatograph for the fists reactor. The syngas

flow was adjusted based on the CO conversion, to obtain comparable data with the standard Fischer Tropsch test, the flow must be adjusted until obtain approximately 50% CO conversion. This took at least three adjustments with an interval of 12h between them.

During the whole process it is important to keep in mind to remove the products from the hot pots to avoid the accumulation of the melted waxes and water into the system.

The fifth day the catalyst test was concluded and the melted waxes recovered, free of water by decantation.

2.3 Characterization methods

Information of the chemical and structural characteristics of zeolites is an important aspect to establish their sorption and catalytic properties. A single analysis technique is not enough to have a complete description of the complex zeolite structure. The combination of diverse methods must be applied to provide an accurate description of zeolite structure.

According to *van Bekkum et al.* the characterization of a zeolite has to provide information about [22]:

- Its structure and morphology
- Its chemical composition
- Its ability to sorb and retain molecules
- Its ability to chemically convert these molecules

To characterize the four produced zeolite materials different methods were employed. Each method provides specific information about the zeolite structure. To obtain information about the surface area BET measurements was performed. In terms of micro and nano-shape of the powder the SEM and S(T)EM microscopes provide extremely accurate images. Related to the crystalline structure and composition XDR provides relevant information. To obtain information about the metal distribution in the materials Chemisorption was utilized. Standard analytical approaches are summarized in the **Appendix H**.

2.3.1 Brunauer-Emmett-Teller (BET)

The study of microporosity of materials is measured via nitrogen adsorption at constant temperature over the surface material, including the pores and cages. The shape of the isotherm represents the degree of crystalline structures. The ideal case of uniform microporosity is represented in Fig. 2-5 Type I. Any deviation from this shape indicates an amorphous structure in the zeolite crystal, based on micropore volume the degree of crystalline can be calculated. Some zeolites can have a mesopore pore sizes, the typical isotherm of it is shown in the Fig. 2-5 Type IV.

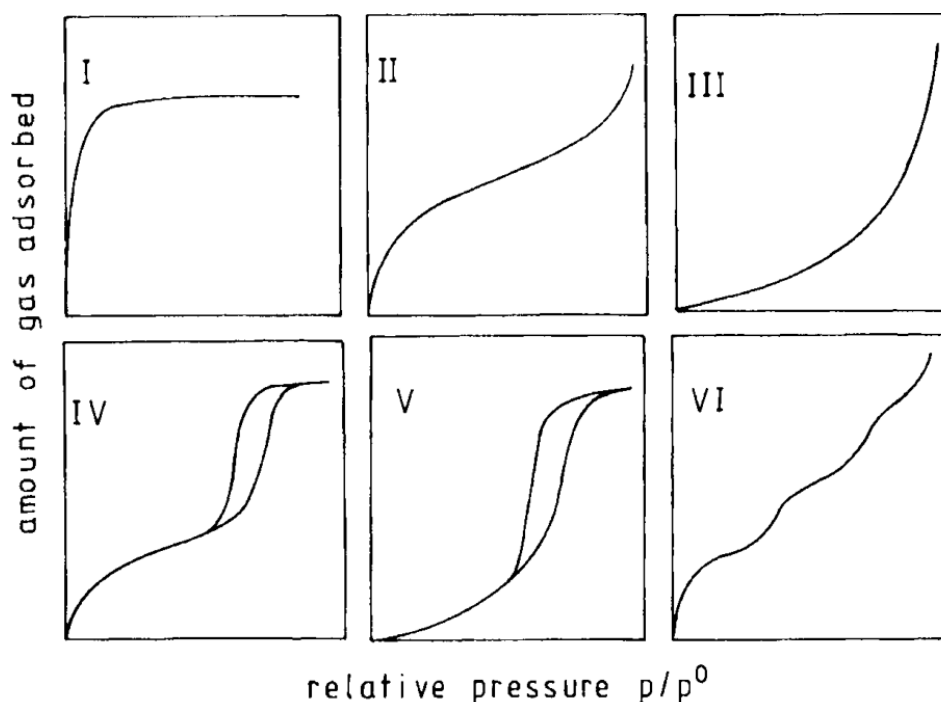


Fig. 2-5 Brunauer classification, Types of sorption isotherms [22]

The classification of the diameter pore sizes is given by IUPAC. The pore sizes are: micropores ranged from 3 to 20 Å, mesopores ranged from 20 to 500 Å and macropores ranged from 500 to 1000 Å. Using molecules considered relatively inert such as noble gases like Argon or small molecules like Nitrogen, the pore distribution sizes and the total pore volume can be determined. Usually the temperature condition to develop the adsorption isotherm is the correspondent condensation temperature of the selected molecule to adsorb. Table 2-11 shows the characteristics of the different types of isotherms.

An advanced technique of adsorption can be applied to measure only the external surface area of the zeolites. The method consists in using a benzene-filled pore to occupy and block temporary the pores access, allowing the nitrogen to adsorb over the surface [19].

Table 2-11 Type and characteristics of sorption isotherms [22]

Type of isotherm	Characteristics	Example
I	Adsorption in micropores	Benzene on zeolites
II	Multilayer adsorption on flat surfaces	N ₂ on SiO ₂ , Al ₂ O ₃
III	Weak gas-solid interactions	H ₂ O on noble metals
IV	Multilayer adsorption and pore condensation	N ₂ on MCM-41 type materials
V	Weak gas-solid interactions	H ₂ O on noble metals
VI	Non porous adsorbent	Kr on graphite

The Brunauer-Emmett-Teller (BET) equation (Eq. 1) is applied to type II and type IV isotherms to determine the specific surface area of the adsorbents.

$$\frac{p}{(p_0 - p)V} = \frac{1}{cV_{mon}} + \frac{(c-1)p}{cV_{mon}p_0} \quad \text{Eq. 1}$$

where V is the volume of gas adsorbed, V_{mon} the volume of gas adsorbed in a monolayer, p_0 the vapor pressure of the gas, c is proportional to $\exp(-(\Delta H_d - H_{vap})/RT)$, ΔH_d is the enthalpy of adsorption in the first layer and H_{vap} the heat of vaporization. The BET surface area is determined from the correlation of $\frac{p}{p_0}$ vs. $\frac{p}{(p_0 - p)V}$ using the range pressure range

$$0.05 < \frac{p}{p_0} < 0.30 \quad [22].$$

For zeolites with micropores the concept of multilayer is not applicable due to pore size limitations, the adsorbent molecule fills completely the pore. The size of the pore suppresses the multilayer formation. The BET isotherms reported for zeolites are used an empirical value to compare the porosity of the material with the reference one. It does not correspond to the internal area of the pores and cavities.

However, for mesopores and macropores, the multilayer adsorption can occur giving comparative results of the pore sizes and distribution.

Robson and Lillerud report that measurements based on the BET method can be performed in zeolites taking into account some precautions. The $\frac{p}{p_0}$ must be kept below 0.25 to avoid capillary condensation in the interstice between the crystals. The low value in the pressure ratio also prevents a significant physical adsorption over the external surface of the crystal. Very small crystals increase the error at high values of the pressure ratio [39]. The ideal pressure ratio range is between 0.05 to 0.25.

Despite the fact that N_2 is the common molecule used in BET surface area measurements, N_2 is not the most appropriate option to measure the micropore zeolite volume because N_2 isotherms frequently show changes in the packing density resulting in a possible quadruple interaction of N_2 with the zeolite. This interaction results in hysteresis of the isotherm. Most suitable molecules that prevent this effect are Ar and O_2 [39].

2.3.2 X-ray diffraction (XDR)

X-ray diffraction (XRD) is a technique to identify the crystal phase and the purity of the zeolite crystals. The degree of crystalline formation could be estimated from the diffraction intensity, wide-based peaks represent an amorphous phase while high and sharp narrow peaks represent high crystalline structures.

XRD is defined as the elastic scattering of x-ray photons by atoms in a periodic lattice. Relevant aspect of the XRD measurements is crystal size and the orientation of the crystal. During sample preparation, to minimize the possibility that some large crystals remain standing up in a parallel position, the zeolite sample must be grinded to ensure that only small and uniform powder is used. This allows a random orientation of the crystals in the sample holder, resulting in a standard powder diffraction pattern [19].

Bragg's law described the reflection observed in a polycrystalline material at a given angle 2θ , measured at the wavelength λ , related to lattice planes with a distance d and an orientation indicated by the Miller's indices hkl . The parameter n is an integer called the order of reflection, which is often taken as unity. Eq. 2 represents the Bragg's equation.

$$n\lambda = 2d_{(hkl)} \sin \theta \quad \text{Eq. 2}$$

An illustration of the Bragg's law based on the XDR allowing to derive lattices planes is shown in the Fig. 2-6.

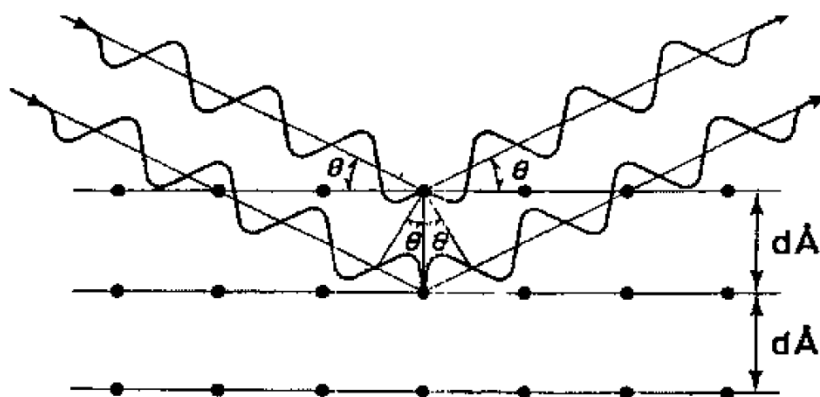


Fig. 2-6 Schematic representation of Bragg's Law [43]

Zeolites possess unique structures characterized for the ultra regular structure, pore size, pore distribution and surface area. It is not hard to conclude that also XRD powder patterns for each zeolite are well defined and unique. The predicted peak position and intensity match with the expected ones. To verify the chemical structure of some zeolites a collection of

simulated powder patterns was published by IZA [44]. The zeolites regular structure must fit with the one simulated by IZA in order to verify the obtained structure.

The adsorbed molecules inside of the zeolite structure could alter the diffraction pattern, it is important to remove any component that is not part of the original structure before performing the measurements.

The size of the crystals is a relevant parameter for the XRD powder pattern determination, the materials with powder crystals below 100 nm present some problems due to incomplete scattering directions. The ratio that relates the crystal size to line width is the Scherrer equation (Eq. 3).

$$L = \frac{K\lambda}{\beta \cos \theta} \quad \text{Eq. 3}$$

Where L is a measure of the dimension of a particle in the direction perpendicular to the reflecting plane, λ is the x-ray wavelength, β is the peak width, θ is the angle between the beam and the normal on the reflection plane, and K is a constant, which is often taken as unity. This provides an incredible fast estimation of the particle size despite that it is not always reliable [43].

The wavelength λ , is based in a material radiation. The most common used element is copper (Cu-K α 1) with a radiation of 1.54056 Å [17]. The span of the individual measurements is based on the definition of the peaks, more points means more accurate peak description. The angle range depends on the material, for zeolites the range between 5 to 50° of 2θ covers the complete peaks. The elapsed time of the measurement in the equipment is a function of the range and the span.

2.3.3 Scanning electron microscope (SEM)

The crystal size and the crystal morphology could be obtained via scanning electron microscopy (SEM). The resulting images do not guarantee a crystalline structure; they only provide a precise image of the micro- or nano-shape of the external surface of the crystal but not the detailed characterization of surface.

A charging effect is an issue that modifies the resolution of the SEM images. To avoid the charging effect, diverse coating materials are employed. The cheapest coating material is carbon and the most common is gold. For zeolites, the layer that is created with the carbon coating is not enough to avoid charging effects, the alternative of gold is more reliable in terms of avoiding charging but is not the best option because gold creates nano-islands that can interfere with the image resolution and mislead perception of zeolite nanoparticles. The best coating material for zeolites is platinum/palladium (80:20 composition ratio). The coated layer is very thin compare to gold, additionally this alloy creates islands many times smaller than gold.

The sputter coating machine is supplementary equipment that works in vacuum under inert argon conditions with high current to deposit the metal over the surface of the zeolite. In addition de development of new technologies as low voltage field emission electron sources for SEM brought significant reduction of the charging effect. This advanced equipments allow to observe particles as small as 12 Å [20].

The functionality principle of SEM is the focus of an electron beam in a very small spot to produce an image of the surface (Fig. 2-7). Additionally to the produced images by the SEM, the electron beam emits the X-ray fluorescence and the Auger electrons. X-ray fluorescence could provide a composition of the zeolite based on typically wavelength.

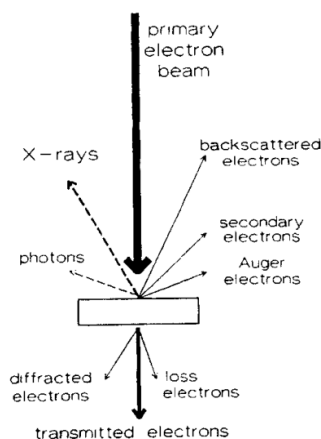


Fig. 2-7 Interaction of the primary electron beam with the sample [22]

2.3.4 Chemisorption

Chemisorption according to IUPAC is defined as: “*Adsorption which results from chemical bond formation (strong interaction) between the adsorbent and the adsorbate in a monolayer on the surface*” [45].

Chemisorption is a useful characterization method that allows to count metal surface atoms. Crystallite sizes based on this technique are surface-weighted average sizes. To get the right measurements of the metal surface dispersion the stoichiometry relation between the metal and the adsorbed gas plays an important role, this ratio must be known or at least a good approximation of it should be available.

This stoichiometry ratio is determined by many factors as; the metal itself, how the crystals are distributed in the exposed planes, the crystallite size, the temperature and other experimental factors. Chemisorption was shown to be a reliable method to measure very small metal particles due to the strong irreversible bonds that occur in the metal surface while the adsorption on the support is considerable weak.

The support with weak adsorption is described by Henry’s Law, while the metal surface with strong adsorption bonds is perfectly described by Langmuir-type isotherm. Fig. 2-8 depicted support adsorption (1), metal unsupported adsorption (2), and metal supported adsorption (3)[35].

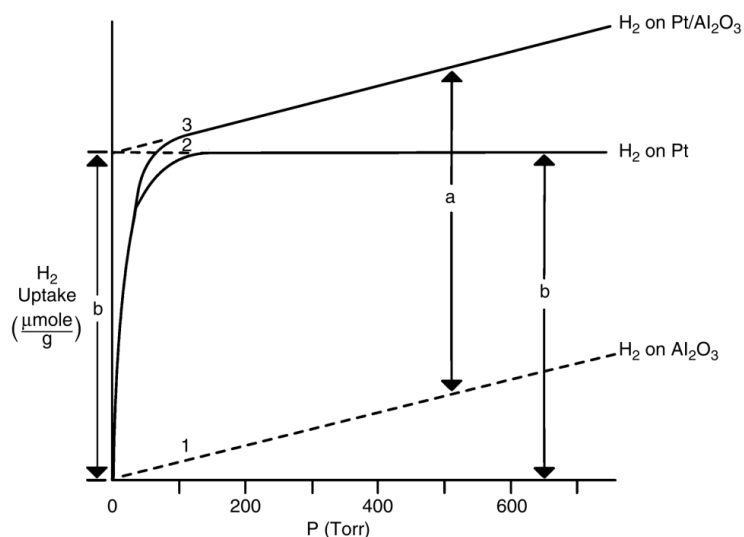


Fig. 2-8 Adsorption isotherms for Pt dispersed on Al₂O₃: 1) H₂ adsorption on Al₂O₃ in Henry’s law region, 2) H chemisorption on Pt, 3) Total H₂ chemisorption on Pt/Al₂O₃ catalyst [35]

The most used adsorbate chemisorption gas is hydrogen. Hydrogen is commonly adsorbed dissociatively at 26.85°C and is widely used with many metals. In the specific case of Fischer-Tropsch cobalt-based catalyst the adsorbate gas is hydrogen with a stoichiometry factor of two, it means that two cobalt active sites absorbed one hydrogen molecule and rhenium does not participate in the chemisorption[15][46].

The chemisorption measurements were performed evacuating the samples for 1h at room temperature; this pre-step was done to ensure that the system is completely sealed.

The chemisorption sequence was:

1. Evacuation of the gases for 1h at 60°C.
2. Leak test of the system at 60°C under vacuum at low temperature.
3. Injection of hydrogen gas to perform *in situ* reduction, the reduction temperature was 350°C with a heat rate of 1°C/min, once the temperature was reach the system remains at 350°C for 10h under hydrogen atmosphere.
4. Evacuation at 330°C for 1h, to remove completely hydrogen reduction atmosphere at high temperature.
5. Evacuation at 100°C for 0.5h, to remove completely reduction atmosphere hydrogen at medium temperature.
6. Leak test of the system at 100°C under vacuum medium temperature.
7. Analysis with hydrogen at 40°C. The pressure range was 10 to 520 mmHg containing 11 points.

Chemisorption was employed to measure the crystallite size for particles in the nanosize range with very high accuracy [15]. The formula is applicable to monodisperse spherical cobalt particles. The Eq. 4 estimates the crystallite size of the cobalt particles.

$$d(\text{Co}^0)(\text{nm}) = \frac{96}{D(\%)} \quad \text{Eq. 4}$$

3. Results and discussion

It was decided that the results and discussion of the present work would be incorporated in only one chapter.

For practical purposes this chapter is divided in two main sections:

- The synthesis of the tailored β -zeolite/Fischer Tropsch catalyst and characterization (Section 3.1).
- The Fischer Tropsch test results of six different tested samples (Section 3.2).

3.1 β -zeolite/Fischer Tropsch catalyst

The hydrothermal synthesis of zeolites constantly presents a challenge because regardless of the precision or the precise control of the hydrothermal conditions, the exact addition of the chemical components and the rigorous follow up of the treatment procedures, the structure of the resulting zeolites could not be identical; but if care is taken, it is very similar.

The reaction conditions were an important aspect to be kept under strict control. During the syntheses of β -zeolite/FT catalysts, the temperature was kept constant by the temperature controller. Despite the temperature was controlled, it was noticed that the heat distribution inside of the Parr autoclave was not constant. A temperature gradient between the center of the reactor liner and the walls of the liner was detected. This gradient originated that the reaction conditions were not completely homogeneous inside the reactor Teflon liner.

This abnormality in the synthesis conditions was the same during all the performed syntheses, the remaining uncertainty is how the temperature profile in the reactor is affected by the changes in the recipes. As a consequence of the synthesis conditions variation, in particular temperature, the crystallinity of the products change.

The Parr autoclave reactor was a fully sealed equipment to work up to 70 barg and 250°C but unfortunately, the Teflon liner inside the reactor does not contain a lid to seal completely the Teflon liner. Therefore at reaction conditions, the solution (zeolite components), contained in the Teflon liner was in contact with the metal top cover of the autoclave and internal thermowell and propeller of the agitation device.

These metal components must be inert for the reaction conditions, but the zeolite reaction conditions inside the Teflon liner was highly basic medium at high temperature and

equilibrium pressure, that promote the ionic exchange to stabilize the aluminum charge in the zeolite structure. The effect of the additional components (unexpected counter ions) in the β -zeolite/FT catalyst is taken in account but only as side effect; no measurements were performed to determine the amount of migrating ions in the β -zeolite/FT catalyst.

The results of the conducted research were based on the synthesized β -zeolite, β -zeolite/FT catalyst and Fischer Tropsch catalyst cobalt-based catalyst characterization. The characterization methods that were employed are BET, XRD, SEM, and Chemisorption. Diverse measurements were followed to perform the BET adsorption/desorption isotherms. Extended 2θ angle range was employed to measure the powder pattern diffraction. SEM microscope was also used.

3.1.1 Brunauer-Emmett-Teller (BET)

The performed adsorption/desorption BET isotherms was considered in two different ranges. The decision of use two ranges was supported by the fact that zeolites are structures in the micropores range and standard BET methods are based on the multilayer concept. This concept cannot apply directly to the zeolites structures, the alternative solution proposed by IZA is to use a reduced pressure ratio range.

The pressure ratios range was from 0.01 to 0.95 and from 0.01 to 0.30. This last range exceed slightly IZA's suggestion but the decision of using it is based on the consideration that the synthesized materials are a bifunctional catalysts that share the same alumina support that is normally measured in the wide pressure ratio range. The results of pore volume and pore size were based on Barrett-Joyner-Halenda (BJH) method, the desorption isotherm was selected to calculate both pore properties [15].

The results from BEA-01 AUT to BEA-03 AUT were intentionally excluded of the discussion because these zeolites do not represent the real structure of β -zeolite due to reactor failures.

To facilitate the understanding of the pressure ratio ranges from this point forward, the 0.01 to 0.95 range will be referred as long pressure range, and the 0.01 to 0.30 range will be referred as short pressure range.

The long pressure range will be employed to determine the alumina properties and the short pressure range to determine the β -zeolite properties and the β -zeolite/FT catalyst properties.

As expected the measurement of the BET surface area and BJH pore volume was always higher when the product is already calcined as is depicted in Fig. 3-1 a) and b). The product without calcination contains the organic template trapped inside the pores and cavities, this organic compound prevents the nitrogen molecule from entering the pores to create a nitrogen gas layer. The exact same behavior of the product without calcination was found for the short pressure range no matter the difference in the pressure ratio.

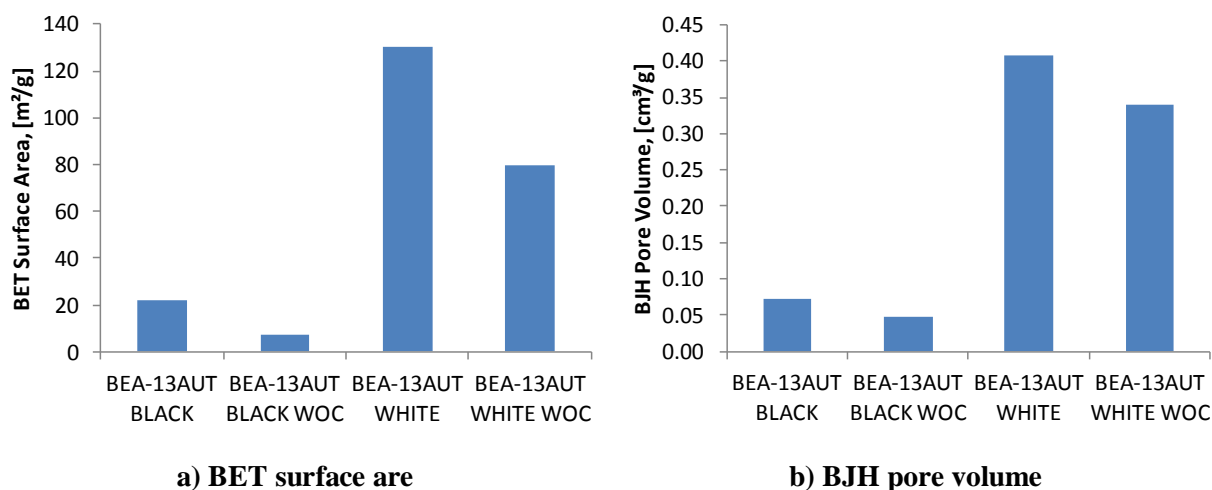


Fig. 3-1 β -zeolite/FT catalyst BET surface area comparison, long pressure range

By the contrast, the BJH pore size resulted in abnormal behavior because it was expected that the pore size would follow the same tendency as the BET surface area and BHJ pore volume (Fig. 3-2).

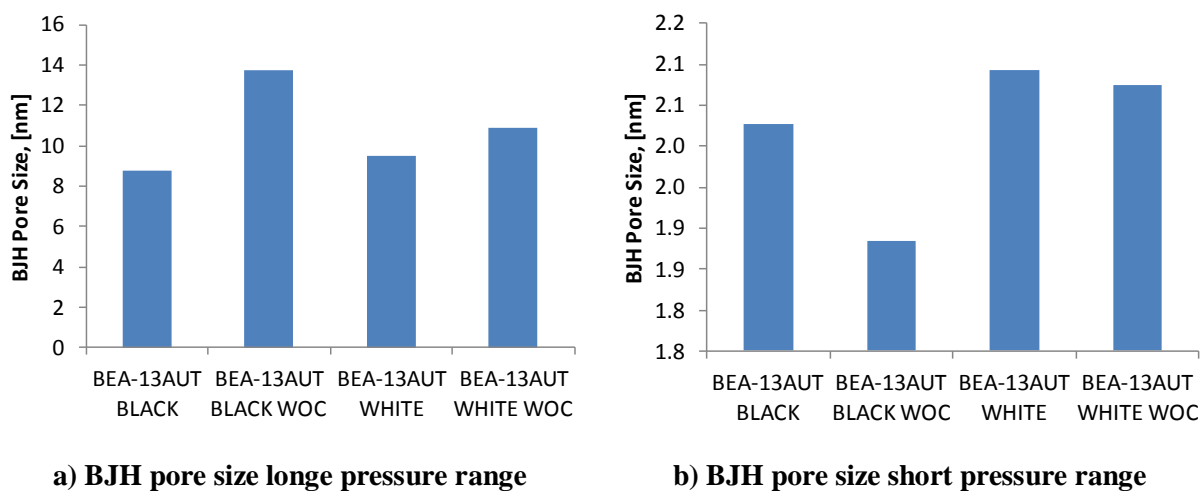


Fig. 3-2 β -zeolite/FT catalyst BET BJH pore size comparison

This abnormal results are well documented by IZA, the BET technique to measure pore size cannot be applied to zeolites with a small structure, smaller than 8-rings, because the nitrogen molecule does not penetrate the small pore at low temperature. Moreover, nitrogen is not the best choice to measure micropore size because nitrogen could lead quadruple interactions, resulting in complex packing density, this probably can cause hysteresis in the isotherm. The alternative to obtain reliable results is change the probe molecule for Ar or O₂.

The long pressure range and short pressure range also offers different results in BET surface area (Fig. 3-3), BJH pore volume and BJH pore sizes, included in **Appendix C**. In the BET surface area the recommended range is the short pressure ratio, the resulted surface area is comparable with the reported in the literature for zeolites.

Based on the literature information and the obtained results of the surface areas, the results for the short pressure range are consistent with the amount of zeolite that the β -zeolite/FT catalyst contains. The higher the amount of zeolite in the β -zeolite/FT catalyst, the higher the surface area, as depicted in Fig. 3-4. However, when performing the analysis with the long pressure range, BJH pore volume and BJH pore sizes were consistent with the zeolite content.

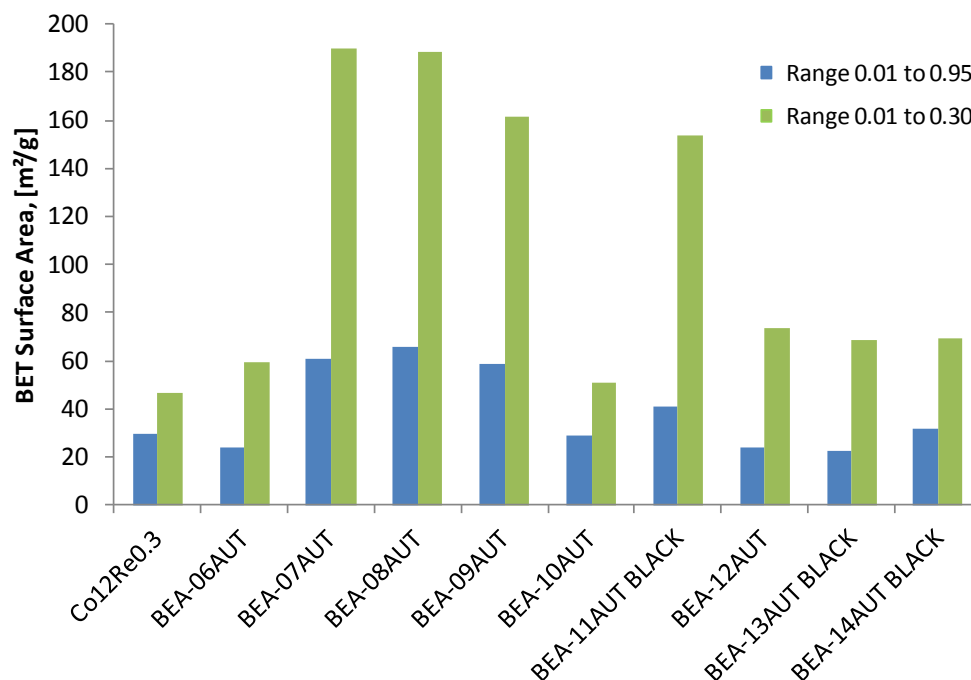


Fig. 3-3 β -zeolite/FT catalyst BET surface area between long pressure range and short pressure range

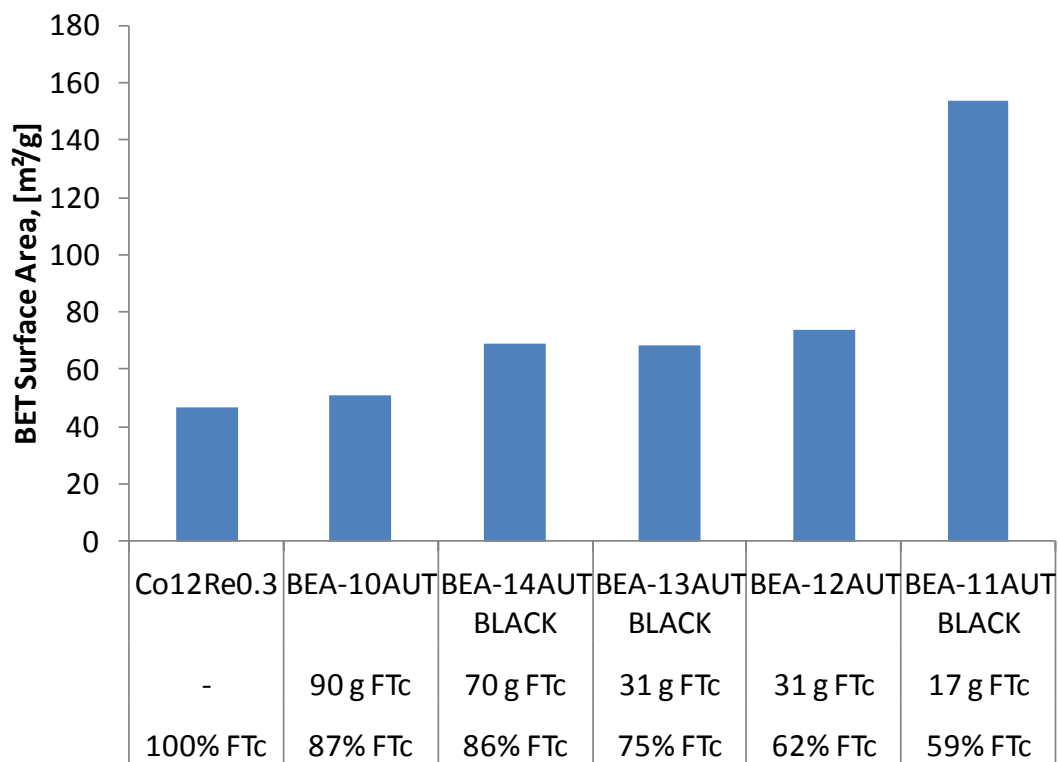


Fig. 3-4 β -zeolite/FT catalyst BET surface area short pressure range

The complete set of results, plots, and isotherms is included in **Appendix C**.

3.1.2 X-ray diffraction (XDR)

The different powder patterns obtained via XRD were compared to the literature. The results show in most cases that β -zeolite and β -zeolite/FT catalyst were synthesized in the same way as the reference. The slight deviations from the reference pattern in some plots is because the interactions between β -zeolite and FT catalyst.

The analyses were performed between 2θ 5° to 75° as a trade-off between the recommended angles for zeolites and supported metal catalysts. The recommended 2θ for zeolites is 5° to 50° , according to IZA [21]; while the recommended 2θ for supported metal catalysts is 20° to 90° [15]. It is also noteworthy to comment that the step between measurements is 0.1° , for 2θ 5° to 75° .

BEA-01 AUT to BEA-05 AUT are pure β -zeolite samples. BEA-06 AUT to BEA-14 AUT are β -zeolite/FT catalyst samples. As mentioned previously, some samples generated two phases, BLACK and WHITE. These phases were separated and analyzed separately. The white phase of BEA-11 AUT, BEA-13 AUT, and BEA-14 AUT was identified as being composed of pure β -zeolite (Fig. 3-5); while the black phase of these same samples was identified as β -zeolite/FT catalyst (Fig. 3-7).

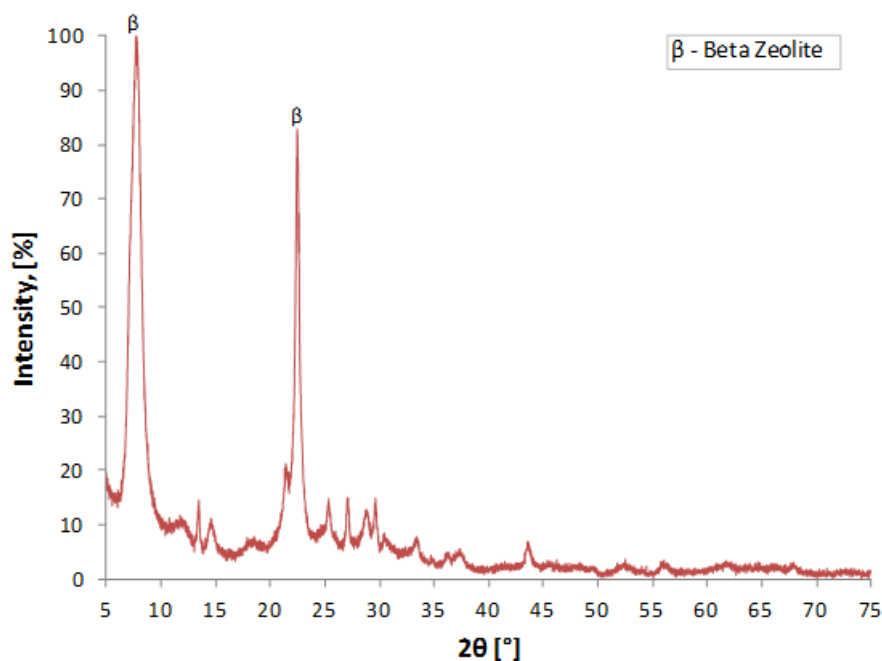


Fig. 3-5 XRD powder pattern for pure β -zeolite sample BEA-14AUT, white calcined sample

The γ -alumina characteristic peaks cannot be observed in the same pattern as the FT cobalt-based catalyst characteristic peaks because the former overlaps the angle of the γ -alumina peaks, as depicted in Fig. 3-6.

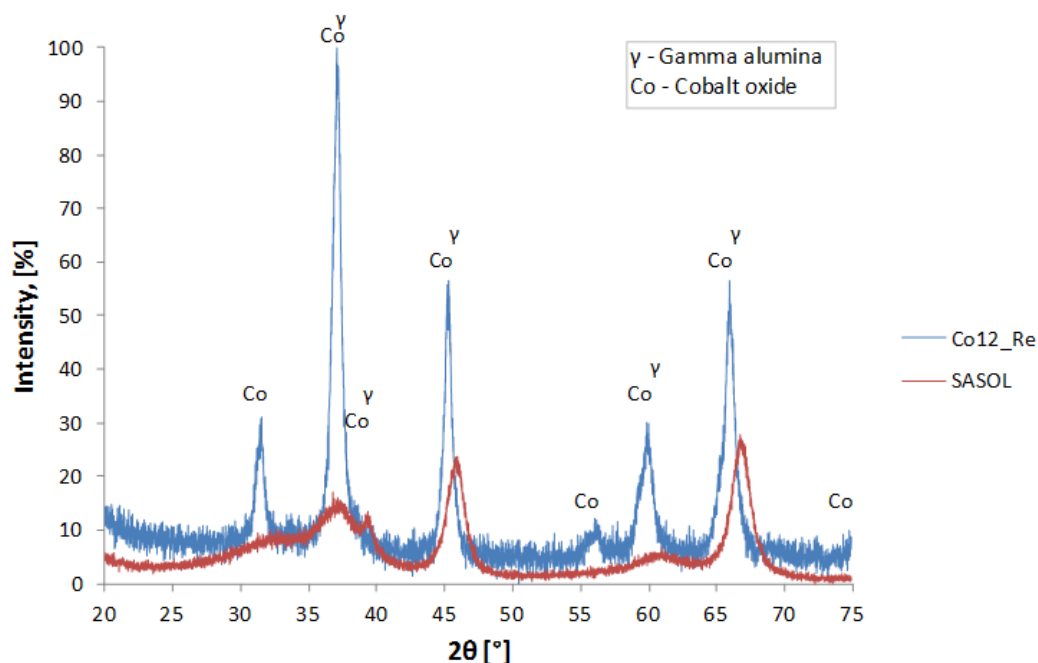


Fig. 3-6 Comparison of XRD patterns of γ -alumina and FT catalyst

XRD was used to prove that calcination at 550°C, which was used to remove the organic compound from the zeolite structure, did not damage the crystalline structure or the metal dispersion over the alumina support. This can be observed in Fig. 3-7, in which the peaks of the calcined and the not calcined samples match almost perfectly. In the same figure, the peaks of β -zeolite, γ -alumina, and FT cobalt-based catalyst are present as expected.

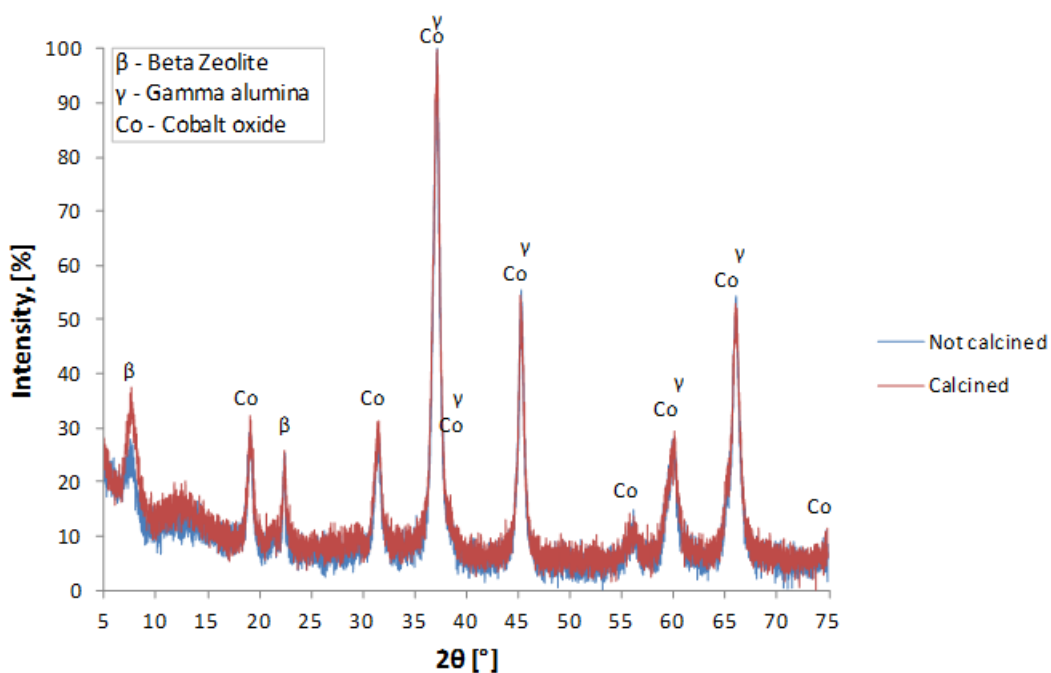


Fig. 3-7 XRD powder pattern for β -zeolite/FT catalyst sample BEA-14AUT, black sample

All the XRD analysis of pure β -zeolite samples are depicted in Fig. 3-8. In the case of the β -zeolite white samples that were separated from the β -zeolite/FT-catalyst, it can be observed that the those that were generated in reaction conditions with a higher content of FT-catalyst have a wider peak, denoting lower crystallinity. For example, BEA-14 AUT, which was generated with 70 g of FT cobalt-based catalyst and 24.3 g of zeolite solid precursors, has a wider peak than BEA-11 AUT, which was prepared with 16.5 g of FT cobalt-based catalyst and 34.2 g of zeolite solid precursors.

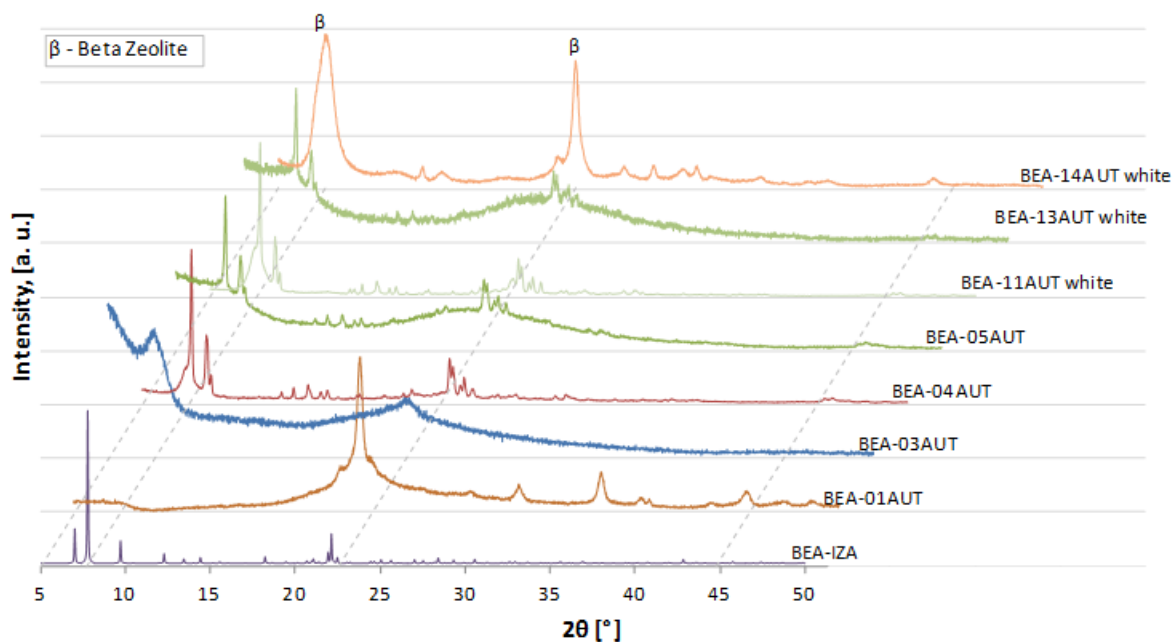


Fig. 3-8 XRD powder pattern for β -zeolites collection. Greek letter β represents the main peaks of pure β -zeolite reference pattern from IZA [21]. Dotted gray lines are spatial reference lines

The results from BEA-01 AUT to BEA-03 AUT were intentionally excluded from the discussion because these zeolites do not represent the real structure of β -zeolite due to reactor failures.

Fig. 3-9 depicts the XRD characterization of all the β -zeolite/FT cobalt-based catalyst full collection. As reference, the line depicted at the bottom is pure β -zeolite and the second line from the bottom is pure FT cobalt-based catalyst.

The third line from the bottom is a physical mixture of pure β -zeolite and pure FT cobalt-based catalyst (25:75, weight), prepared separately and mixed with thorough agitation. It can be observed that, except for the very low angle, this physical preparation is very similar to BEA-06, which was prepared in the reactor. This similarity is only in crystallinity; however, it would not be expected that this physically prepared sample would have good results for the FT reaction because the FT catalyst and the β -zeolite would separate due to solid density, size, and shape differences.

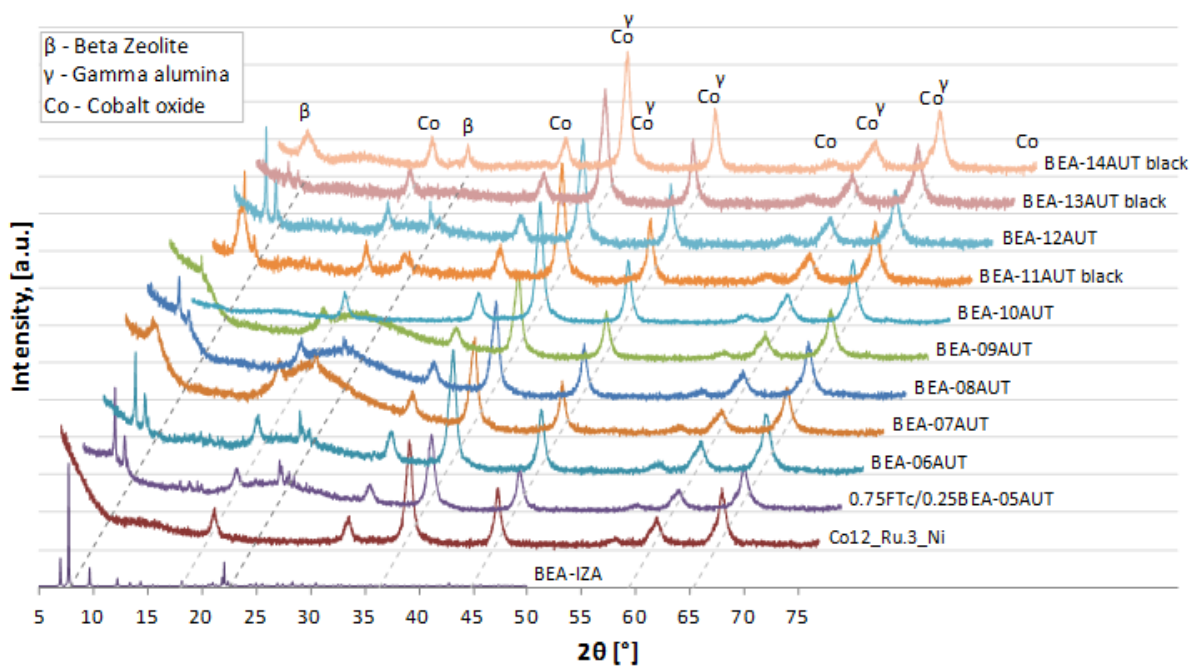


Fig. 3-9 XRD powder pattern for β -zeolites/FT catalyst collection. Greek letter β represents the main characteristic peaks of β -zeolite reference pattern from IZA [21], Co represents the main characteristic peaks for cobalt oxide [15] and Greek letter γ represents the main characteristic peaks of γ -alumina. Dotted gray lines are spatial references

Fig. 3-10 depicts the catalyst samples that were selected to be tested in the FT reactor. The XRD analysis of pure β -zeolite and pure FT cobalt-based catalysts are also depicted as a reference. The angle that is typically used to analyze alumina is from 2θ 20° to 90° , and this analysis was done from 5° to 70° . Therefore, the plots in literature typically do not depict the first part of the trend that can be seen in Fig. 3-10 for the FT cobalt-based catalyst.

All samples in Fig. 3-10, present the characteristic peaks of FT cobalt-based catalyst and β -zeolite. In BEA-10 AUT, the peaks corresponding to β -zeolite are very small because it is the sample that was prepared with a higher catalyst/zeolite ratio. In BEA-11 AUT, the peaks corresponding to β -zeolite are very larger because it is the sample that was prepared with a lower catalyst/zeolite ratio.

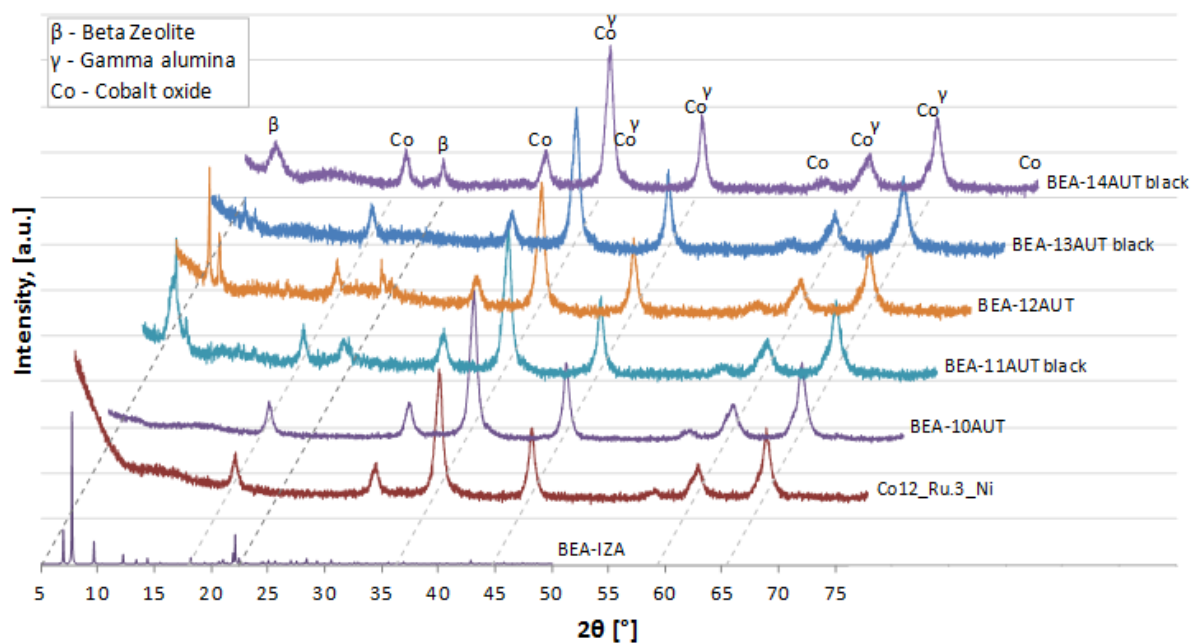


Fig. 3-10 XRD powder pattern for β -zeolites/FT catalysts that were tested in the FT reactor. Greek letter β represents the main characteristic peaks of β -zeolite reference pattern from IZA [21], Co represents the main characteristic peaks for cobalt oxide [15] and Greek letter γ represents the main characteristic peaks of γ -alumina. Dotted gray lines are spatial references

The rest of the XRD analyses can be consulted in **Appendix D**.

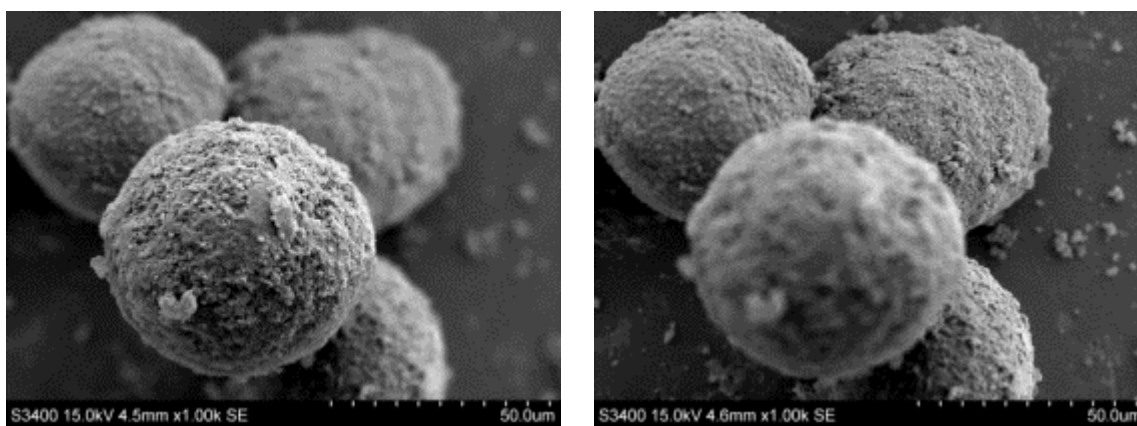
3.1.3 Scanning electron microscope (SEM)

All the images of the zeolite samples were taken all SEM. The samples were coated with different materials and different amounts of material. The two main materials employed to coat the zeolites were carbon and gold. Regardless the amount of the carbon coat the images were not good. The gold coating was more reliable for zeolites in SEM.

Several current intensities were tested. It was observed that the higher the current intensity the higher contrast but the lower the resolution. It was found that 15 kV and a 30% probe gave detailed enough images with high resolution.

Several coating times using gold were also tested and based on the quality of the images, it was determined that 2.5 minutes at maximum intensity of the equipment was an appropriate coating time. If coating lasted less time, less charge was obtained, and the quality of the images decreased. On the other hand, very long times would produce a very thick layer which would avoid the visualization of the shape of the surface.

As the catalyst has a spherical shape, the focus is an important parameter to get a good image. In Fig. 3-11 it can be observed that by changing the focused plane, the image shows different aspects of the analyzed spheres.



BEA-11AUT BLACK, 50 μ m

BEA-11AUT BLACK, 50 μ m

Fig. 3-11 SEM images of BEA-11 AUT BLACK using different focus

Fig. 3-12 (a-e) shows BEA-14 AUT, black phase, with different magnifications. Fig. 3-12 (f) shows the image of pure FT cobalt-based catalyst. It can be observed that while pure catalyst has a smooth appearance, β -zeolite present in BEA-14 AUT is evident in the rest of the images. β -zeolite has a characteristic appearance of “cabbage-like” agglomerates, which are observed in the BEA-14 AUT images.

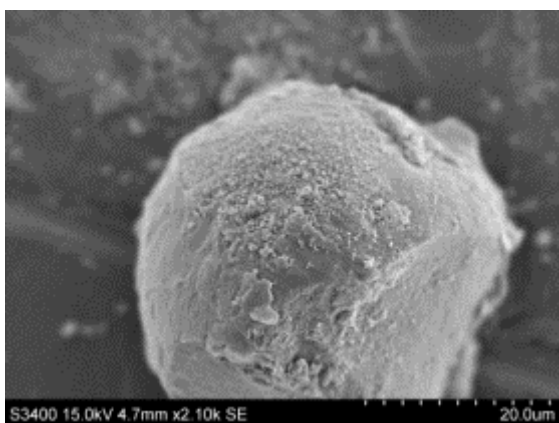
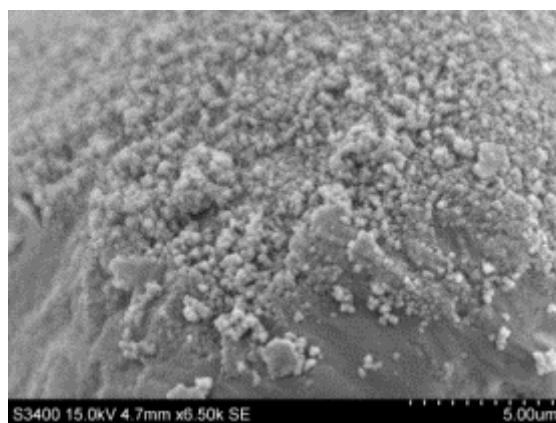
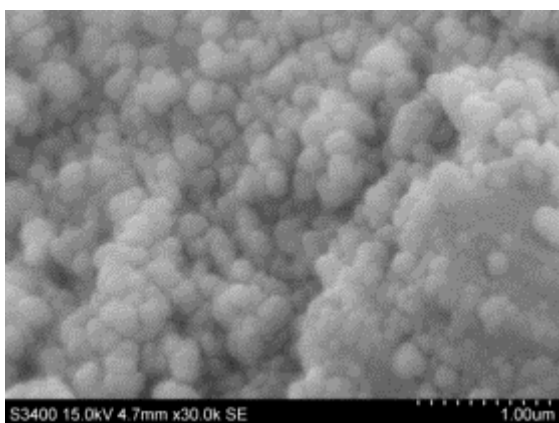
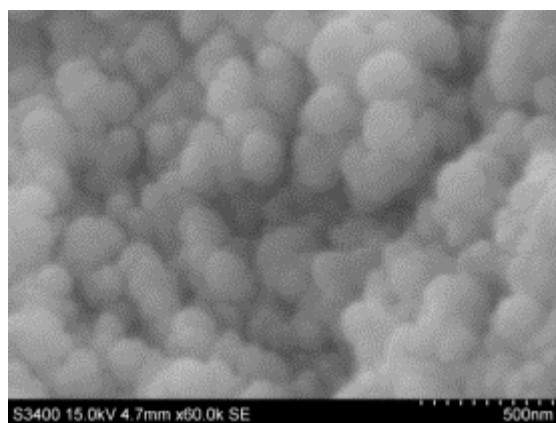
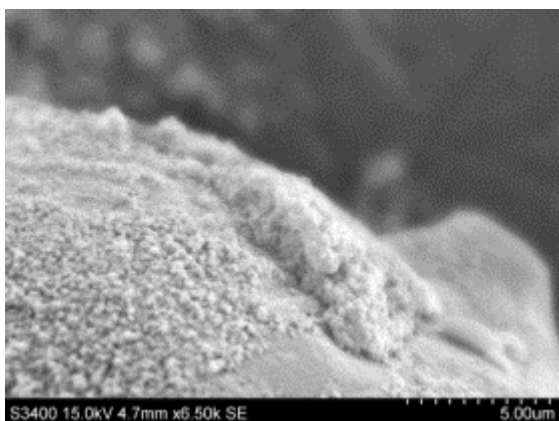
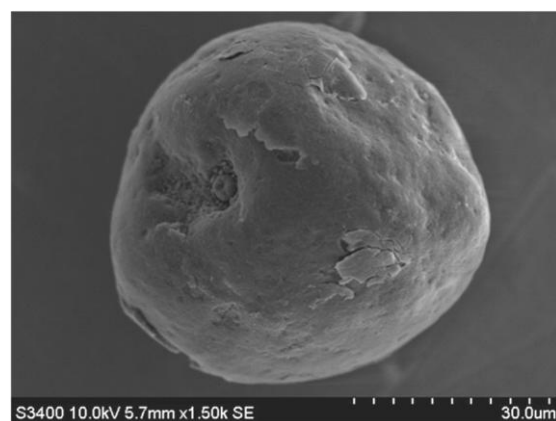
a) BEA-14AUT BLACK, 20 μ mb) BEA-14AUT BLACK, 5 μ mc) BEA-14AUT BLACK, 1 μ md) BEA-14AUT BLACK, 0.5 μ me) BEA-14AUT BLACK, 5 μ mf) Fischer Tropsch catalyst, 30 μ m

Fig. 3-12 β -zeolite/FT cobalt-based catalyst BEA-14AUT BLACK and FT catalyst, gold-coated

Fig. 3-13 shows BEA-10 AUT, which is the β -zeolite/FT catalyst that contains the highest amount of Fischer Tropsch cobalt-based catalyst. In other samples, such as the one shown in Fig. 3-12, zeolite can be observed in the surface. However, in the case of BEA-10 AUT, this is not the case and only a few small zeolite agglomerates were present.

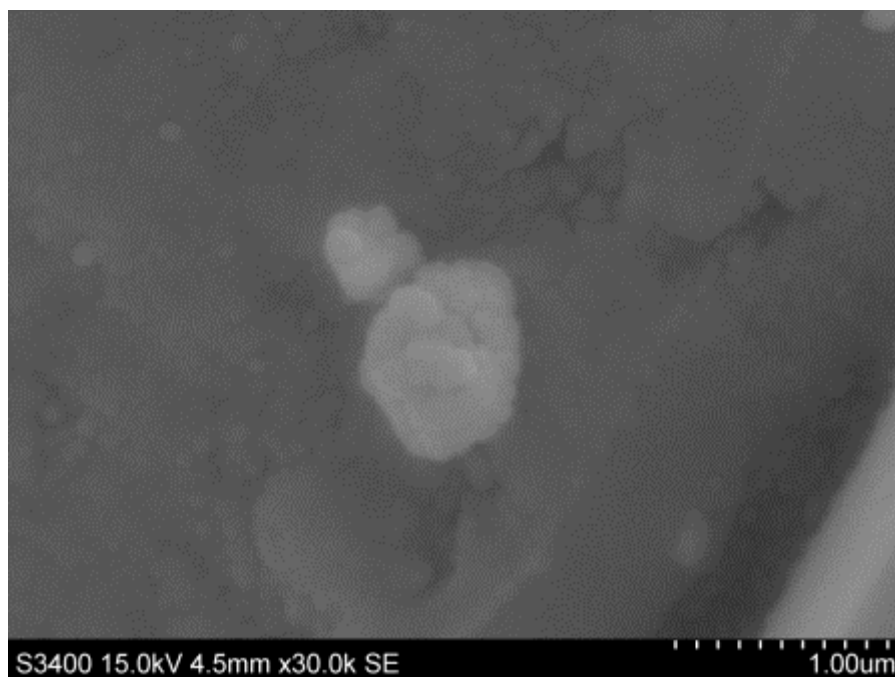


Fig. 3-13 β -zeolite/FT catalyst BEA-10AUT 1 μ m, gold-coated

The rest of the images can be consulted in **Appendix E**.

3.1.4 Chemisorption

Hydrogen chemisorption was performed to obtain the different isotherms and metal dispersion only in the samples that contain FT cobalt-bases catalyst. The samples were BEA-06 AUT to BEA-14AUT. It is also possible to use chemisorption to measure some properties in zeolites but the absorbed gas and measurement conditions are different, these measurements and characterization procedures are out of the scope of the present work.

The chemisorption was performed in calcined and not calcined samples. One important result that was observed during the chemisorption measurements was the fact that the samples without calcination lost more weight during the analysis.

This could be explained based on the presence of the organic template in the β -zeolite/FT catalyst sample, due to the very high vacuum and high reducing temperature during the chemisorption, the decomposition point of the template must change. At atmospheric pressure conditions, the complete decomposition and removal of the organic template from the pores and cavities was at 550°C.

At chemisorption conditions, very low pressure and 350°C, the decomposed template abandons the β -zeolite/FT catalyst sample pores, dragged by the reduction gas (hydrogen).

It was expected that the higher the amount of β -zeolite in the catalyst, the lower the metal dispersion value but in the not calcined samples, the results were irregular due to template decomposition (Table 3-1).

The estimated FT catalyst will be described in section 3.2.

Table 3-1 Hydrogen chemisorption results for the β -zeolite/FT catalyst samples without calcination. The catalysts were sorted by high to low FT catalyst weight content

		BEA-10AUT	BEA-14AUT	BEA-13AUT	BEA-12AUT	BEA-11AUT
		WOC	WOC	WOC	WOC	WOC
Estimated FT catalyst	wt%	87	86	75	62	59
Metal Dispersion:	%	7.3	3.2	7.3	6.6	4.8
Metallic Surface	m ² /g _{sample}	5.2	2.3	4.5	3.3	2.3
Area:	m ² /g _{metal}	49.5	21.9	49.7	44.9	32.7

Chemisorption was utilized to measure the metal dispersion in the β -zeolite/FT calcined catalyst, the catalyst are listed in Table 3-2. Pure FT cobalt-based catalyst (Co12-Re0.3) shows the higher amount of cobalt, higher the metal dispersion as is expected. Some of the produced β -zeolite FT catalyst showed different results because BEA-11 AUT and BEA-14 AUT are out of the expected metal dispersion. This difference could be attributed to the β -zeolite presence. The present work does not study the influence of the zeolites in the chemisorption measurements.

Table 3-2 Hydrogen chemisorption results for the β -zeolite/FT catalyst samples that were tested in the FT reactor. The catalysts were sorted by high to low FT catalyst weight content

		Co12- Ru0.3	BEA- 10AUT	BEA- 14AUT	BEA- 13AUT	BEA- 12AUT	BEA- 11AUT
Estimated FT catalyst	wt%	100	87	86	75	62	59
Cobalt	wt%	12.0	10.5	10.4	9.0	7.4	7.1
Metal Dispersion:	%	8.3	6.7	6.1	6.6	5.9	6.5
Metallic Surface Area:	m ² /g _{sample}	6.7	4.7	4.3	4.0	3.0	3.1
	m ² /g _{metal}	54.8	45.2	41.3	44.9	39.9	44.2

The crystallite size could be estimated by the chemisorption, based on the percentage of the metal dispersion. In the β -zeolite/FT calcined catalyst the crystallite size is apparently larger than the size in the pure FT cobalt-based catalyst. The increment in the crystallite size is because β -zeolite was distributed uniformly over the FT cobalt-based catalyst surface resulting in a coverage layer of the crystals (Table 3-3).

BEA-14 AUT crystallite factor is different but a correction was performed using crystallite factor of 99.6. This crystallite factor is slightly different from the reported in the reference, the reported value was 96 [15]. The difference could be caused because the β -zeolite presence during the chemisorption measurements. It has been reported in the literature that slight differences are expected in the chemisorption test from laboratory to laboratory.

Table 3-3 Hydrogen chemisorption crystal sizes for the β -zeolite/FT catalyst samples that were tested in the FT reactor. The catalysts were sorted by high to low FT catalyst weight content

		Co12- Ru0.3	BEA- 10AUT	BEA- 14AUT	BEA- 13AUT	BEA- 12AUT	BEA- 11AUT
FT catalyst	wt%	100	87	86	75	62	59
Cobalt	wt%	12.0	10.5	10.4	9.0	7.4	7.1
Metal Dispersion:	%	8.3	6.7	6.1	6.6	5.9	6.5
Crystallite Factor		99.6	92.9	99.6	99.6	99.6	99.6
Crystallite Size	nm	12	14	16	15	17	15
Est. Crystallite Size*:	nm	12	15	16	15	17	15

* Estimated crystallite size based on: $d(\text{Co}^0)(\text{nm}) = \frac{99.6}{D(\%)}$

The complete set of results and isotherms is included in **Appendix F**.

3.1.5 Silicon source

The silicon source constitutes a considerable origin of poisoning components to the Fischer Tropsch catalyst during the hydrothermal synthesis, due to the sodium content. There is some uncertainty in how the sodium reacts and where ends. One option is that sodium ends as an ion in high concentration over the catalyst surface. Another option is that it ends in high concentration in the solvent. A third option is that it distributes in both parts of the system.

Sodium is diluted in the system to the presence of water, organic template, silicon source, aluminum source, and FT catalyst. However, a questionless point is the fact that, regardless of this dilution, the very low concentrations of sodium in Ludox are still high enough (180 ppm) to affect FT catalyst performance. Ludox was used only for BEA-01 AUT to BEA-05 AUT, which are pure β -zeolite samples. All the β -zeolite/FT catalysts, from BEA-06 to BEA-14, were prepared either with fumed silica or TEOS, to avoid the undesirable effect of sodium in the FT reaction.

In principle TEOS would be the best option in terms of purity because it is virtually sodium free. Fumed silica may contain up to 100 ppm, but due to the dilution effect, this concentration is reduced. In order to analyze the difference between using TEOS and fumed silica, two samples (BEA-10 AUT and BEA-11 AUT) were prepared with fumed silica and tested in the FT reactor, and two samples (BEA-12 AUT and BEA-12 AUT) were prepared with TEOS.

The results of the FT reaction test will be discussed in section 3.2. At this point, it can be said that, when analyzing the results of BEA-10 AUT to BEA-13 AUT, no evident difference was observed between the effect of sodium content in those samples prepared with fumed silica compared and those samples prepared with TEOS. Based on these results, it was determined to prepare BEA-14 AU with fumed silica. The silicon sources are listed in Table 3-4.

Table 3-4 Silicon source for the β -zeolite/FT catalyst samples that were tested in the FT reactor

BEA-10AUT	BEA-11AUT	BEA-12AUT	BEA-13AUT	BEA-14AUT
Fumed Silica	Fumed Silica	TEOS 99.999%	TEOS 99.999%	Fumed Silica

3.2 Fischer Tropsch reaction test

It was decided to test five different samples of β -zeolite/FT catalysts and one of pure Fischer Tropsch cobalt-based catalyst to obtain a reference line of the activity and selectivity of the pure catalyst.

The tested β -zeolite/FT catalyst BEA-10 AUT to BEA-14 AUT were synthesized with the method of pretreated FT catalyst with TEA-OH followed by standard hydrothermal synthesis, the procedure was describe in section 2.1.4.

The first set of tested catalysts was BEA-10 AUT to BEA-13 AUT. In the case of the products with white and black phase, only black phases were tested because those are the ones with the active FT catalyst. The results from the first test called RUN360 show that the silicon source did not have a relevant impact.

Additionally, RUN361 was run using pure FT cobalt-based catalyst. This run provided a baseline that would serve as reference for the analysis.

The composition for BEA-14 AUT was defined based on the following:

- The results of activity and selectivity in the test RUN360 showed that fumed silica as silicon source gives good results. Therefore, BEA-14 AUT was synthesized with fumed silica.
- It was required to cover the gap between the results of RUN360 and RUN361, in terms of rate, selectivity, and final product composition.

The last tested material was BEA-14 AUT in test RUN362.

In all the Fischer Tropsch plots the legend names of the tested β -zeolite/FT catalyst were simplified. Instead of BEA-10 AUT to BEA-14 AUT, BEA10 to BEA14 were used. The data represented in the bar plots was based in the average of the last adjustment of syngas flow to obtain approximately 50% CO conversion.

An important assumption was used to estimate the amount of the FT catalyst in the β -zeolite/FT catalyst hydrothermal products. The assumption was that the total amount of pure FT cobalt-based catalyst was employed in the hydrothermal synthesis ends in the final β -zeolite/FT catalyst product. The recovered product from the hydrothermal synthesis after treatment was weighted and the difference between the final weight and the original amount of pure FT catalyst added in each recipe was the fixed β -zeolite to the FT catalyst.

The mass composition of the tested products is described in Table 3-5. Column A represents the amount of pure Fischer Tropsch cobalt-based catalyst employed in the hydrothermal synthesis as reactant. Column B represents the estimated percentage of FT catalyst in the final product β -zeolite/FT catalyst after the hydrothermal synthesis and column C is the balance of the β -zeolite/FT catalyst.

Table 3-5 Mass composition of the β -zeolite/FT catalyst and pure FT cobalt-based catalyst tested in the Fischer Tropsch reactor

	A	B	C
		wt% FTc	wt% β -zeolite
BEA-10 AUT	90 g FTc	87%	13%
BEA-11 AUT	17 g FTc	59%	41%
BEA-12 AUT	31 g FTc	62%	38%
BEA-13 AUT	31 g FTc	75%	25%
BEA-14 AUT	70 g FTc	86%	14%
Co12Re0.3	-	100%	0%

Despite the higher content of FT cobalt-based in the recipe of some β -zeolite/FT catalyst the final products contain less. The reduction of the FT catalyst presence in the final product was originated by the spontaneous phase separation at the end of the hydrothermal synthesis. For example BEA-12 AUT contains large amount of pure FT catalyst as reactant (31g) in the hydrothermal synthesis compared with BEA-11 AUT that contains almost half (17g) of the FT catalyst amount, however the final percentage in the β -zeolite/FT catalyst was practically the same (Table 3-6).

This fact also explain the difference between BEA-13 AUT and BEA-12 AUT that contain exactly the same FT catalyst amount as reactant (31g), nevertheless the estimated weight percentage was different. BEA-12 AUT contains 38 wt% of β -zeolite while BEA-13 AUT contains only 25 wt% of β -zeolite, the weight percentage difference is because in BEA-12 AUT β -zeolite/FT catalyst product did not present phase separation at the end of the hydrothermal synthesis.

Table 3-6 Mass composition of the β -zeolite/FT catalyst and pure FT cobalt-based catalyst, including white and black phases, seed-assisted procedure and TEA-OH pretreatment. Samples are sorted according to FT catalyst content

	FT catalyst as reactant	Estimated wt% FTc	White/Black phase	Seed-Assisted	TEA-OH pretreatment
Co12Re0.3	-	100	No	No	Yes
BEA-10 AUT	90 g FTc	87	No	No	Yes
BEA-14 AUT	70 g FTc	86	Yes	No	Yes
BEA-13 AUT	31 g FTc	75	Yes	Yes	Yes
BEA-12 AUT	31 g FTc	62	No	No	Yes
BEA-11 AUT	17 g FTc	59	Yes	No	Yes

Besides the rigorous control of temperature, pressure, and syngas flow during the complete Fischer Tropsch synthesis, syngas flow was adjusted based on CO conversion. To obtain comparable data with the standard Fischer Tropsch test, the flow must be adjusted until approximately 50% CO conversion is obtained, as depicted in Fig. 3-14.

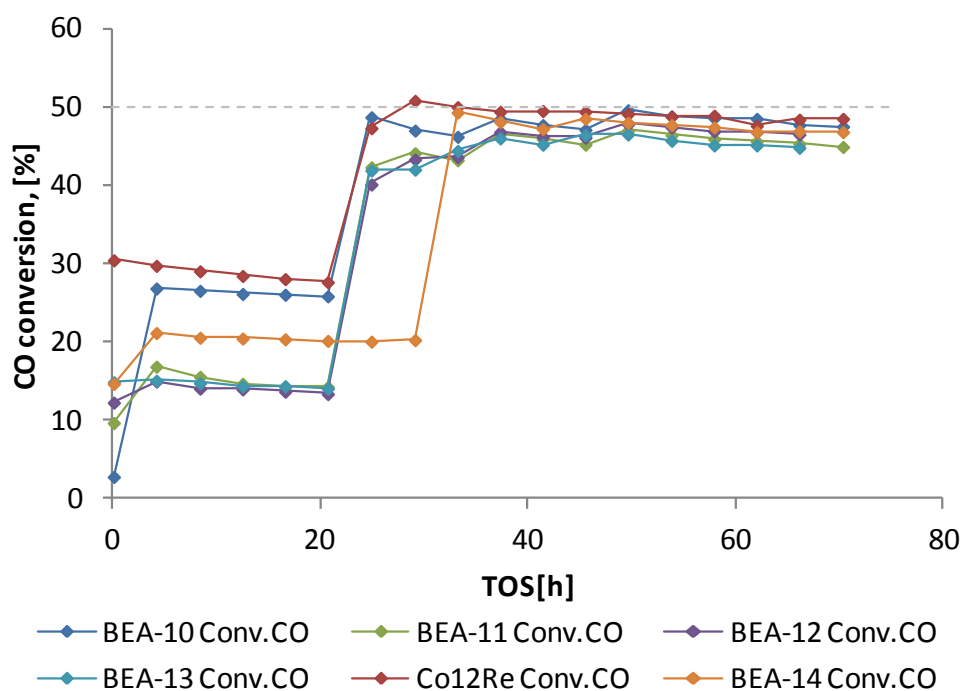


Fig. 3-14 Carbon Monoxide conversion in the Fischer Tropsch reaction test

Typical syngas flow adjustments for the conventional Fischer Tropsch cobalt-based catalyst did not work as was expected. The presence of the β -zeolite creates different reaction conditions that made difficult the exact estimation of the syngas adjustment as depicted in Fig. 3-15. The adjustments in the gas flow to obtain approximately 50% CO conversion in

BEA-13 AUT did not have the same behavior as the other β -zeolite/FT catalyst tested in RUN360.

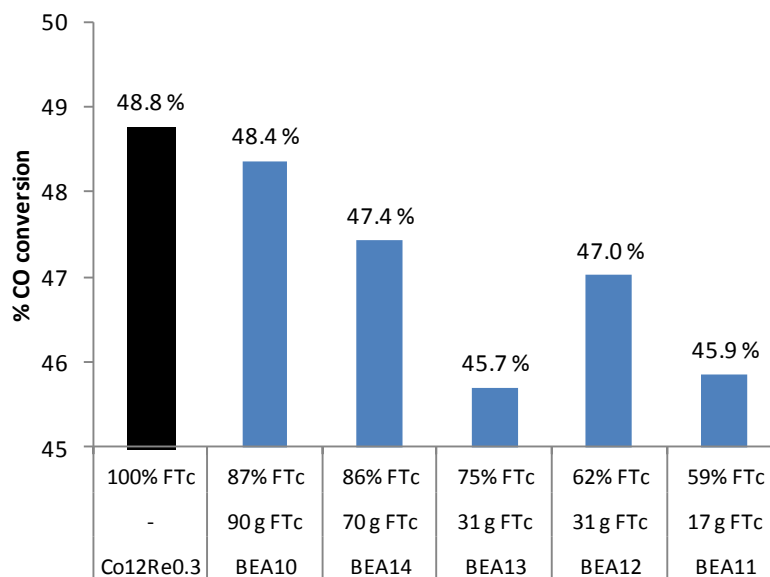


Fig. 3-15 Carbon Monoxide 50% conversion in the Fischer Tropsch reaction test. Samples are sorted according to FT catalyst content

The unexpected result for BEA-13 AUT suggests that further syngas flow adjustments would have been required to obtain 50% CO conversion. This evidence suggests that the activity in the catalyst was decremented faster because more adjustments were required in the same process conditions. The others β -zeolite/FT catalysts behaved as expected, higher amounts of β -zeolite in the catalyst composition lower activity the β -zeolite/FT catalyst in the Fischer Tropsch synthesis.

The difference in BEA-13 AUT was the use of the seed-assisted procedure described in section 2.1.4. There is evidence that the seed assisted procedure might generate a different structure in the β -zeolite/FT catalyst. This finding was supported by the XRD powder pattern of BEA-13 AUT, that presents very short peaks compared to BEA-12 AUT that have the same chemical components in the recipe.

Fig. 3-16 shows that as the percentage of β -zeolite increases, the generation of methane also increases. This can be explained as a negative effect of the β -zeolite's acidic sites promotion of methane generation. This effect was also noticed in ethane and ethene generation, the amount of these hydrocarbon gases increment as the percentage of β -zeolite increases.

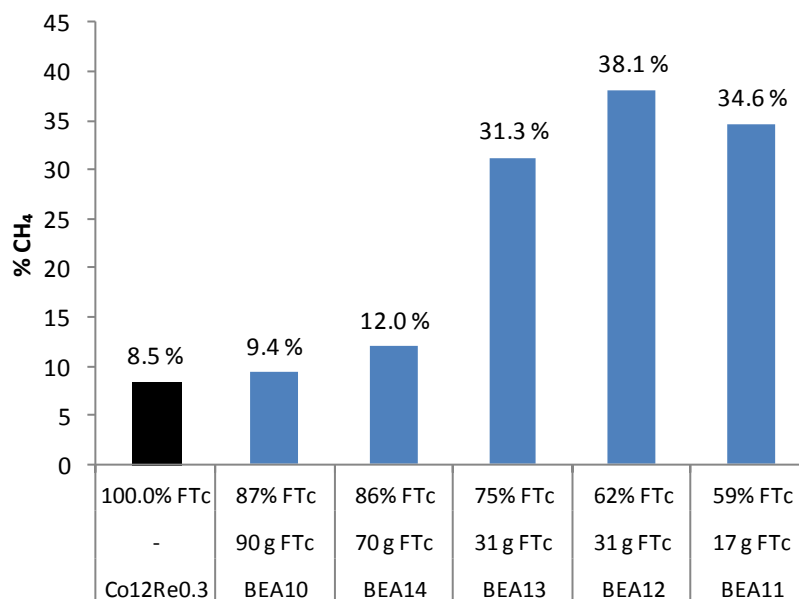


Fig. 3-16 Methane generation of the different samples in FT reaction test. Samples are sorted according to FT catalyst content

The effect of the acidic sites of β -zeolite is a trade-off that should be accepted in order to generate jet fuel hydrocarbons. The optimal trade-off is still to be definitely established, but BEA-14 AUT should be close to an appropriate value.

It was observed that from C₃ to C₆ hydrocarbon products (Fig. 3-17), the sum of the percentage of the olefins and paraffins in the FT synthesis product remains relatively constant among the different tested β -zeolite/FT catalysts that were sampled.

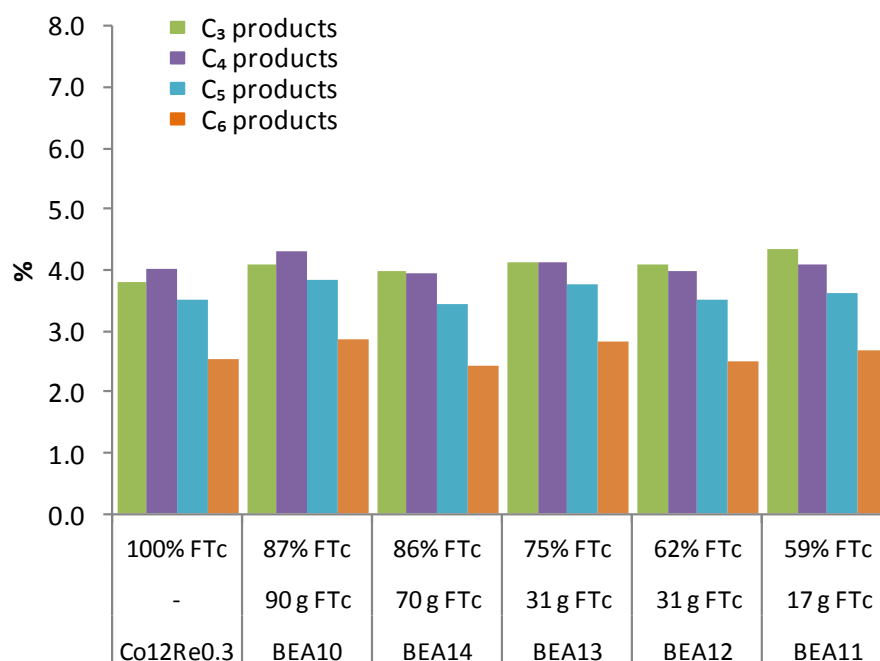


Fig. 3-17 C₃ to C₆ hydrocarbon products of the different samples in FT reaction test. Samples are sorted according to FT catalyst content

It was expected mass and heat transfer limitation in the β -zeolite/FT catalyst. β -zeolite is a material with ultra regular micropore structure, the micropore structures of zeolites cause diffusion limitations during the desorption of products from the surface to the pore system and the diffusion of products out of the pore system. The presences of β -zeolite change the performance of catalyst when is comparing with and standard Fischer Tropsch cobalt-based catalyst (Co12Re0.3).

However, the olefin/paraffin ratio varied among the tested FT catalysts. Fig. 3-18 shows the variations in the olefin/paraffin ratio. This effect can be explained with the fact that as the percentage of zeolite increases, diffusion restrictions become more severe and the hydrogen pressure higher, leading to secondary hydrogenation of the olefins. In order to understand the increase of diffusion restrictions it is important to remember that zeolite pores are in the range of micropores, while FT catalyst alumina support pores are in the range of mesopores. Micropores offer many times very high selectivity of products but the diffusion limitation is still an important concern.

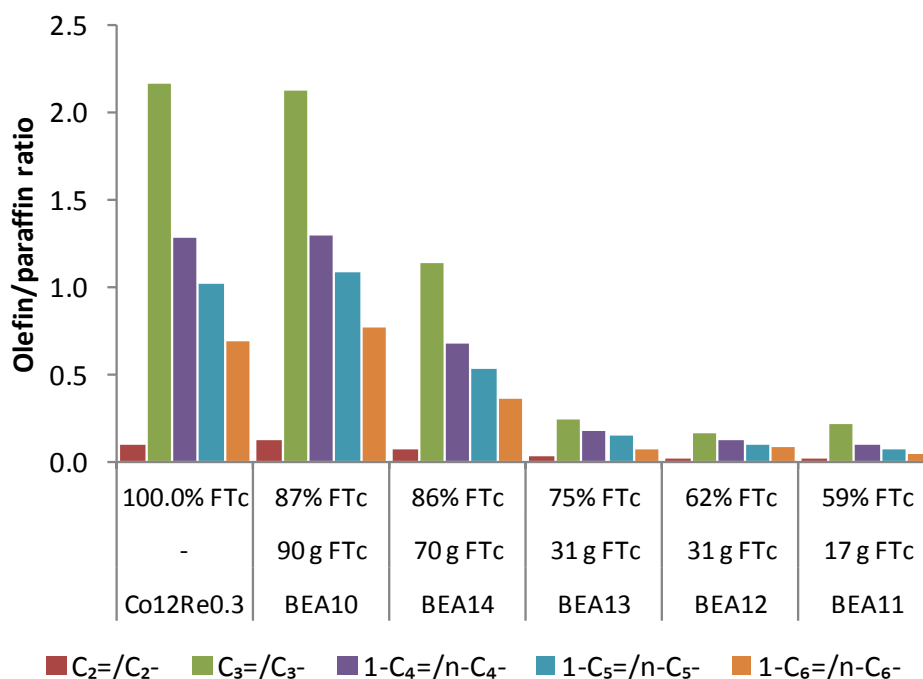


Fig. 3-18 Olefin to paraffin ratio of the different samples in FT reaction test. Samples are sorted according to FT catalyst content

The Anderson-Schulz-Flory distribution equation predicts the distinct production of hydrocarbons in the Fischer Tropsch synthesis. The distributions estimate to products with

high selectivity, methane or waxes. The selection of which one would be the predominant product is based in the FT metal-based catalyst, the process conditions and the promoters used during the synthesis of the FT catalyst. The proper amount of β -zeolite could alter this distribution promoting the generations of low amount of methane but shifting the wax range from lowering the proportion of heavy waxes and increasing the proportion of medium waxes.

As the amount of methane increases due to the high content of β -zeolite in the tested catalyst, the quantity of C_5+ components decreases (Fig. 3-19). This predictable behavior could be easily explained by the fact that the source of hydrocarbons were carbon monoxide and hydrogen. If those components react as methane the availability of the reactant gases decreases resulting in less abundance of the various long-chained products compared to methane.

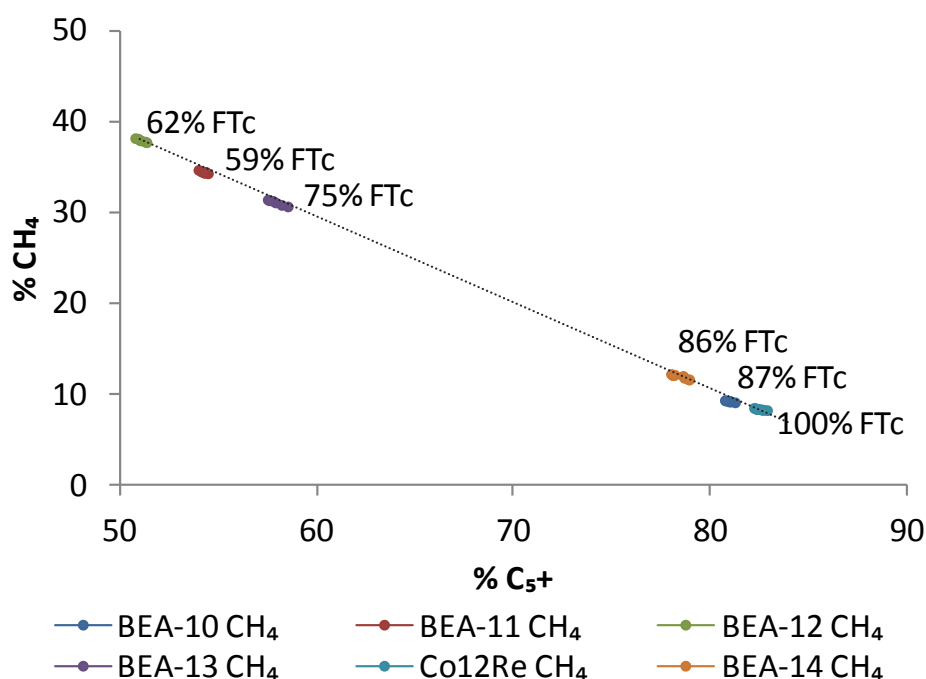


Fig. 3-19 Methane as function of C_5+ components. The plotted data were based in the last adjustment of gas flow to obtain approximately 50% CO conversion. Dotted line is used as reference to show the linearity of the results

The linear relationship between methane and C_5+ products for the tested β -zeolite/FT catalyst offers a practical way to estimate the amount of pure FT catalyst during the hydrothermal synthesis. The synthesized product could cover the gap between BEA-13 AUT (75 wt% FT estimated) and BEA-14 AUT (86 wt% FT estimated). The estimation would be performed by a simple linear interpolation.

The abnormal behavior of BEA-12 AUT and BEA-11 AUT could be described by the fact that the Parr autoclave is not the proper reactor to perform hydrothermal zeolite synthesis because the Teflon liner is not full sealed. This could lead to obtaining two different products at the end of the hydrothermal synthesis, some products with only one phase and some products with two phases (black and white).

In standard zeolite synthesis is typical it to obtain two phases at the end of the hydrothermal synthesis. One of the phases is the liquids in the solutions as water and organic template free of solids. The other phase contains the solids such as the silicon source and the aluminum source. In the particular case of the β -zeolite/FT catalyst hydrothermal synthesis when two phases were obtained the liquid phase contained almost pure β -zeolite and the solid phase contained the β -zeolite/FT catalyst. This could be avoided changing the Parr autoclave reactor with a reactor with a fully enclosed liner.

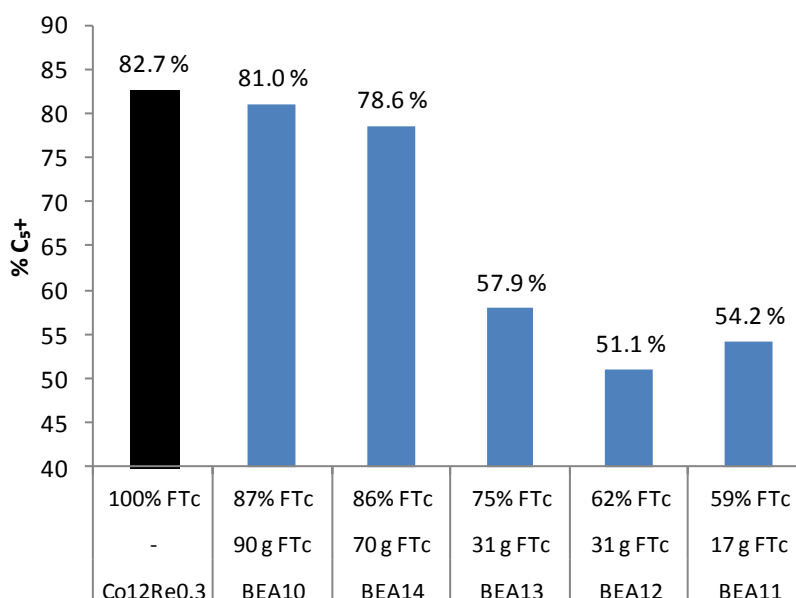


Fig. 3-20 Total percentage of C₅₊ generated during the FT tests. The data were based in the average of the last adjustment of gas flow to obtain approximately 50% CO conversion

As methane increases with high amount of β -zeolite in the β -zeolite/FT catalyst the opposite effect is expected in the C₅₊ generation. As depicted in Fig. 3-20 the presence of higher amounts of β -zeolite reduce the amount of C₅₊. This is a positive result in terms of jet fuel production, the obtained solid hydrocarbon products with the β -zeolite/FT catalyst are softer waxes compare to the obtained with pure Fischer Tropsch cobalt-based catalyst.

It was noted that the recovered waxy products from the FT synthesis of the β -zeolite/FT catalysts were consistently softer compared to waxes generated from the pure FT cobalt-based catalyst. This fact is a clear qualitative evidence that the wax produced with β -zeolite/FT catalyst are hydrocarbons with lower molecular weight as is expected when β -zeolite is included in the structure of the FT cobalt-based catalyst.

The jet fuel products could be obtained with the inclusion of β -zeolite in the FT cobalt-based catalyst. BEA-14 AUT was the most promising β -zeolite/FT catalyst to obtain jet fuel products. Further chromatography analysis must be performed to the waxy products to identify and classify the complete set of produced hydrocarbons in the presences of β -zeolite in the FT catalyst and establish how the molecular weight was shifted to the low molecular weight solid hydrocarbons.

The complete set of results of the FT tests can be consulted in **Appendix G**.

4. Conclusions

BET technique is a very precise method to measure the surface area and pore characteristics in many materials but in the particular case of zeolites, that possess ultra regular pores and cages in the micro range scale, BET must be adapted to obtain meaningful results. Performed measurements in two different ranges from 0.01 to 0.95 and from 0.01 to 0.30 offer diverse results. The short pressure range shows that when increasing β -zeolite content, the overall surface area also increases, as expected. The large pressure range shows that increasing β -zeolite content, pore size and volume decrease, also as expected.

XRD proved to be a useful tool to prove that calcination at 550°C removes the template completely and does not damage the crystalline structure of FT cobalt-based catalyst and there is not any evidence of sintering of the metal. XRD showed that is a useful tool to determine the presence of β -zeolite and FT cobalt-based catalyst in the β -zeolite/FT catalyst samples. Moreover, it was possible to determine the crystallinity of the final product. As expected, when increasing the amount of β -zeolite, crystallinity of the final product increases. XRD demonstrated that the γ -alumina powder pattern peaks were overlapped by the FT cobalt-based catalyst peaks.

SEM images show perfectly how the β -zeolite is attached to the Fischer Tropsch cobalt-based spherical particle. The smooth surface in the original FT catalyst turns to a powdered surface. A high magnification of the samples shows the evident presence of β -zeolite due to their characteristic appearance of “cabbage-like” agglomerates. SEM is a reference that helps to determine the presence of the β -zeolite over the surface, but cannot be employed as a quantitative tool to determine the abundance of the β -zeolite over the surface. Advanced techniques of sample preparation could be used to obtain images of the internal pores of the alumina covered by β -zeolite via SEM, the images could show the β -zeolite layer over the alumina pores and cavities. S(T)EM images could provide useful information about the chemical composition of the different components present in the β -zeolite/FT catalyst.

Chemisorption helps to determine the metal dispersion of cobalt over the β -zeolite/FT catalyst surface. The not calcined samples lost more weight during the chemisorption sequence due to template decomposition. The crystallite size was determined with the metal dispersion result. The slight difference between the obtained crystallite factor (99.6) and the reported in the references (96) shows how β -zeolite change the surface of the catalyst including the crystallite sizes.

Regarding the different available silicon sources, Ludox would have negative effects in the FT reaction due to its high sodium content. When analyzing the performance of catalysts prepared with fumed silica and TEOS 99.999%, no evident difference was observed. As fumed silica is a much less expensive silicon source, it seems to be the appropriate option.

The characterization techniques provided vast amount of useful information about the physical and chemical composition of the synthesized β -zeolite/FT catalyst and how the presence of β -zeolite increases the surface area and can cause interferences during the metals dispersion measurements in chemisorption.

Seed assisted procedure accomplishes the idea of obtaining a different product that could change the syngas conversion. Unfortunately this change is not optimal, the result is against the expected one. The recommendation is to not use this procedure in further investigations of β -zeolite/FT catalyst synthesis.

It is relevant to perform further investigations of the spontaneous phase separation, in order to have full control of the hydrothermal synthesis products. The collected information in the present work does not offer a clear evidence of when or how one or two phase products were produced. Crucial change to have better control of the hydrothermal synthesis is the Parr autoclave reactor substitution.

Fischer Tropsch reaction test is the most relevant tool to prove how the selectivity of the synthesized β -zeolite/FT catalyst was tailored to obtain higher amounts of C_5 - C_{17} , soft wax hydrocarbons, in the range of jet fuel.

The current efforts related to the novel FT catalyst developments are to minimize as much as possible the methane generation without the excessive generation of hard waxes. FT synthesis results of the β -zeolite/FT catalyst show that the amount of β -zeolite could generate softer waxes but the amount of the zeolite must not exceed 25 wt% because the production of methane would be very high, at least 4 times more than the pure FT cobalt-based catalyst. The recommendation is a β -zeolite/FT catalyst that produce 15 vol% of methane.

Based on the linear relation of methane and C_{5+} , β -zeolite/FT catalyst that produce 15 vol% of methane would produce 75.4 vol% of C_{5+} .

The total amount of Ethene/Ethane had similar behavior to methane. At higher content of β -zeolite in the catalyst, the generation of Ethene/Ethane increases. This increase was at least two times compared to pure FT cobalt-based catalyst.

For the rest of the measured components, the total amount of Propene/Propane, 1-Butene/n-Butane, 1-Pentene/n-Pentane, and 1-Hexene/n-Hexane remains almost the same. The notorious difference was the change in the olefin/paraffin ratio due to the high content of β -zeolite. As diffusion restrictions become more severe and the hydrogen pressure higher, the percentage of olefins decreases and the paraffins increase because secondary hydrogenation of the olefins occurs.

Among the synthesized catalysts, based on the FT synthesis test BEA-14 AUT shows the best performance and properties to be the ideal candidate in the production of jet fuel hydrocarbon products range.

The linear relation of methane and C_{5+} among the different β -zeolite/FT catalyst tested allows estimating the composition of a catalyst that can cover the gap between BEA-14 AUT (86 wt% estimated FT catalyst) and BEA-13 AUT (75 wt% estimated FT catalyst). A product with 80 wt% of FT catalyst and without phase separation during hydrothermal synthesis would be have an optimal trade-off between soft waxes production and low methane generation.

The differences in the C_{5+} production between BEA-12 AUT and BEA-11 AUT under the same FT synthesis conditions, is evidence that the spontaneous phase separation must be controlled in order to keep the percentage of FT catalyst and β -zeolite as is planning in the recipe. An autoclave with fully enclosed liner can provide this stability during the hydrothermal synthesis.

During the FT synthesis products recovery, physical evidence of soft wax materials was noticed with the inclusion on β -zeolite in the FT catalyst. This evidence supports the fact that the hard waxes were shifted to more soft waxes. Jet fuel product can be produced from this soft waxes.

Further investigation of the composition of the waxy products can provide better results about the quantity of jet fuel that could be produce by β -zeolite/FT catalyst.

5. Further work

- Analyze the solid products (waxes), obtained during the Fischer Tropsch reaction test of the β -zeolite/FT catalyst. The analysis would provide useful data of C_5 to C_{17} content to estimate jet fuel production.
- Improve the autoclave reactor and Teflon liner to perform further β -zeolite/FT catalyst synthesis. A fully enclosed liner will provide much better reaction conditions.
- Change the agitation method, autoclave reactor rotating instead of a propeller inside the liner. This agitation improvement also guarantees better distribution of the heat inside the sealed Teflon liner.
- Employ S(T)EM images to obtain information about the chemical composition of the different components present in the β -zeolite/FT catalyst.
- Perform SEM images inside the catalyst pores.
- Develop a method that includes the influence of zeolites during metals dispersion via chemisorption.

6. Bibliography

- [1] S. Kulprathipanja, *Zeolites in Industrial Separation and Catalysis*. Great Britain: John Wiley & Sons, 2010, p. 569.
- [2] M. E. Dry, “The Fischer–Tropsch process: 1950–2000,” *Catal. Today*, vol. 71, no. 3–4, pp. 227–241, Jan. 2002.
- [3] A. de Klerk and E. Furimsky, *Catalysis in the Refining of Fischer-Tropsch Syncrude*. Cambridge: Royal Society of Chemistry, 2010.
- [4] J. A. Moulijn, M. Makkee, and A. E. van Diepen, *Chemical Process Technology*, 2nd ed. Wiley, 2013, p. 580.
- [5] J. G. Speight, *The Biofuels Handbook*. The Royal Society of Chemistry, 2011, pp. P001–555.
- [6] A. H. Lillebø, E. Patanou, J. Yang, E. A. Blekkan, and A. Holmen, “The effect of alkali and alkaline earth elements on cobalt based Fischer–Tropsch catalysts,” *Catal. Today*, vol. 215, pp. 60–66, Oct. 2013.
- [7] Y. Richardson, J. Blin, and A. Julbe, “A short overview on purification and conditioning of syngas produced by biomass gasification: Catalytic strategies, process intensification and new concepts,” *Prog. Energy Combust. Sci.*, vol. 38, no. 6, pp. 765–781, 2012.
- [8] R. A. Meyers, Ed., *Encyclopedia of Sustainability Science and Technology*. New York, NY: Springer New York, 2012.
- [9] R. Oukaci, A. H. Singleton, and J. G. Goodwin, “Comparison of patented Co F–T catalysts using fixed-bed and slurry bubble column reactors,” *Appl. Catal. A Gen.*, vol. 186, no. 1–2, pp. 129–144, Oct. 1999.
- [10] J. M. Andersson, “Controlling the Formation and Stability of Alumina Phases,” Department of Physics, Chemistry and Biology, 2005.
- [11] N. P. Østbø, “Evolution of Alpha Phase Alumina in Agglomerates upon Addition to Cryolitic Melts,” Faculty of Natural Sciences and Technology, 2002.
- [12] D. Schanke, S. Eri, E. Rytter, C. Aaserud, A.-M. Hilmen, O. A. Lindvåg, E. Bergene, and A. Holmen, “Fischer-Tropsch synthesis on cobalt catalysts supported on different aluminas,” *Studies in Surface Science and Catalysis*, vol. 147. Statoil R and D, Research Centre, Postuttak, N-7005 Trondheim, Norway, pp. 301–306, 2004.
- [13] M. Ojeda, R. Nabar, A. U. Nilekar, A. Ishikawa, M. Mavrikakis, and E. Iglesia, “CO activation pathways and the mechanism of Fischer–Tropsch synthesis,” *J. Catal.*, vol. 272, no. 2, pp. 287–297, Jun. 2010.

- [14] Ø. Borg, S. Eri, E. Rytter, and A. Holmen, "Fischer-Tropsch synthesis over different alumina supported cobalt catalysts," in *ACS National Meeting Book of Abstracts*, 2006, vol. 232.
- [15] Ø. Borg, "Role of Alumina Support in Cobalt Fischer-Tropsch Synthesis," Faculty of Natural Sciences and Technology, 2007.
- [16] E. Rytter, L. Lefferts, R. Keiski, Ø. Borg, N. Hammer, S. Eri, O. A. Lindvåg, R. Myrstad, E. A. Blekkan, M. Rønning, and A. Holmen, "Fischer-Tropsch synthesis over un-promoted and Re-promoted γ -Al₂O₃ supported cobalt catalysts with different pore sizes," *Catal. Today*, vol. 142, no. 1–2, pp. 70–77, 2009.
- [17] K. H. J. Buschow, R. W. Cahn, M. C. Flemings, B. Ilschner, E. J. Kramer, and S. Mahajan, *Encyclopedia of Materials: Science and Technology, Vol 1-11*. Elsevier, 2001, p. 9913.
- [18] C. Colella and W. S. Wise, "The IZA Handbook of Natural Zeolites: A tool of knowledge on the most important family of porous minerals," *Microporous Mesoporous Mater.*, no. 0, Aug. 2013.
- [19] M. Niwa, N. Katada, and K. Okumura, *Characterization and Design of Zeolite Catalysts*, vol. 141. Berlin, Heidelberg: Springer Berlin Heidelberg, 2010.
- [20] J. Čejka, A. Corma, and S. Zones, Eds., *Zeolites and Catalysis*. Weinheim, Germany: Wiley-VCH Verlag GmbH & Co. KGaA, 2010.
- [21] IZA, "International Zeolite Association," 2013. [Online]. Available: <http://www.iza-online.org/default.htm>. [Accessed: 01-Dec-2013].
- [22] H. van Bekkum, E. M. Flanigen, P. A. Jacobs, and J. C. Jansen, Eds., *Studies in Surface Science and Catalysis*, vol. 137. Elsevier, 2001, p. 1062.
- [23] WILEY, Ed., *Wiley Critical Content - Petroleum Technology, Volume 1-2*. John Wiley & Sons, 2007, p. 2000.
- [24] C. Baerlocher, L. B. McCusker, and D. H. Olson, *Atlas of Zeolite Framework Types*. Elsevier, 2007, p. 404.
- [25] L. Lloyd, *Handbook of Industrial Catalysts*. Boston, MA: Springer US, 2011.
- [26] J. Weitkamp, "Zeolites and catalysis," *Solid State Ionics*, vol. 131, no. 1–2, pp. 175–188, Jun. 2000.
- [27] O. L. Eliseev, M. V. Tsapkina, O. S. Dement'eva, P. E. Davydov, A. V. Kazakov, and A. L. Lapidus, "Promotion of cobalt catalysts for the Fischer-Tropsch synthesis with alkali metals," *Kinet. Catal.*, vol. 54, no. 2, pp. 207–212, Apr. 2013.
- [28] A. L. Lapidus, O. L. Eliseev, M. V. Tsapkina, O. S. Belousov, and V. V. Gushchin, "Potassium as a promoter in the Co-based Fischer-Tropsch catalysis," *Russ. Chem. Bull.*, vol. 59, no. 9, pp. 1834–1835, Jan. 2011.

- [29] C. M. Balonek, A. H. Lillebø, S. Rane, E. Rytter, L. D. Schmidt, and A. Holmen, "Effect of Alkali Metal Impurities on Co–Re Catalysts for Fischer–Tropsch Synthesis from Biomass-Derived Syngas," *Catal. Letters*, vol. 138, no. 1–2, pp. 8–13, May 2010.
- [30] A. A. Adesina, "Hydrocarbon synthesis via Fischer-Tropsch reaction: travails and triumphs," *Appl. Catal. A Gen.*, vol. 138, no. 2, pp. 345–367, May 1996.
- [31] A. Y. Khodakov, A. Holmen, C. Mirodatos, Y. Wang, W. Ma, G. Jacobs, J. Kang, D. E. Sparks, M. K. Gnanamani, V. R. R. Pendyala, W. D. Shafer, R. A. Keogh, U. M. Graham, G. A. Thomas, and B. H. Davis, "Fischer–Tropsch synthesis. Effect of alkali, bicarbonate and chloride addition on activity and selectivity," *Catal. Today*, vol. 215, pp. 73–79, 2013.
- [32] A. Nakhaei Pour, S. M. K. Shahri, Y. Zamani, M. Irani, and S. Tehrani, "Deactivation studies of bifunctional Fe-HZSM5 catalyst in Fischer-Tropsch process," *J. Nat. Gas Chem.*, vol. 17, no. 3, pp. 242–248, Sep. 2008.
- [33] L. a. Vytnova, E. I. Bogolepova, a. N. Shuikin, V. I. Kurkin, E. V. Marchevskaya, and G. a. Kliger, "Fischer-Tropsch synthesis on aluminum oxide-and zeolite-diluted catalysts," *Pet. Chem.*, vol. 46, no. 2, pp. 103–109, Mar. 2006.
- [34] I. Chorkendorff and J. W. Niemantsverdriet, *Concepts of Modern Catalysis and Kinetics*. Weinheim, FRG: Wiley-VCH Verlag GmbH & Co. KGaA, 2003.
- [35] M. A. Vannice, *Kinetics of Catalytic Reactions*. Boston, MA: Springer US, 2005.
- [36] ASME-D1655, "D1655-13 - Standard Specification for Aviation Turbine Fuels." ASTM International, p. 17, 2013.
- [37] ASME-D7566, "D7566-13 - Standard Specification for Aviation Turbine Fuel Containing Synthesized Hydrocarbons." ASTM International, p. 25, 2013.
- [38] I. LEE, "Rhodium supported on thermally enhanced zeolite as catalysts for fuel reformation of jet fuels," *Catal. Today*, vol. 136, no. 3–4, pp. 258–265, Jul. 2008.
- [39] H. Robson and K. P. Lillerud, Eds., *Verified Synthesis of Zeolitic Materials*, Second. Amsterdam: Elsevier Science, 2001, p. 177.
- [40] Parr Instrument Company, "Series 4560 Mini Reactors," *June 2014*, 2014. [Online]. Available: <http://www.parrinst.com/products/stirred-reactors/series-4560-100-600-ml-mini-reactors/>.
- [41] R. R. Willis and A. I. Benin, *From Zeolites to Porous MOF Materials - The 40th Anniversary of International Zeolite Conference, Proceedings of the 15th International Zeolite Conference*, vol. 170. Elsevier, 2007, pp. 242–249.
- [42] C. J. Brinker, "Hydrolysis and condensation of silicates: Effects on structure," *J. Non. Cryst. Solids*, vol. 100, no. 1–3, pp. 31–50, Mar. 1988.

- [43] V. S. Ramachandran and J. J. Beaudoin, *Handbook of Analytical Techniques in Concrete Science and Technology*. New York, NY, USA: William Andrew Publishing, 2001, p. 934.
- [44] M. M. J. Treacy and J. B. Higgins, Eds., *Collection of Simulated XRD Powder Patterns for Zeolites*. Amsterdam: Elsevier Science B.V., 2007, p. 586.
- [45] V. Gold, *Compendium of Chemical Terminology*. International Union of Pure and Applied Chemistry - IUPAC, 1987, p. 1670.
- [46] S. Todorova, V. Zhelyazkov, and G. Kadinov, "IR, TPR and chemisorption study of alumina-supported cobalt catalysts," *React. Kinet. Catal. Lett.*, vol. 57, no. 1, pp. 105–110, Jan. 1996.
- [47] M. Camblor, A. Corma, and S. Valencia, "Spontaneous nucleation and growth of pure silica zeolite- β free of connectivity defects," *Chem. Commun.*, no. 20, p. 2365, 1996.
- [48] R. N. Bhat and R. Kumar, "Synthesis of zeolite beta using silica gel as a source of SiO₂," *J. Chem. Technol. Biotechnol.*, vol. 48, no. 4, pp. 453–466, Apr. 2007.
- [49] Ø. B. Vistad, D. E. Akporiaye, and K. P. Lillerud, "Identification of a Key Precursor Phase for Synthesis of SAPO-34 and Kinetics of Formation Investigated by in Situ X-ray Diffraction," *J. Phys. Chem. B*, vol. 105, no. 50, pp. 12437–12447, Dec. 2001.

7. Appendixes

Appendix A

Synthesis of various zeotype materials

Via hydrothermal synthesis four different types of zeolites were prepared in SINTEF-Oslo. Using different recipes per each synthesis to gain inside for this master project work.

Chemical components

For the zeolites synthesis the following materials were used to obtain the specific structure and reaction conditions. Table A-1 and Table A-2 show the chemical involved in this work.

Table A-1 Chemical zeolite components A

	Material	Chemical name	CAS Number
Solvent	Water	Distillate water [39]	7732-18-5
Basics	NaOH	Sodium hydroxide	1310-73-2
Acids	H ₃ PO ₄	Phosphoric acid	7664-38-2
	HF	Hydrofluoric acid	7664-39-3
Template	20% TPA-OH 80% H ₂ O	Tetrapropylammonium hydroxide	4499-86-9
	40% TEA-OH 60% H ₂ O	Tetraethylammonium hydroxide	77-98-5
	MTEA-Br	Methyltriethylammonium bromide	2700-16-5
	C ₄ H ₉ O	Morpholine	110-91-8

Table A-2 Chemical zeolite components B

	Material	Chemical name	CAS Number	
Silica Source	30% SiO ₂ 70% H ₂ O	Colloidal silica suspension (LUDOX® AS-30)	7631-86-9	
	40% SiO ₂ 60% H ₂ O	Colloidal silica suspension (LUDOX® HS-40)	7631-86-9	
	SiO ₂	Fumed Silica	112945-52-5	
	1.0 SiO ₂ 0.5 H ₂ O	Silicic Acid	1343-98-2	
	Si(OC ₂ H ₅) ₄	Tetraethyl orthosilicate (TEOS)	78-10-4	
	Aluminum source	NaAlO ₂	Sodium aluminate	11138-49-1
		Al(OH) ₃	Aluminium hydroxide	1330-44-5
70% Al ₂ O ₃ 30% H ₂ O		Pseudoboehmite Catapal-B	8006-30-2	

In addition, an ion exchange technique was tested in the resulting zeolites to exchange sodium with cobalt and ammonium. The materials used during this test are shown in Table A-3.

Table A-3 Ion exchange chemical

	Material	Chemical name	CAS Number
Solvent	Water	Distillate water [39]	7732-18-5
		Water, with 0.04 μ S conductivity	
Salts	$\text{Co}(\text{NO}_3)_2 \cdot 6\text{H}_2\text{O}$	Cobalt(II) nitrate hexahydrate	10026-22-9
	NH_4Cl	Ammonium chloride	12125-02-9

Synthesis equipment

To perform all the experiments, autoclave equipments played an important role during the zeolite synthesis. Hydrothermal conditions must prevail during the crystallization.

In addition to develop the hydrothermal temperature conditions, a laboratory oven with a range temperature between 0-240°C was employed. The oven includes an internal fan to distribute the heat more homogenously; all the synthesis were made using the fan at 100% speed. The option to exchange the air into the oven was omitted to preserve homogeneous and constant temperature. The substitution of the air inside the oven chamber is only mandatory during drying procedures, not for heating uses. The used oven design was modified to include a rotating option; this modification in the oven allows very high dispersion of the materials inside the autoclave, changing the crystallization. The rotating autoclave option was used for a few zeolites syntheses, not for all of them.

After the synthesis period, the product was recovered and washed. To wash the material a Büchner flask, Büchner funnel and filter paper under vacuum system were used. The amount of water is not fixed, it depends on the quantity of zeolite. Normal values of water were 0.5 l per sample.

Some zeolites plugged the filter. An alternative to wash these materials was centrifugation. A centrifuge with 3400 rpm was used to sediment zeolites, the amount of water remains in the same value 0.5 l per sample.

The product was recovered either by filtration or centrifugation in a plastic Petri dish to dry. During drying an oven with a forced draft air fan was employed, to avoid losses of the zeolite mug when it was dry. The speed of the fan was very low, only to ensure a continue

movement of the air into the chamber. The incoming air accelerates the drying effect and prevents air water saturation inside the oven. The regular period of drying time was overnight, at 60°C.

Before calcination the zeolite was crushed and grounded with a mortar and pestle until a uniform white powder free of agglomerates or flakes was obtained. This step allows uniform heating of the sample during calcination.

To remove the remaining water and template from the zeolites micropores, a calcination step was required. The calcination was performed using an electrical muffle furnace with a sequence program, the sample was carried in a crucible. The first step was to remove traces of water, with a ramp of constant heat of 5°C/min, the temperature range was from room temperature to 100°C, once reached the temperature was kept for two hours. After two hours, the temperature was increased from 100°C to 550 °C, with a ramp of 2 °C/min and kept at 550-600°C for six hours. The temperature guarantees the complete decomposition and removal of the organic template. During this time, changes of color occurred during this step due to decomposition of the organic compound in the zeolite structure. The final step was the cooling from 550 to 30°C with a ramp of 3°C/min.

Zeolites recipes and treatment

A recipe is a procedure to synthesize zeolites. The main parts described in a recipe are: type of material, batch composition, source materials, batch preparation including amounts of each component, temperature conditions, synthesis time, recovery steps of the zeolite, and the expected results in the product characterization.

Reliable recipe sources are papers and books as the compendium of recipes published by the Synthesis Commission of the IZA called “*Verified Syntheses of Zeolitic Materials*” [39]. Some zeolites were synthesized via two different methods. The selected synthesized zeolites were shown in Table A-4.

Table A-4 Selected zeolite recipes to perform synthesis

IZA code	Reference document
BEA	<i>Camblor, Corma, and Valencia</i> [47]
	<i>Bhat and Kumar</i> [48]
CHA	Vistad, Akporiaye and Lillerud [49]
MFI	Robson and Lillerud [39]
MTW	Robson and Lillerud [39]

The general steps to perform a zeolite synthesis are listed below:

The first step to synthesize a zeolite is to follow exactly the recipe and kept a strict respect of the amounts of each component. The amounts determine the final ratio composition in the zeolite structure. The main components are: a source of silica oxide (SiO_2), a source of aluminum oxide (Al_2O_3), a source of template (organic compound), a source of counter ion (eg. Na^+ , K^+), and water (H_2O).

The second step is to mix all reactants. It is important to follow the right sequence to avoid agglomerates in the final solution. In the case of basic solutions it is good practice to dissolve the solids in water first, before the addition of the silica source. After the preparation of the solid-water solution and the addition of the silica source, it is relevant to stir, as much as possible to avoid flocks formation. Based on the recipe and the water content in the recipe, often the final mix of reactants looks like a very viscous whitish liquid. It is important to mix well all components, to get the same composition in the complete solution.

One recipe included the pre-step of preparing the seed for the MFI zeolite. The seed was prepared with a short time hydrothermal, around 16 h, process to obtain a seed gel. This gel contains very small crystals that were used as a nucleation material in the zeolite synthesis. The gel was sedimented for two hours, the solution was split in a light and heavy phase. The heavy phase was added to the rest of the reactants in an autoclave and follows the same reaction steps as a standard zeolite synthesis procedure.

Table A-5, Table A-6, as well as Table A-7 and Table A-8, include the information related to the reactants, amount of reactants and the molar composition of the solution.

Table A-5 BEA zeolite reactants recipe

Molar composition		Reactants	Amount, [g]
Recipe one			
1.00	SiO_2 :	Tetraethyl orthosilicate	25.98
0.54	HF:	Hydrofluoric acid	3.37
0.27	TEAOH:	Tetraethylammonium hydroxide	24.80
10.91	H_2O	Water	7.01
Recipe two			
59.80	SiO_2 :	Colloidal silica, Ludox 30	40.54
1.10	Al_2O_3 :	Sodium aluminate	0.79
3.10	Na_2O :	Sodium hydroxide	0.42
5.00	TEAOH:	Tetraethylammonium hydroxide	12.41
1500.00	H_2O	Water	55.38

Table A-6 CHA zeolite reactants recipe

Molar composition	Reactants	Amount, [g]
Recipe		
1.00 SiO ₂ :	Colloidal silica, Ludox 30	34.67
1.00 Al ₂ O ₃ :	Pseudoboehmite	12.26
1.00 P ₂ O ₅ :	Phosphoric acid	39.92
2.10 C ₄ H ₉ O:	Morpholine	31.99
60.00 H ₂ O	Water	154.67

Table A-7 MFI zeolite reactants recipe

Molar composition	Reactants	Amount, [g]
Recipe seed		
30.00 SiO ₂ :	Colloidal silica, Ludox 30	65.18
3.25 Na ₂ O:	Pseudoboehmite	5.66
2.27 TPAOH:	Tetrapropylammonium hydroxide	47.99
958.00 H ₂ O	Water	291.35
Recipe zeolite		
25.43 SiO ₂ :	Colloidal silica, Ludox 30	109.54
1.00 Al ₂ O ₃ :	Sodium aluminate	5.84
1.00 Na ₂ O:	Sodium hydroxide	3.45
1115.00 H ₂ O	Water	779.17

Table A-8 MTW zeolite reactants recipe

Molar composition	Reactants	Amount, [g]
Recipe		
100.00 SiO ₂ :	Colloidal silica, Ludox 30	65.54
1.00 Al ₂ O ₃ :	Aluminium hydroxide	1.71
10.00 Na ₂ O:	Sodium hydroxide	8.78
20.00 MTEA-Br:	Methyltriethylammonium bromide	42.79
2000.00 H ₂ O	Water	390.46

The third step is the hydrothermal synthesis process in which the zeolite structure is formed. The process conditions vary based on the zeolite structure. Typical syntheses crystallize between room temperature up to 200°C under autoclave equilibrium pressure; the required time ranges from hours to days. Synthesis times range for the four selected zeolites from less than a day up to 16 days of continued heating and crystal structure formation. The

complete set of reaction times and temperature conditions per each synthesis is shown in Table A-9.

Table A-9 Temperature and time conditions

Sample Name	Reaction time [days]	Reaction Temperature, [°C]	Sample batch
BEA-01	2.0	140	Batch 1
BEA-02	5.6	150	Batch 2
BEA-03	6.6	150	Batch 2
BEA-04	7.6	150	Batch 2
BEA-05	8.6	150	Batch 2
CHA-01	1.0	200	Batch 1
CHA-02	2.0	200	Batch 1
CHA-03	0.7	200	Batch 2
CHA-04	1.7	200	Batch 2
CHA-05	2.0	200	Batch 2
MFI-01	4.5	180	Batch 1
MFI-02	4.5	180	Batch 2
MTW-01	16.0	140	Batch 1
MTW-02	2.0	140	Batch 2
MTW-03	5.0	140	Batch 2
MTW-04	6.0	140	Batch 2

The evolution of some zeolites structure and crystallization was tracked with the preparation of one batch divided in different autoclaves. These samples were put at the same time in the oven and took out one by one, in a programmed sequence of reactions days. The purpose of this method was to follow the crystal evolution structure.

The fourth step is autoclave cooling. When the reaction was considered as finished, the autoclave was taken out of the oven. The cooling procedure is a very simple step with relevant considerations during the implementation, to avoid contamination of the final product. There are many ways to do it. The fastest way is to put the autoclave under water flow for a couple of minutes; the important part of this cooling strategy was to avoid water from entering into the autoclave due to the fast contraction of the metal against the internal Teflon liner. The addition of water unwittingly could lead in a change of composition and include more ions than expected. A safer and obviously longer procedure is cooling down by natural convection with air ambient temperature.

The water cooling method took around 10 min, while the natural cooling by convection took around 4 hours for the same size autoclave. The fast cooling does not affect the crystalline structure or morphology of the zeolite.

The fifth step is recovery. Once cooled the sample at room temperature, there is a standard procedure followed to recover the zeolites. The first step is to remove the water excess by decantation, the remaining sediment is the zeolite, with a metallic spatula removed the solid from the bottom of the Teflon liner. This solid was transferred to a Büchner flask with a Büchner funnel with a filter paper and washing three to four times (approximately 0.5 l) with distillate water under vacuum. In the last wash, the filtered water in the flask must be clear and free of any sediment or color. Excessive washing is not recommended; it is possible that the pH varies too much in the zeolite and the flocks deagglomerate and the filter paper cannot retain the small grains anymore. A signal of excessive washing is if after obtaining clear water in the flask, it turns to cloudy water appearance.

An option to recover and wash the zeolite is centrifugation. This was chosen when the washing liquid remained for more than five minutes into the Büchner funnel. The amount of water to use is the same as filtered.

The sixth step is drying. After the last wash, the zeolite contains large amounts of water trapped in the intraparticle structure. The filter paper containing the zeolite sample was placed in plastic Petri dishes without cover. This procedure was performed to remove the water retained over the zeolite surface. An oven under stagnant condition was used; the temperature was set at 60 °C. The oven was equipped, with a fan with a variable speed, the fan speed was set between 20-30% allowing continuous exchange of fresh air, and the samples remain into the oven for at least 6 h. The time varies based on the amount of the sample and the dispersion of the mug over the filter paper.

The seventh step is calcination. Before calcination the zeolite was crushed and grounded with a mortar and pestle until, obtaining a uniform white powder free of agglomerates or flakes. Calcination was performed to remove the template from the zeolite structure. The sample was weighted before and after calcination to follow how much organic material is removed. The process is performed in an electrical muffle furnace with a conventional fan to mix the internal air of the chamber, ensuring a uniform temperature.

The calcination procedure has several of steps, which are listed below:

1. The first step of the calcination is to remove completely any trace of water from the surface zeolites but also from the internal pores. With a programmed sequence the crucible that contains the zeolite sample was heated from room temperature up to 100 °C, with a ramp of 5°C/min and kept at 100°C for 2 h.
2. Two hours elapsed; the temperature was increased from 100°C to 550 °C with a ramp of 2°C/min, and kept at 550°C for 6 h. The high temperature guarantees the complete decomposition and remotion of the organic template. It is crucial heating up with a regular slow step size sequence as a ramp, the sudden increasing of heat destroy the internal structure of the zeolite due to the very fast expansion and evaporation of the water and the template.

A quick visual effect of wrong heating ramp procedure, after calcination is when the resulting powder is finer than the initial one. This destroys the pores and cavities in the zeolite structure.

During this time, changes of powder color occurred over the zeolite surface due to decomposition of the organic compound. The initial color of the zeolites powder was white, during calcination the color changes gradually from light color to dark and from dark to light again. The initial change of color occurred at 250°C a light beige color was in the zeolite, at 300°C a yellow color was present, at 350°C a light brown, at 400°C a dark brown was observed. The colors were the decomposition of the organic material in the zeolite. After six hours elapsed, the color of the powder returned to white in most cases with a few exceptions that remained in a slightly beige color.

3. Once accomplished the remotion of the template from the zeolite structure; the muffle furnace was cooled down to 30°C with a ramp of 3°C/min. The ramp sequence is not compulsory during the cooling step because the muffle furnace remains hot for a long period, but it is a good practice to perform as a normal procedure. The sudden cooling from 500°C to ambient temperature in a few minutes could lead to the damage the zeolite structure due to stress contracting forces.

The already calcined zeolite samples were collected in 10 ml wide mouth glass bottles with plastic lid, labeled with a three-letter code similar to the IZA code followed by a sequential sample number and stored for further characterization.

Additional procedures

Additional procedures were tested in order to cover a complete overview of the zeolite synthesis. The additional aspects covered were zeolite ionic exchange and the pelletization or tablet process.

Ionic exchange is a chemical technique that allows the exchange of ions in the zeolite structure in order to replace the counter ion for another one. The cation A (original one in the zeolite structure), is completely displaced by the selective uptake of cation B from the aqueous phase (the one in the solution).

The performed ionic exchange was a simple preparation of a salt dissolved in water with a known molar concentration (e.g. 0.1M). The salt must contain the ion to exchange (cation B). Based on the final requisites of the zeolite, different methods of ionic exchange could be performed. The first one includes a very high molar concentration of the ionic exchange solution, this method allows to exchange the desirable amount of ions in only two or three exchanges. Once realized each ionic exchange, the sample must be washed to remove the excess of solution to avoid the impregnation of the salt over the zeolite surface, to guaranty the substitution of the ions. A more reliable option is to prepare a solution with lower molar concentration and double ionic exchange contacts.

In both methods the samples are stirred for one hour with the solution that contain the ion to exchange, one hour elapsed the zeolite was washed and filtered with a very small amount of water to remove the small droplets of solution over the surface. Over-washing can remove the ion that was fixed and must be avoided. The final number of exchanged ions depended on how many counter ions the initial zeolite has. Finally, the zeolite sample must be dried again after the last ion exchange. The zeolite must be crushed and grounded again with a mortar and pestle until a uniform white powder free of agglomerates or flakes is obtained.

The pelletization process or tablet process is a useful method because zeolites are very fine powders; normally materials with a very small particle size are hard to handle due to static effects, ultra lightweight of each particle, and very compact bulk structure. The compact bulk structure origins a very high-pressure drop and the challenge of retaining very small particles inside a reactor, making difficult to avoid losses. The tablet process is only required if the zeolites will be used as a catalyst in the reactor. Zeolite tables are not easy to make, they do not stick together for long time. The use of binders as a zeolite adhesive is a common alternative to obtain uniform and stable tablets.

Appendix B

Risk Assessment

Before operate and run any experiment in the Parr autoclave risk assessment was elaborate to take in account the risk of the hydrothermal synthesis.

The risk value was obtained base on the risk matrix provided to perform the risk assessment that is accomplish with the regulations of Natural science faculty at Norwegian University of Science and Technology. This risk value was weighted in the human risk as a priority factor.

The risk assessment content 5 pages included in this appendix. The images depicted the performed risk assessment elaborated in February 2014.

NTNU  HSE	Hazardous activity identification process	Prepared by HSE section Approved by The Rector	Number HMSRV-26/01	Date 09.01.2013 Replaces 01.12.2006	
--	---	---	-----------------------	--	---

Unit: Department of Chemical Engineering, IKP **Date:** February 04th, 2014

Line manager: Edd Anders Blekkan

Participants in the identification process: Magnus Rønning (supervisor), Mario Ernesto Casalegno Garduño (student)

Short description of the main activity/main process: Master project for student: Mario Ernesto Casalegno Garduño.

Project title: Fischer-Tropsch catalysts for jet fuel production

Is the project work purely theoretical? (YES/NO): NO *Answer "YES" implies that supervisor is assured that no activities requiring risk assessment are involved in the work. If YES, briefly describe the activities below. The risk assessment form need not be filled out.*

Signatures: Responsible supervisor:  Student: 

ID nr.	Activity/process	Responsible person	Existing documentation	Existing safety measures	Laws, regulations etc.	Comments
1	Zeolite synthesis	Mario Casalegno	NTNU procedures.	Working conditions are below the max. operating conditions	NTNU-HSE regulations	Max operating conditions: temperature up to 250°C and pressure up to 70 bar
2	Zeolite-Catalyst support synthesis	Mario Casalegno	NTNU procedures.	Working conditions are below the max. operating conditions	NTNU-HSE regulations	Max operating conditions: temperature up to 250°C and pressure up to 70 bar
3						
4						
5						
6						

1

 HSE/KS	Risk assessment	Prepared by	Number	Date	
		HSE section	HMSRV2603E	04.02.2011	
		Approved by		Replaces	
		The Rector		01.12.2006	

Unit: Department of Chemical Engineering, IKP

Date: February 04th, 2014

Line manager: Edd Anders Blekkan

Participants in the identification process: Magnus Rønning (supervisor), Mario Ernesto Casalegno Garduño (student)

Short description of the main activity/main process: Master project for student: Mario Ernesto Casalegno Garduño.

Project title: Fischer-Tropsch catalysts for jet fuel production

Signatures: Responsible supervisor:  Student: 

Activity from the identification process form	Potential undesirable incident/strain	Likelihood:		Consequence:			Risk Value (human)	Comments/status Suggested measures
		Likelihood (1-5)	Human (A-E)	Environment (A-E)	Economy/material (A-E)			
Zeolite synthesis	Steam relief due to depressurization. Burns.	2	C	A	A	2C	Ensure that the seal is in perfect conditions, to support the pressure (16 bar) at 200°C. The rupture disc relief tubing is located in the back part of the foam hood. Use a sign of warning during running operation.	
Zeolite-Catalyst support synthesis	Steam relief due to depressurization. Burns.	2	C	A	A	2C	Ensure that the seal is in perfect conditions, to support the pressure (16 bar) at 200°C. The rupture disc relief tubing is located in the back part of the foam hood. Use a sign of warning during running operation.	

2

 HSE/KS	Risk assessment	Prepared by	Number	Date	
		HSE section	HMSRV2603E	04.02.2011	
		Approved by		Replaces	
		The Rector		01.12.2006	

--	--	--	--	--	--	--	--

Likelihood, e.g.:

1. Minimal
2. Low
3. Medium
4. High
5. Very high

Consequence, e.g.:

- A. Safe
- B. Relatively safe
- C. Dangerous
- D. Critical
- E. Very critical

Risk value (each one to be estimated separately):

- Human = Likelihood x Human Consequence
 Environmental = Likelihood x Environmental consequence
 Financial/material = Likelihood x Consequence for Economy/material

Potential undesirable incident/strain

Identify possible incidents and conditions that may lead to situations that pose a hazard to people, the environment and any materiel/equipment involved.

Criteria for the assessment of likelihood and consequence in relation to fieldwork

Each activity is assessed according to a worst-case scenario. Likelihood and consequence are to be assessed separately for each potential undesirable incident. Before starting on the quantification, the participants should agree what they understand by the assessment criteria:

Likelihood

Minimal 1	Low 2	Medium 3	High 4	Very high 5
Once every 50 years or less	Once every 10 years or less	Once a year or less	Once a month or less	Once a week

Consequence

Grading	Human	Environment	Financial/material
E Very critical	May produce fatality/ies	Very prolonged, non-reversible damage	Shutdown of work >1 year.
D Critical	Permanent injury, may produce serious serious health damage/sickness	Prolonged damage. Long recovery time.	Shutdown of work 0.5-1 year.

3

NTNU	Risk assessment	Prepared by	Number	Date	
		HSE section	HMSRV2603E	04.02.2011	
HSE/KS		Approved by		Replaces	
		The Rector		01.12.2006	

C Dangerous	Serious personal injury	Minor damage. Long recovery time	Shutdown of work < 1 month
B Relatively safe	Injury that requires medical treatment	Minor damage. Short recovery time	Shutdown of work < 1week
A Safe	Injury that requires first aid	Insignificant damage. Short recovery time	Shutdown of work < 1day

The unit makes its own decision as to whether opting to fill in or not consequences for economy/materiel, for example if the unit is going to use particularly valuable equipment. It is up to the individual unit to choose the assessment criteria for this column.

Risk = Likelihood x Consequence

Please calculate the risk value for "Human", "Environment" and, if chosen, "Economy/materiel", separately.

About the column "Comments/status, suggested preventative and corrective measures":

Measures can impact on both likelihood and consequences. Prioritise measures that can prevent the incident from occurring; in other words, likelihood-reducing measures are to be prioritised above greater emergency preparedness, i.e. consequence-reducing measures.

4

NTNU	Risk matrix	prepared by	Number	Date	
		HSE Section	HMSRV2604	8 March 2010	
HSE/KS		approved by	Page	Replaces	
		Rector	4 of 4	9 February 2010	

MATRIX FOR RISK ASSESSMENTS at NTNU

CONSEQUENCE	Extremely serious	E1	E2	E3	E4	E5
	Serious	D1	D2	D3	D4	D5
	Moderate	C1	C2	C3	C4	C5
	Minor	B1	B2	B3	B4	B5
	Not significant	A1	A2	A3	A4	A5
		Very low	Low	Medium	High	Very high
		LIKELIHOOD				

Principle for acceptance criteria. Explanation of the colours used in the risk matrix.

Colour	Description
Red	Unacceptable risk. Measures must be taken to reduce the risk.
Yellow	Assessment range. Measures must be considered.
Green	Acceptable risk Measures can be considered based on other considerations.

5

Appendix C

Brunauer-Emmett-Teller (BET)

Table C-1 β -zeolite (calcined) BET results with a pressure ratio 0.01 to 0.95

	BET Surface Area	Single point Pore Volume		BJH Pore Volume		BJH Pore Sizes	
		Ads	Des	Ads	Des	Ads	Des
	[m ² /g]	[cm ³ /g]	[cm ³ /g]	[cm ³ /g]	[cm ³ /g]	[nm]	[nm]
BEA-01AUT	0.4	-	-	0.0003	0.0006	2.45	22.79
BEA-03AUT	42.8	0.0697	0.0704	0.0822	0.0872	5.53	4.86
BEA-04AUT	198.2	0.2147	0.2166	0.1118	0.1112	3.22	3.13
BEA-05AUT	197.0	0.1898	0.1911	0.1797	0.1757	3.56	3.57
BEA-11AUT WHITE	103.6	0.2297	0.2288	0.0844	0.0810	3.71	4.03
BEA-13AUT WHITE	130.6	0.1898	0.1905	0.4132	0.4072	9.08	9.51
BEA-14AUT WHITE	142.1	0.2708	0.2688	0.2016	0.1989	5.15	5.39

Table C-2 β -zeolite/FT catalyst (calcined) BET results with a pressure ratio 0.01 to 0.95

	BET Surface Area	Single point Pore Volume		BJH Pore Volume		BJH Pore Sizes	
		Ads	Des	Ads	Des	Ads	Des
	[m ² /g]	[cm ³ /g]	[cm ³ /g]	[cm ³ /g]	[cm ³ /g]	[nm]	[nm]
Co12Re0.3	29.6	0.0231	0.0228	0.1730	0.1741	14.46	13.40
γ-alumina	175.0	0.0885	0.0884	-	-	-	-
BEA-06AUT	23.6	0.0325	0.0322	0.0839	0.0783	7.19	7.65
BEA-07AUT	60.4	0.0948	0.0958	0.1736	0.1426	4.98	6.12
BEA-08AUT	65.9	0.0948	0.0966	0.2327	0.2057	7.00	8.34
BEA-09AUT	58.5	0.0789	0.0797	0.2475	0.2459	8.66	9.07
BEA-10AUT	28.5	0.0258	0.0243	0.1304	0.1319	12.12	11.83
BEA-11AUT BLACK	40.8	0.0773	0.0783	0.0591	0.0635	5.09	4.35
BEA-12AUT	23.9	0.0364	0.0374	0.0670	0.0683	9.60	8.25
BEA-13AUT BLACK	22.4	0.0337	0.0327	0.0657	0.0726	13.72	8.75
BEA-14AUT BLACK	31.6	0.0380	-	0.1288	0.1286	9.69	9.96

Table C-3 β -zeolite (not calcined) BET results with a pressure ratio 0.01 to 0.95

	BET Surface Area	Single point Pore Volume		BJH Pore Volume		BJH Pore Sizes	
		Ads	Des	Ads	Des	Ads	Des
	[m ² /g]	[cm ³ /g]	[cm ³ /g]	[cm ³ /g]	[cm ³ /g]	[nm]	[nm]
BEA-11AUT WHITE WOC	41.8	0.0822	0.0823	0.0515	0.0499	5.86	6.14
BEA-13AUT WHITE WOC	79.9	0.0846	0.0823	0.3401	0.3391	10.66	10.91

Table C-4 β -zeolite/FT catalyst (not calcined) BET results with a pressure ratio 0.01 to 0.95

	BET Surface Area	Single point Pore Volume		BJH Pore Volume		BJH Pore Sizes	
		Ads	Des	Ads	Des	Ads	Des
	[m ² /g]	[cm ³ /g]	[cm ³ /g]	[cm ³ /g]	[cm ³ /g]	[nm]	[nm]
BEA-09AUT WOC	49.5	0.0637	0.0645	0.2115	0.2132	10.02	9.69
BEA-10AUT WOC	25.9	0.0237	0.0217	0.1121	0.1149	12.20	10.84
BEA-11AUT BLACK WOC	12.7	0.0214	0.0214	0.0246	0.0250	7.68	7.24
BEA-12AUT WOC	12.4	0.0151	0.0150	0.0480	0.0481	11.18	11.75
BEA-13AUT BLACK WOC	7.6	0.0090	0.0080	0.0447	0.0469	17.46	13.72
BEA-14AUT BLACK WOC	18.6	0.0177	0.0159	0.0912	0.0946	14.18	11.91

Table C-5 β -zeolite (calcined) BET results with a pressure ratio 0.01 to 0.30

	BET Surface Area	Single point Pore Volume		BJH Pore Volume		BJH Pore Sizes	
		Ads	Des	Ads	Des	Ads	Des
	[m ² /g]	[cm ³ /g]	[cm ³ /g]	[cm ³ /g]	[cm ³ /g]	[nm]	[nm]
BEA-01AUT	0.7	-	-	-	-	-	-
BEA-03AUT	132.5	0.0628	0.0626	0.0158	0.0167	2.08	2.07
BEA-04AUT	435.0	0.2168	0.2156	0.0622	0.0572	2.15	2.12
BEA-05AUT	386.8	0.1919	0.1901	0.0816	0.0797	2.11	2.11
BEA-11AUT WHITE	461.3	0.2221	0.2220	0.0376	0.0382	2.07	2.06
BEA-13AUT WHITE	382.3	0.1746	0.1747	0.0742	0.0736	2.10	2.09
BEA-14AUT WHITE	535.6	0.2542	0.2538	0.0606	0.0633	2.09	2.08

Table C-6 β -zeolite/FT catalyst (calcined) BET results with a pressure ratio 0.01 to 0.30

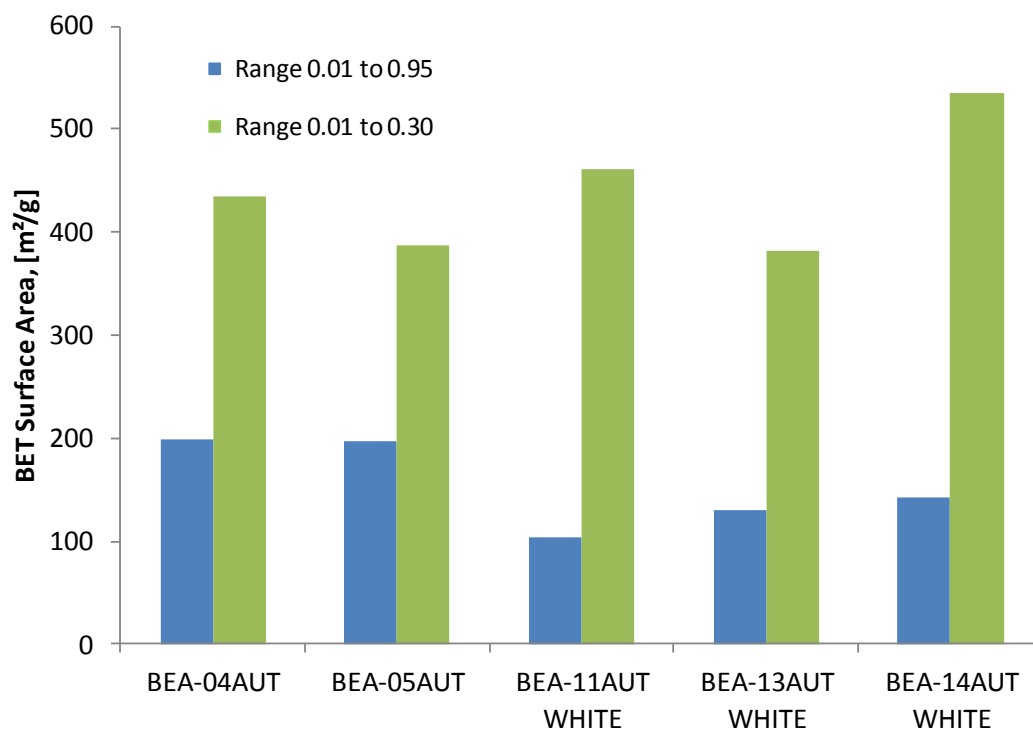
	BET Surface Area	Single point Pore Volume		BJH Pore Volume		BJH Pore Sizes	
		Ads	Des	Ads	Des	Ads	Des
	[m ² /g]	[cm ³ /g]	[cm ³ /g]	[cm ³ /g]	[cm ³ /g]	[nm]	[nm]
Co12Re0.3	46.6	0.0191	0.0189	0.0151	0.0135	2.12	2.09
γ-alumina	174.4	0.0887	0.0886	-	-	-	-
BEA-06AUT	59.2	0.0280	0.0281	0.0072	0.0071	2.04	2.01
BEA-07AUT	190.1	0.0866	0.0873	0.0883	0.0340	2.14	2.09
BEA-08AUT	188.4	0.0864	0.0865	0.0352	0.0346	2.09	2.09
BEA-09AUT	161.8	0.0729	0.0738	0.0703	0.0324	2.13	2.09
BEA-10AUT	50.7	0.0216	-	0.0112	0.0121	2.06	2.05
BEA-11AUT BLACK	153.7	0.0728	0.0730	0.0181	0.0178	2.09	2.07
BEA-12AUT	73.5	0.0340	-	0.0120	0.0113	2.11	2.05
BEA-13AUT BLACK	68.4	0.0322	-	0.0082	0.0079	2.08	2.03
BEA-14AUT BLACK	69.2	0.0327	-	0.0092	0.0087	2.00	2.09

Table C-7 β -zeolite (not calcined) BET results with a pressure ratio 0.01 to 0.95

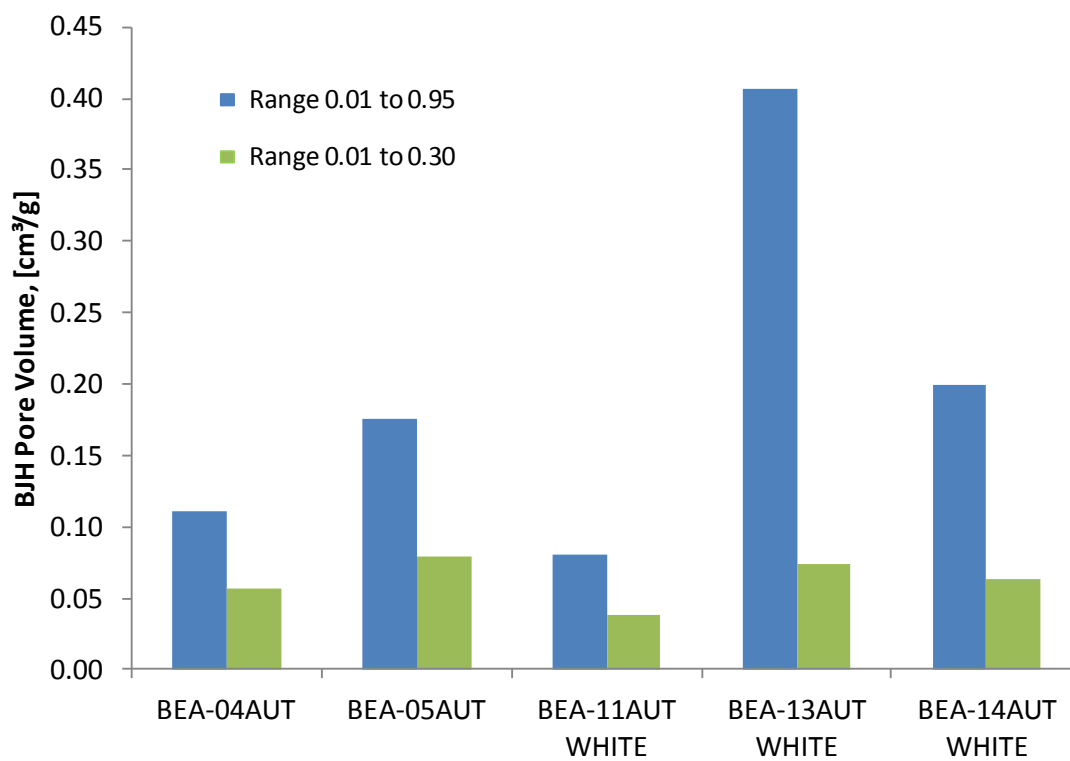
	BET Surface Area	Single point Pore Volume		BJH Pore Volume		BJH Pore Sizes	
		Ads	Des	Ads	Des	Ads	Des
	[m ² /g]	[cm ³ /g]	[cm ³ /g]	[cm ³ /g]	[cm ³ /g]	[nm]	[nm]
BEA-11AUT WHITE WOC	163.7	0.0791	-	0.0130	0.0123	2.02	2.04
BEA-13AUT WHITE WOC	166.8	0.0715	0.0707	0.0362	0.0374	2.07	2.08

Table C-8 β -zeolite/FT catalyst (not calcined) BET results with a pressure ratio 0.01 to 0.95

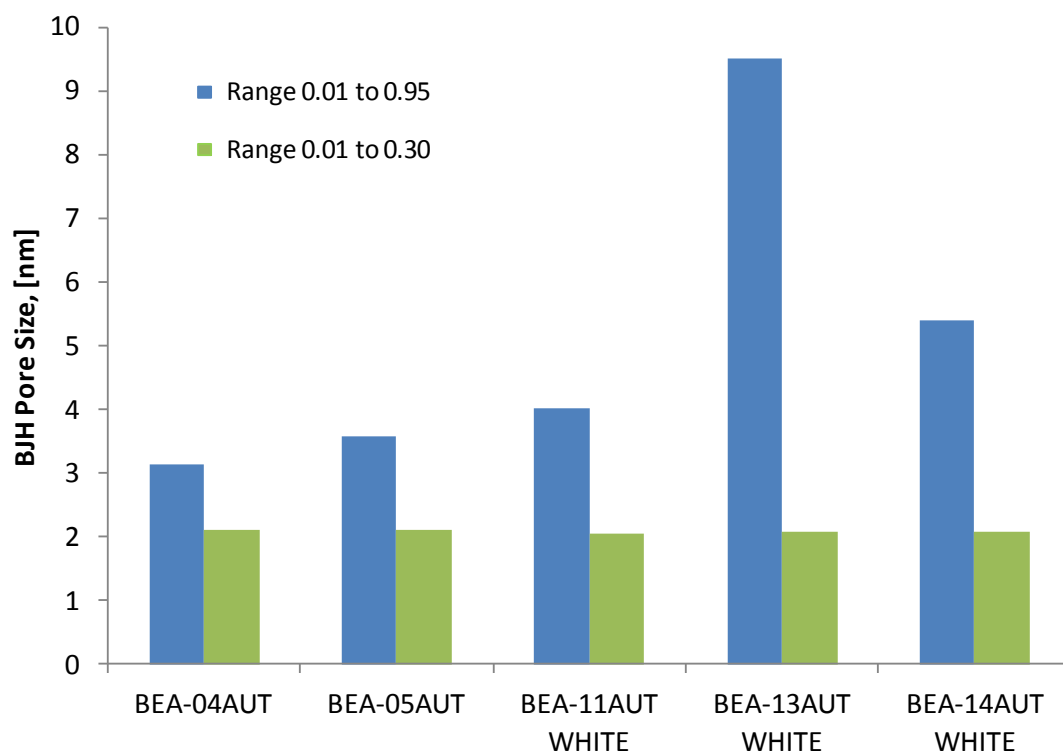
	BET Surface Area	Single point Pore Volume		BJH Pore Volume		BJH Pore Sizes	
		Ads	Des	Ads	Des	Ads	Des
	[m ² /g]	[cm ³ /g]	[cm ³ /g]	[cm ³ /g]	[cm ³ /g]	[nm]	[nm]
BEA-09AUT WOC	131.0	0.0585	0.0589	0.0432	0.0469	2.14	2.14
BEA-10AUT WOC	46.6	0.0200	-	0.0075	0.0086	2.03	2.03
BEA-11AUT BLACK WOC	41.2	0.0201	-	0.0030	0.0026	1.94	1.96
BEA-12AUT WOC	29.9	0.0135	-	0.0050	0.0056	2.00	2.01
BEA-13AUT BLACK WOC	18.5	0.0091	-	0.0041	0.0041	1.86	1.88
BEA-14AUT BLACK WOC	29.4	0.0140	-	0.0033	0.0051	1.88	1.99



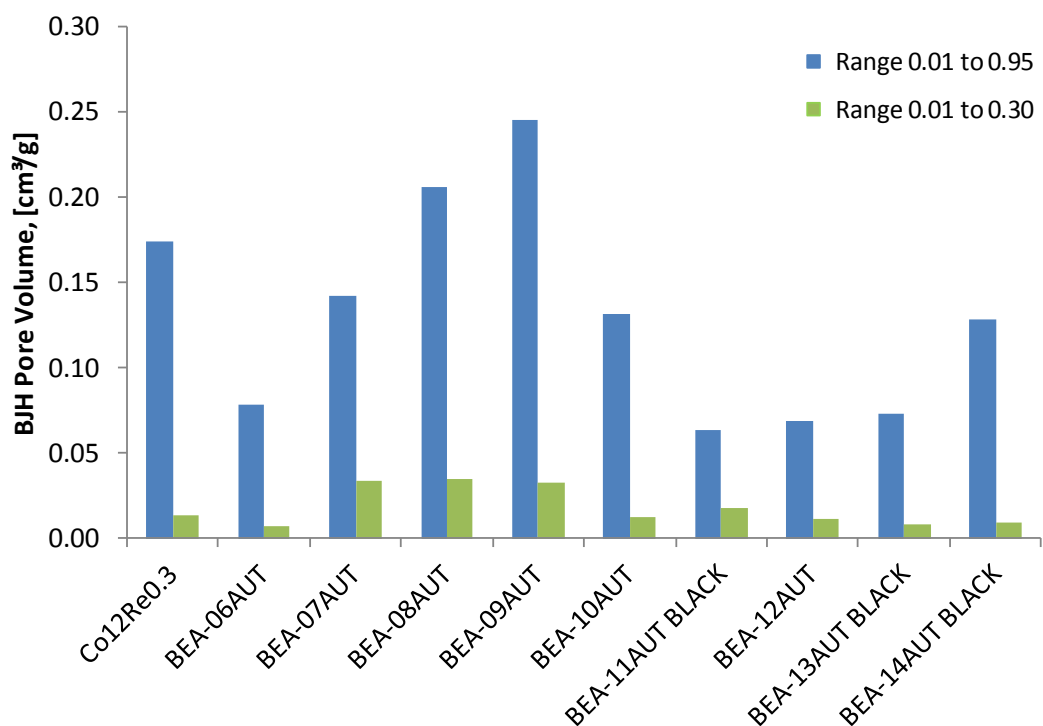
Pure β -zeolite BET surface area between range 0.01 to 0.95 versus range 0.01 to 0.30



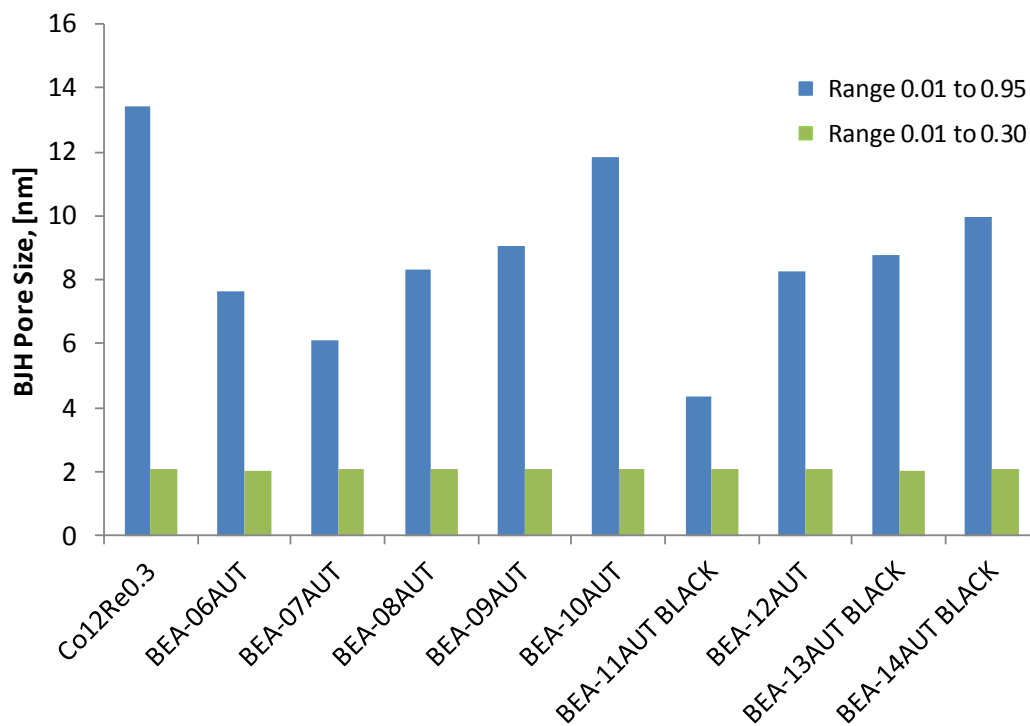
Pure β -zeolite BJH pore volume (desorption isotherm) between range 0.01 to 0.95 versus range 0.01 to 0.30



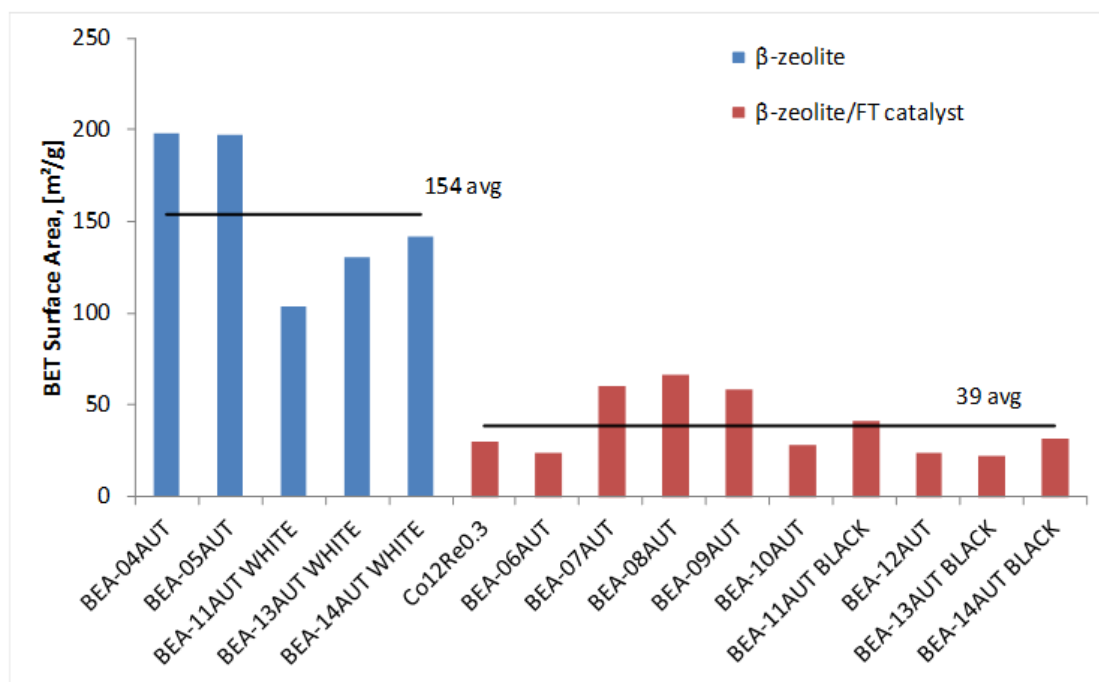
Pure β -zeolite BJH pore sizes (desorption isotherm) between range 0.01 to 0.95 versus range 0.01 to 0.30



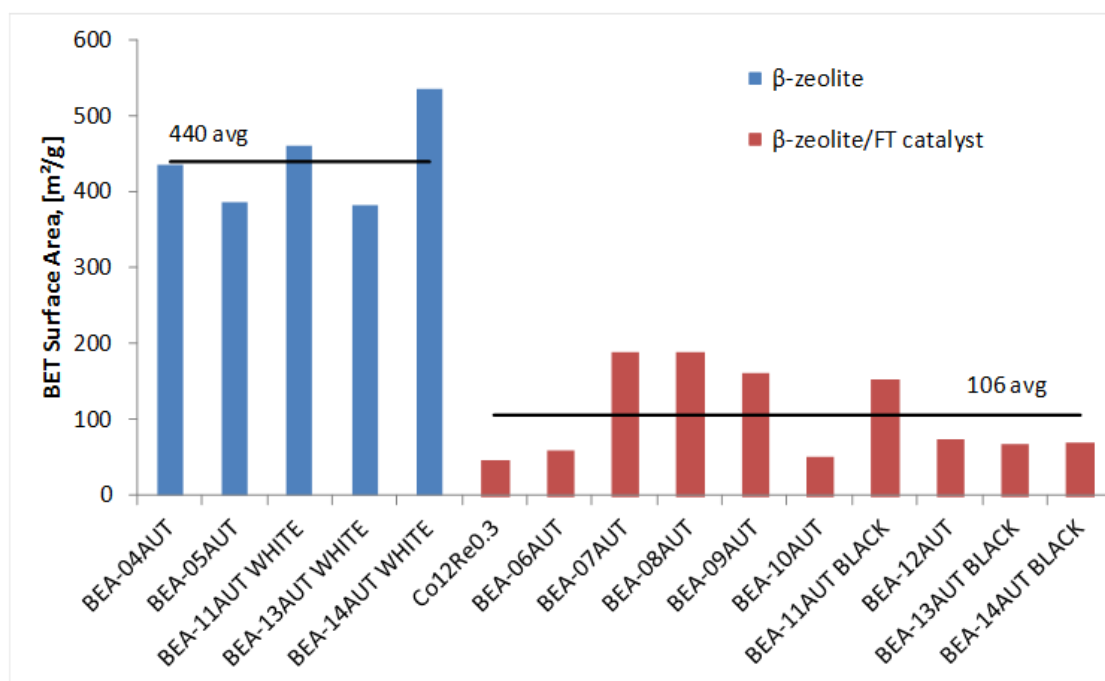
β -zeolite/FT catalyst BJH pore volume (desorption isotherm) between range 0.01 to 0.95 versus range 0.01 to 0.30



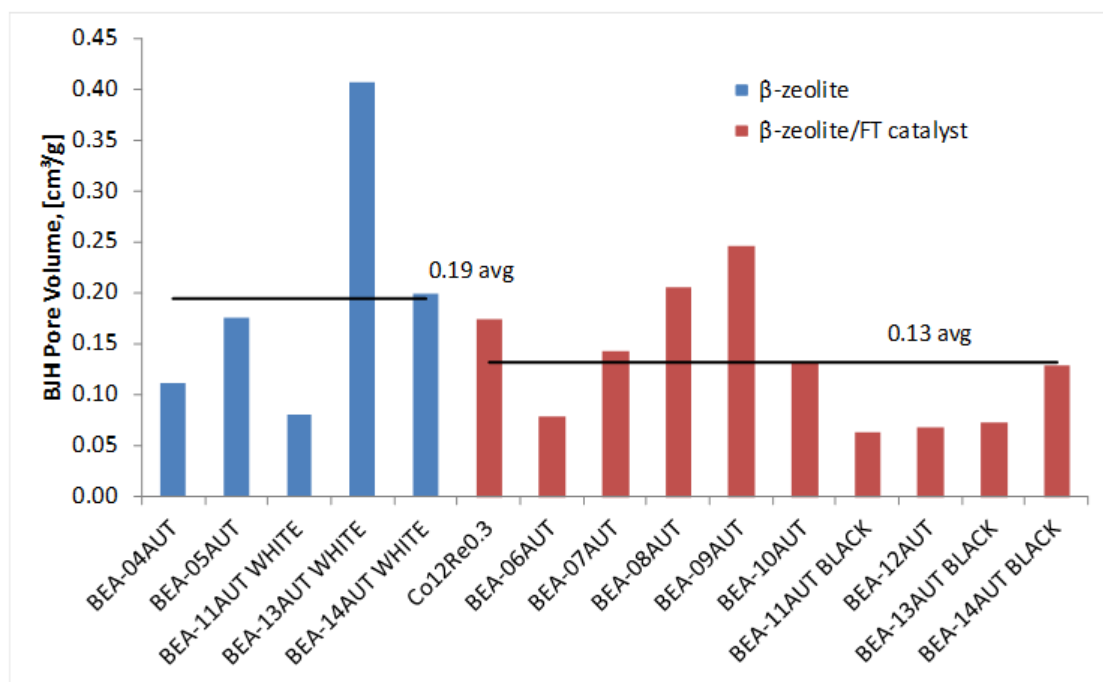
β -zeolite/FT catalyst BJH pore sizes (desorption isotherm) between range 0.01 to 0.95 versus range 0.01 to 0.30



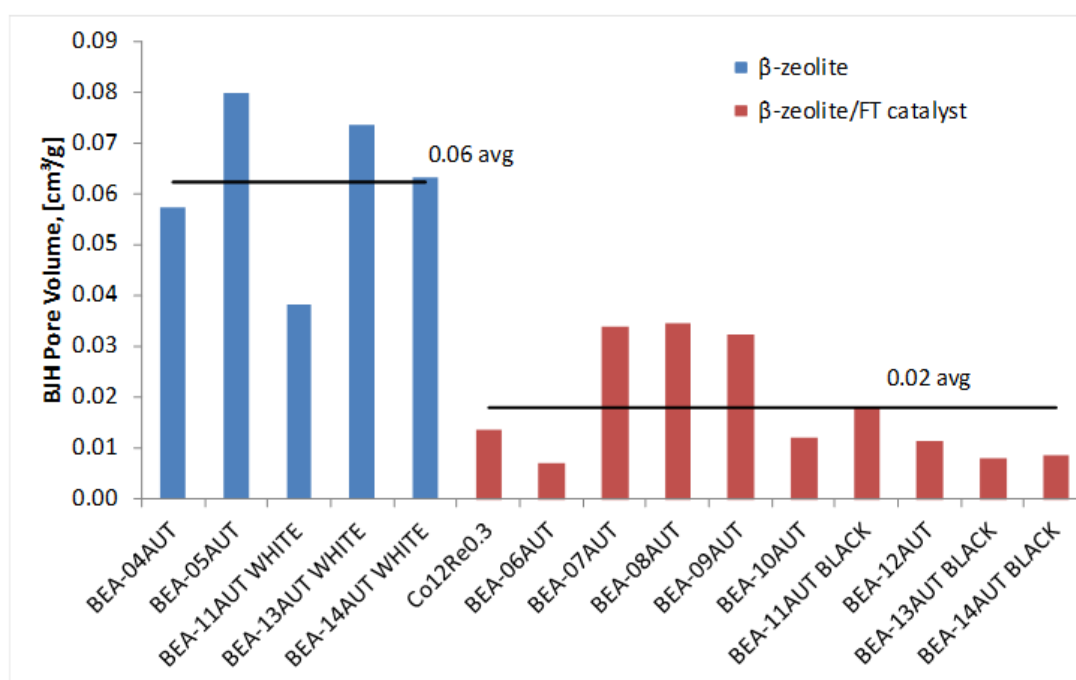
Pure β -zeolite versus β -zeolite/FT catalyst BET surface area range 0.01 to 0.95



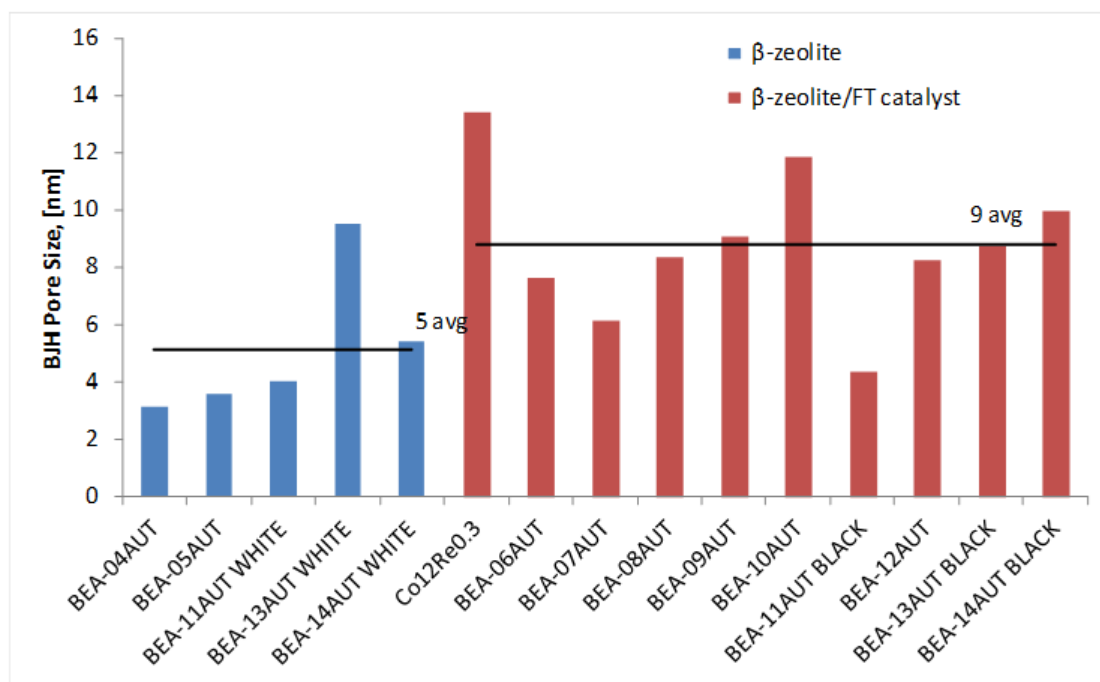
Pure β -zeolite versus β -zeolite/FT catalyst BET surface area range 0.01 to 0.30



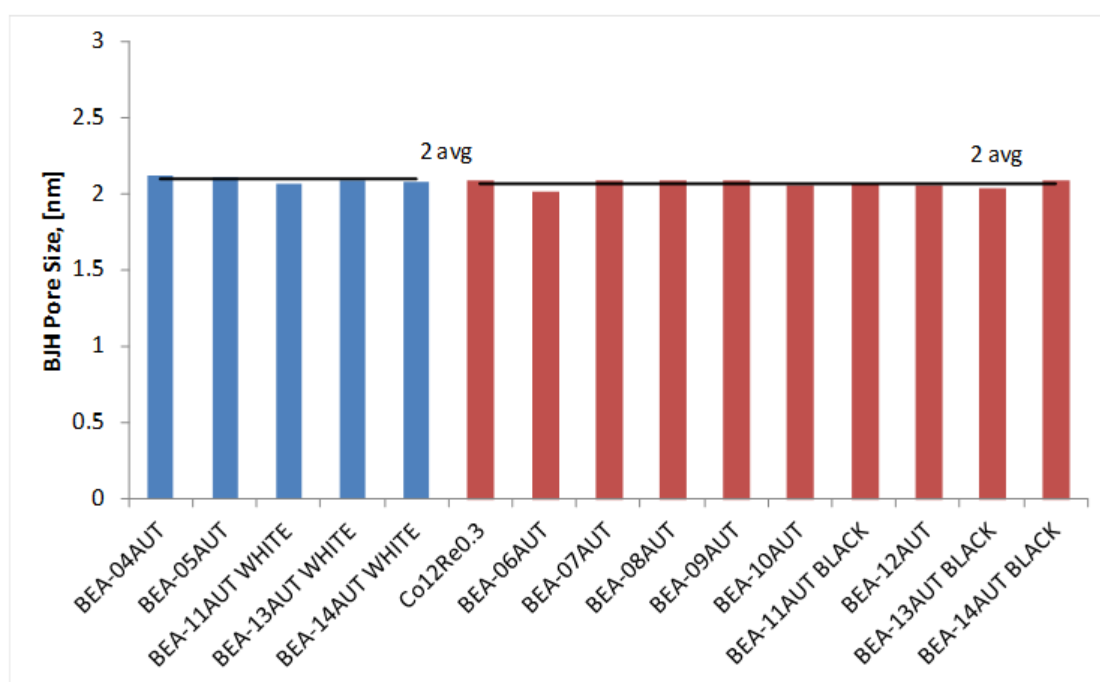
Pure β -zeolite versus β -zeolite/FT catalyst BJH pore volume (desorption isotherm) range
0.01 to 0.95



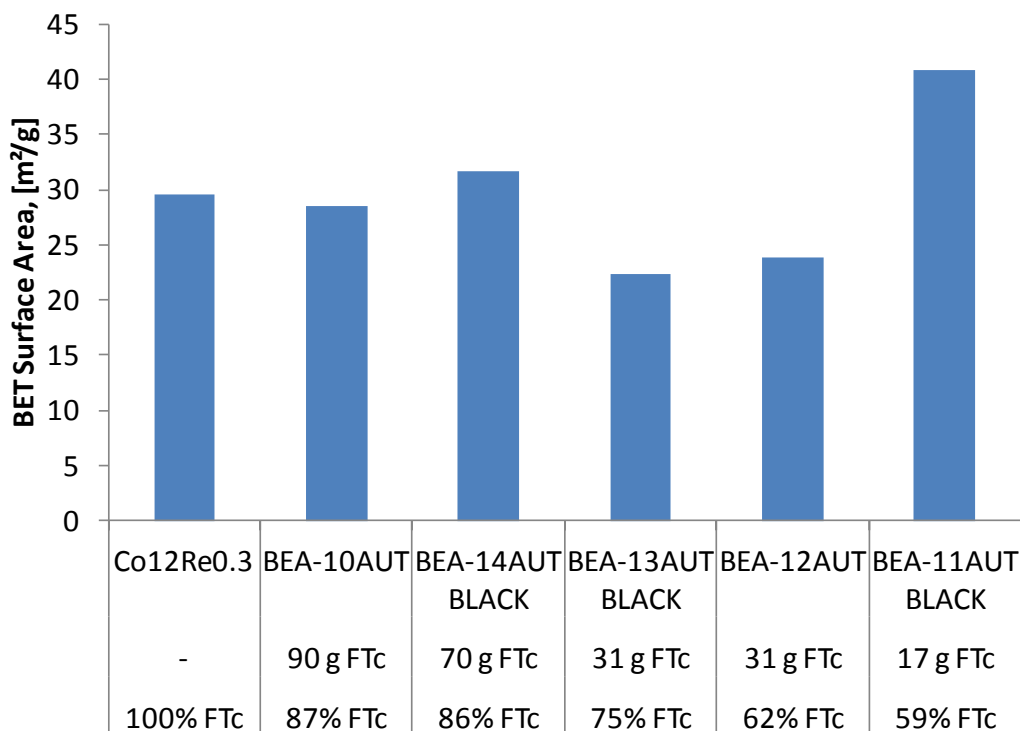
Pure β -zeolite versus β -zeolite/FT catalyst BJH pore volume (desorption isotherm) range
0.01 to 0.30



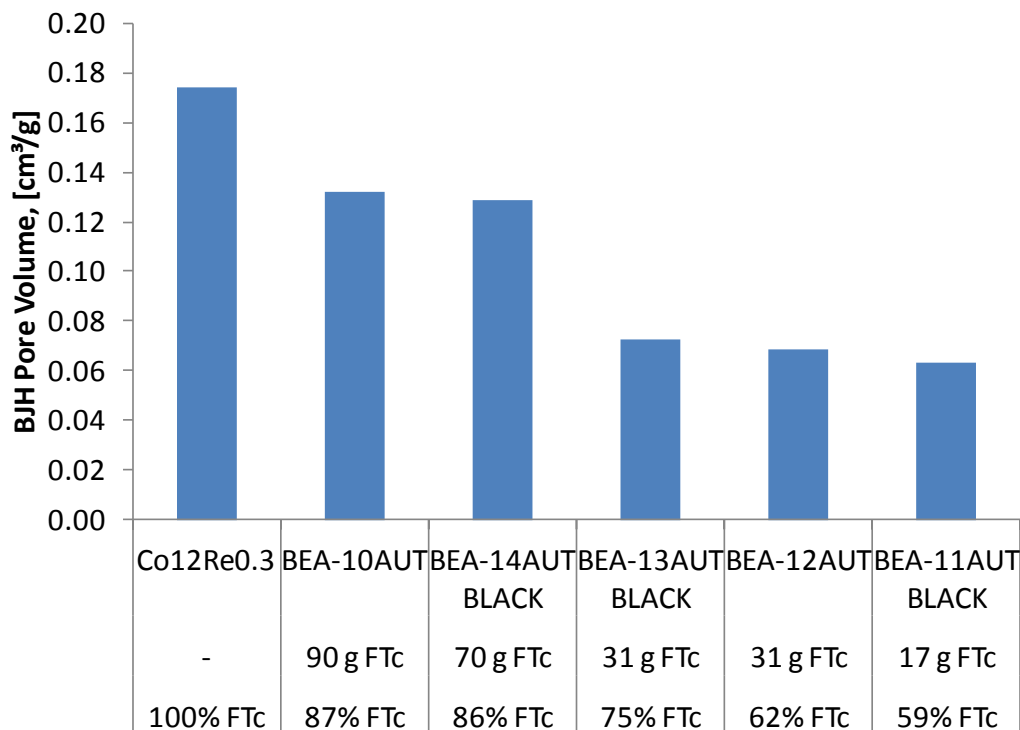
Pure β -zeolite versus β -zeolite/FT catalyst BJH pore sizes (desorption isotherm) range 0.01 to 0.95



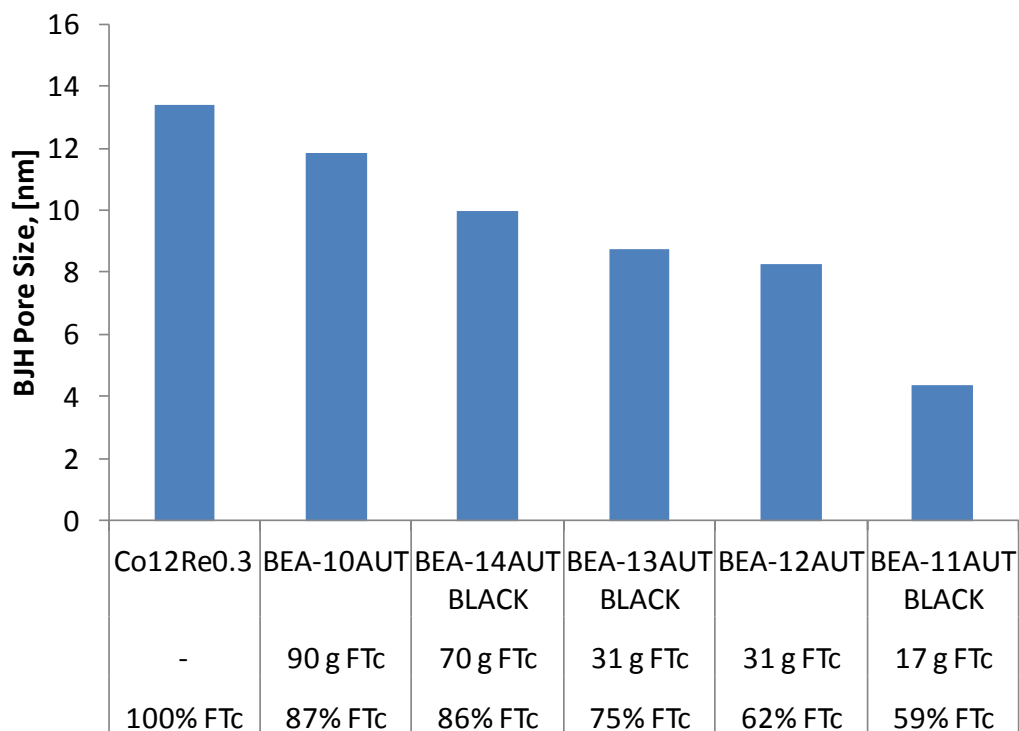
Pure β -zeolite versus β -zeolite/FT catalyst BJH pore sizes (desorption isotherm) range 0.01 to 0.95



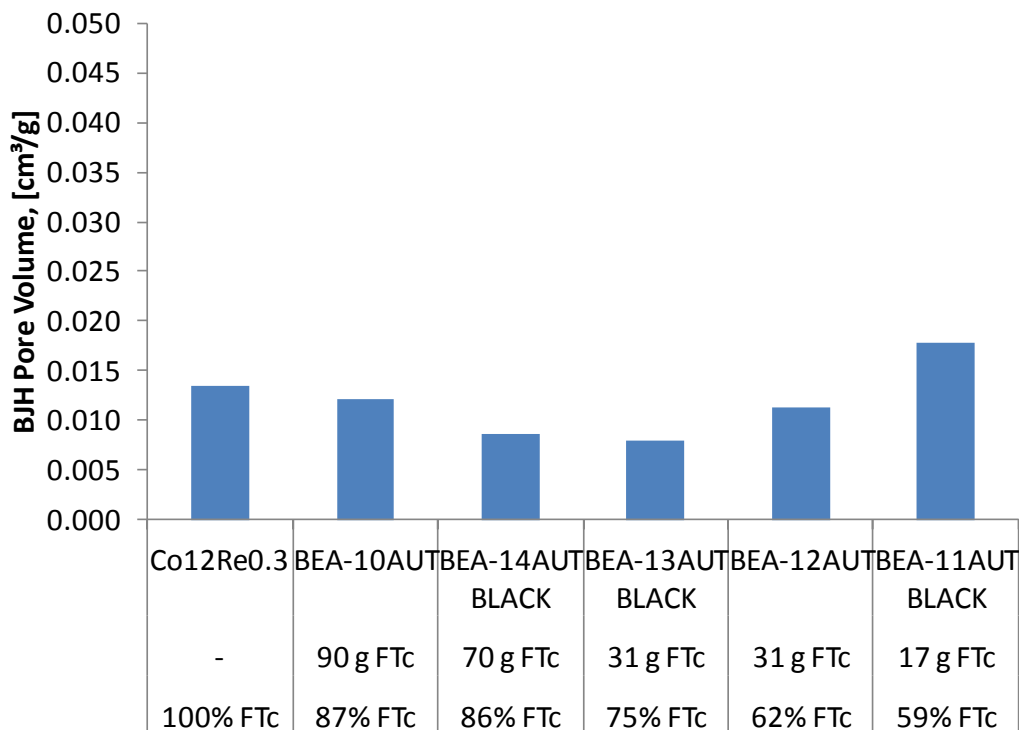
β -zeolite/FT catalyst tested BET surface area range 0.01 to 0.95



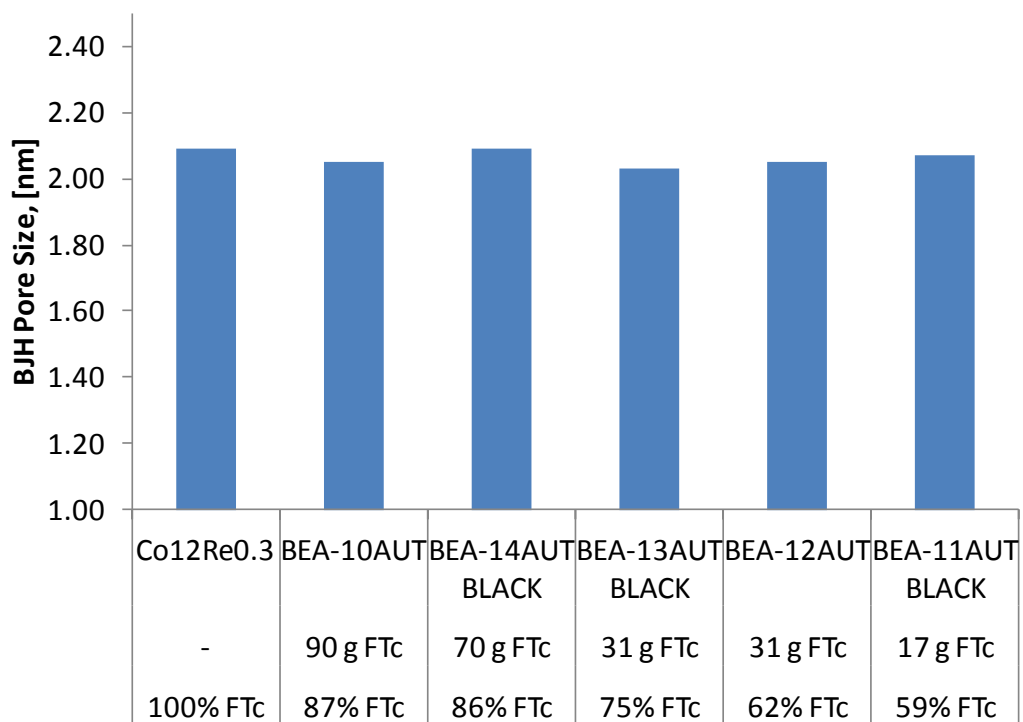
β -zeolite/FT catalyst tested BJH pore volume (desorption isotherm) range 0.01 to 0.95



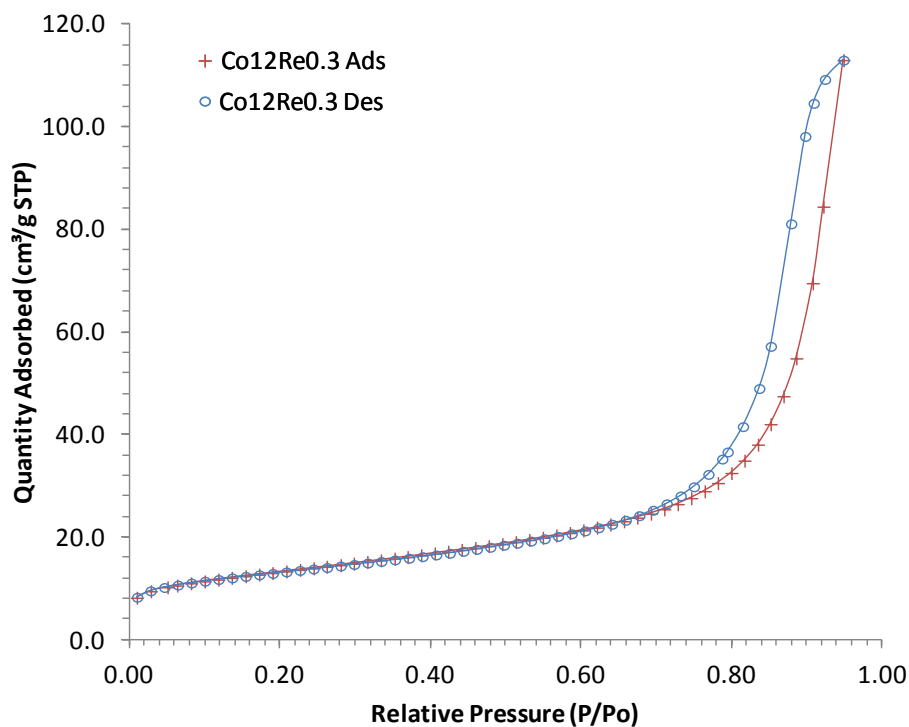
β -zeolite/FT catalyst tested BJH pore size (desorption isotherm) range 0.01 to 0.95



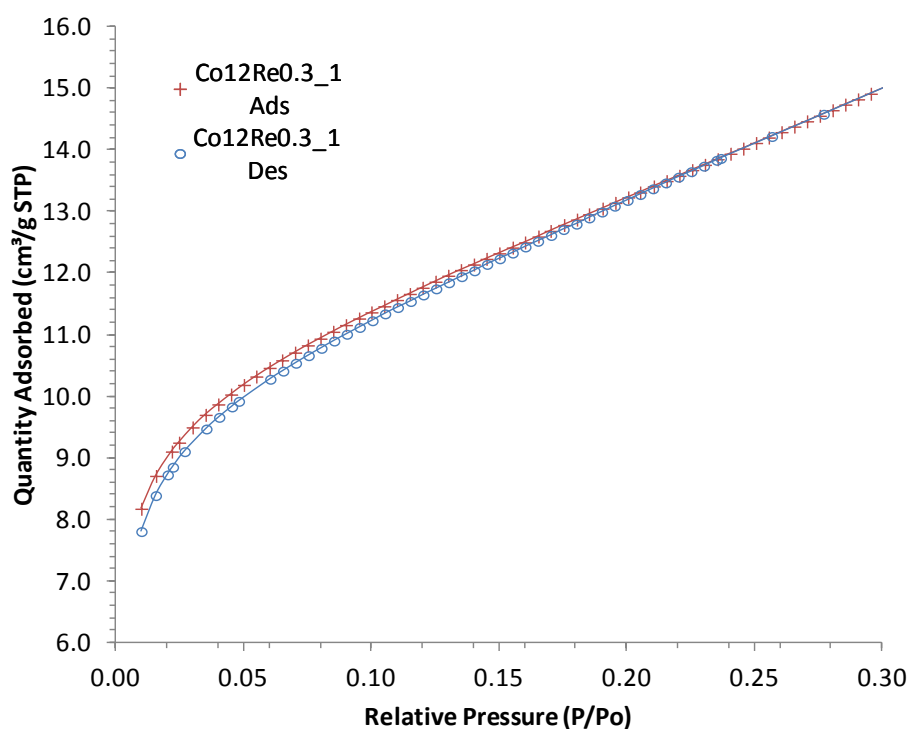
β -zeolite/FT catalyst tested BJH pore volume (desorption isotherm) range 0.01 to 0.30



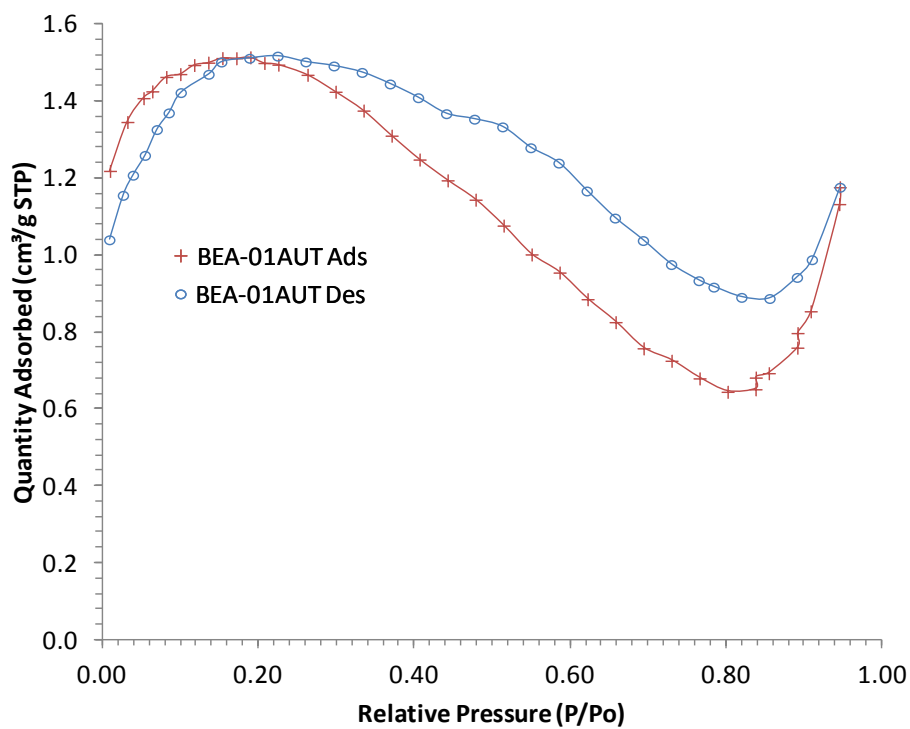
β -zeolite/FT catalyst tested BJH pore size (desorption isotherm) range 0.01 to 0.30



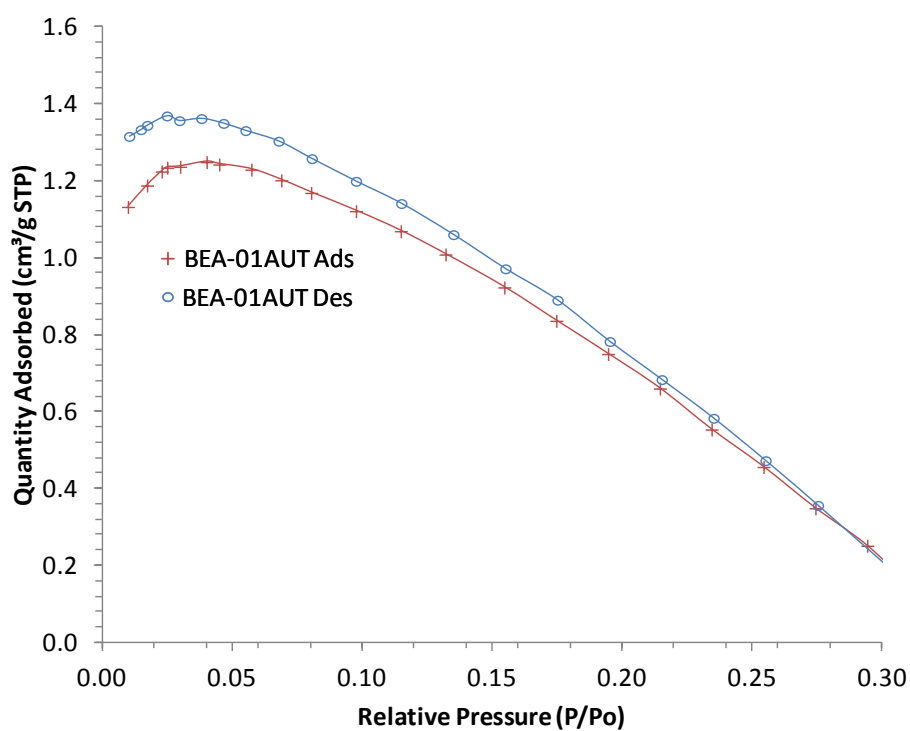
BET adsorption/desorption isotherms for Co12Re0.3, Fischer Tropsch cobalt-based catalyst, with a relative pressure range of 0.01 to 0.95 P/Po



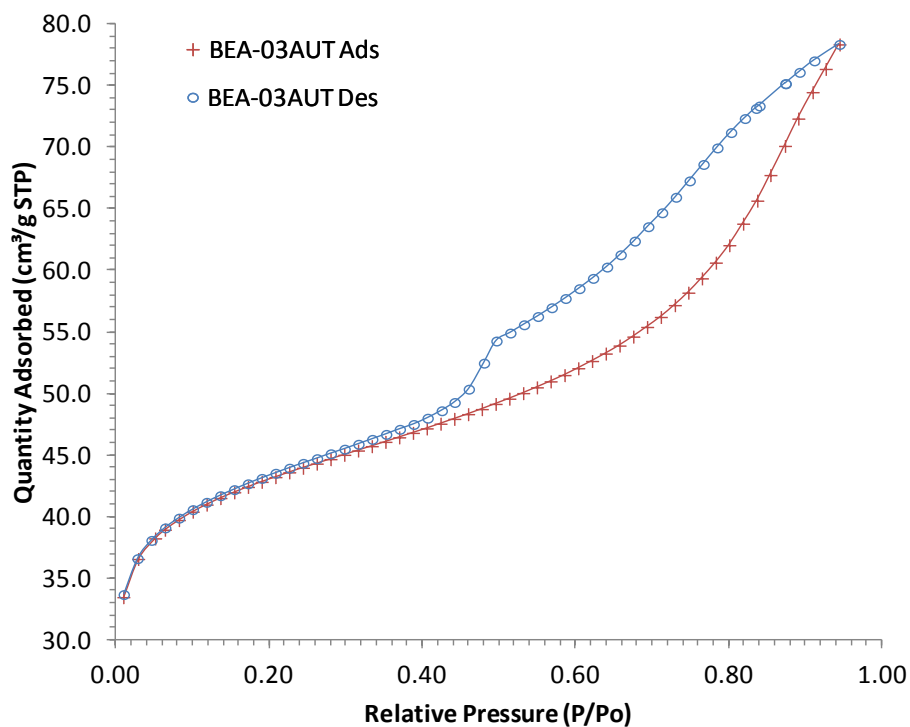
BET adsorption/desorption isotherms for Co12Re0.3, Fischer Tropsch cobalt-based catalyst, with a relative pressure range of 0.01 to 0.30 P/Po



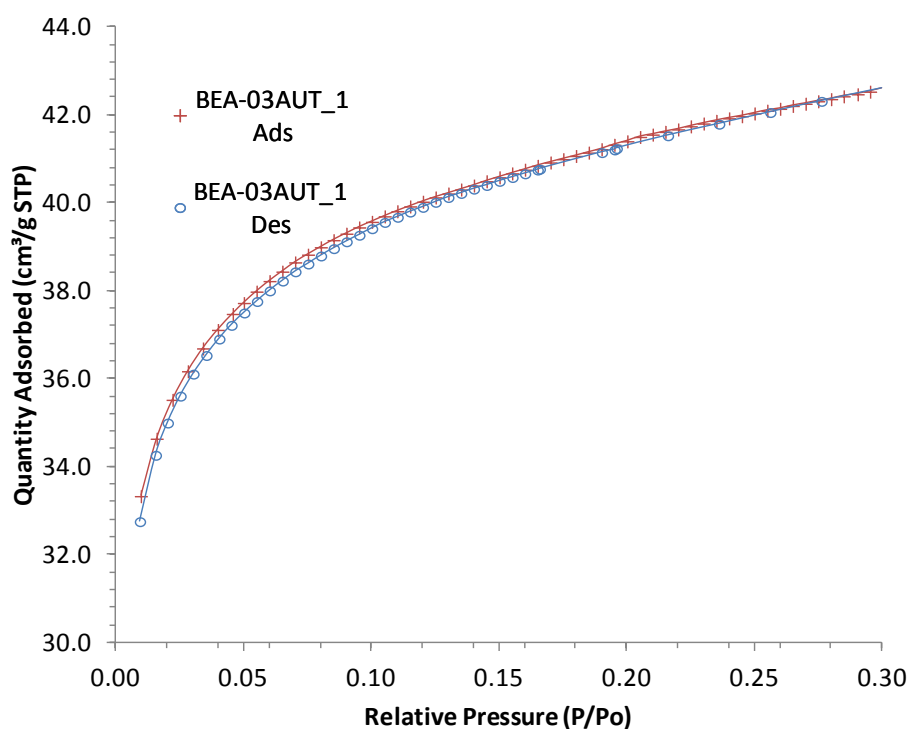
BET adsorption/desorption isotherms for BEA-01AUT, with a relative pressure range of 0.01 to 0.95 P/P_0



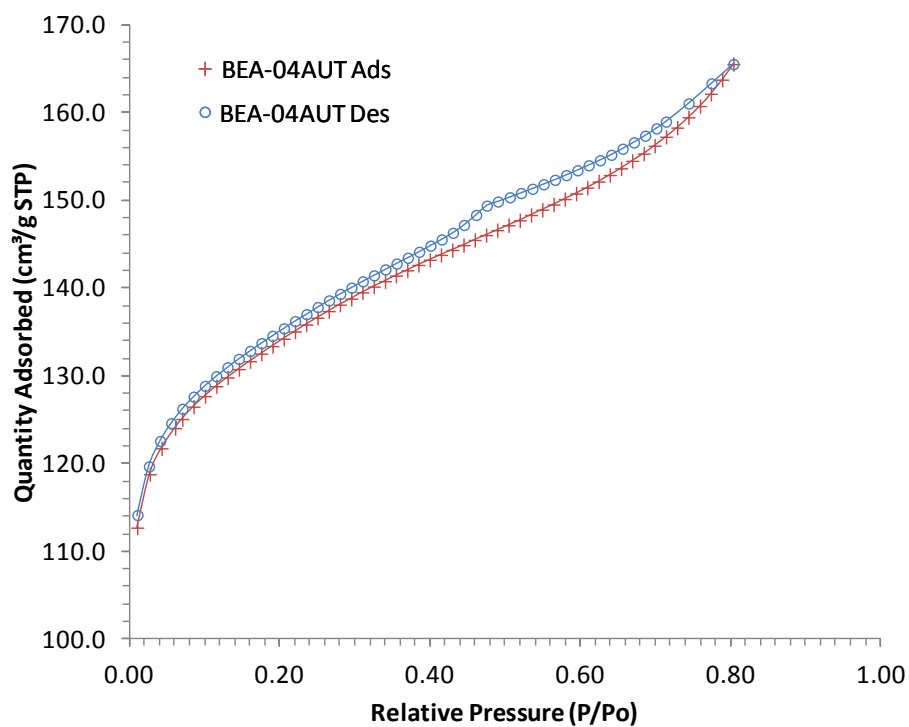
BET adsorption/desorption isotherms for BEA-01AUT, with a relative pressure range of 0.01 to 0.30 P/P_0



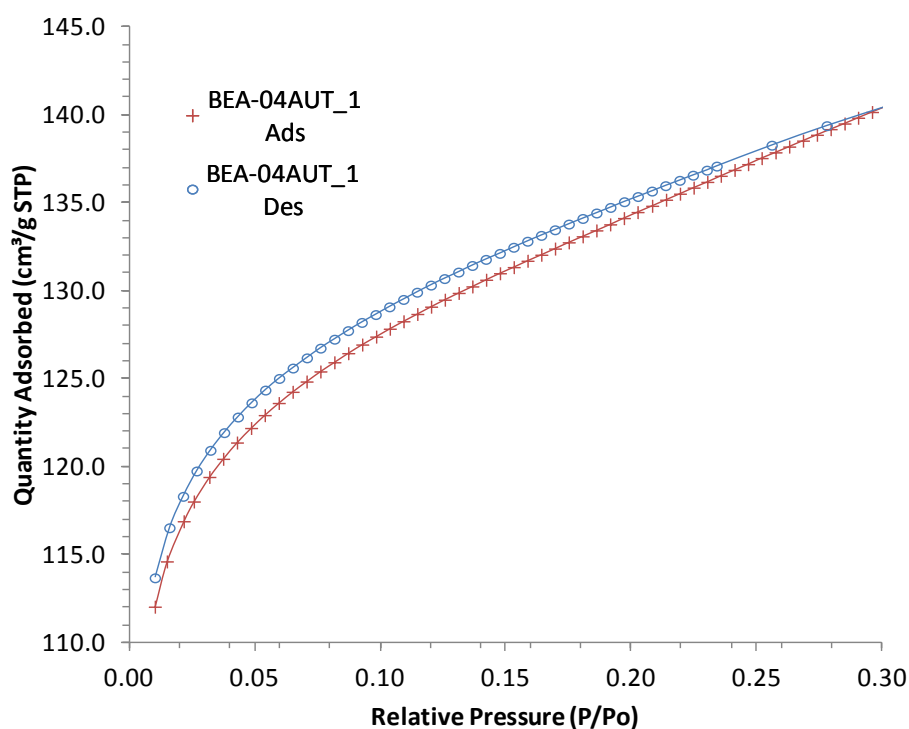
BET adsorption/desorption isotherms for BEA-03AUT, with a relative pressure range of 0.01 to 0.95 P/Po



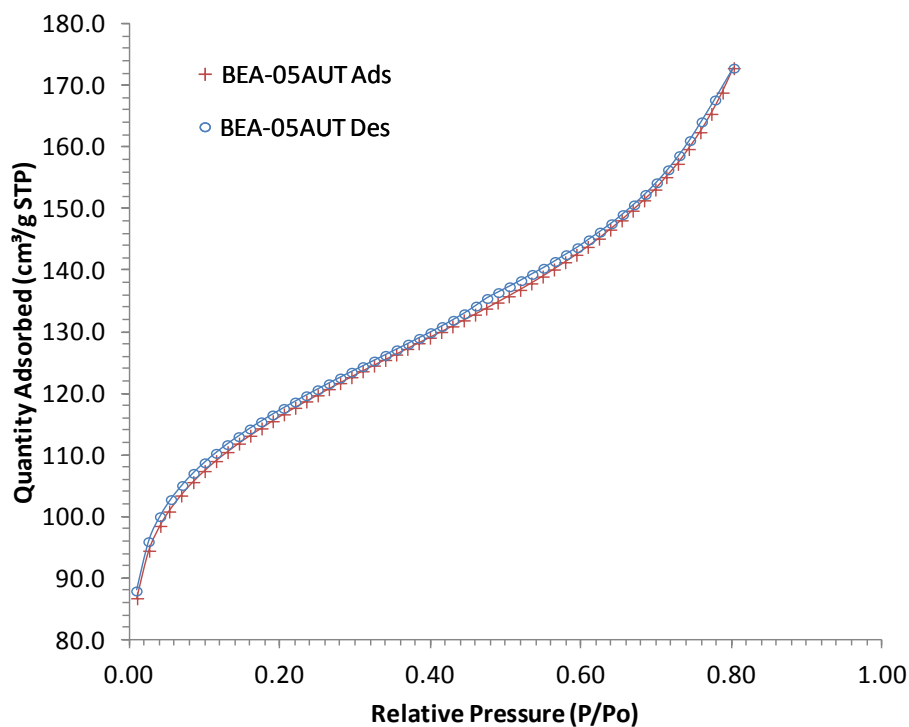
BET adsorption/desorption isotherms for BEA-03AUT, with a relative pressure range of 0.01 to 0.30 P/Po



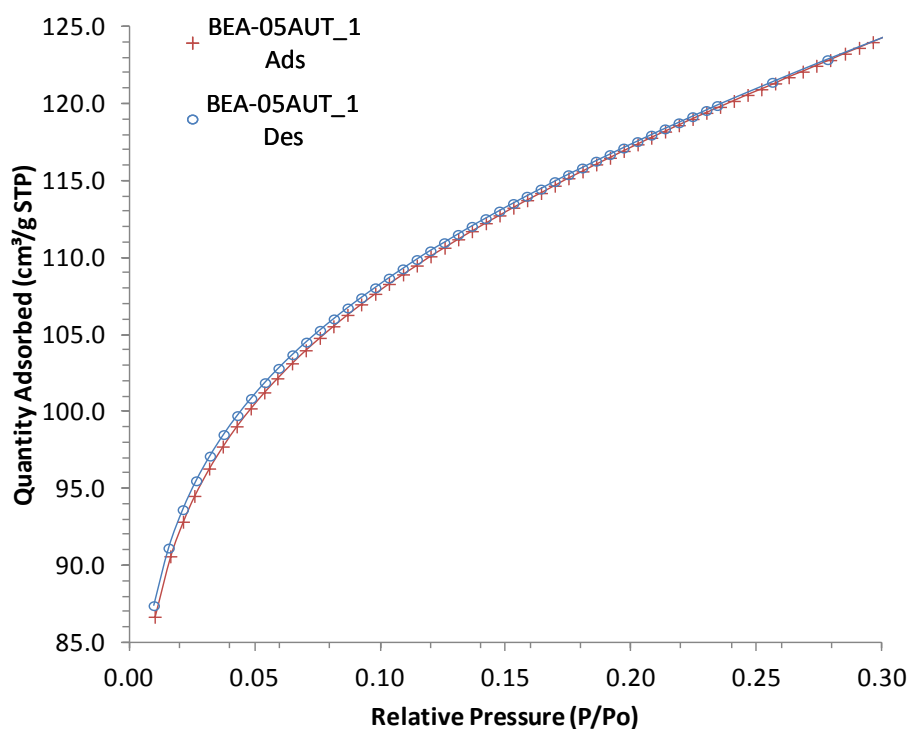
BET adsorption/desorption isotherms for BEA-04AUT, with a relative pressure range of 0.01 to 0.95 P/Po



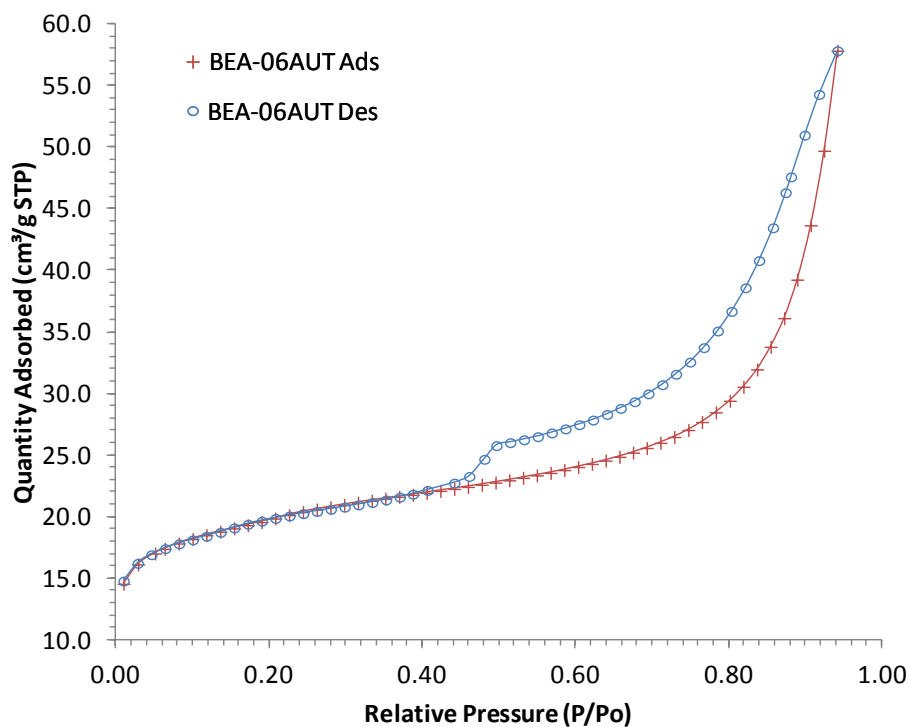
BET adsorption/desorption isotherms for BEA-04AUT, with a relative pressure range of 0.01 to 0.30 P/Po



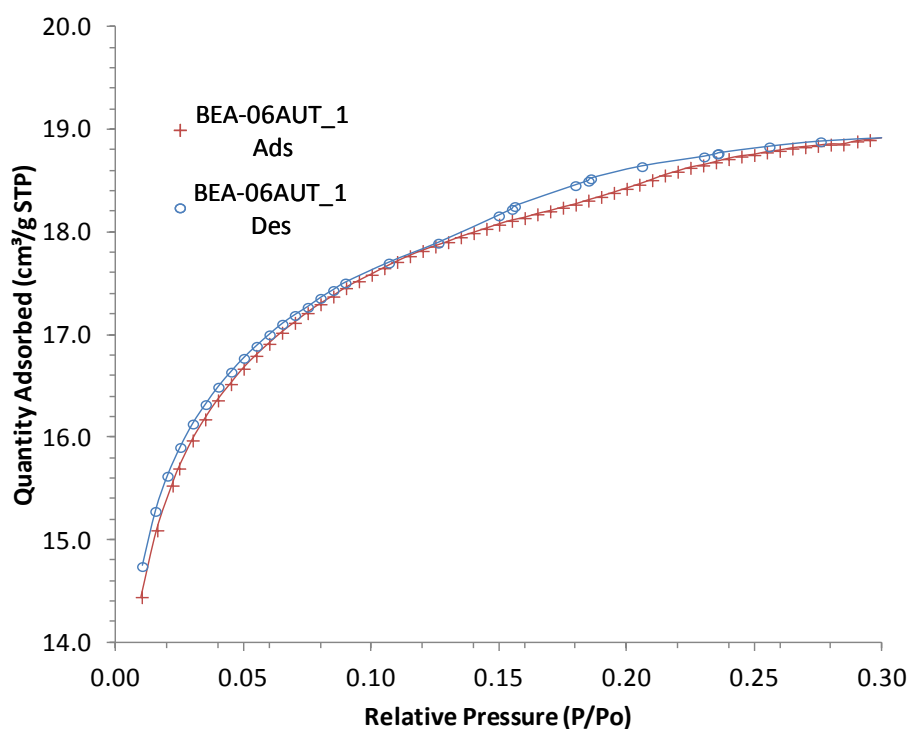
BET adsorption/desorption isotherms for BEA-05AUT, with a relative pressure range of 0.01 to 0.95 P/Po



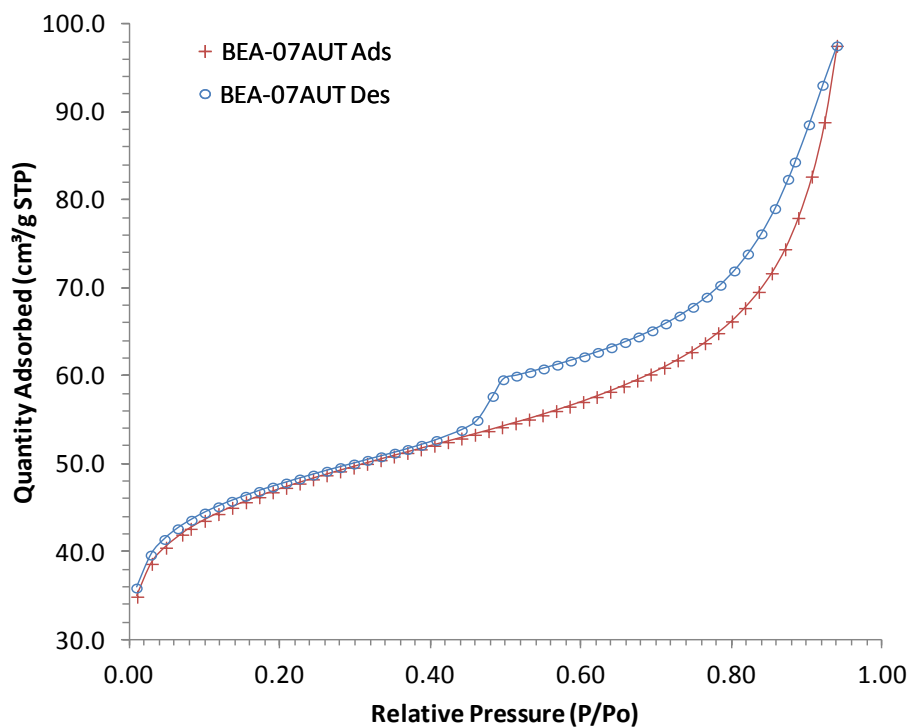
BET adsorption/desorption isotherms for BEA-05AUT, with a relative pressure range of 0.01 to 0.30 P/Po



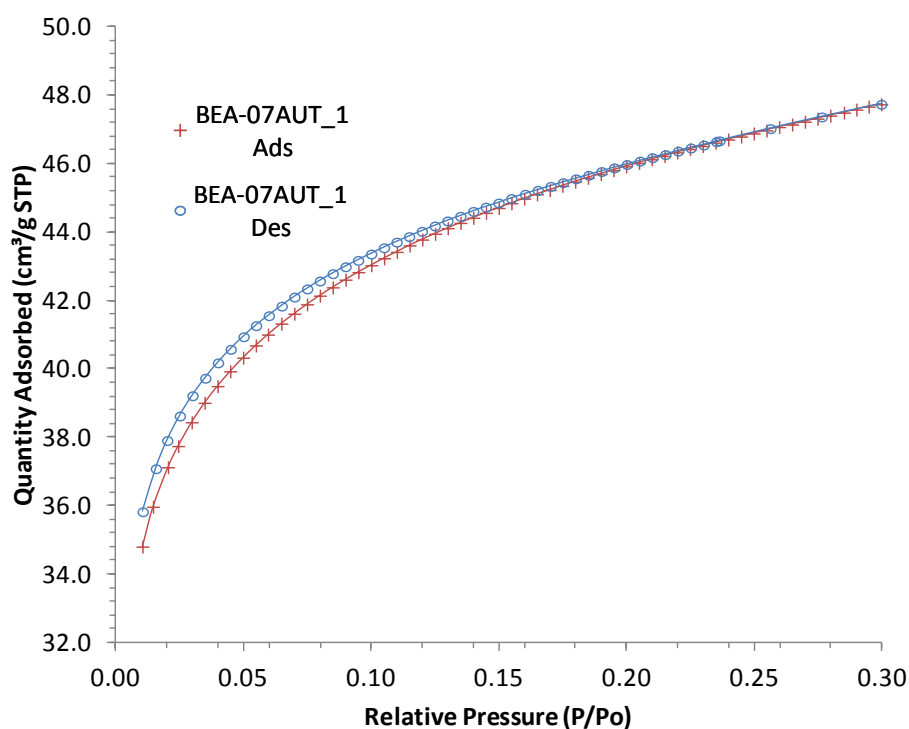
BET adsorption/desorption isotherms for BEA-06AUT, with a relative pressure range of 0.01 to 0.95 P/Po



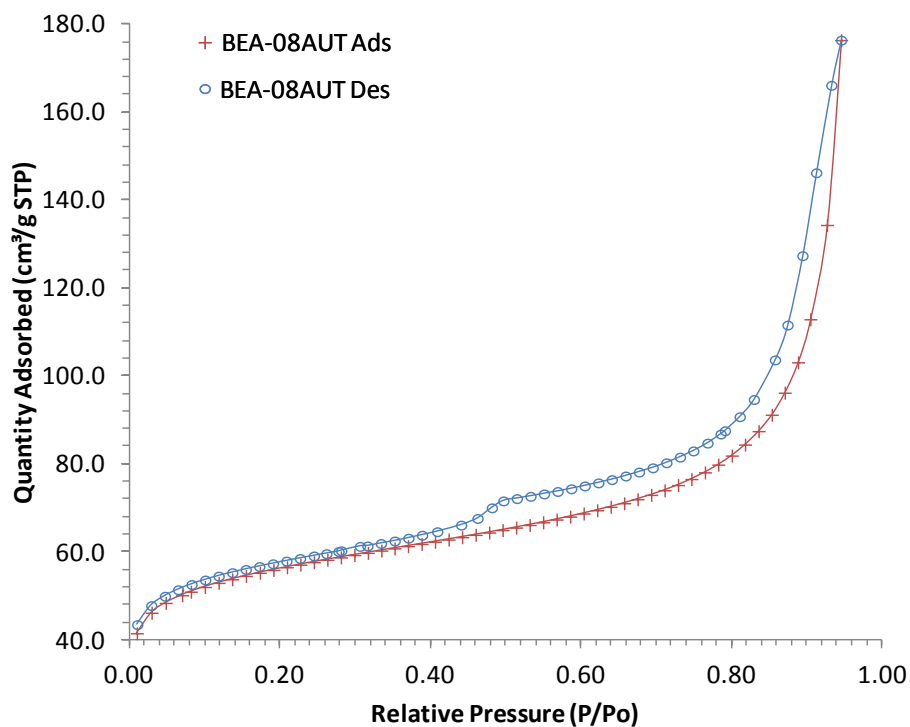
BET adsorption/desorption isotherms for BEA-06AUT, with a relative pressure range of 0.01 to 0.30 P/Po



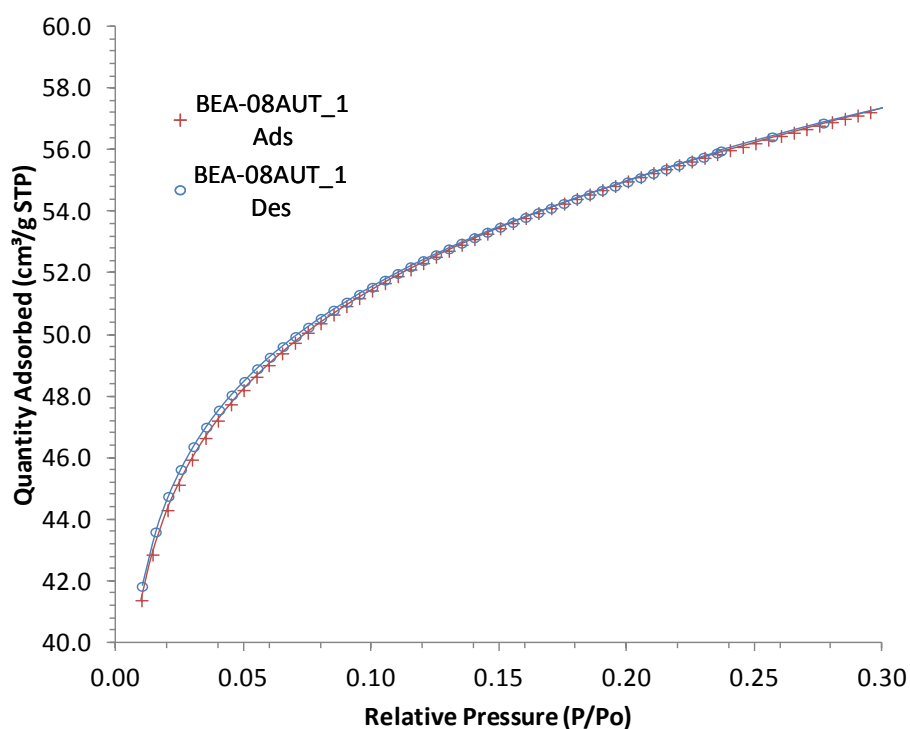
BET adsorption/desorption isotherms for BEA-07AUT, with a relative pressure range of 0.01 to 0.95 P/Po



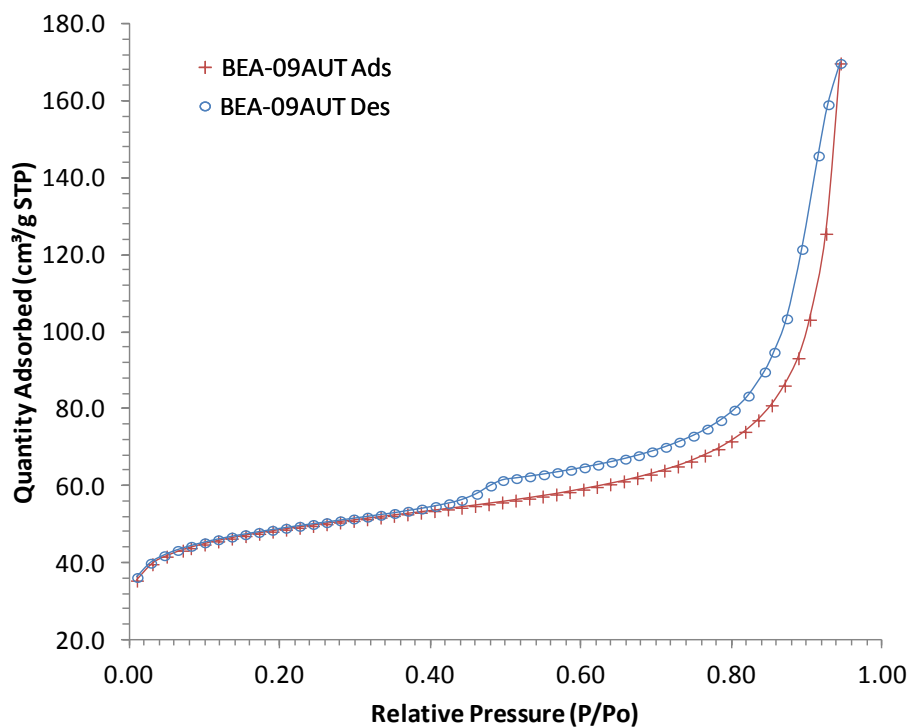
BET adsorption/desorption isotherms for BEA-07AUT, with a relative pressure range of 0.01 to 0.30 P/Po



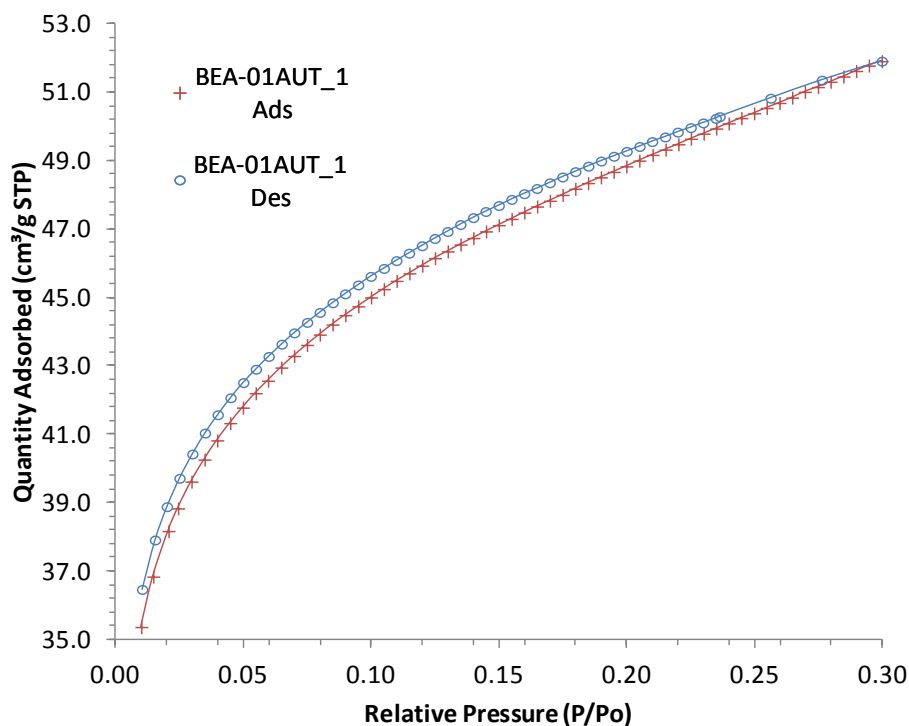
BET adsorption/desorption isotherms for BEA-08AUT, with a relative pressure range of 0.01 to 0.95 P/Po



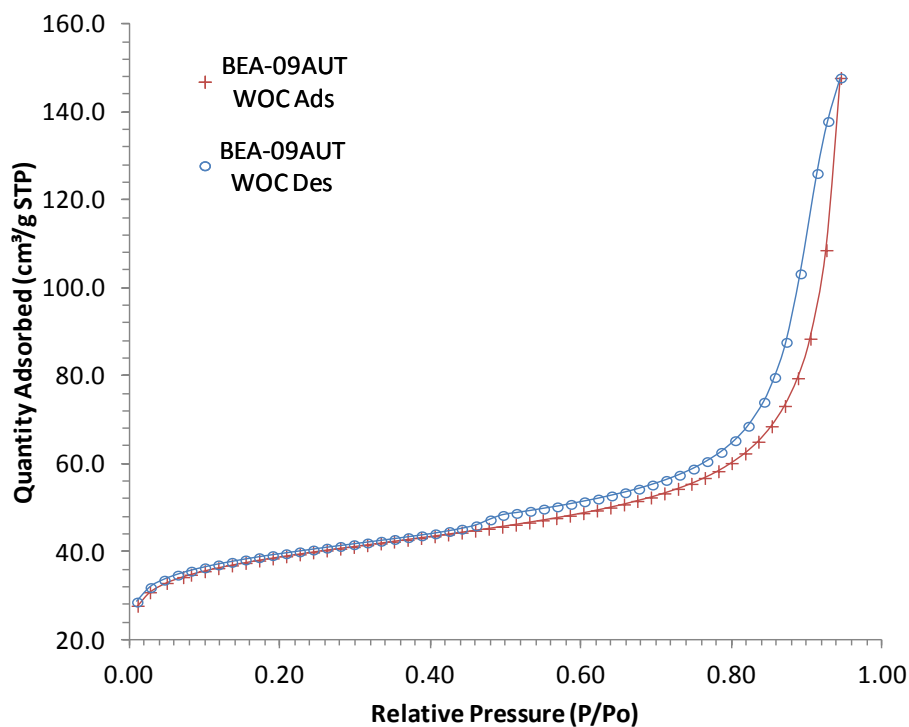
BET adsorption/desorption isotherms for BEA-08AUT, with a relative pressure range of 0.01 to 0.30 P/Po



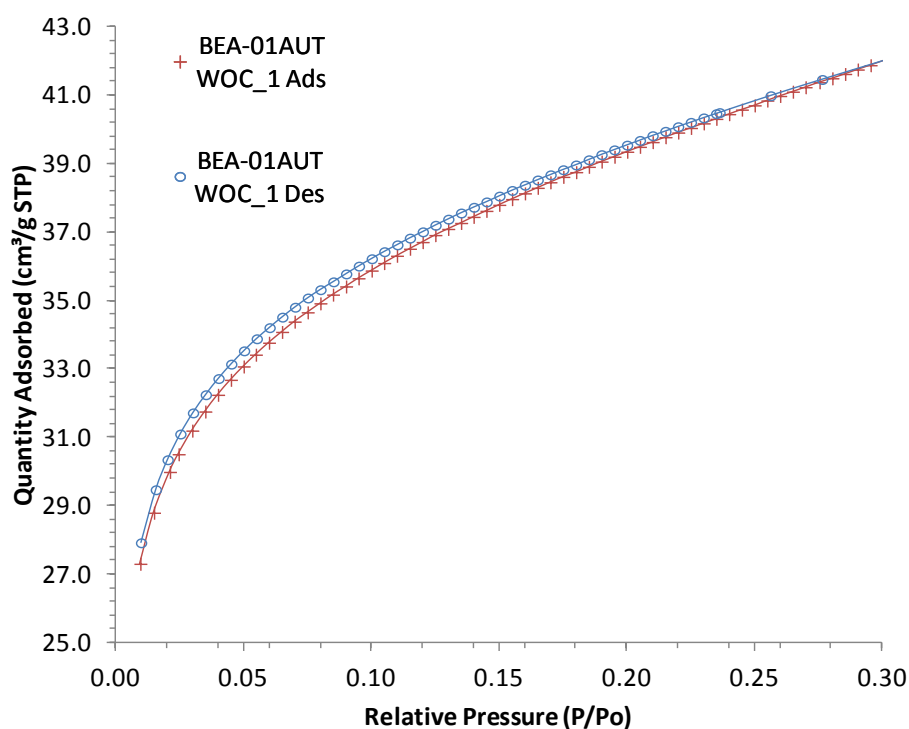
BET adsorption/desorption isotherms for BEA-09AUT, with a relative pressure range of 0.01 to 0.95 P/Po



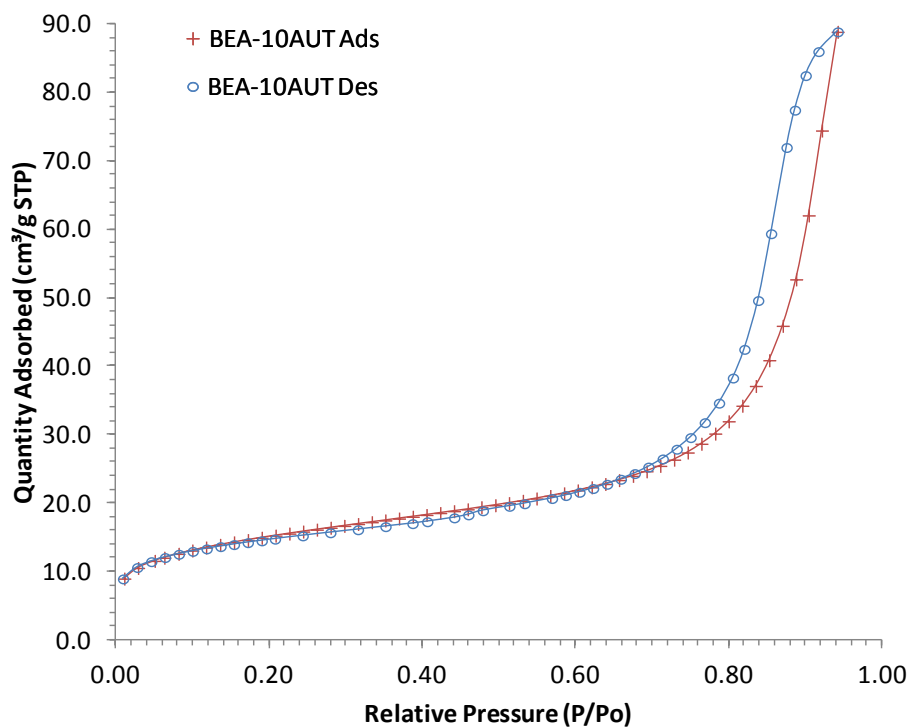
BET adsorption/desorption isotherms for BEA-09AUT, with a relative pressure range of 0.01 to 0.30 P/Po



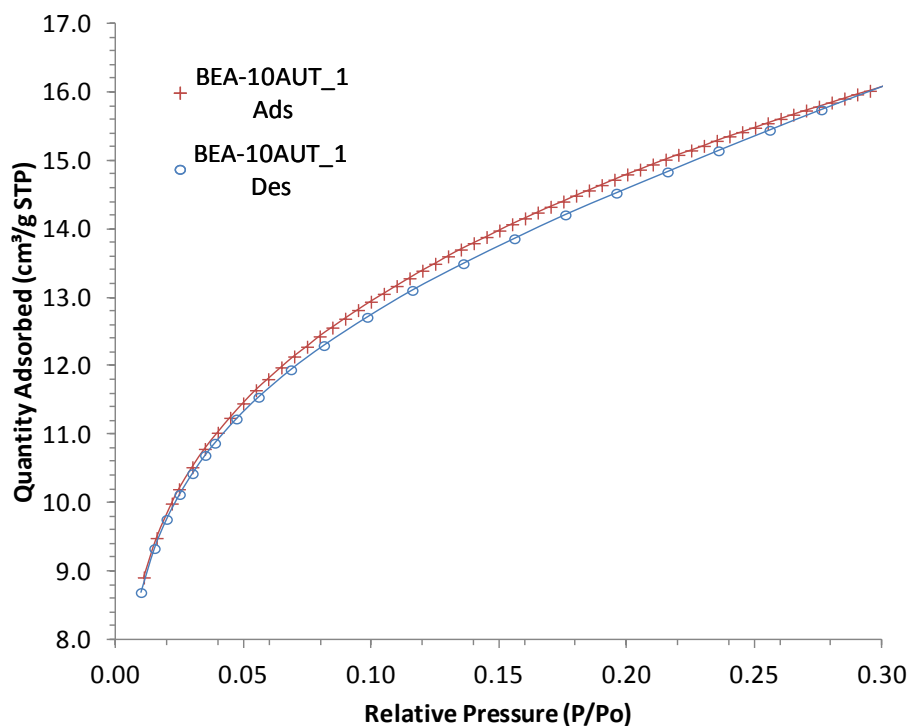
BET adsorption/desorption isotherms for BEA-09AUT WOC, with a relative pressure range of 0.01 to 0.95 P/Po



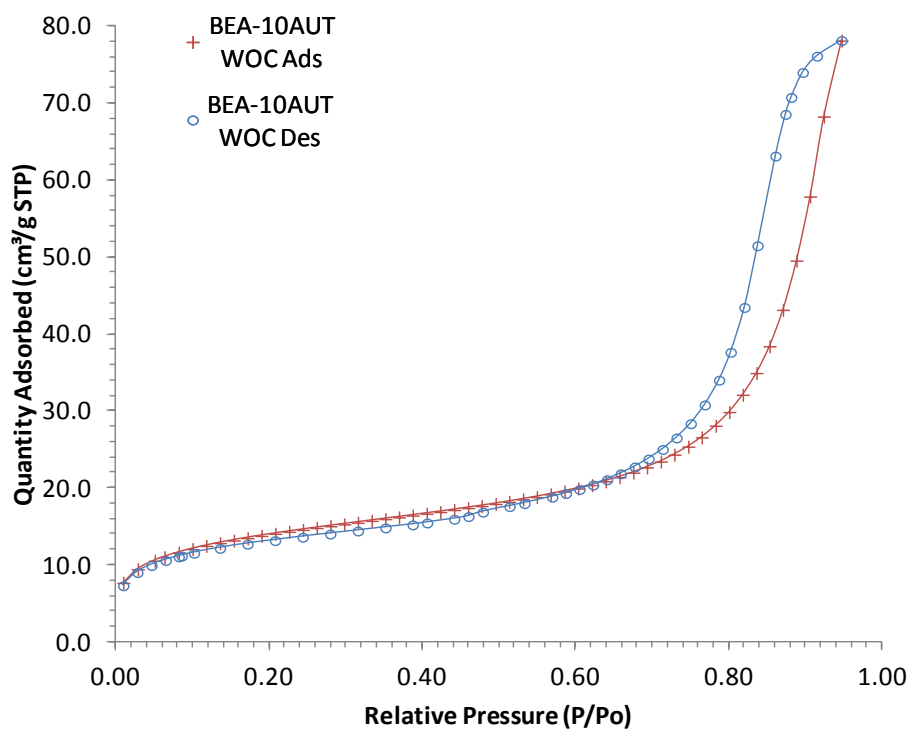
BET adsorption/desorption isotherms for BEA-09AUT WOC, with a relative pressure range of 0.01 to 0.30 P/Po



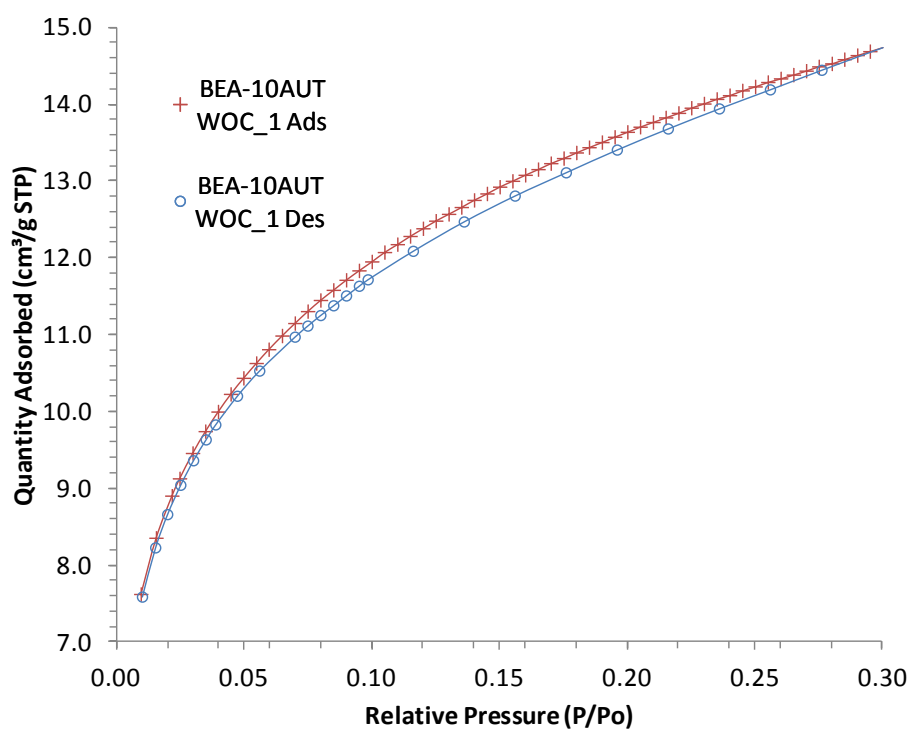
BET adsorption/desorption isotherms for BEA-10AUT, with a relative pressure range of 0.01 to 0.95 P/Po



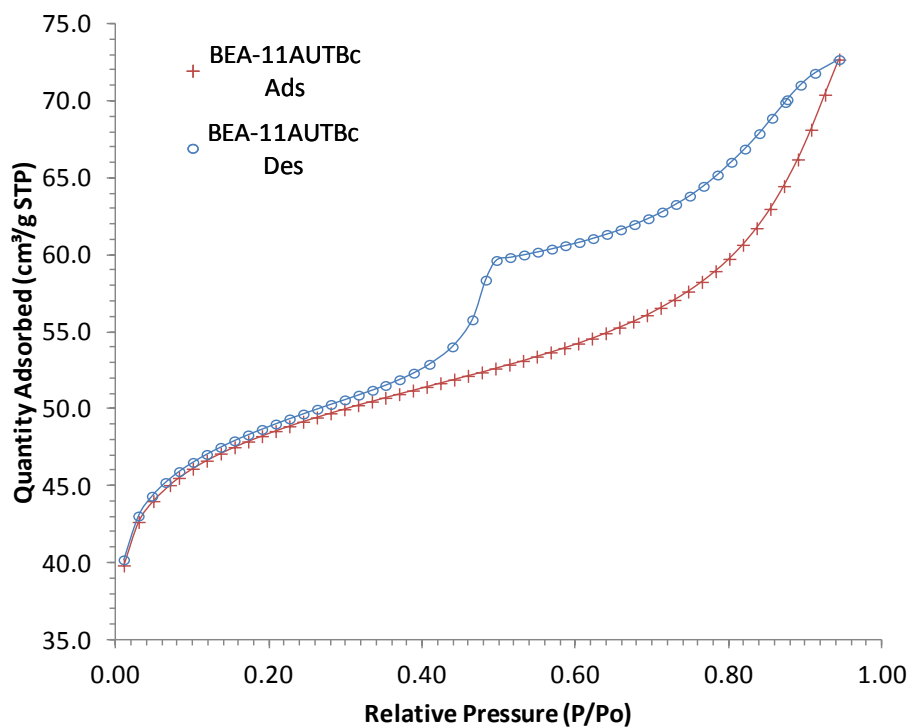
BET adsorption/desorption isotherms for BEA-10AUT, with a relative pressure range of 0.01 to 0.30 P/Po



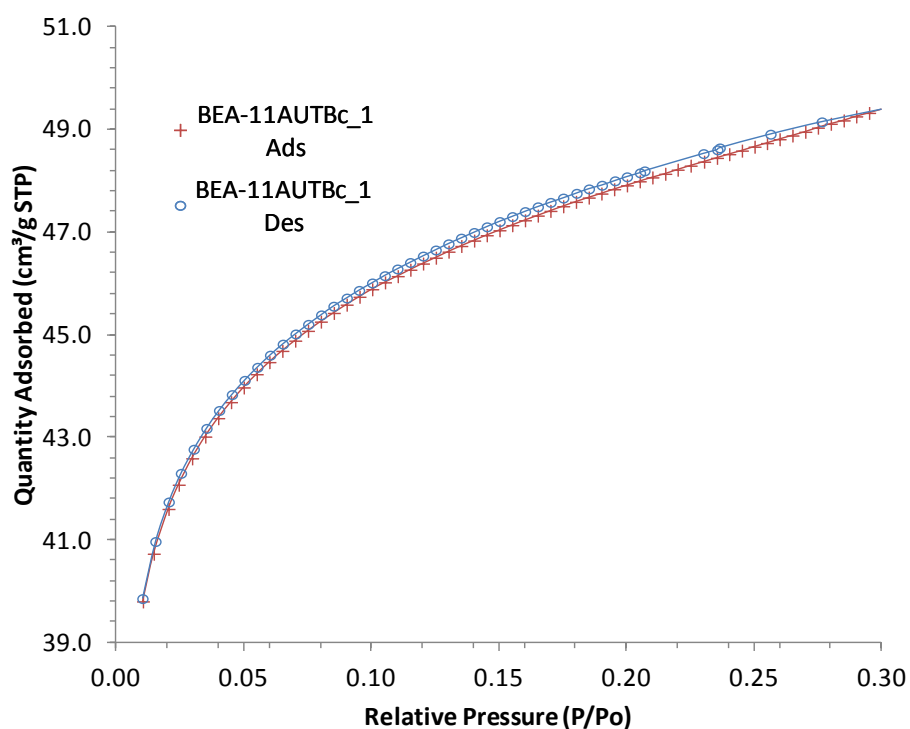
BET adsorption/desorption isotherms for BEA-10AUT WOC, with a relative pressure range of 0.01 to 0.95 P/P_o



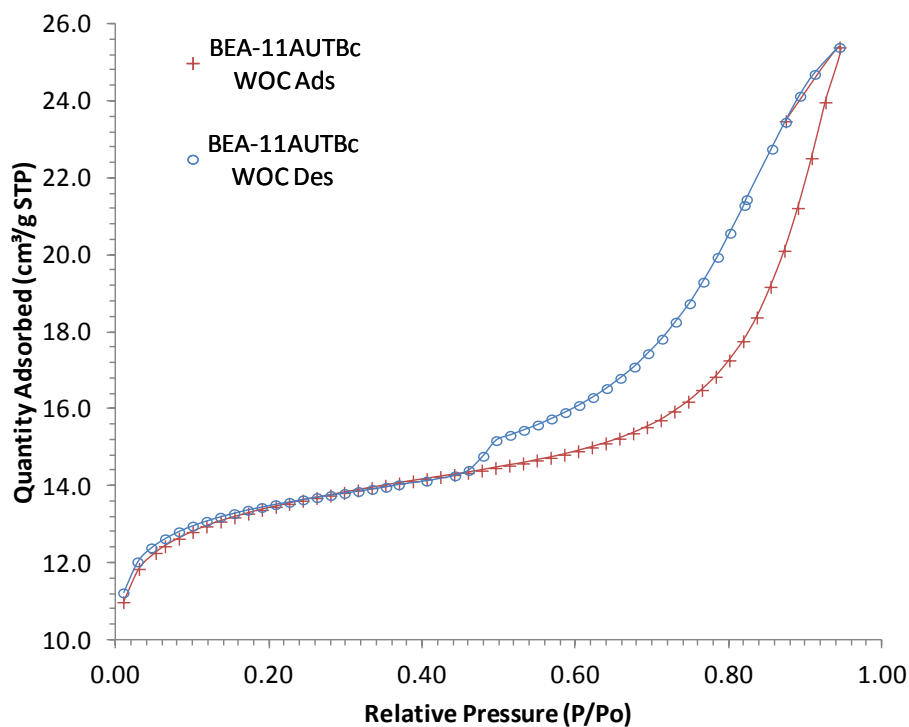
BET adsorption/desorption isotherms for BEA-10AUT WOC, with a relative pressure range of 0.01 to 0.30 P/P_o



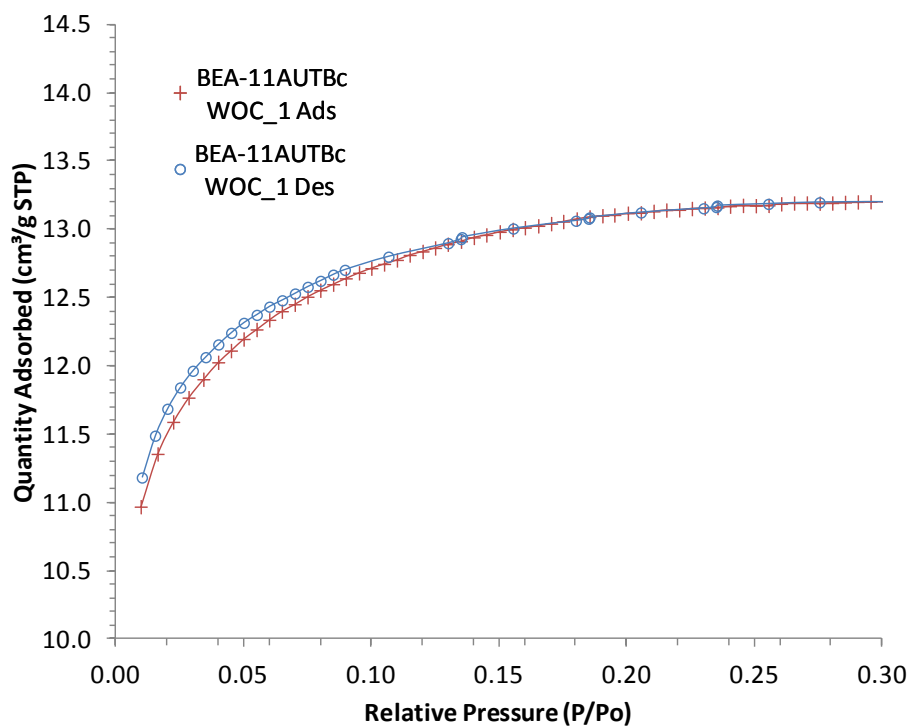
BET adsorption/desorption isotherms for BEA-11AUT BLACK, with a relative pressure range of 0.01 to 0.95 P/Po



BET adsorption/desorption isotherms for BEA-11AUT BLACK, with a relative pressure range of 0.01 to 0.30 P/Po

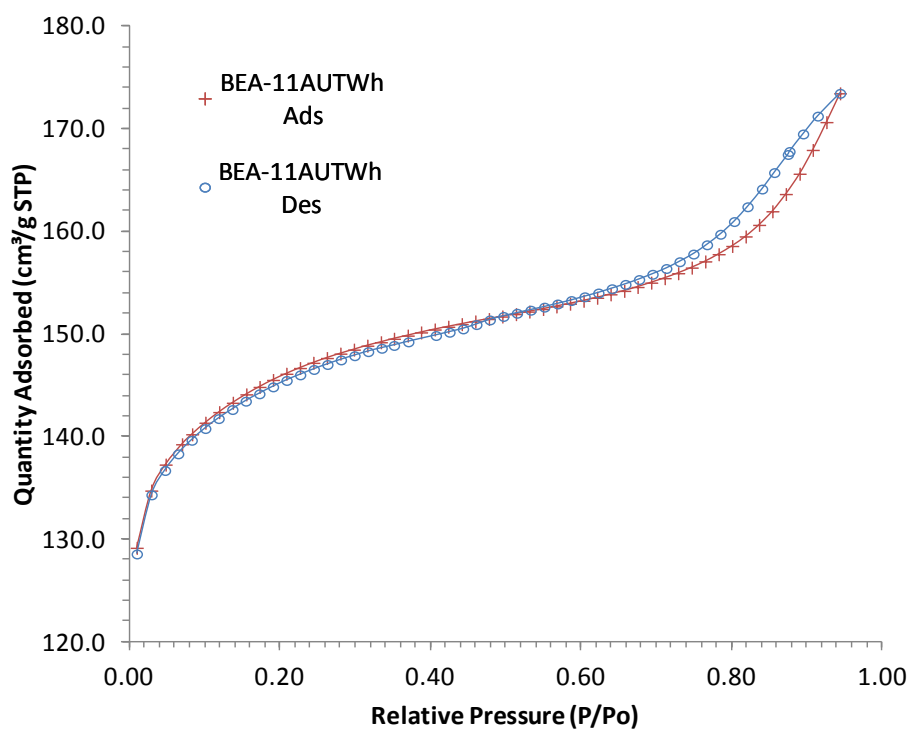


BET adsorption/desorption isotherms for BEA-11AUT BLACK WOC, with a relative pressure range of 0.01 to 0.95 P/P₀

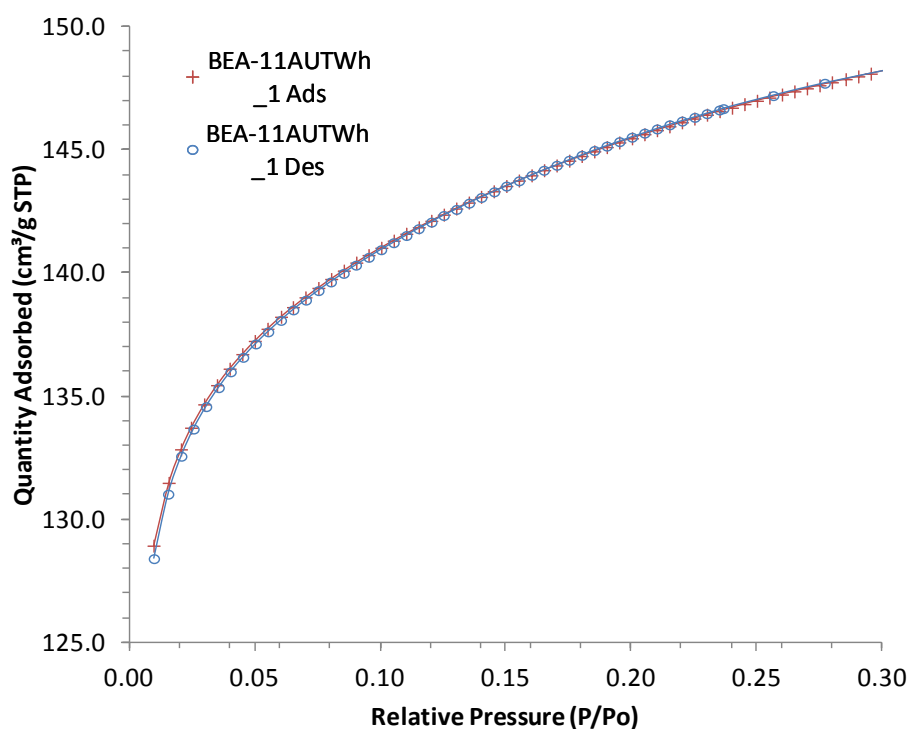


BET adsorption/desorption isotherms for BEA-11AUT BLACK WOC, with a relative pressure range of 0.01 to 0.30

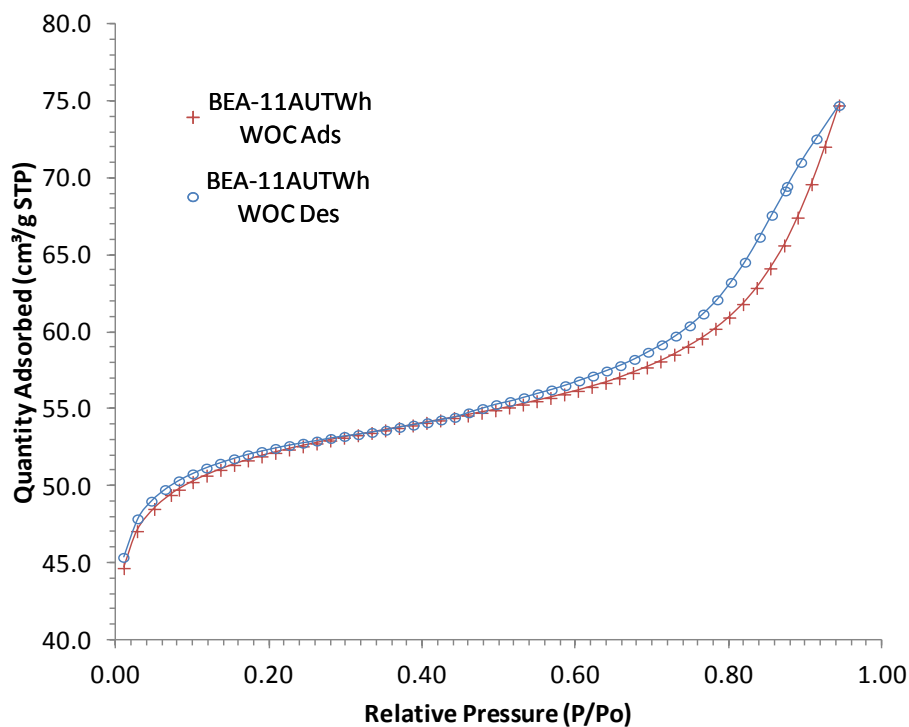
P/P₀



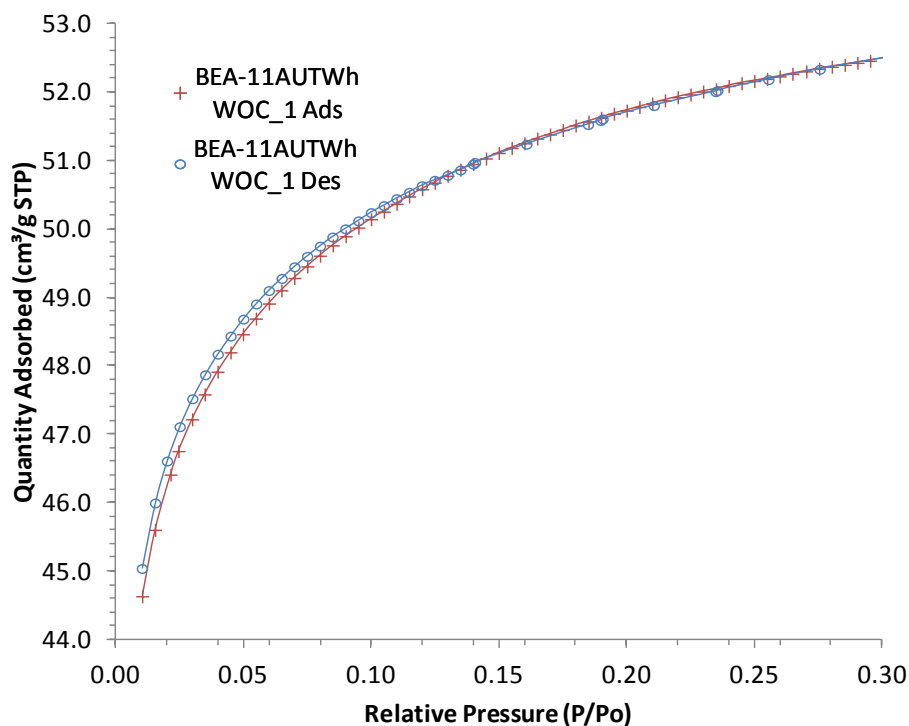
BET adsorption/desorption isotherms for BEA-11AUT WHITE, with a relative pressure range of 0.01 to 0.95 P/Po



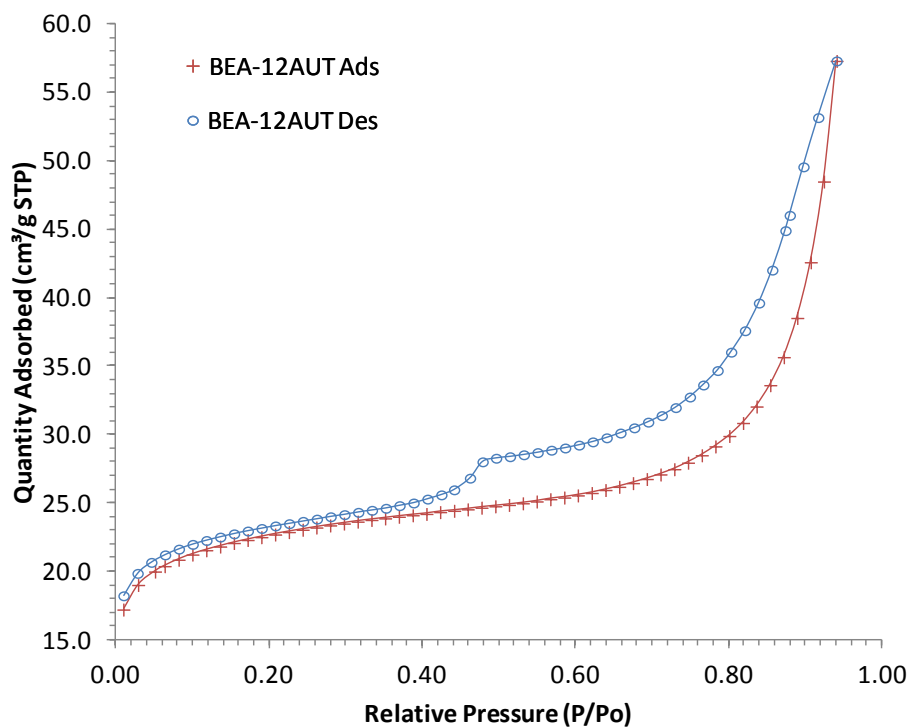
BET adsorption/desorption isotherms for BEA-11AUT WHITE, with a relative pressure range of 0.01 to 0.30 P/Po



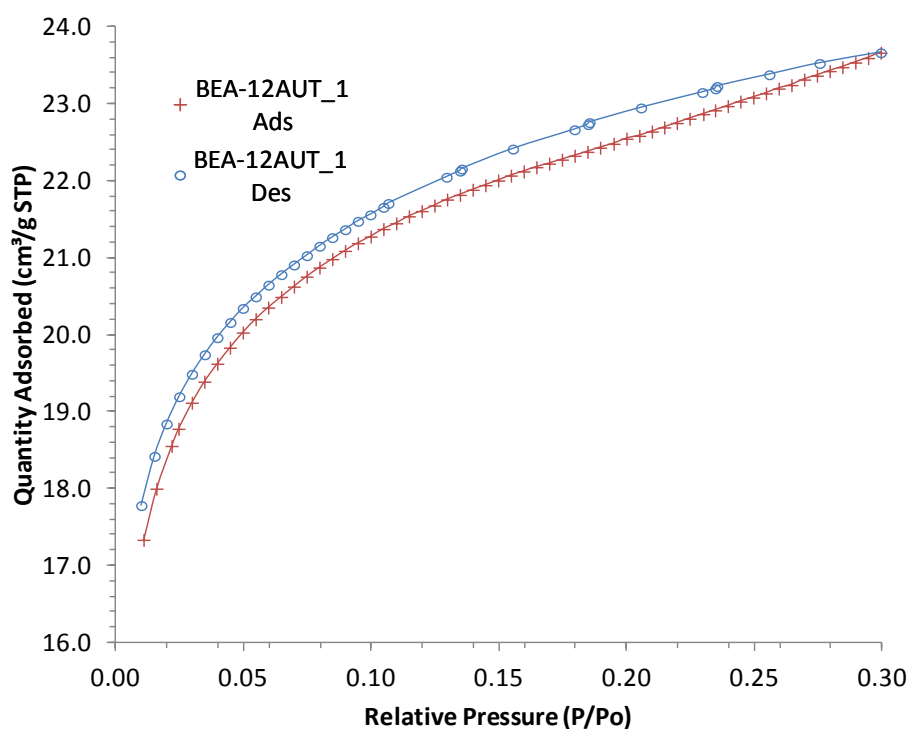
BET adsorption/desorption isotherms for BEA-11AUT WHITE WOC, with a relative pressure range of 0.01 to 0.95 P/Po



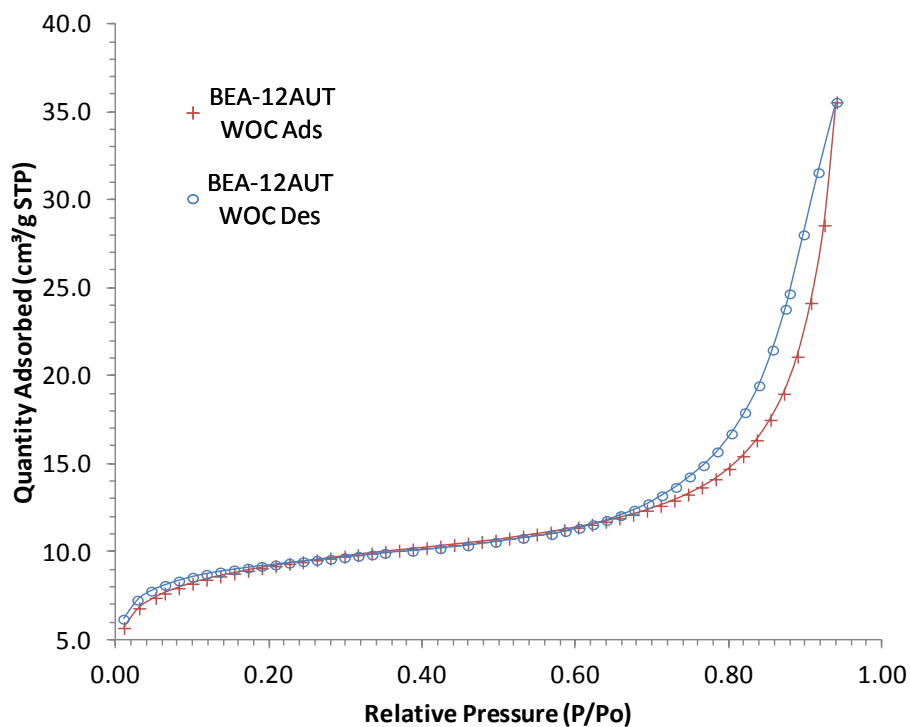
BET adsorption/desorption isotherms for BEA-11AUT WHITE WOC, with a relative pressure range of 0.01 to 0.30 P/Po



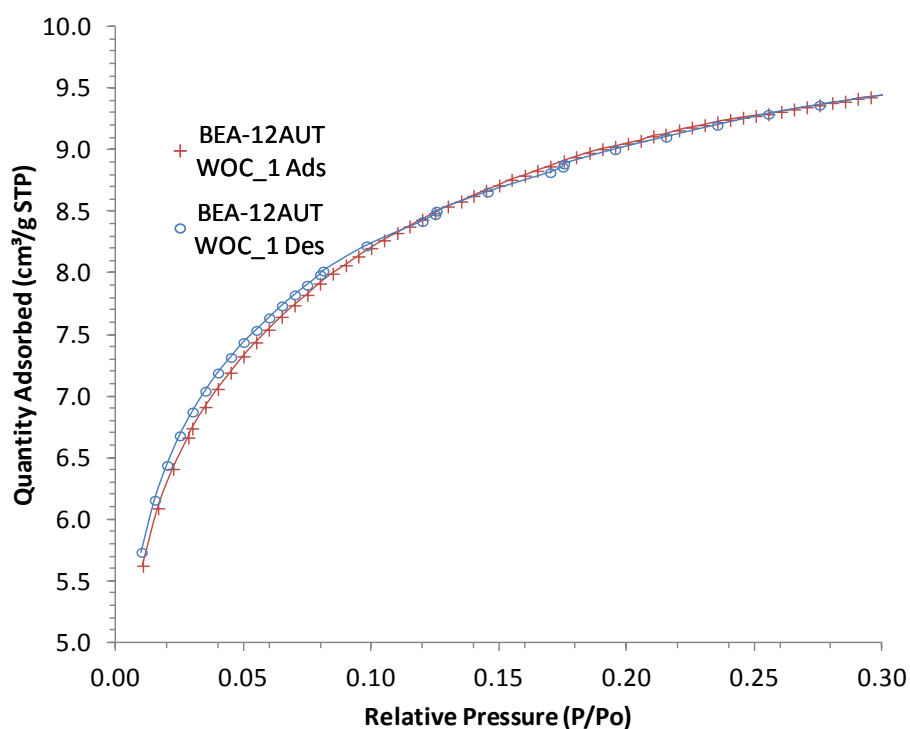
BET adsorption/desorption isotherms for BEA-12AUT, with a relative pressure range of 0.01 to 0.95 P/P_0



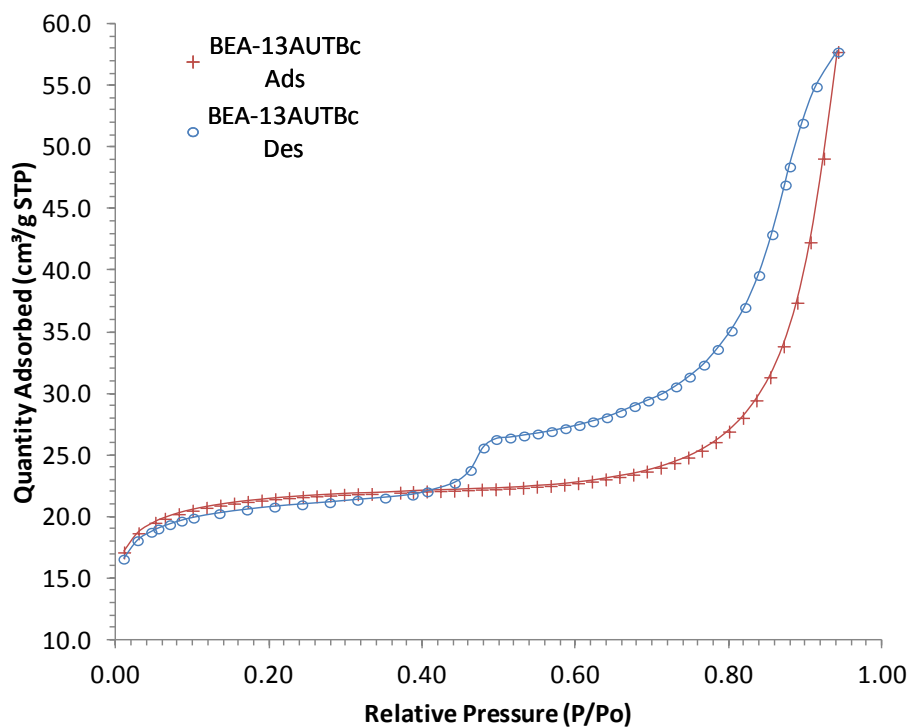
BET adsorption/desorption isotherms for BEA-12AUT, with a relative pressure range of 0.01 to 0.30 P/P_0



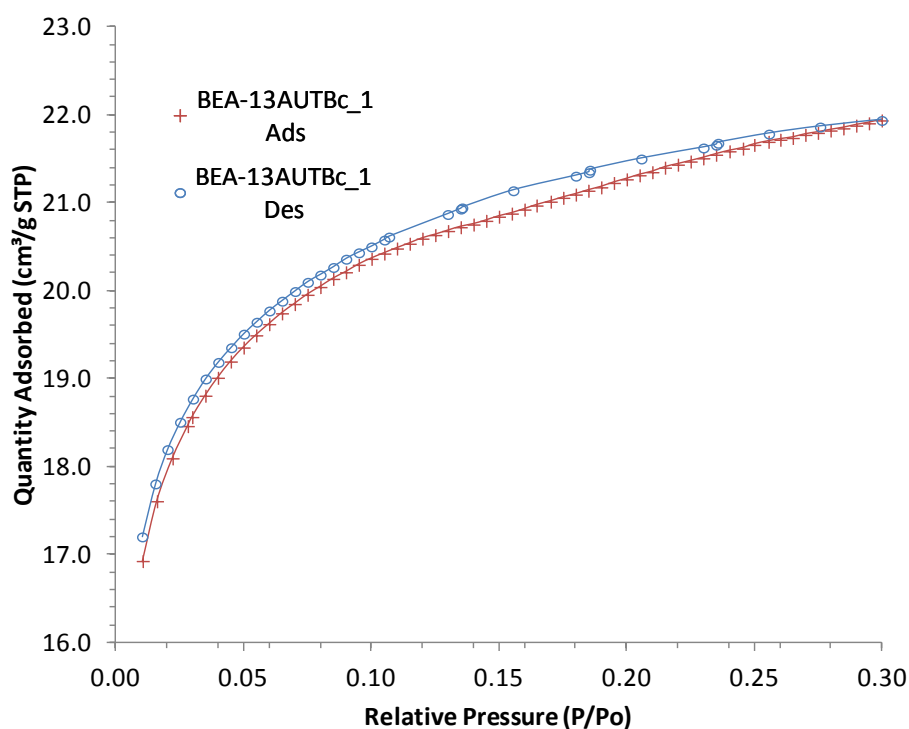
BET adsorption/desorption isotherms for BEA-12AUT WOC, with a relative pressure range of 0.01 to 0.95 P/Po



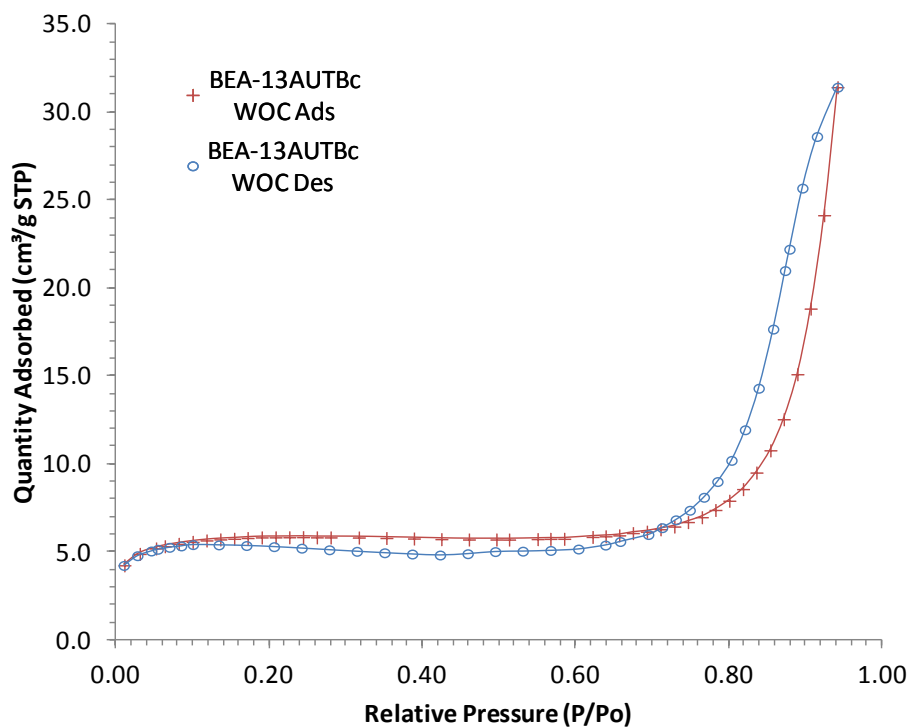
BET adsorption/desorption isotherms for BEA-12AUT WOC, with a relative pressure range of 0.01 to 0.30 P/Po



BET adsorption/desorption isotherms for BEA-13AUT BLACK, with a relative pressure range of 0.01 to 0.95 P/P_0

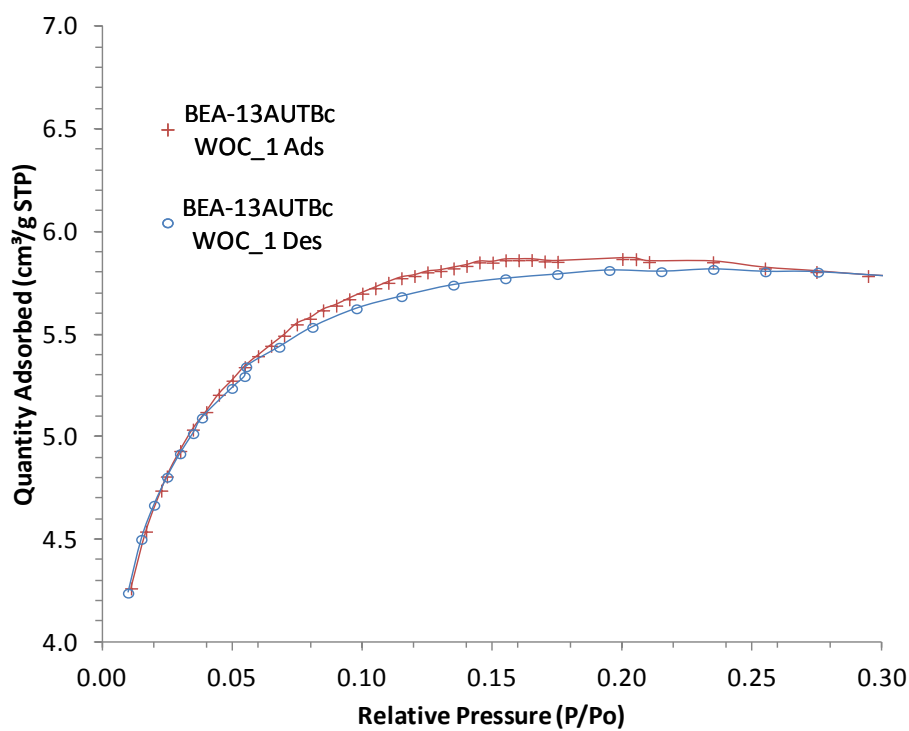


BET adsorption/desorption isotherms for BEA-13AUT BLACK, with a relative pressure range of 0.01 to 0.30 P/P_0

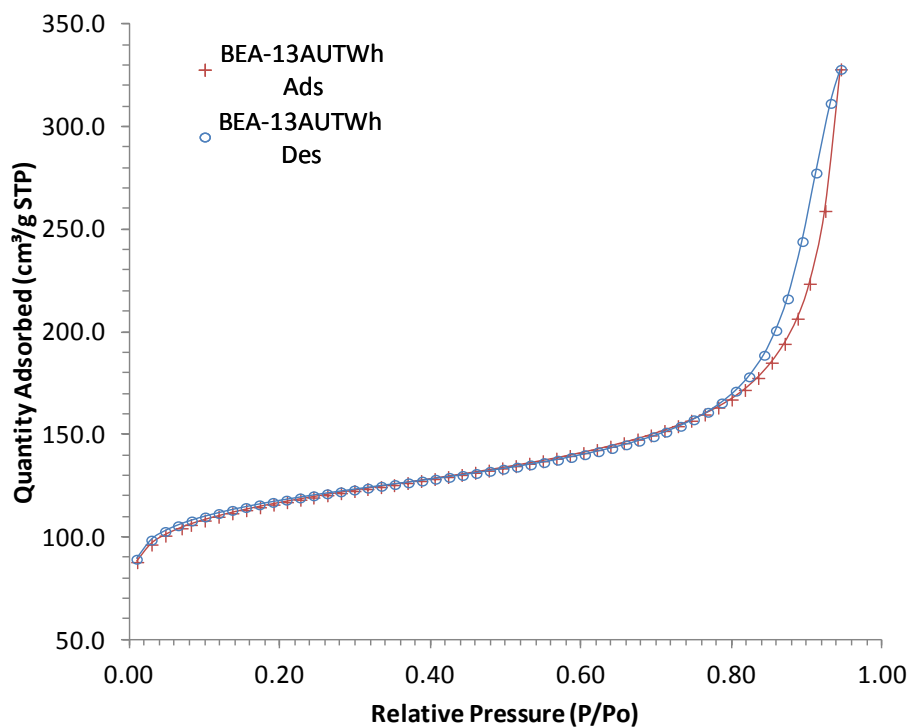


BET adsorption/desorption isotherms for BEA-13AUT BLACK WOC, with a relative pressure range of 0.01 to 0.95

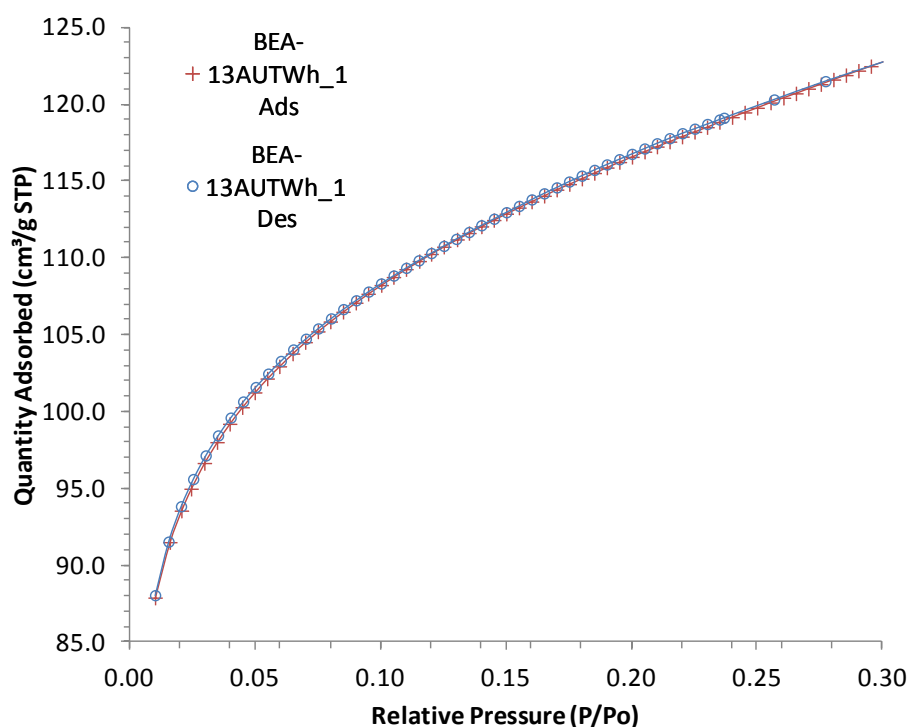
P/Po



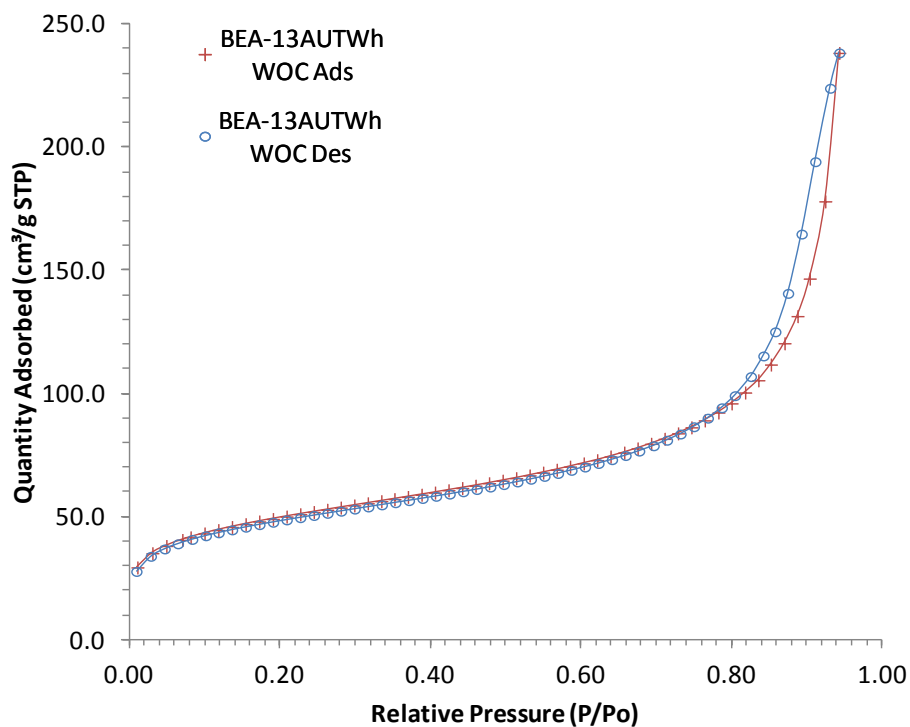
BET adsorption/desorption isotherms for BEA-13AUT BLACK WOC, with a relative pressure range of 0.01 to 0.30 P/Po



BET adsorption/desorption isotherms for BEA-13AUT WHITE, with a relative pressure range of 0.01 to 0.95 P/Po

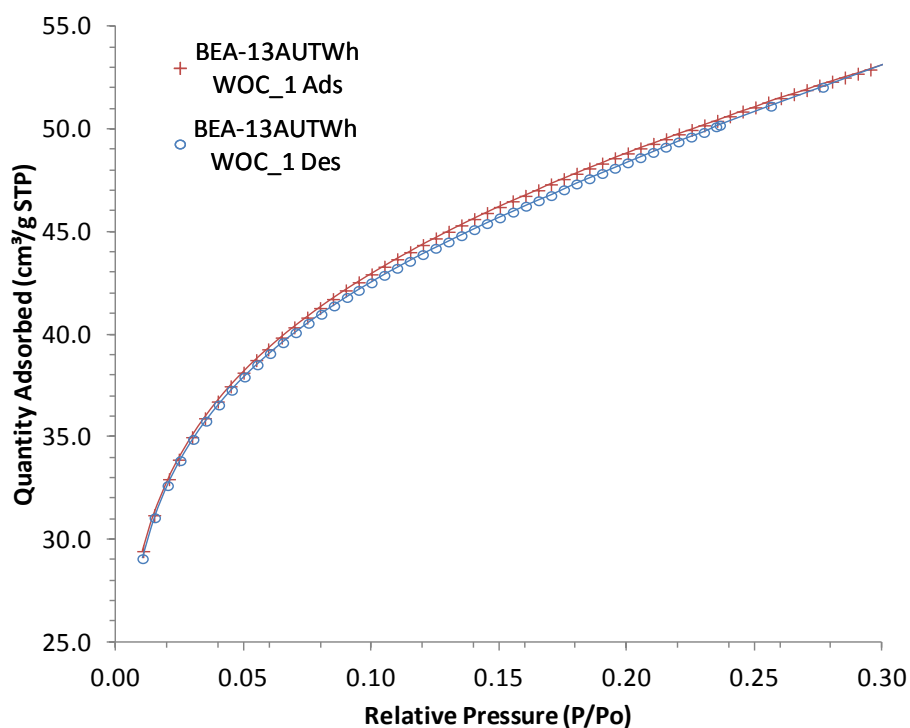


BET adsorption/desorption isotherms for BEA-13AUT WHITE, with a relative pressure range of 0.01 to 0.30 P/Po

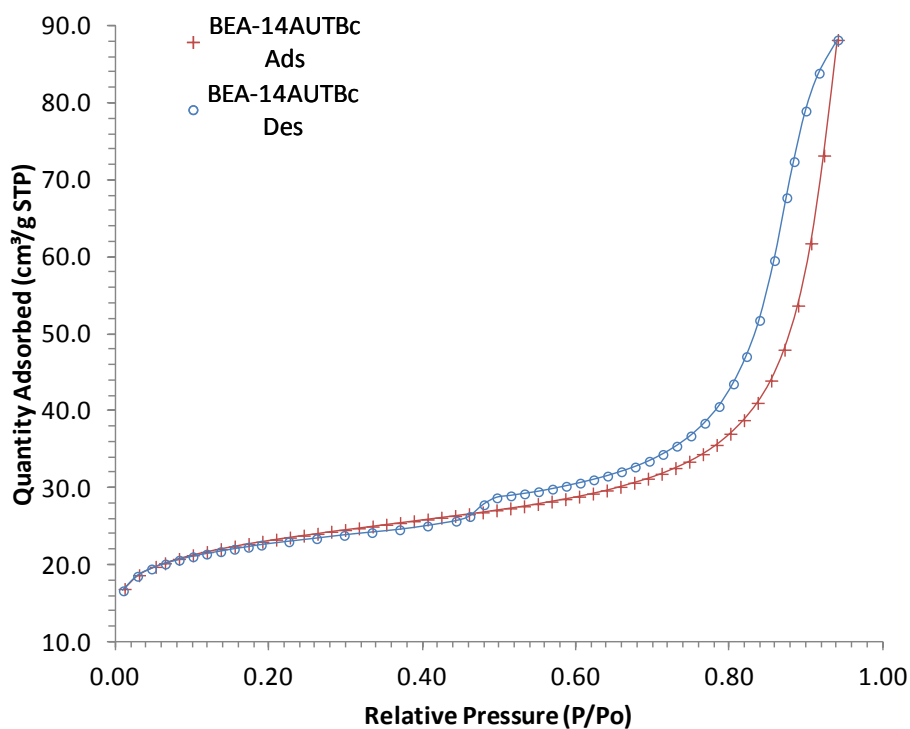


BET adsorption/desorption isotherms for BEA-13AUT WHITE WOC, with a relative pressure range of 0.01 to 0.95

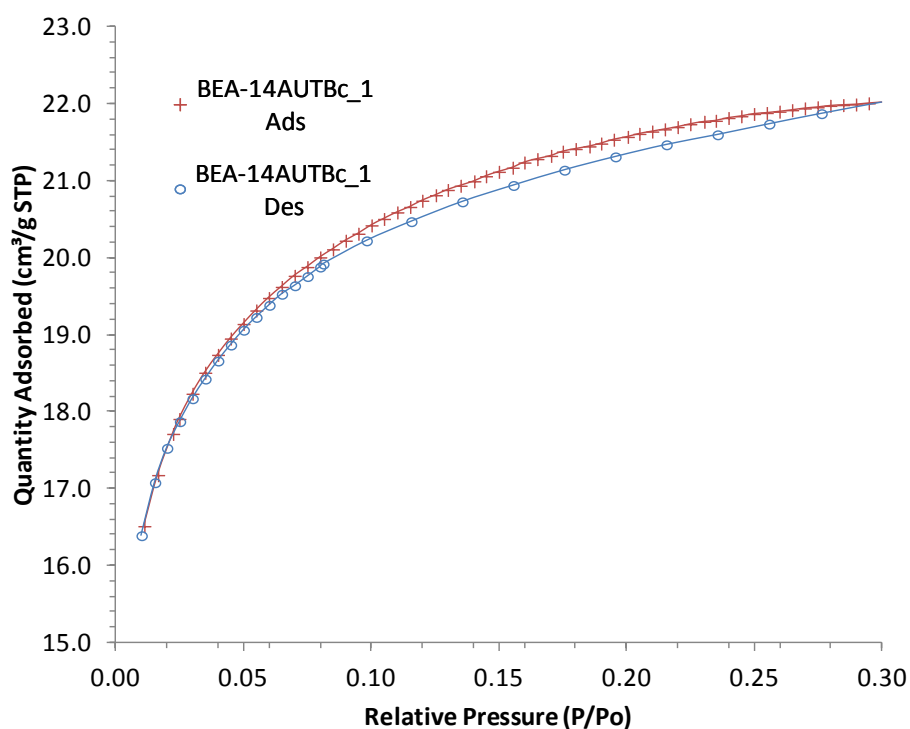
P/P₀



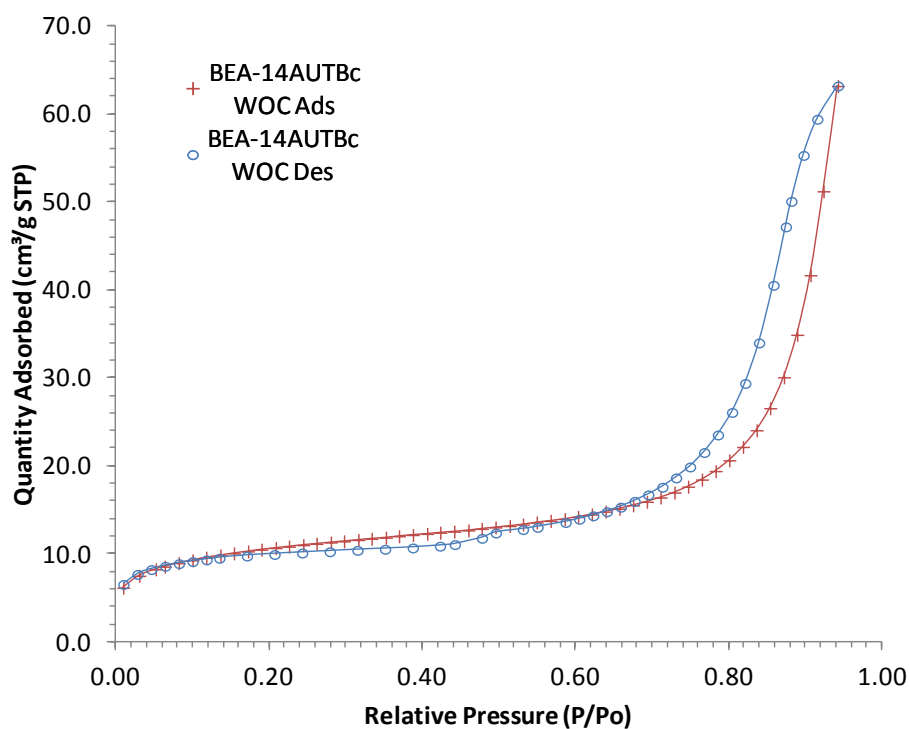
BET adsorption/desorption isotherms for BEA-13AUT WHITE WOC, with a relative pressure range of 0.01 to 0.30 P/P₀



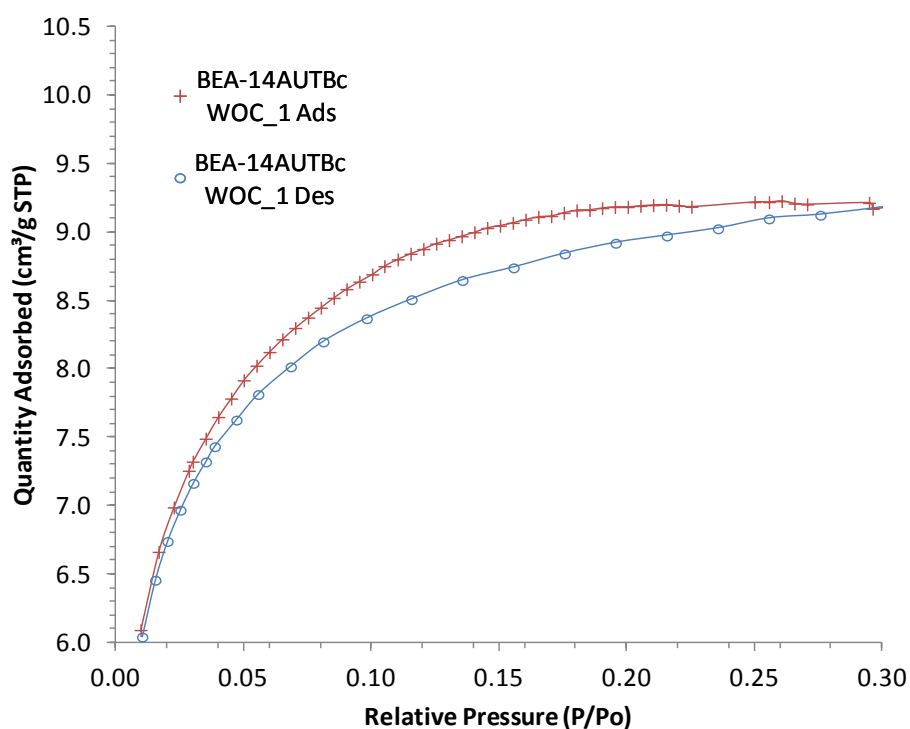
BET adsorption/desorption isotherms for BEA-14AUT BLACK, with a relative pressure range of 0.01 to 0.95 P/Po



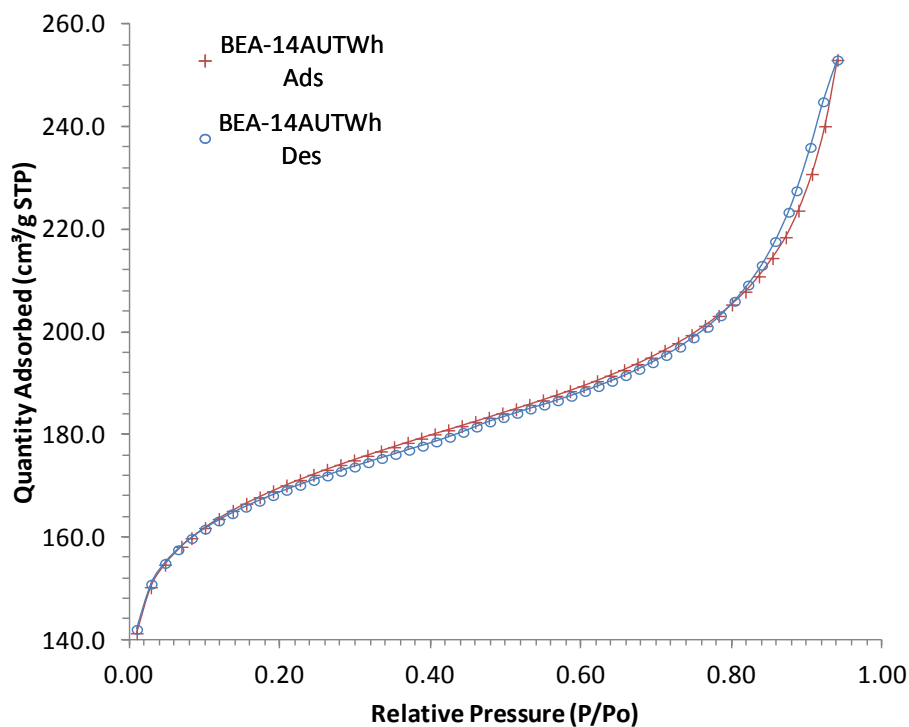
BET adsorption/desorption isotherms for BEA-14AUT BLACK, with a relative pressure range of 0.01 to 0.30 P/Po



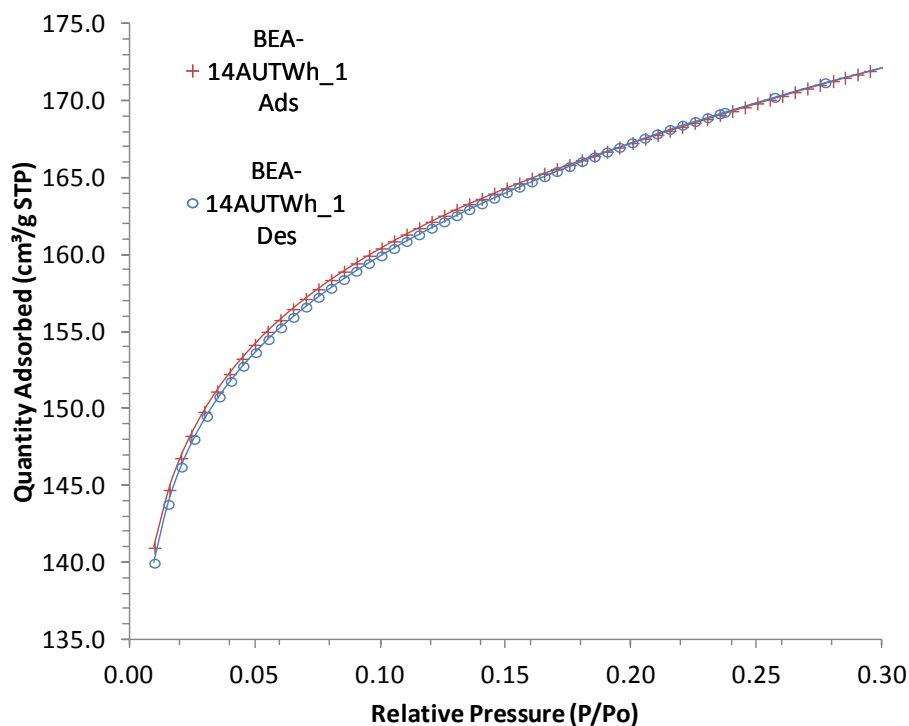
BET adsorption/desorption isotherms for BEA-14AUT BLACK WOC, with a relative pressure range of 0.01 to 0.95 P/Po



BET adsorption/desorption isotherms for BEA-14AUT BLACK WOC, with a relative pressure range of 0.01 to 0.30 P/Po



BET adsorption/desorption isotherms for BEA-14AUT WHITE, with a relative pressure range of 0.01 to 0.95 P/Po



BET adsorption/desorption isotherms for BEA-14AUT WHITE, with a relative pressure range of 0.01 to 0.30 P/Po

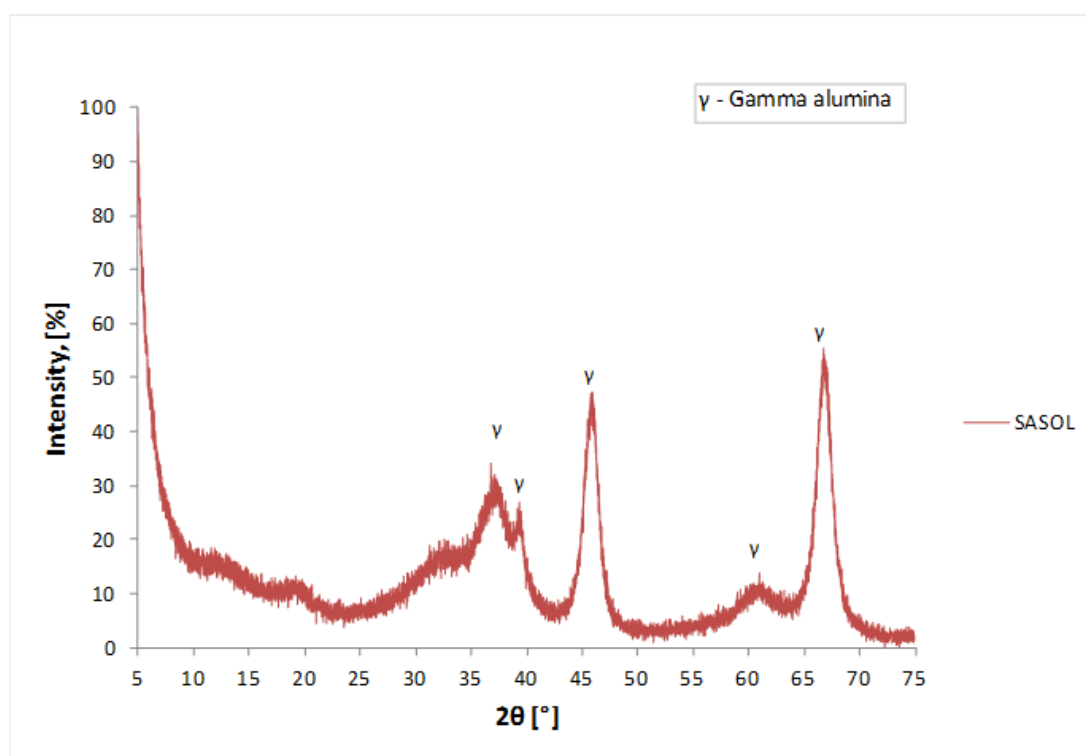
Appendix D

X-ray diffraction (XDR)

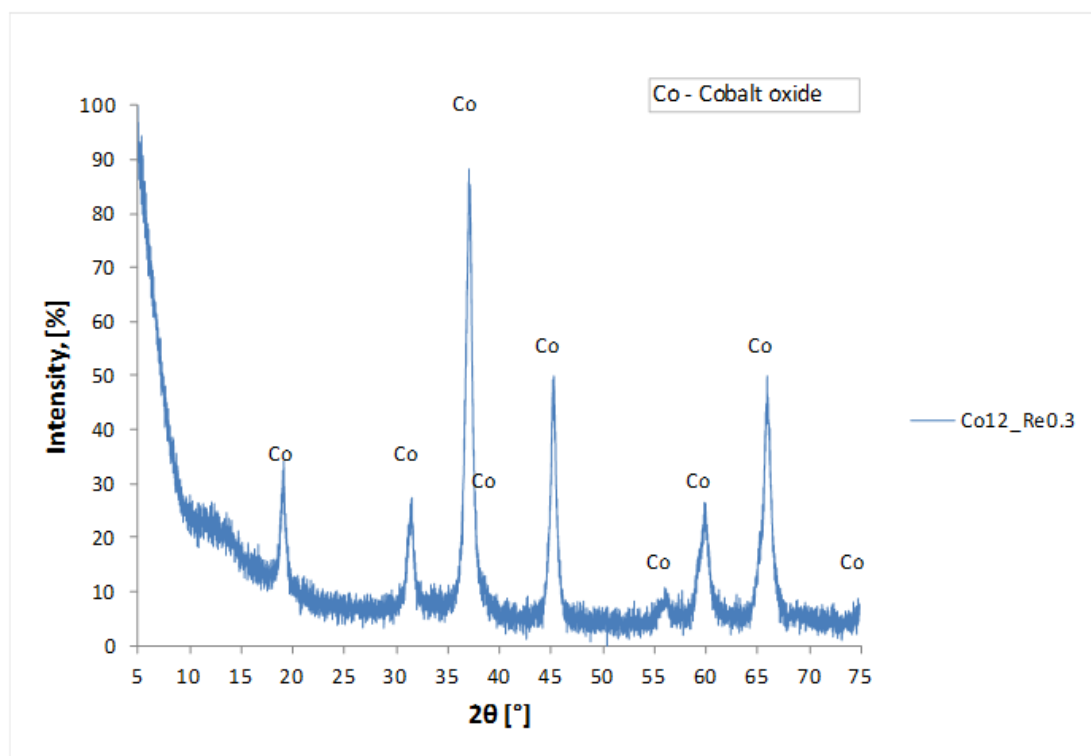
Powder diffraction patterns of zeolites and zeolites/Fischer Tropsch catalyst.

In all the plot is contained in the main peaks some symbols that represents:

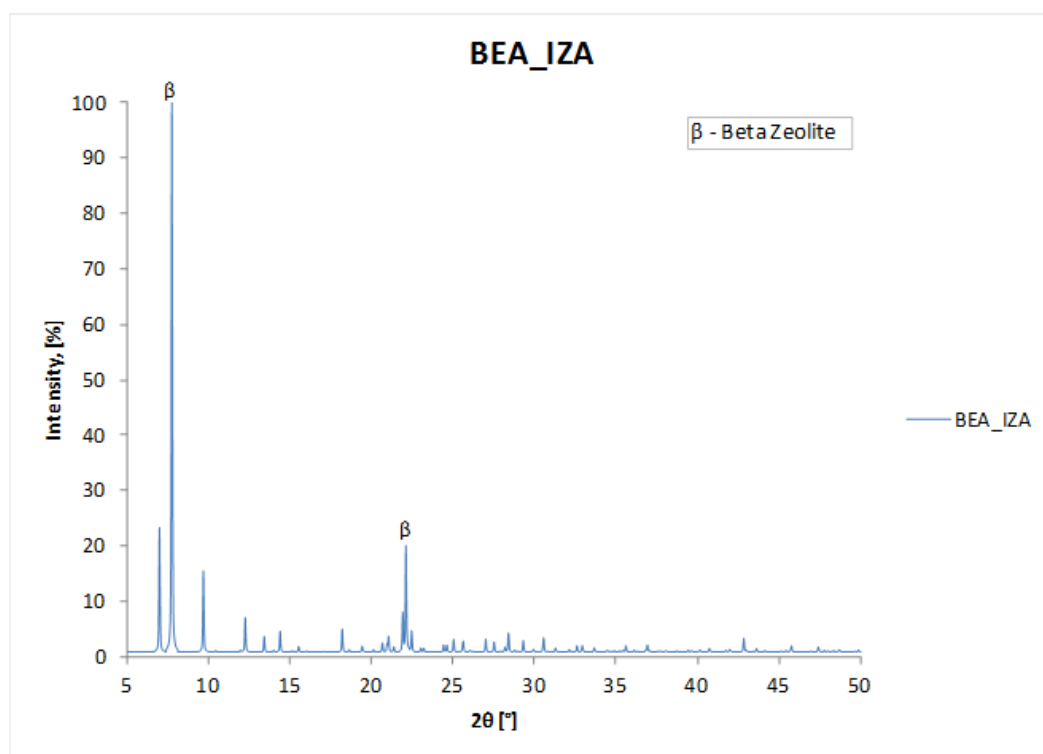
- β represents the main characteristic peaks of β -zeolite, the reference pattern was obtained from IZA [44].
- Co represents the main characteristic peaks for cobalt oxide [15].
- γ represents the main characteristic peaks of gamma alumina [15].



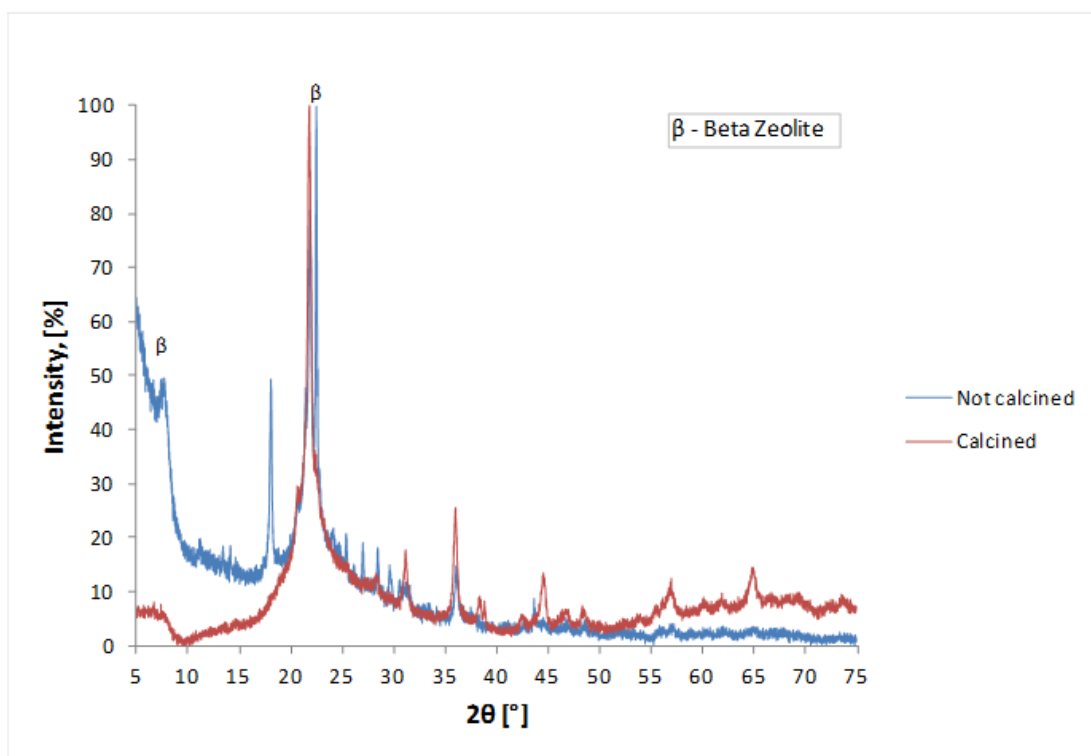
XRD powder pattern for γ -alumina sample, (the alumina is commercialized by Sasol under the brand name PURALOX ®)



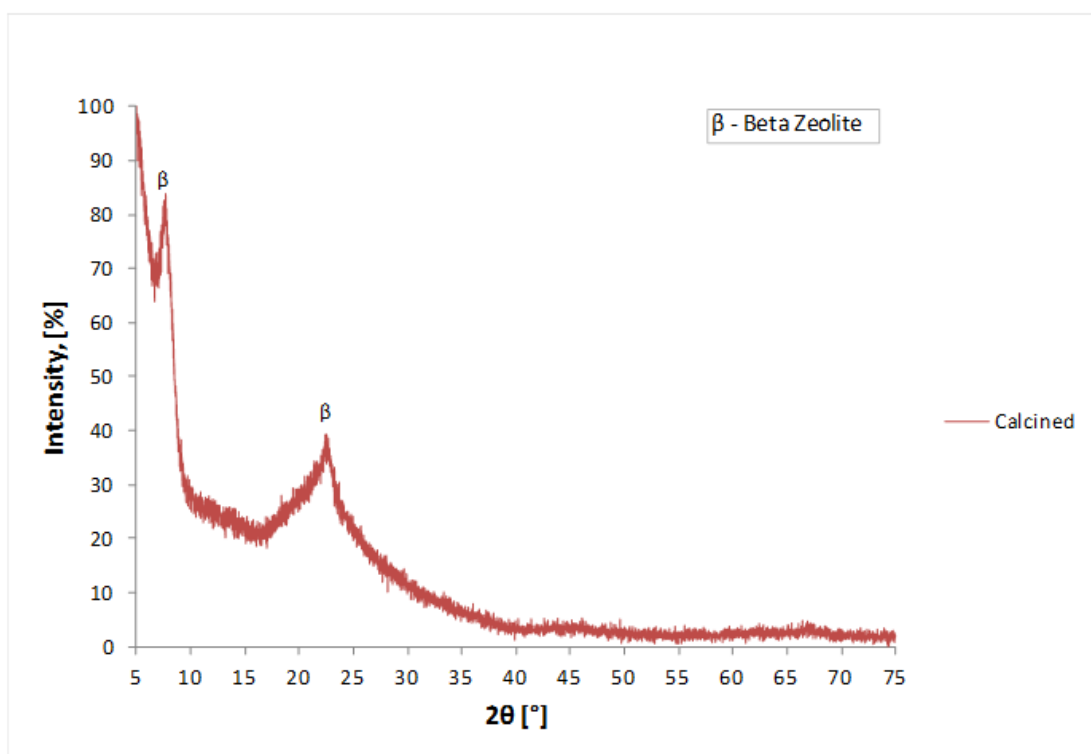
XRD powder pattern for Fischer-Tropsch cobalt-based catalyst sample. The catalyst was provided by Statoil Research Center.



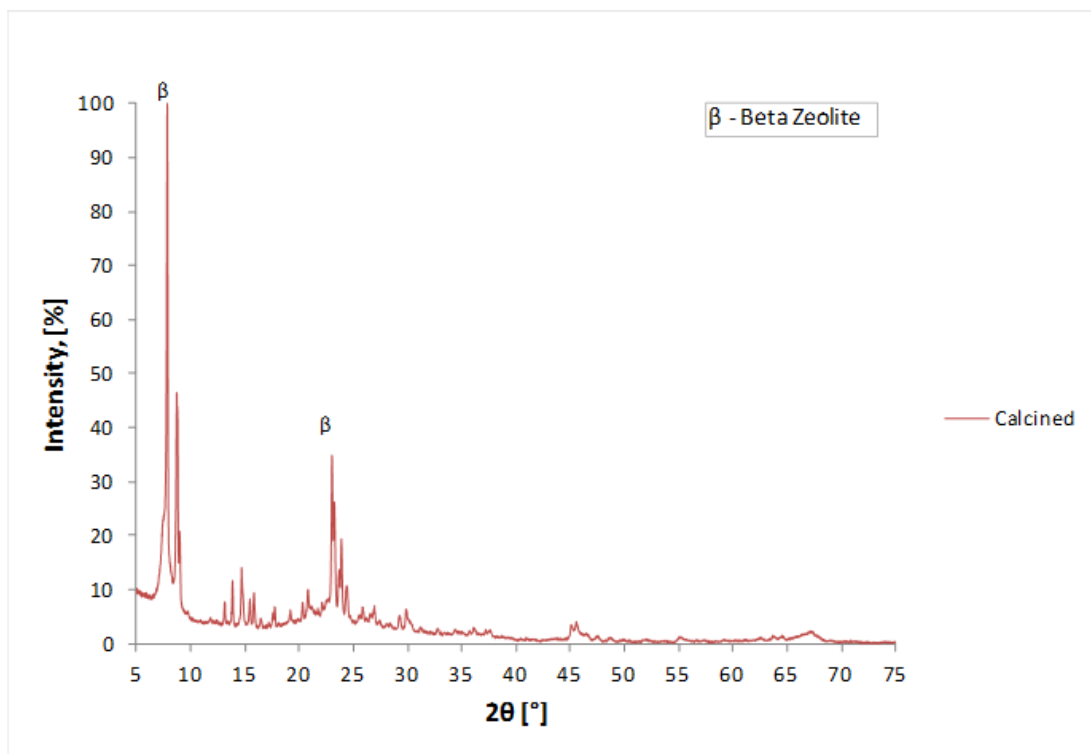
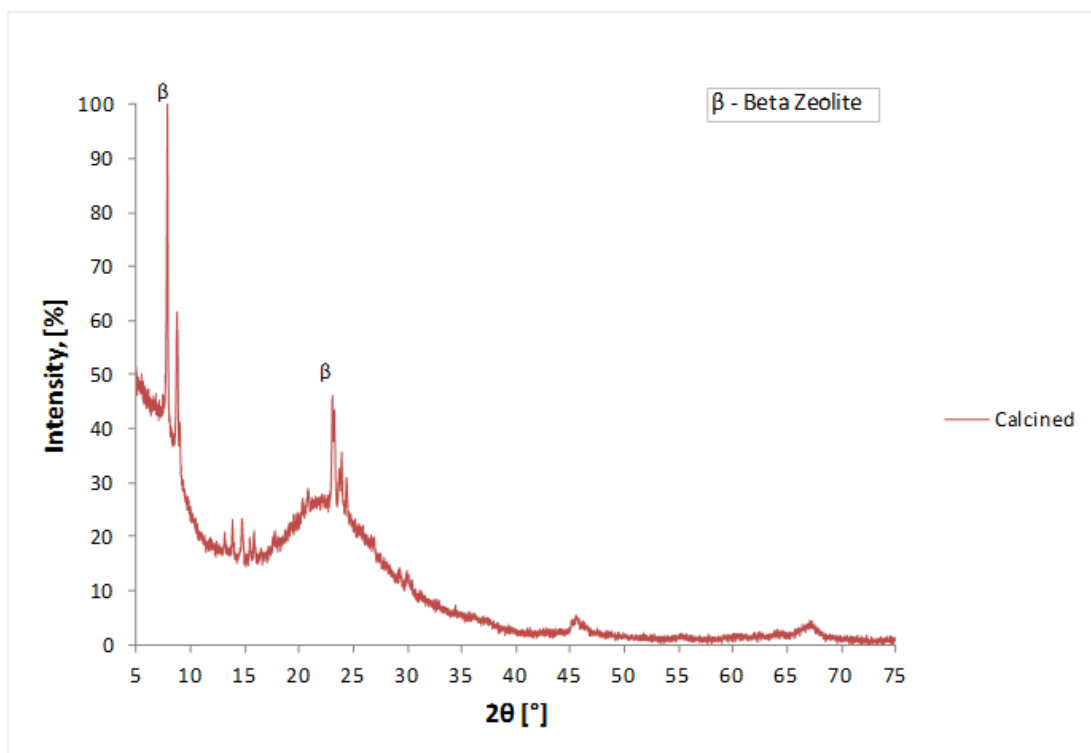
XRD powder pattern for β -zeolite sample, the patter was obtained from the Collection of Simulated XRD Powder Patterns for Zeolites database of IZA [44].

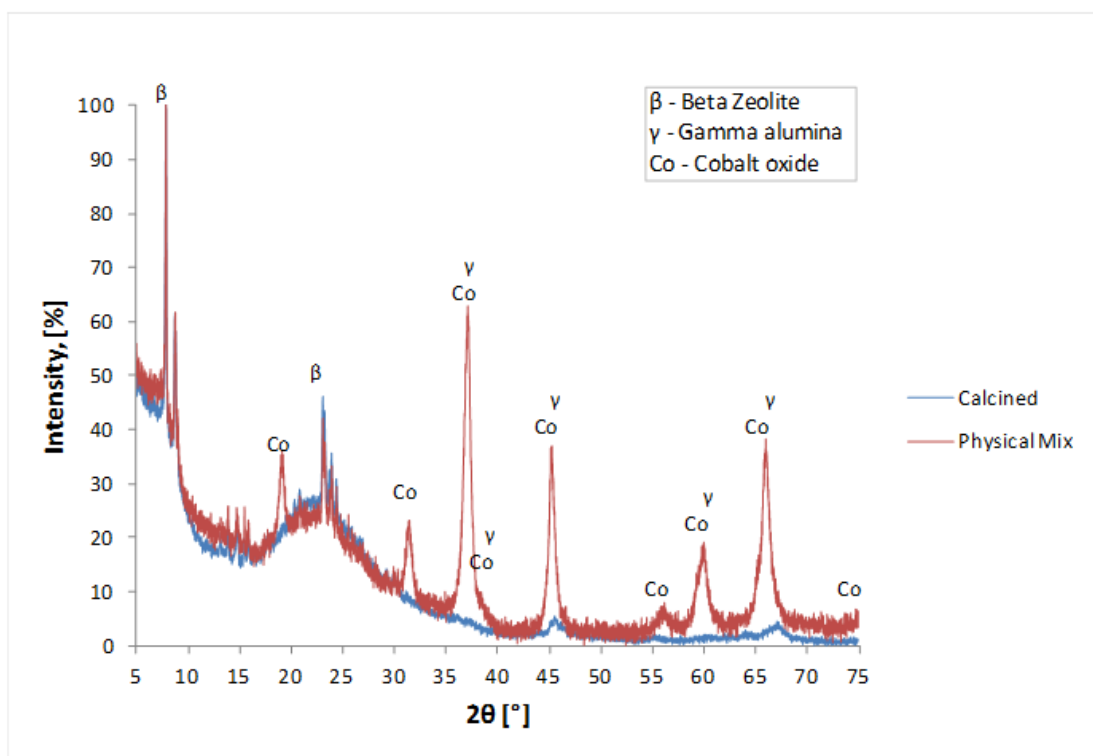


XRD powder pattern for β -zeolite sample BEA-01AUT. The blue line shows the BEA-01AUT sample previous calcination procedure and the red line shows the calcined sample.

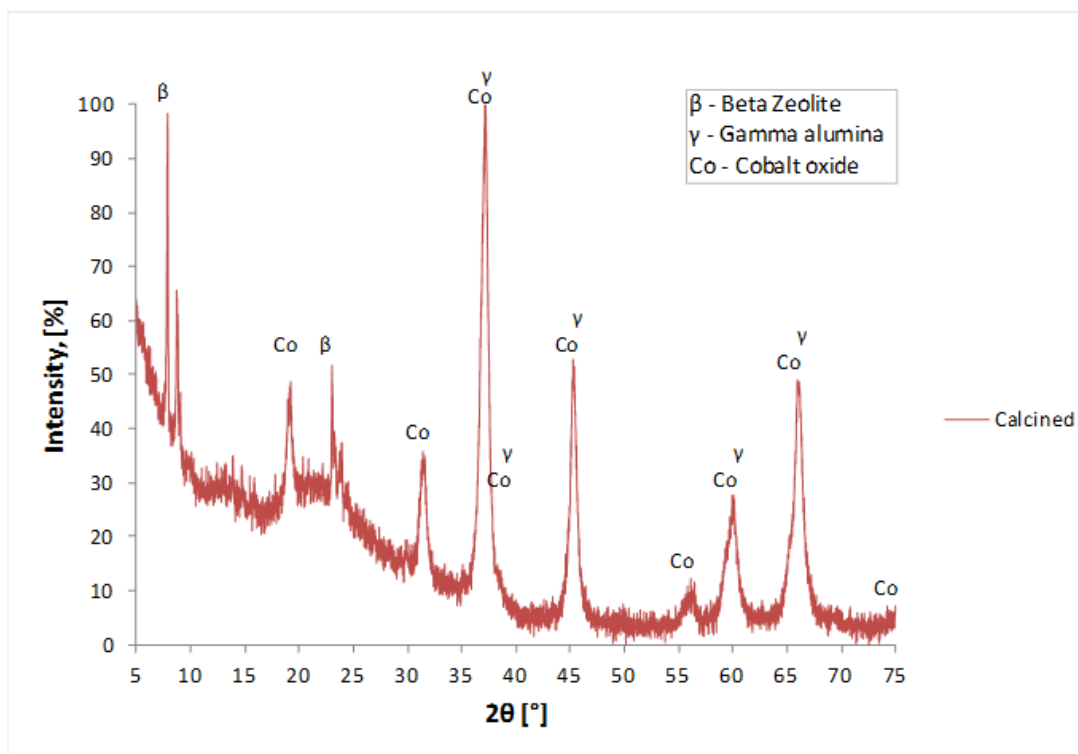


XRD powder pattern for β -zeolite sample BEA-03AUT. The pattern is not completely crystalline due to a failure of the reactor during the synthesis.

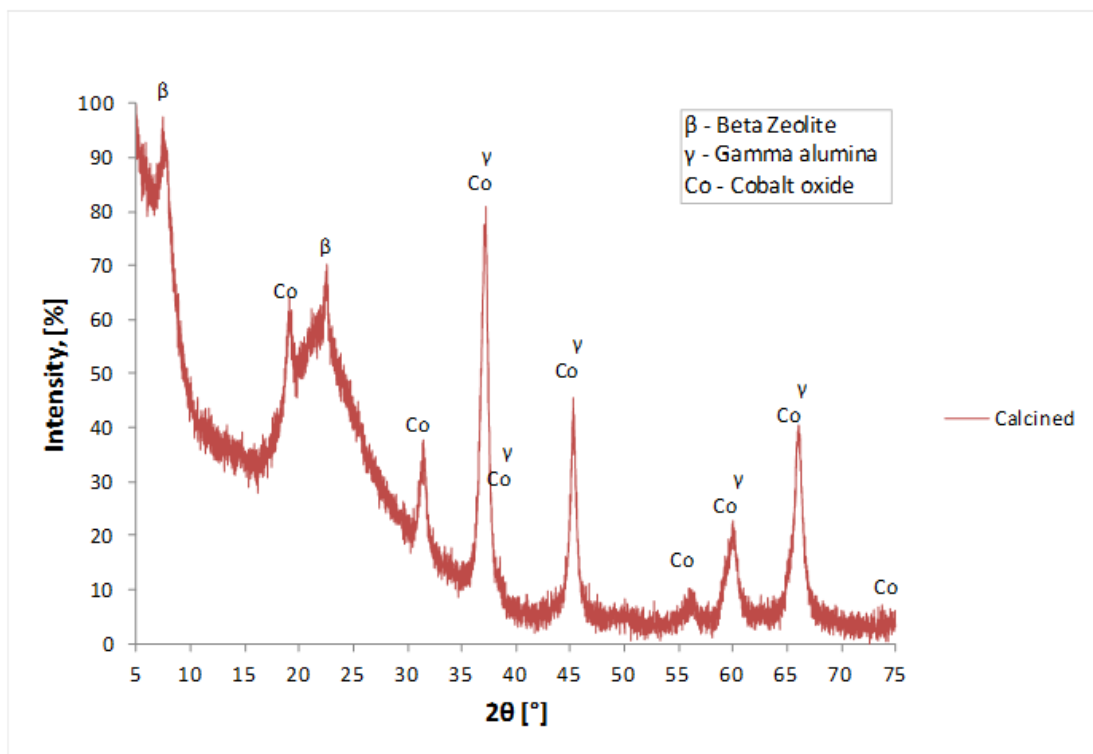
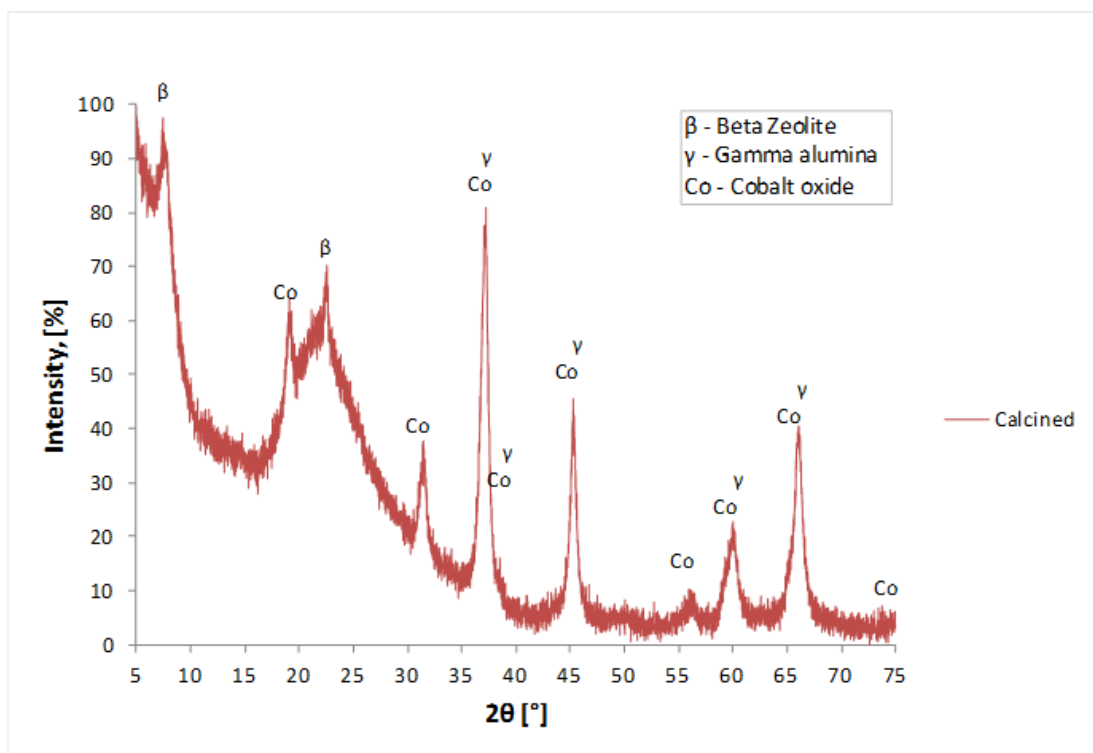
XRD powder pattern for β -zeolite sample BEA-04AUTXRD powder pattern for β -zeolite sample BEA-05AUT

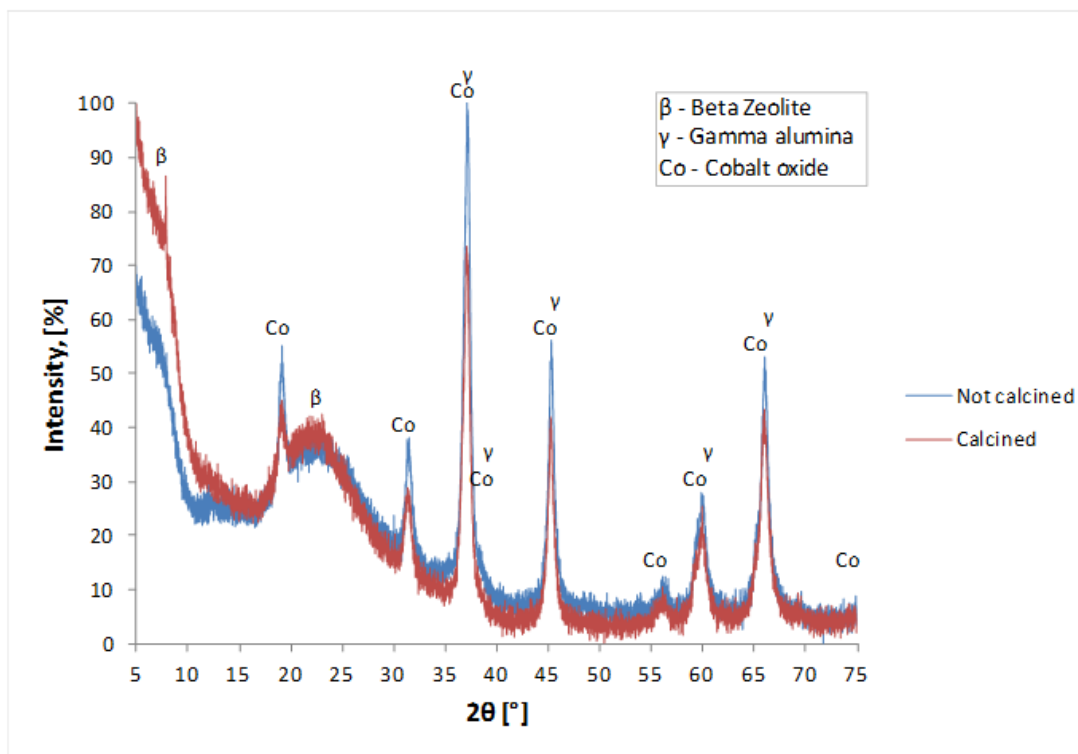
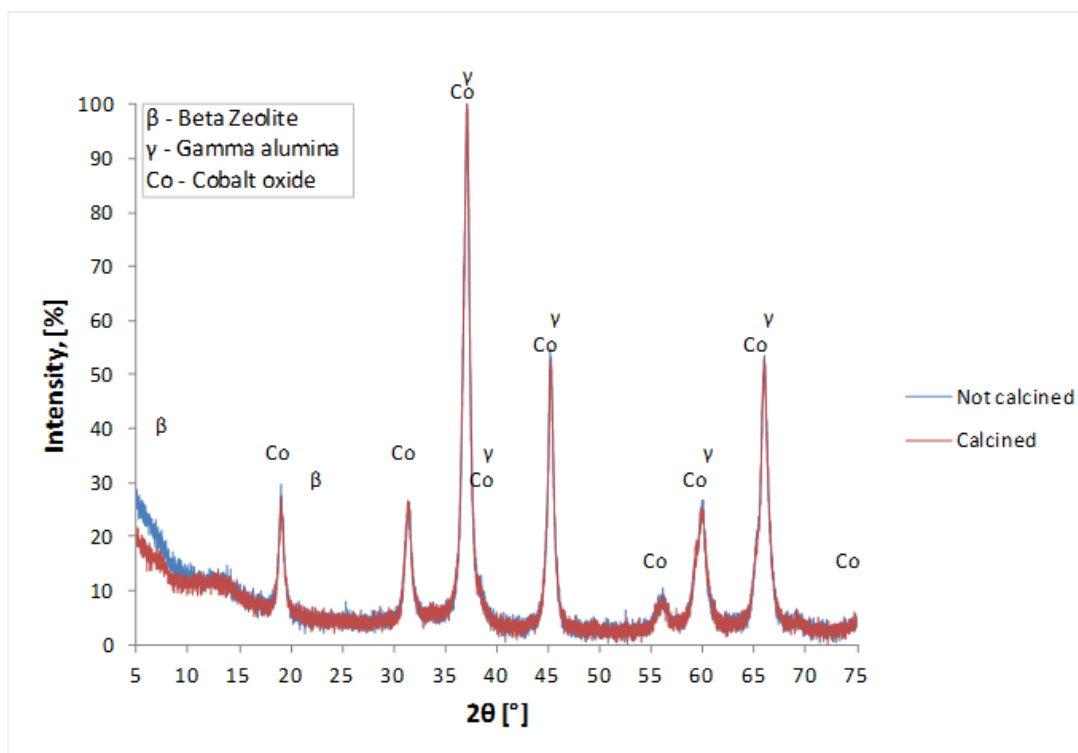


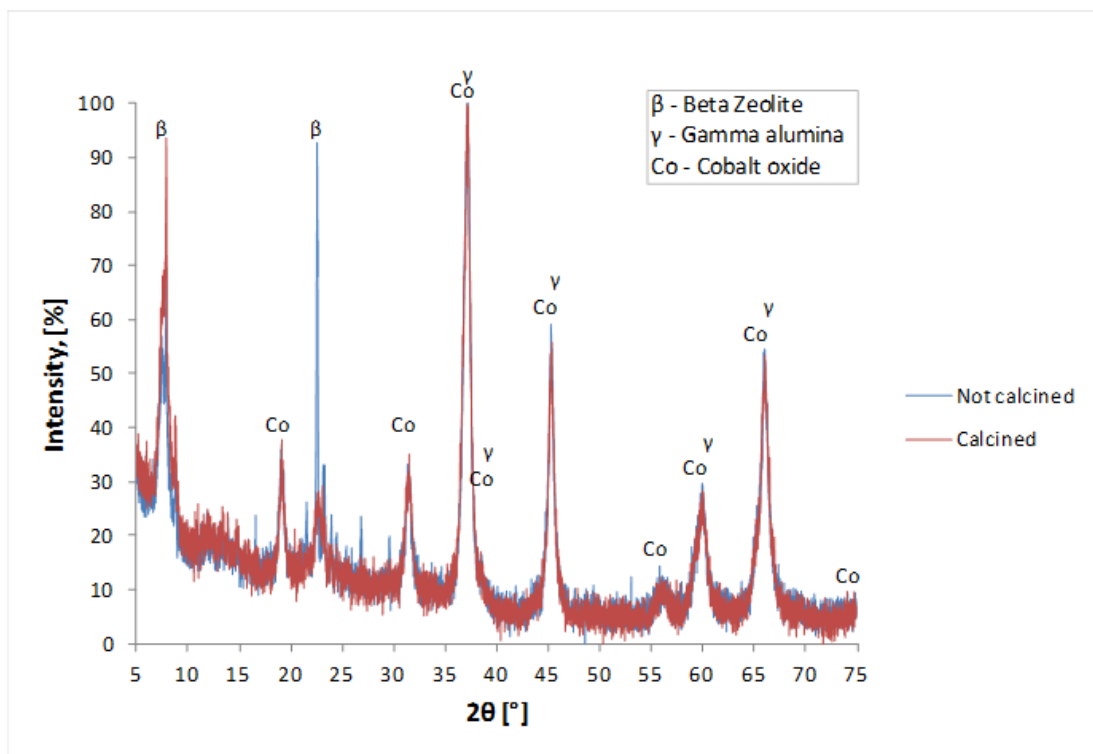
XRD powder pattern for β -zeolite sample BEA-05AUT and Fischer Tropsch catalyst. The sample was a physical mix between both components, the sample was prepared mixing 25 wt% of BEA-05AUT and 75 wt% of Fischer Tropsch catalyst.



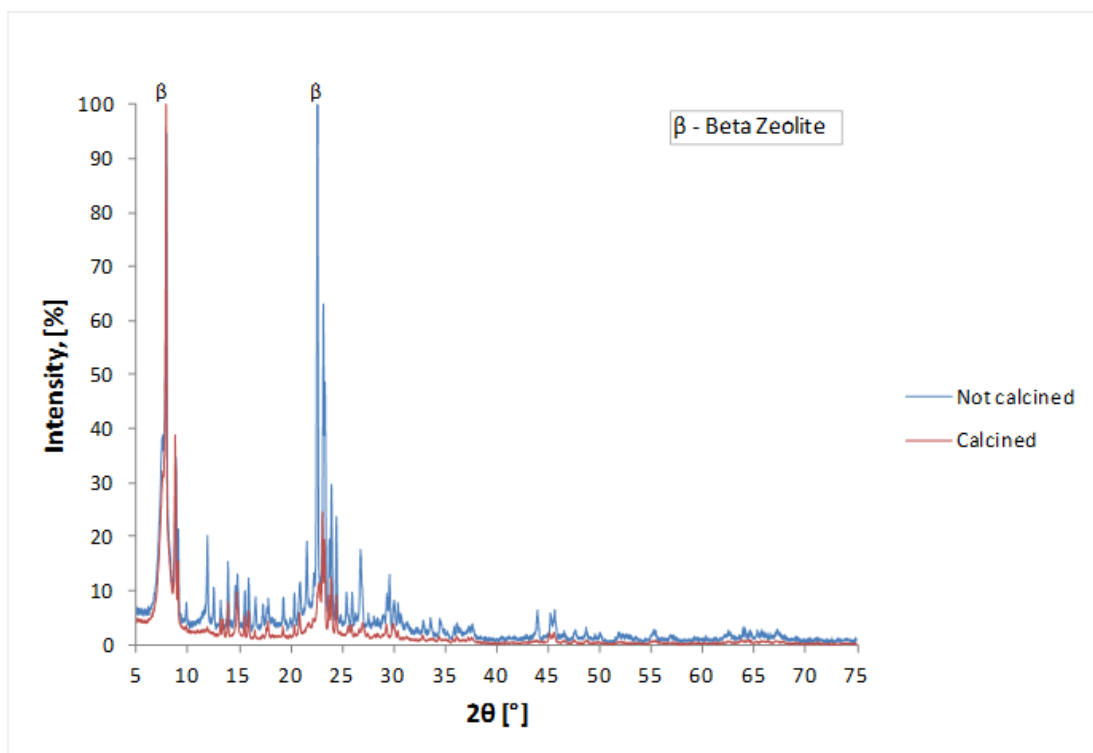
XRD powder pattern for β -zeolite sample BEA-06AUT

XRD powder pattern for β -zeolite sample BEA-07AUTXRD powder pattern for β -zeolite sample BEA-08AUT

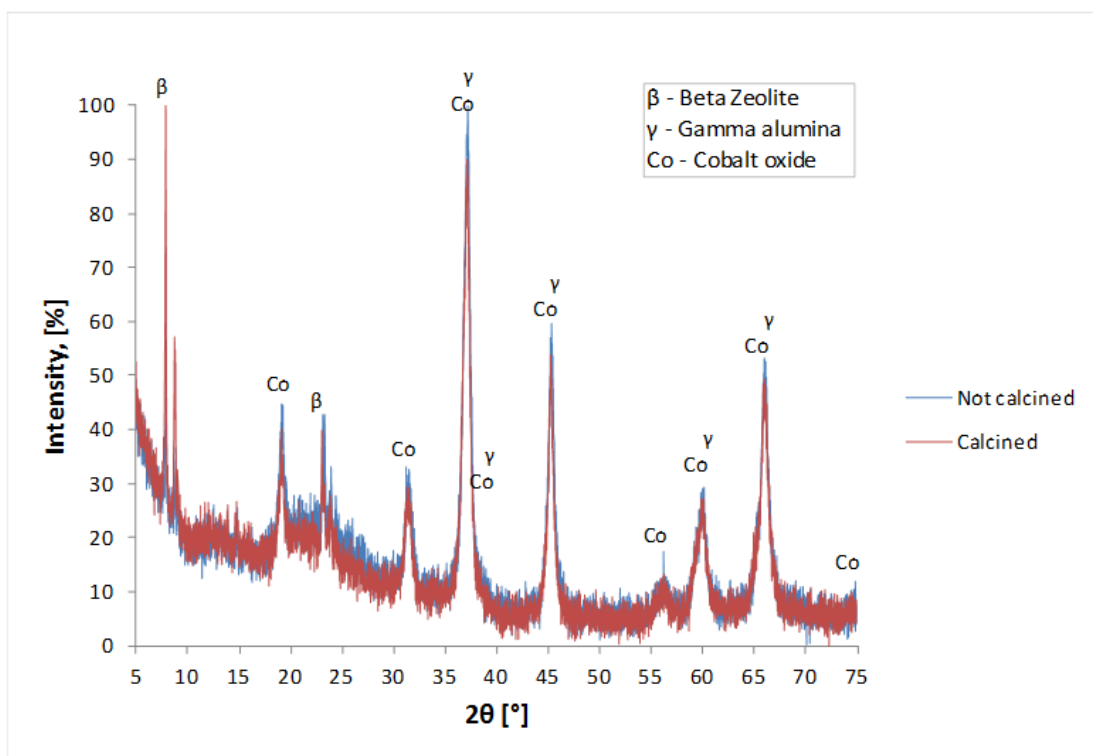
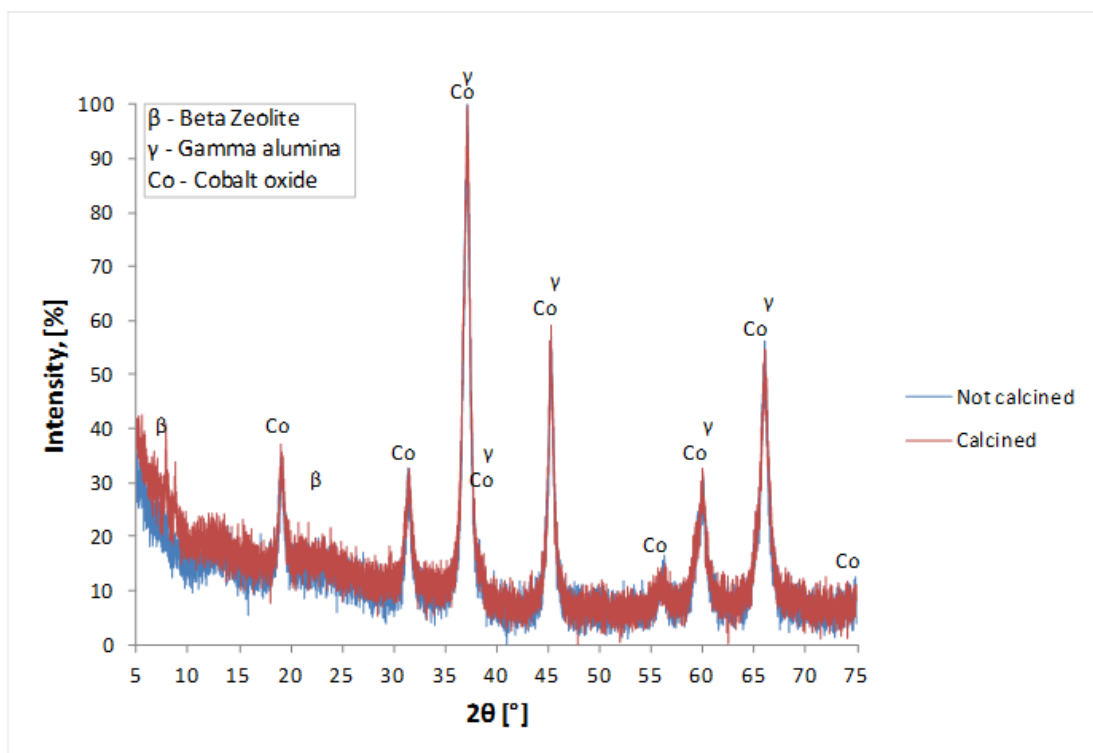
XRD powder pattern for β -zeolite sample BEA-09AUTXRD powder pattern for β -zeolite sample BEA-10AUT

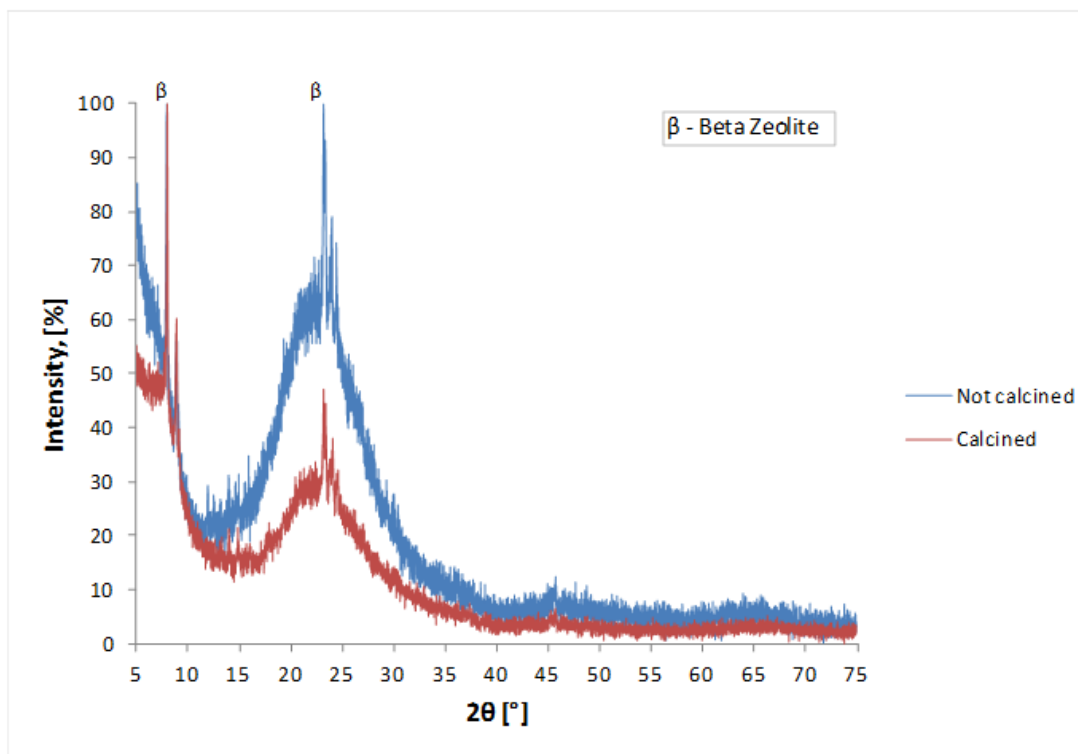


XRD powder pattern for β -zeolite sample BEA-11AUT, Black sample



XRD powder pattern for β -zeolite sample BEA-11AUT, White sample

XRD powder pattern for β -zeolite sample BEA-12AUTXRD powder pattern for β -zeolite sample BEA-13AUT, Black sample



XRD powder pattern for Beta β -zeolite BEA-13AUT, white sample

Appendix E

Scanning electron microscope (SEM)

This appendix shows a collection of different images of the solid components in the final zeolite/FT catalyst. The Images of the solids are γ -alumina, pure β -zeolite, β -zeolite/FT catalyst and β -zeolite from white phase in some of the reactions.

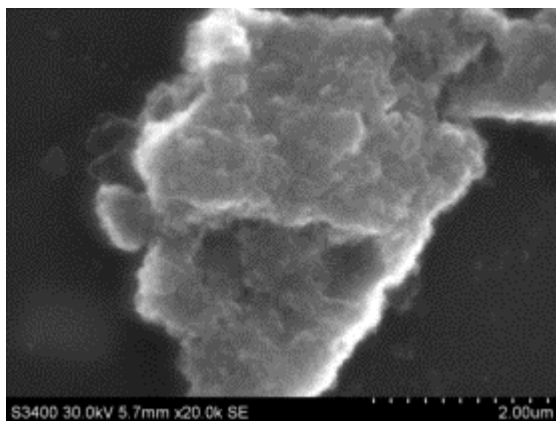
γ -alumina (called SASOL) images that represent the importance of the proper selection of coating material and also the right time to obtain the proper cover layer over the not conducting materials. Two different conducting materials were employed during the coating procedure, carbon and gold.

All the samples included in this appendix are calcined samples, is not any physical difference between calcined and not calcined samples, then SEM cannot provide useful information about it.

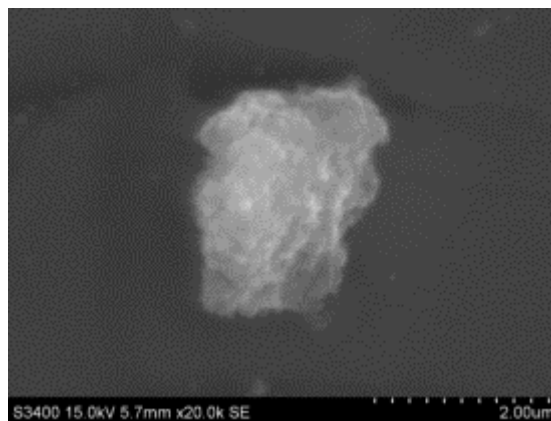
In the case of the pure β -zeolite from BEA-01 AUT to BEA-05 AUT and β -zeolite/FT catalyst from BEA-06AUT to BEA-14 AUT, all the samples were coated with gold for 120 seconds. The only exception is BEA-02 AUT that is not a success material due to reactor failures this sample was not characterized.

In the carbon-coated materials the number represents how many times the automatic coating sequence was used over the particle. The sequence takes 8 seconds every time at maximum intensity.

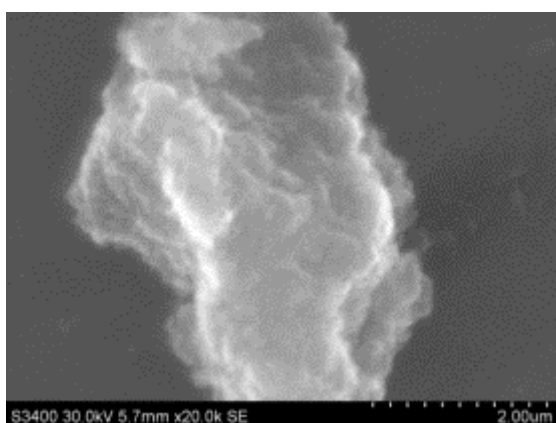
γ -alumina carbon-coated



SASOL, 2 CARBON LAYERS



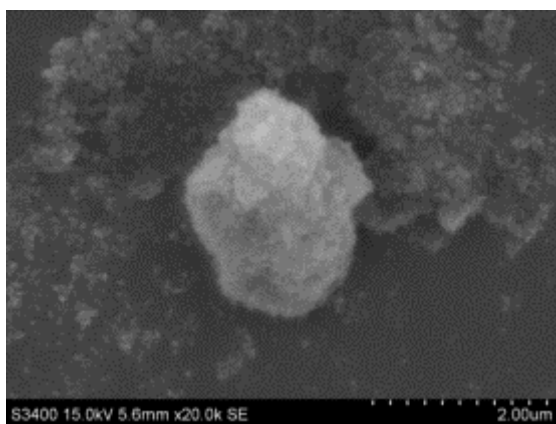
SASOL, 4 CARBON LAYERS



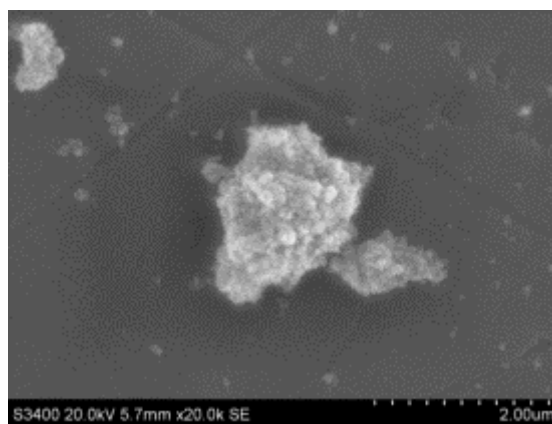
SASOL, 8 CARBON LAYERS

In the gold-coated materials, the number represents the number of seconds that the samples were exposed to the coated source at maximum intensity.

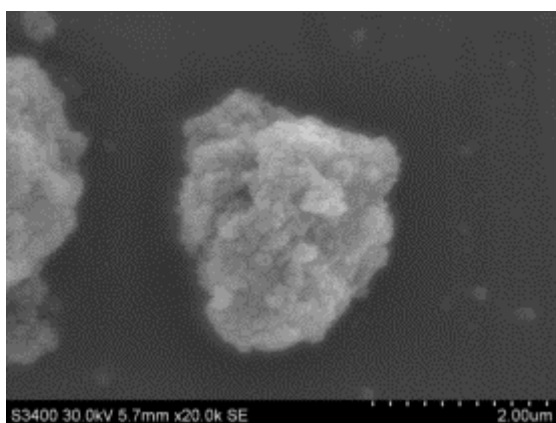
γ -alumina gold-coated



SASOL, 30 SEC GOLD LAYER



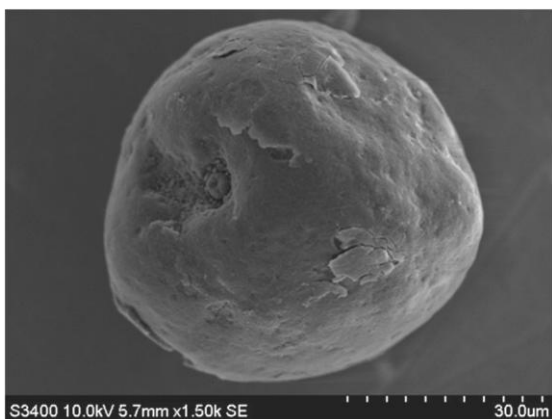
SASOL, 60 SEC GOLD LAYER



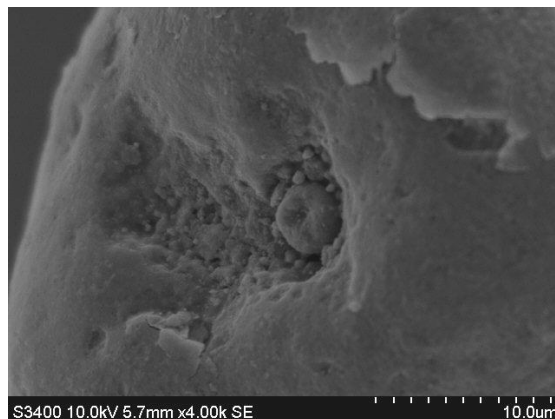
SASOL, 120 SEC GOLD LAYER

The Fischer Tropsch cobalt-based catalyst provided by Statoil Research Center.

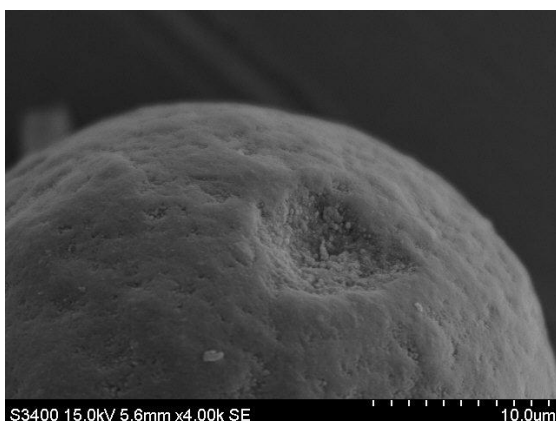
Fischer Tropsch cobalt-based catalyst gold-coated



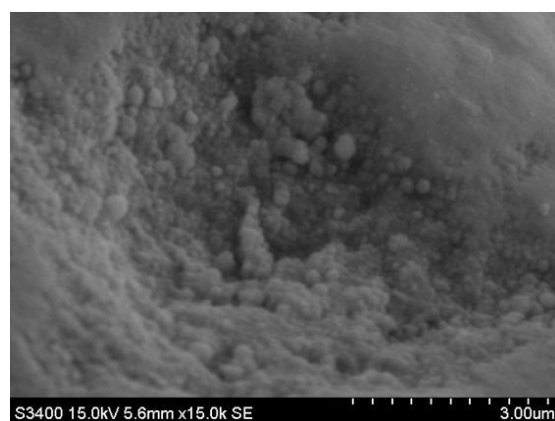
Fischer Tropsch catalyst, 30µm



Fischer Tropsch catalyst, 10µm



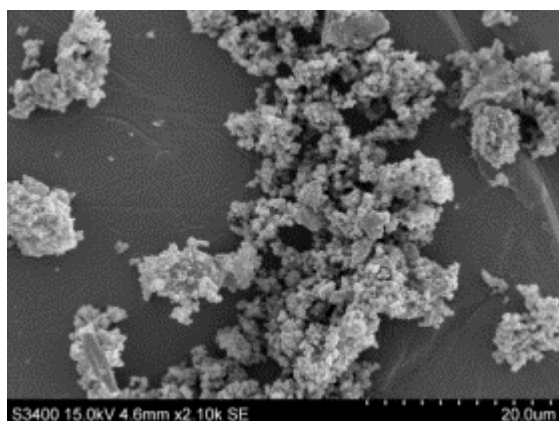
Fischer Tropsch catalyst, 10µm



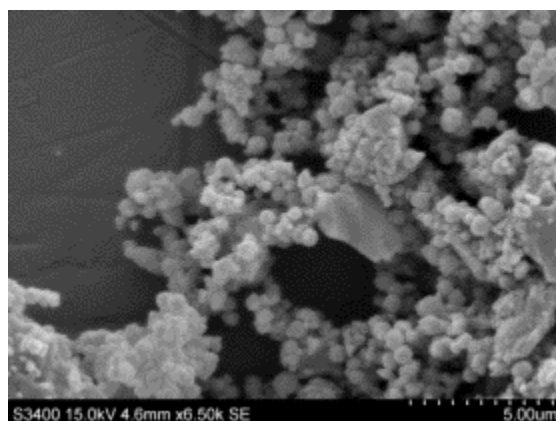
Fischer Tropsch catalyst, 3µm

Images collection that represents the pure β -zeolite products, from BEA-01AUT to BEA-05.

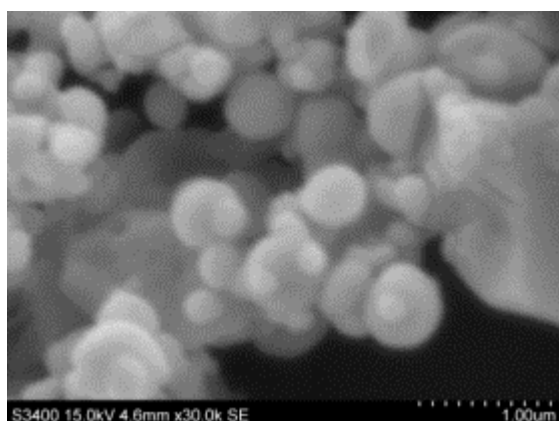
Pure β -zeolite BEA-01AUT gold-coated



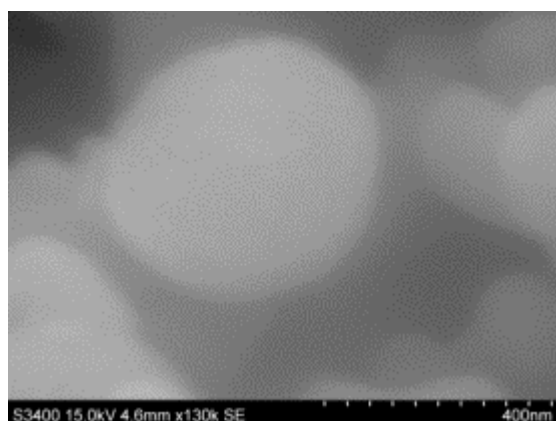
BEA-01AUT, 20 μm



BEA-01AUT, 5 μm

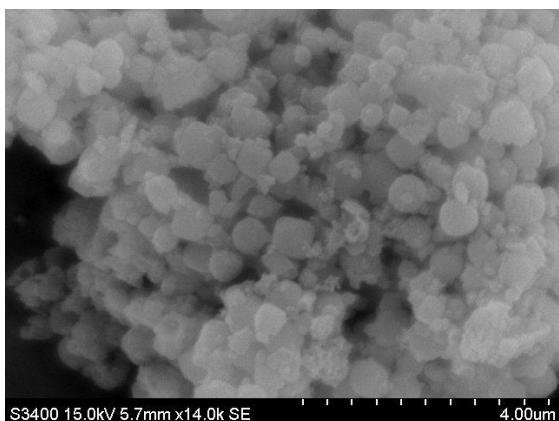


BEA-01AUT, 1 μm

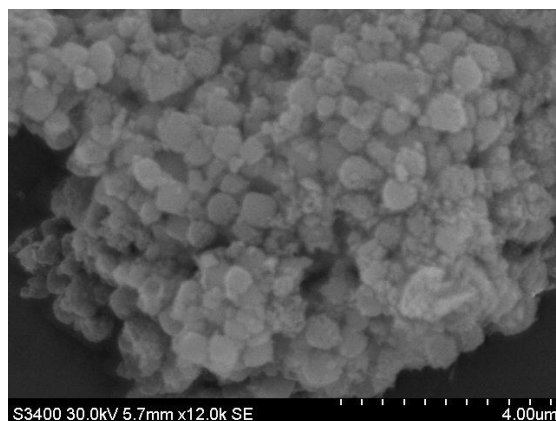


BEA-01AUT, 0.4 μm

Pure β -zeolite BEA-03AUT gold-coated

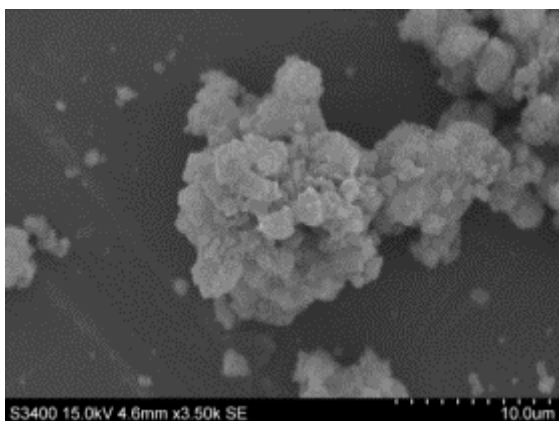


BEA-03AUT, 4 μ m

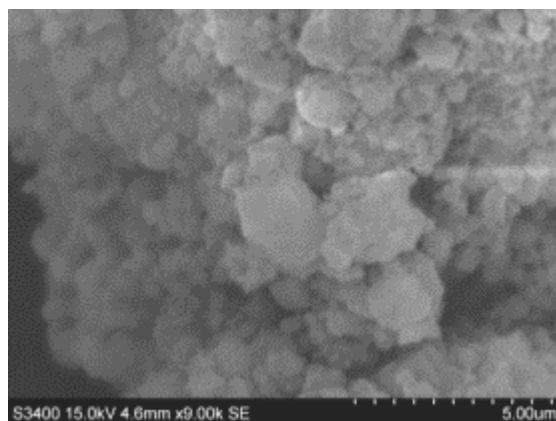


BEA-03AUT, 4 μ m

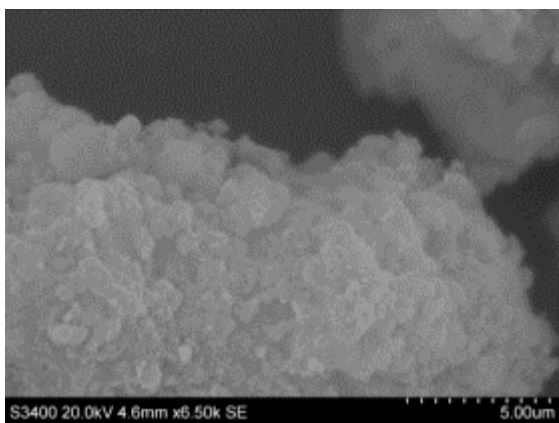
Pure β -zeolite BEA-04AUT gold-coated



BEA-04AUT, 10µm

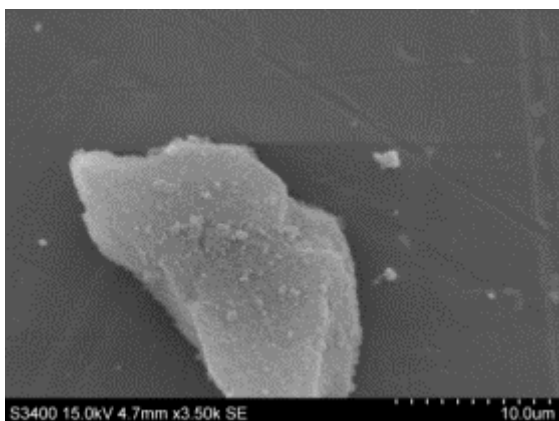


BEA-04AUT, 5µm

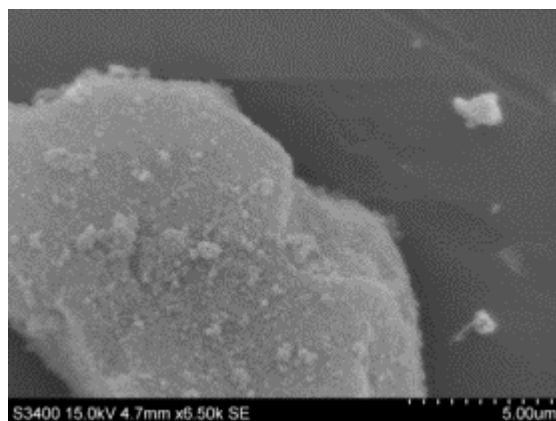


BEA-04AUT, 5µm

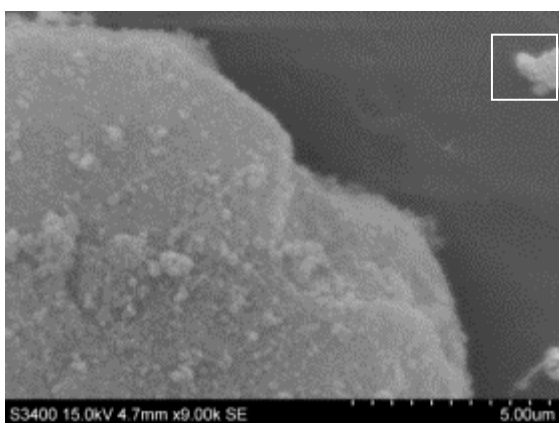
Pure β -zeolite BEA-05AUT gold-coated



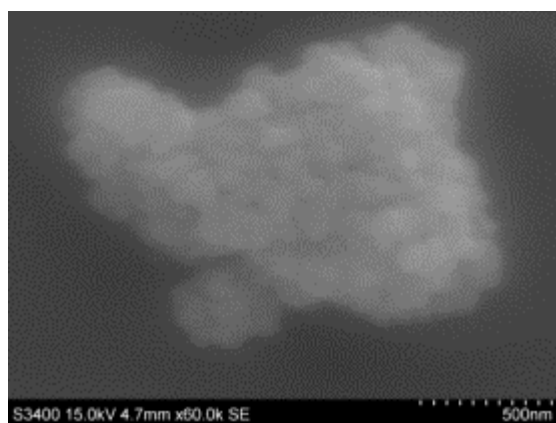
BEA-05AUT, 10µm



BEA-05AUT, 5µm



BEA-05AUT, 5µm



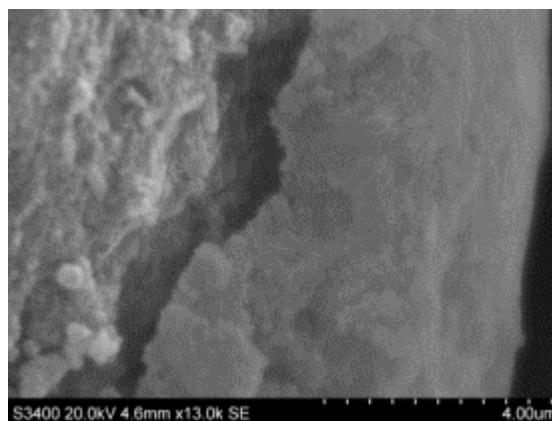
BEA-05AUT, 0.5µm

Images collection that represents the β -zeolite/FT cobalt-based catalyst products, from BEA-06AUT to BEA-14. In the specific cases of BEA-11AUT, BEA-13AUT and BEA-14AUT the two phases are characterized.

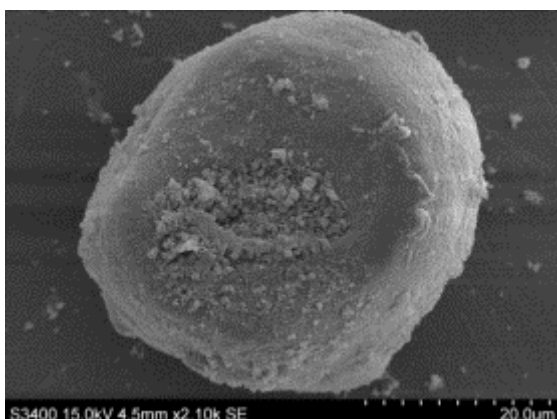
β -zeolite/FT cobalt-based catalyst BEA-06AUT gold-coated



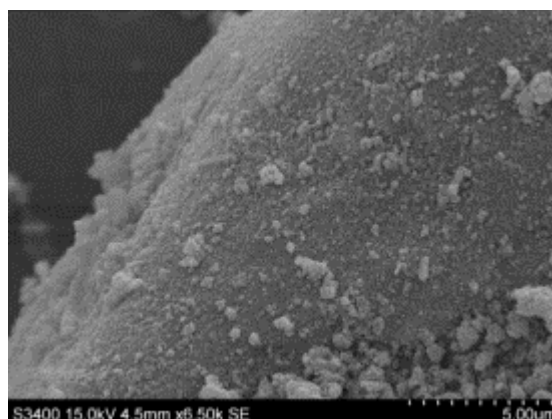
BEA-06AUT, 30 μ m



BEA-06AUT, 4 μ m



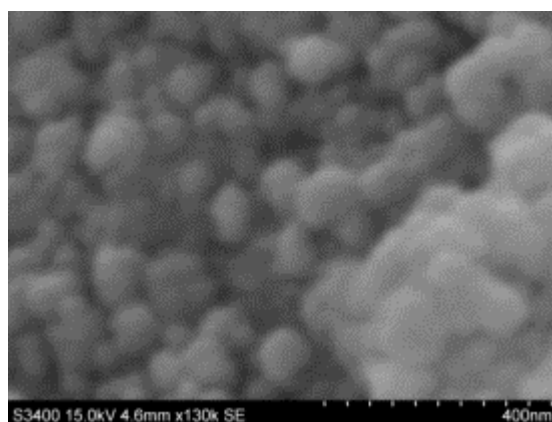
BEA-06AUT, 20 μ m



BEA-06AUT, 5 μ m

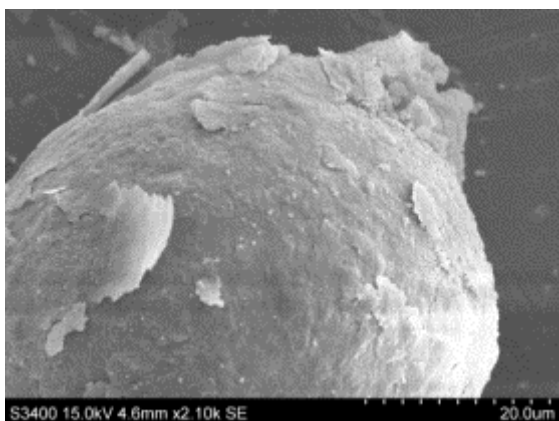


BEA-06AUT, 1 μ m

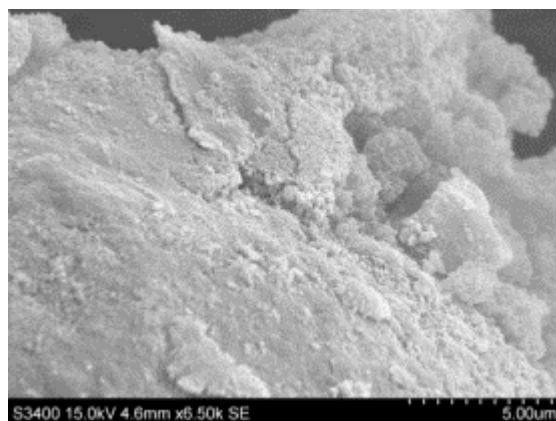


BEA-06AUT, 0.4 μ m

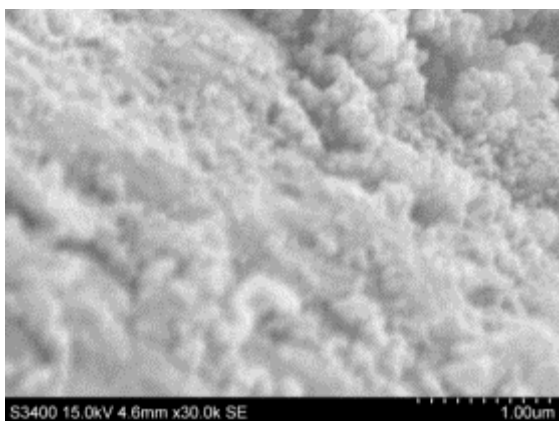
β -zeolite/FT cobalt-based catalyst BEA-07AUT gold-coated



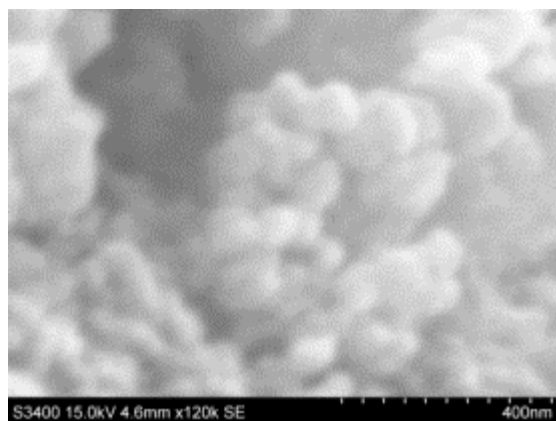
BEA-07AUT, 20 μm



BEA-07AUT, 5 μm



BEA-07AUT, 1 μm

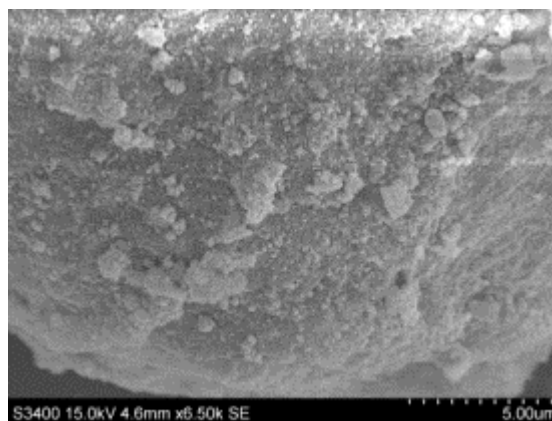


BEA-07AUT, 0.4 μm

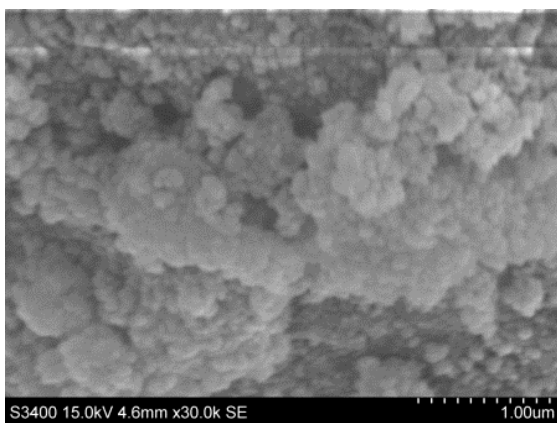
β -zeolite/FT cobalt-based catalyst BEA-08AUT gold-coated



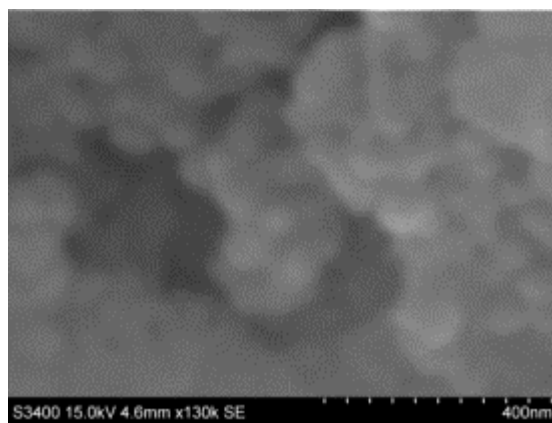
BEA-08AUT, 20μm



BEA-08AUT, 5μm

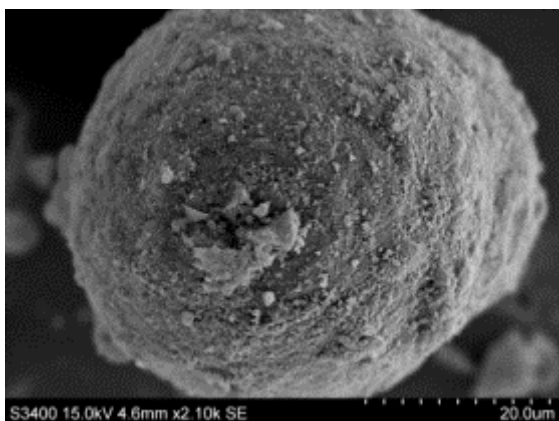


BEA-08AUT, 1μm

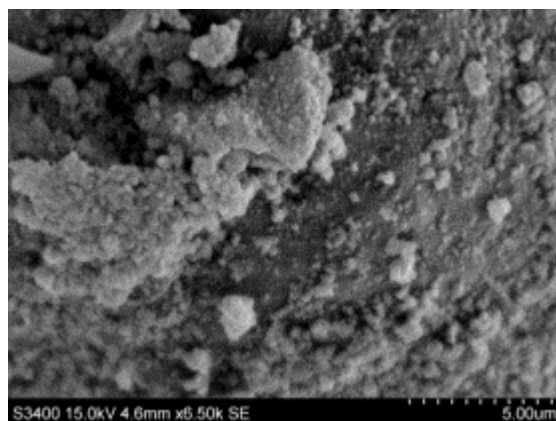


BEA-08AUT, 0.4μm

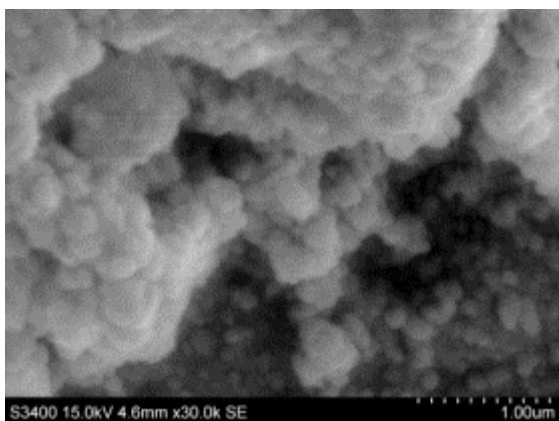
β -zeolite/FT cobalt-based catalyst BEA-09AUT gold-coated



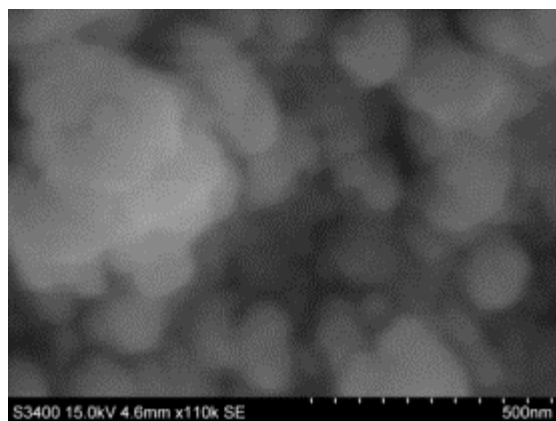
BEA-09AUT, 20 μ m



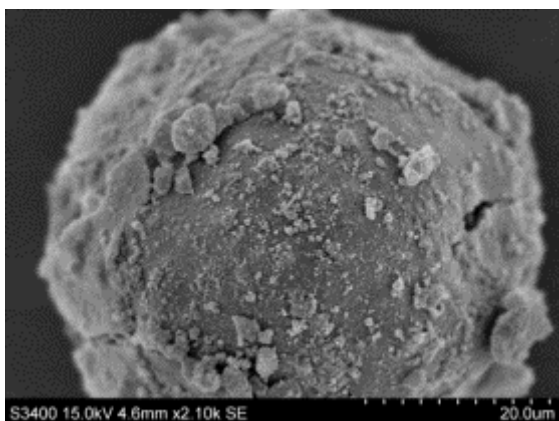
BEA-09AUT, 5 μ m



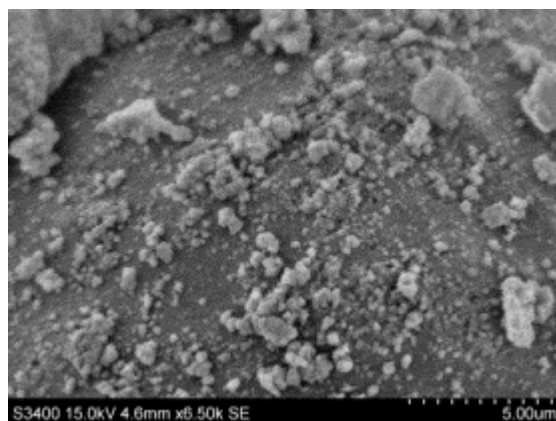
BEA-09AUT, 1 μ m



BEA-09AUT, 0.4 μ m

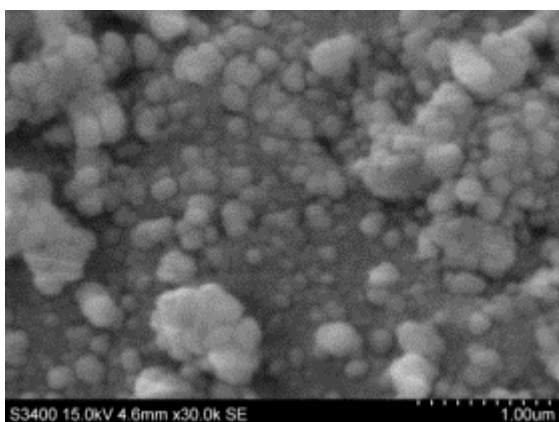


BEA-09AUT, 20 μ m

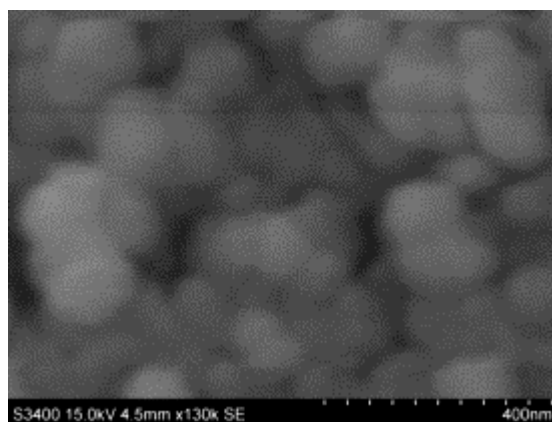


BEA-09AUT, 5 μ m

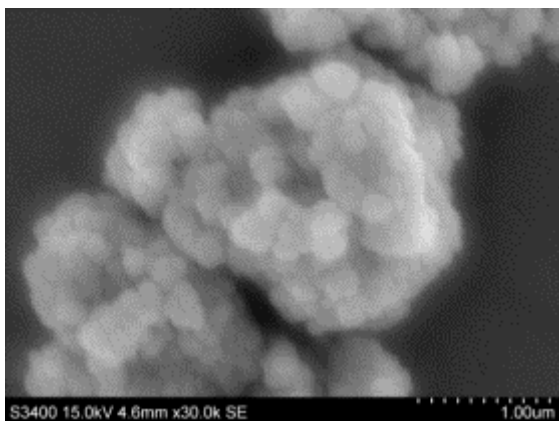
β -zeolite/FT cobalt-based catalyst BEA-09AUT gold-coated (*continued*)



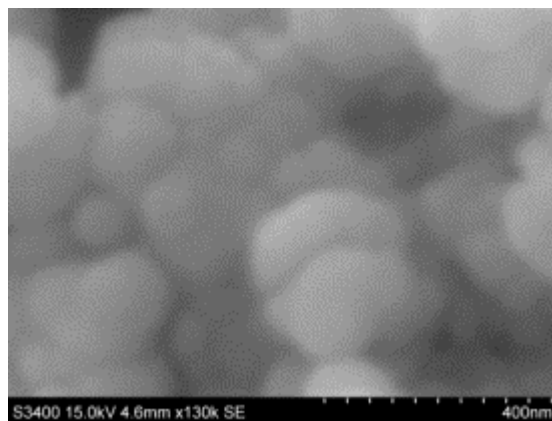
BEA-09AUT, 1 μm



BEA-09AUT, 0.4 μm

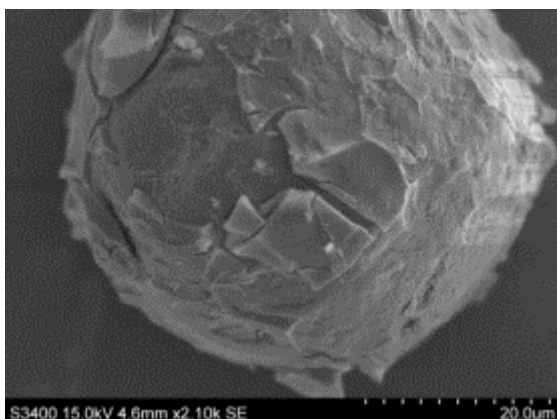


BEA-09AUT, 1 μm

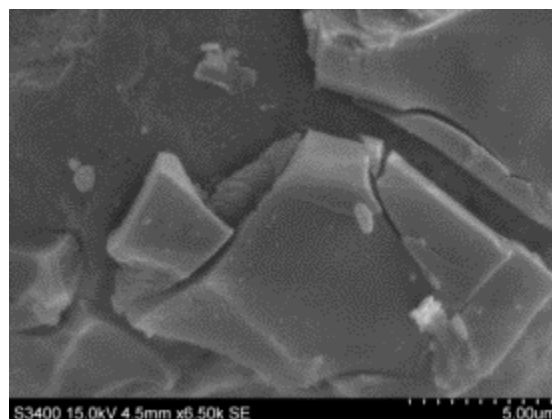


BEA-09AUT, 0.4 μm

β -zeolite/FT cobalt-based catalyst BEA-10AUT gold-coated



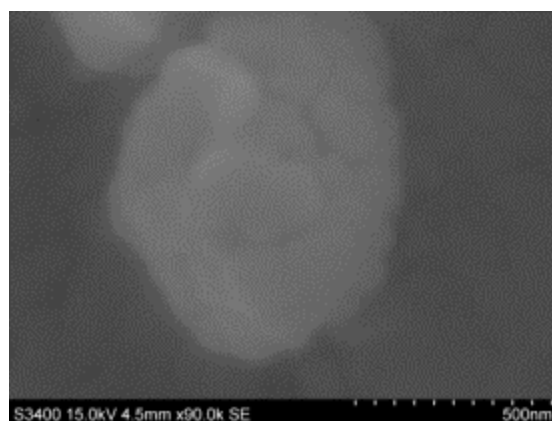
BEA-10AUT, 20 μ m



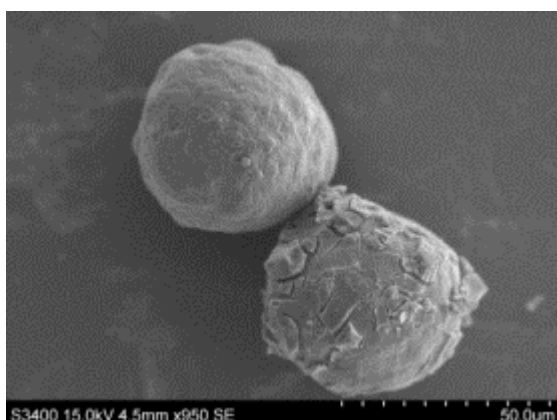
BEA-10AUT, 5 μ m



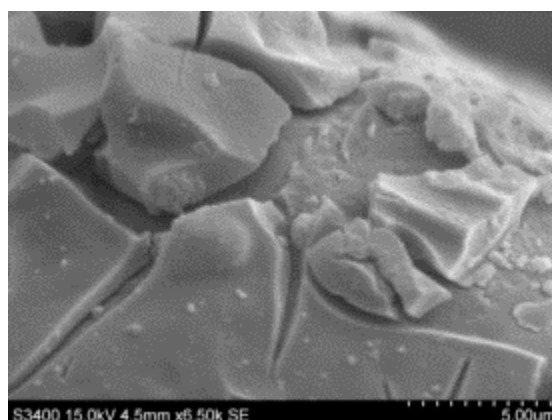
BEA-10AUT, 1 μ m



BEA-10AUT, 0.5 μ m

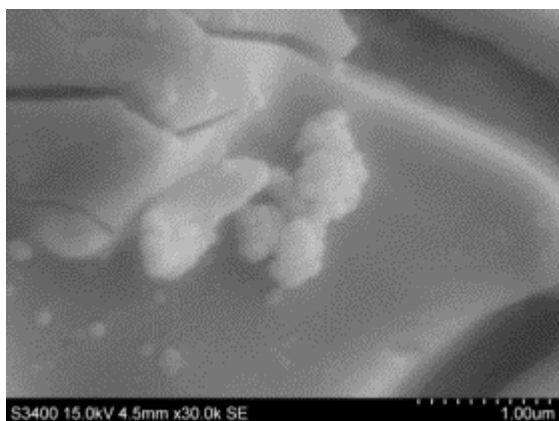


BEA-10AUT, 50 μ m

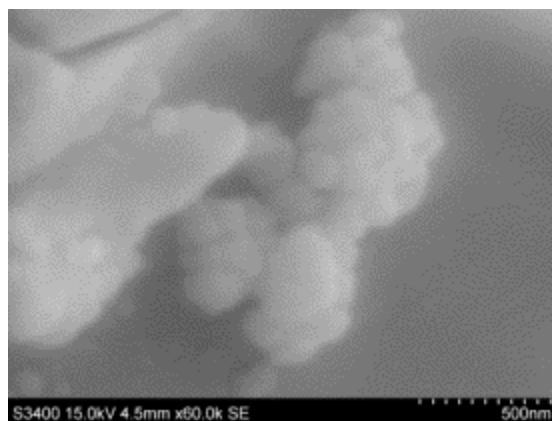


BEA-10AUT, 5 μ m

β -zeolite/FT cobalt-based catalyst BEA-10AUT gold-coated (*continued*)

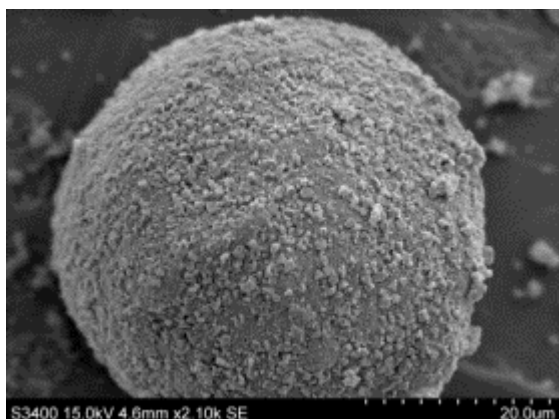


BEA-10AUT, 1 μm

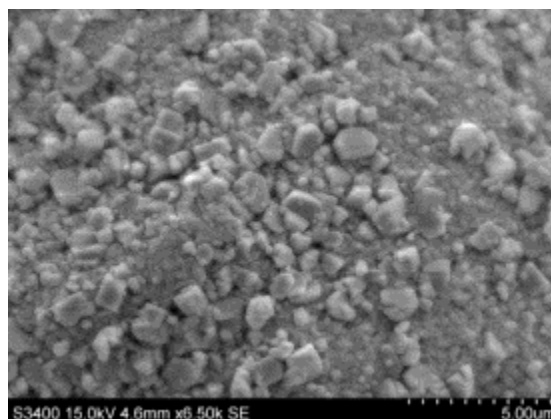


BEA-10AUT, 0.5 μm

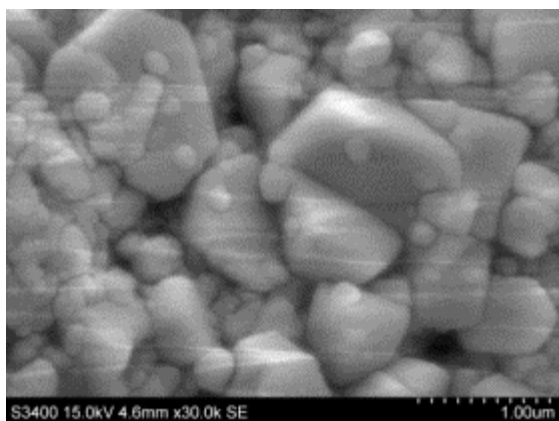
β -zeolite/FT cobalt-based catalyst BEA-11AUT BLACK gold-coated



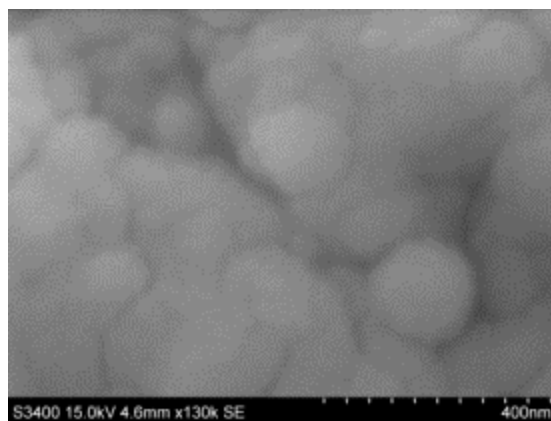
BEA-11AUT BLACK, 20μm



BEA-11AUT BLACK, 5μm

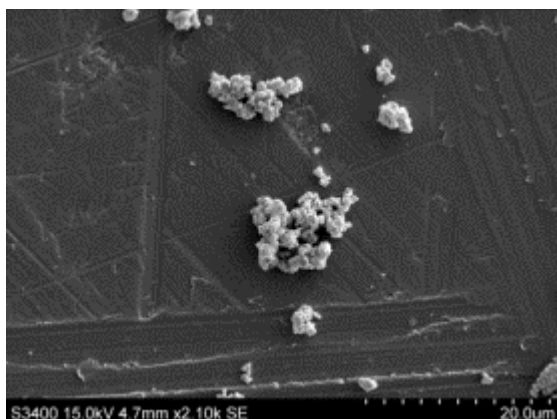


BEA-11AUT BLACK, 1μm

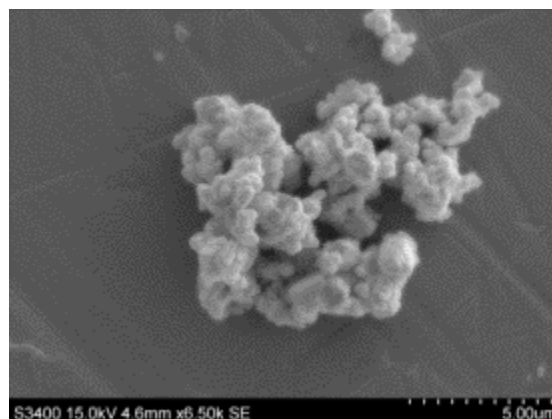


BEA-11AUT BLACK, 0.4μm

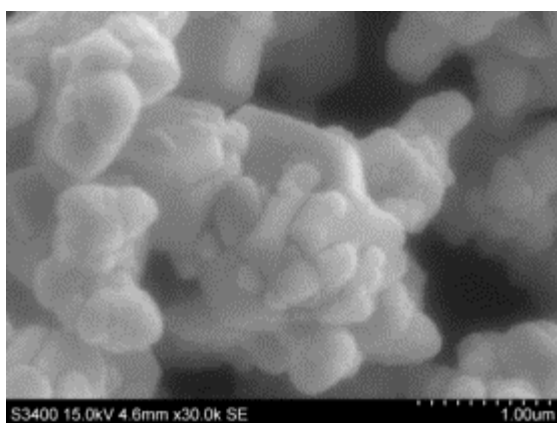
β -zeolite/FT cobalt-based catalyst BEA-11AUT WHITE gold-coated



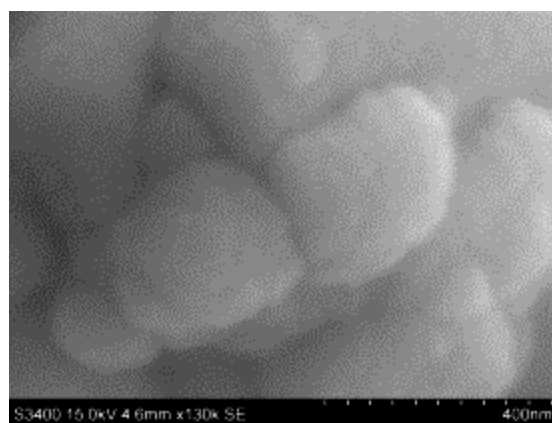
BEA-11AUT WHITE, 20μm



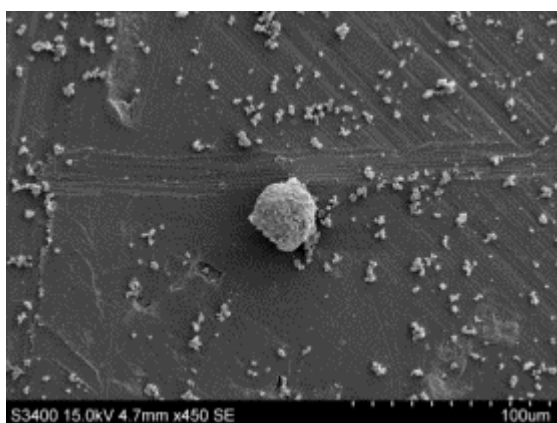
BEA-11AUT WHITE, 5μm



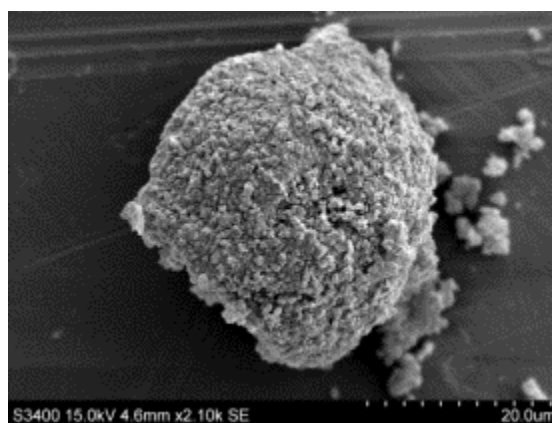
BEA-11AUT WHITE, 1μm



BEA-11AUT WHITE, 0.4μm

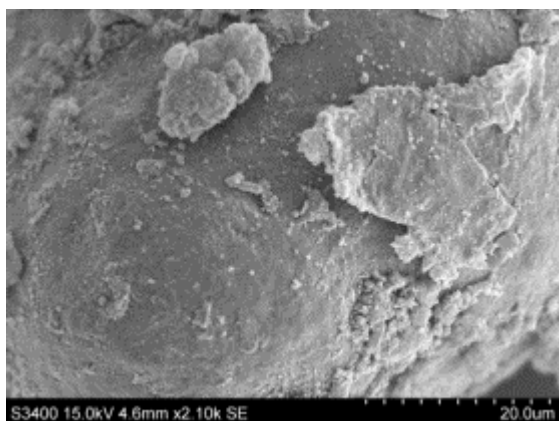


BEA-11AUT WHITE, 100μm

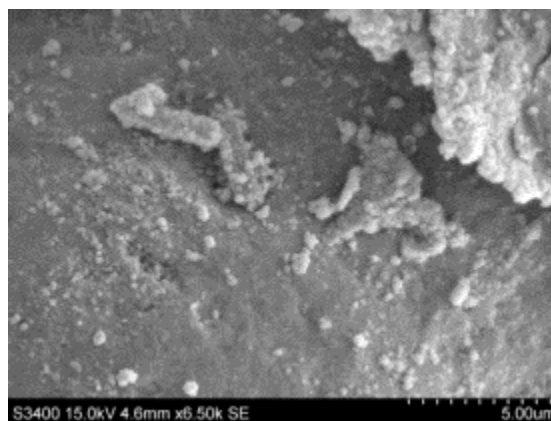


BEA-11AUT WHITE, 20μm

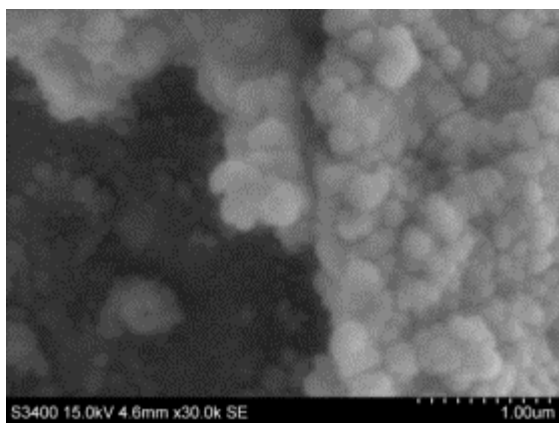
β -zeolite/FT cobalt-based catalyst BEA-12AUT gold-coated



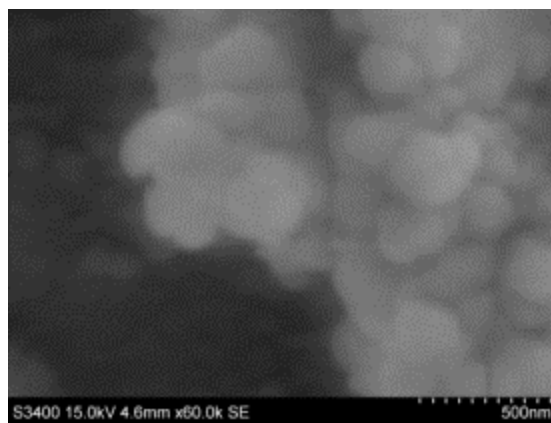
BEA-12AUT , 20μm



BEA-12AUT , 5μm

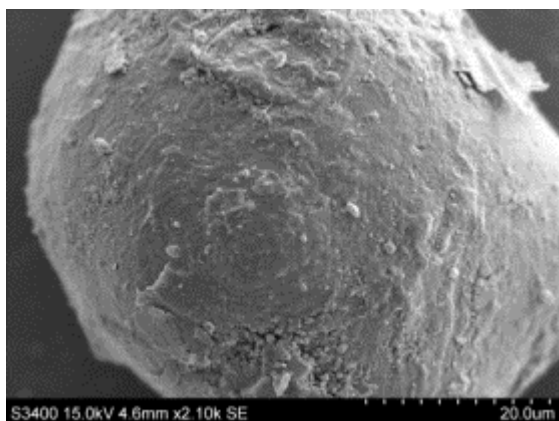


BEA-12AUT , 1μm



BEA-12AUT , 0.5μm

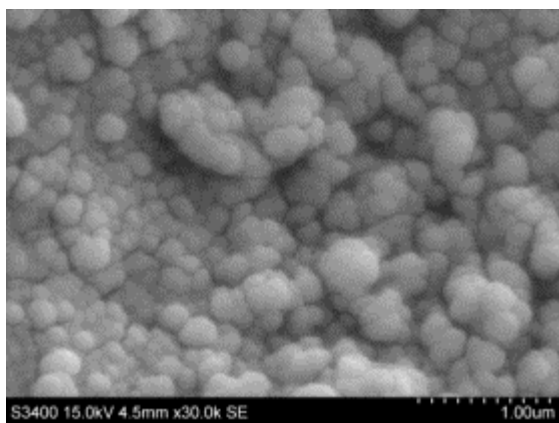
β -zeolite/FT cobalt-based catalyst BEA-13AUT BLACK gold-coated



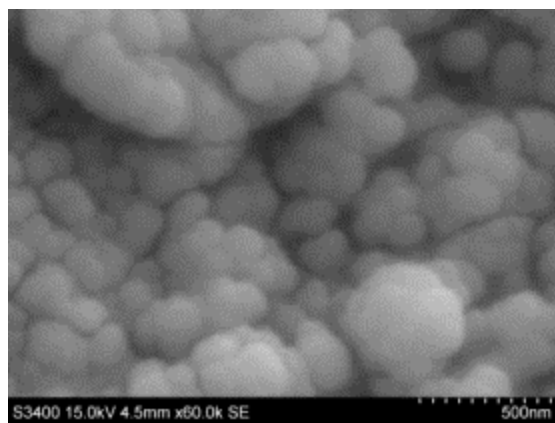
BEA-13AUT BLACK, 20μm



BEA-13AUT BLACK, 5μm

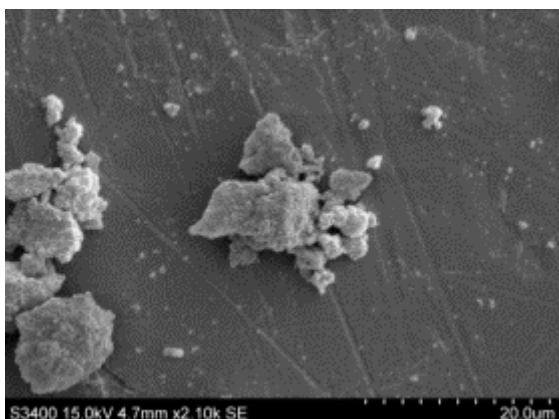


BEA-13AUT BLACK, 1μm

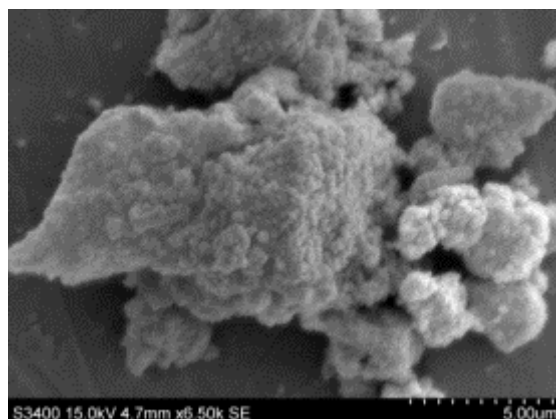


BEA-13AUT BLACK, 0.5μm

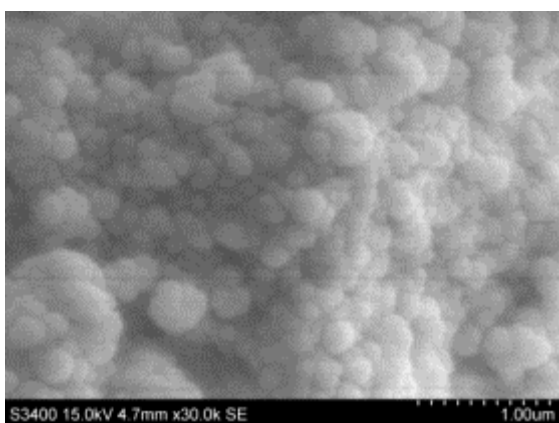
β -zeolite/FT cobalt-based catalyst BEA-13AUT WHITE gold-coated



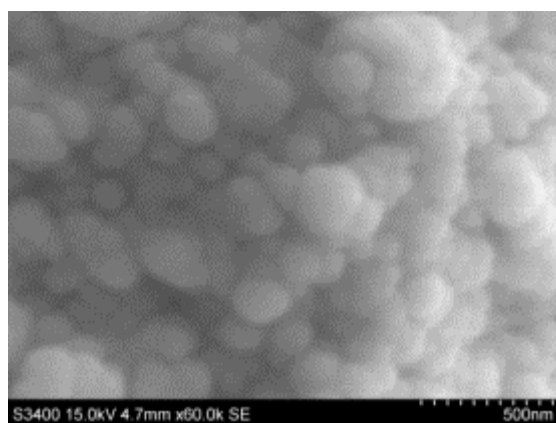
BEA-13AUT WHITE, 20μm



BEA-13AUT WHITE, 5μm

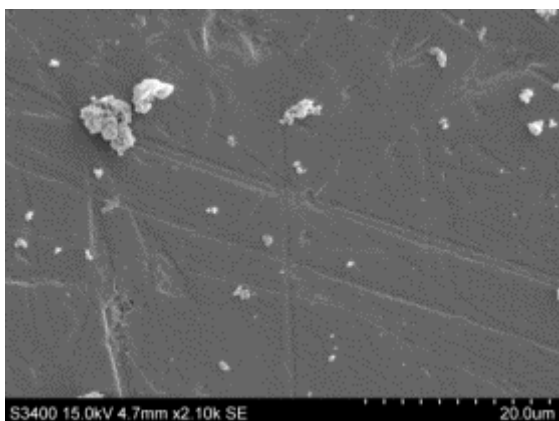


BEA-13AUT WHITE, 1μm

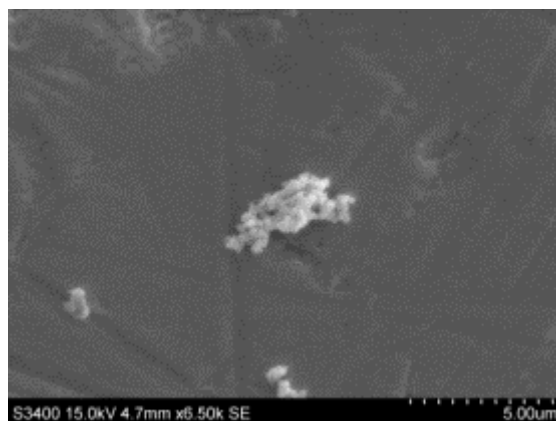


BEA-13AUT WHITE, 0.5μm

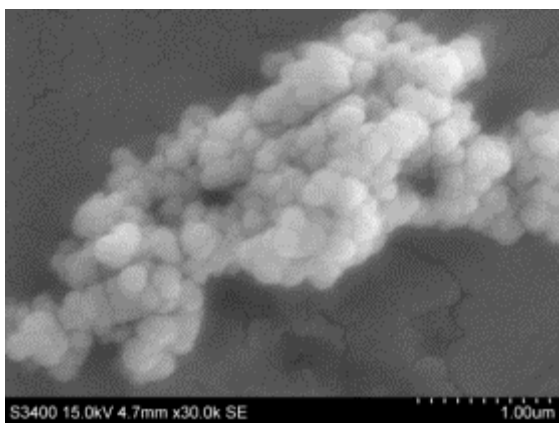
β -zeolite/FT cobalt-based catalyst BEA-14AUT WHITE gold-coated



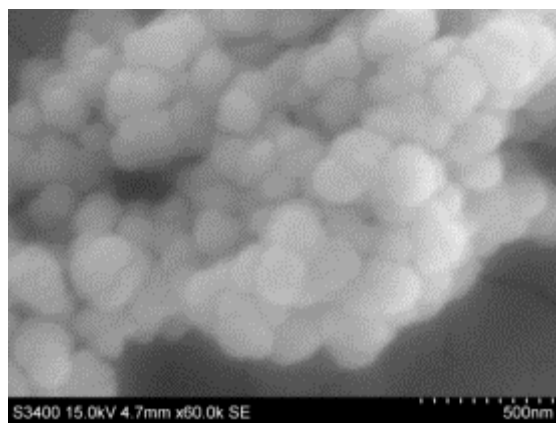
BEA-14AUT WHITE, 20μm



BEA-14AUT WHITE, 5μm



BEA-14AUT WHITE, 1μm



BEA-14AUT WHITE, 0.5μm

Appendix F

Chemisorption

The chemisorption calculations were based in the manual of the equipment Micrometrics ASAP 2020 unit. All the calculations match perfectly with the results report of the equipment. The follow tables content the chemisorption calculation data for the β -zeolite/FT cobalt-based catalysts that are calcined, in the case of the samples that are black and white phase only black calcined phase is included.

		BEA-06AUT	BEA-07AUT	BEA-08AUT	BEA-09AUT
Cobalt	% wt	5.88	4.26	6.34	5.97
Rhenium	% wt	0.00	0.00	0.00	0.00
Sample Mass:	g	0.4625	0.3524	0.3071	0.3656
Metal Dispersion:	%	5.7	4.9	5.9	5.6
Metallic Surface Area:	m ² /g _{sample}	2.3	1.4	2.5	2.3
	m ² /g _{metal}	38.5	33.0	39.8	38.1
Crystallite Factor		99.6	99.6	99.6	203.2
Crystallite Size	nm	17.5	20.4	16.9	36.1
Est. Crystallite Size*:	nm	17.5	20.4	16.9	17.7

* Estimated crystallite size based on: $d(\text{Co}^0)(\text{nm}) = \frac{99.6}{D(\%)}$

		Co12-Ru0.3	BEA-10AUT	BEA-11AUT	BEA-12AUT	BEA-13AUT	BEA-14AUT
Cobalt	% wt	12.00	10.49	7.09	7.40	8.98	10.37
Rhenium	% wt	0.00	0.00	0.00	0.00	0.00	0.00
Sample Mass:	g	0.5925	0.6716	0.6586	0.5992	0.7488	0.6691
Metal Dispersion:	%	8.3	6.7	6.5	5.9	6.6	6.1
Metallic Surface Area:	m ² /g _{sample}	6.7	4.7	3.1	3.0	4.0	4.3
	m ² /g _{metal}	54.8	45.2	44.2	39.9	44.9	41.3
Crystallite Factor		99.6	92.9	99.6	99.6	99.6	99.6
Crystallite Size	nm	12.2	13.9	15.2	16.9	15.0	16.3
Est. Crystallite Size*:	nm	12.0	14.9	15.2	16.9	15.0	16.3

* Estimated crystallite size based on: $d(\text{Co}^0)(\text{nm}) = \frac{99.6}{D(\%)}$

The follow table contents the chemisorption calculation data for the β -zeolite/FT cobalt-based catalyst that are not calcined, in the case of the samples that are black and white phase only black calcined phase is included.

		BEA-09AUT WOC	BEA-10AUT WOC	BEA-11AUT WOC	BEA-12AUT WOC	BEA-13AUT WOC	BEA-14AUT WOC
Cobalt	% wt	5.97	10.49	7.09	7.40	8.98	10.37
Rhenium	% wt	0.00	0.00	0.00	0.00	0.00	0.00
Sample Mass:	g	0.3934	0.5169	0.6261	0.5990	0.7021	0.6682
Metal Dispersion:	%	5.7	7.3	4.8	6.6	7.3	3.2
Metallic Surface Area:	m ² /g _{sample}	2.3	5.2	2.3	3.3	4.5	2.3
	m ² /g _{metal}	38.9	49.5	32.7	44.9	49.7	21.9
Crystallite Factor		203.2	92.9	99.6	99.6	99.6	99.6
Crystallite Size	nm	35.4	12.7	20.6	15.0	13.6	30.8
Est. Crystallite Size*:	nm	17.3	13.6	20.6	15.0	13.6	30.8

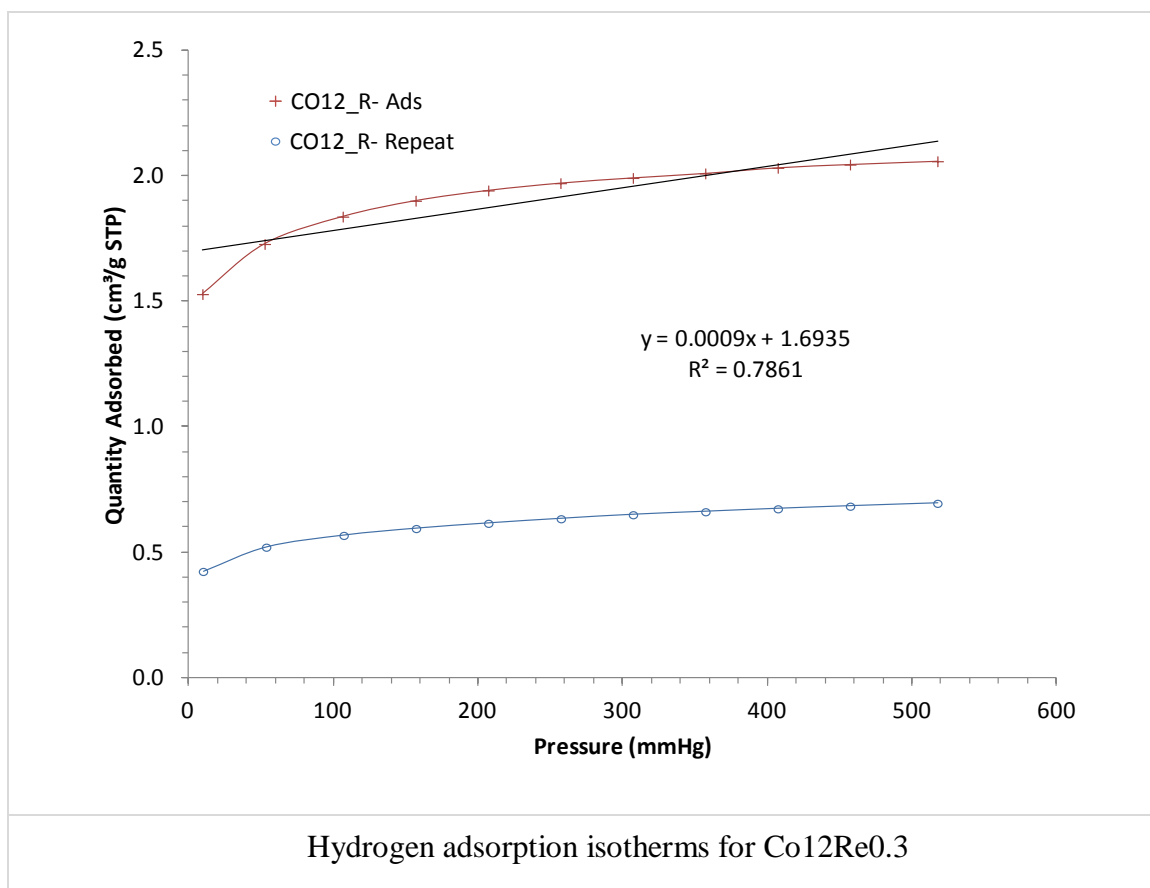
* Estimated crystallite size based on: $d(\text{Co}^0)(\text{nm}) = \frac{99.6}{D(\%)}$

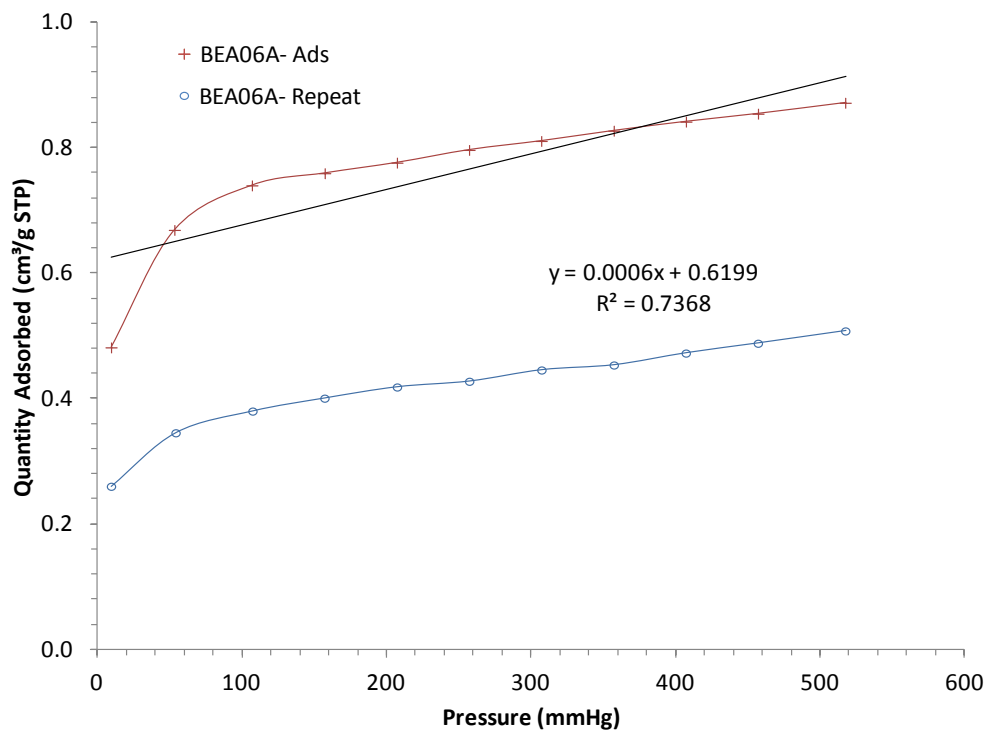
The follow table contents the chemisorption calculation data for the β -zeolite/FT cobalt-based catalyst that are calcined and not calcined, only the white phases is included.

		BEA-11AUT WHITE	BEA-11AUT WHITE WOC	BEA-13AUT WHITE	BEA-13AUT WHITE WOC
Cobalt	% wt	0.20	0.20	0.20	0.20
Rhenium	% wt	0.00	0.00	0.00	0.00
Sample Mass:	g	0.2702	0.2197	0.2227	0.2275
Metal Dispersion:	%	5.4	6.4	-1.2	5.1
Metallic Surface Area:	m ² /g _{sample}	0.1	0.1	0.0	0.1
	m ² /g _{metal}	36.2	43.4	-8.4	34.5
Crystallite Factor		99.6	99.6	99.6	99.6
Crystallite Size	nm	18.6	15.6	-80.1	19.5
Est. Crystallite Size*:	nm	18.6	15.6	-80.0	19.5

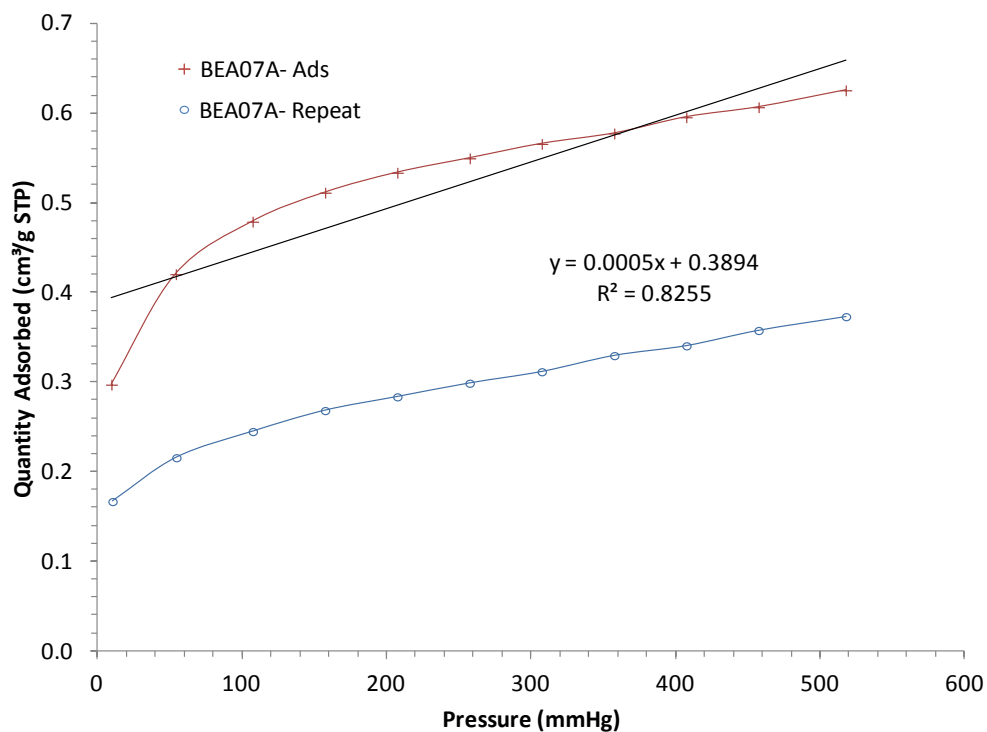
* Estimated crystallite size based on: $d(\text{Co}^0)(\text{nm}) = \frac{99.6}{D(\%)}$

The samples that were measured are the ones that contain FT cobalt-based catalyst, the samples are from BEA-06AUT to BEA-14AUT. It is also measure the FT cobalt-based catalyst provided by Statoil Research Center. The hydrogen adsorption isotherms for the different β -zeolite/FT cobalt-based catalyst

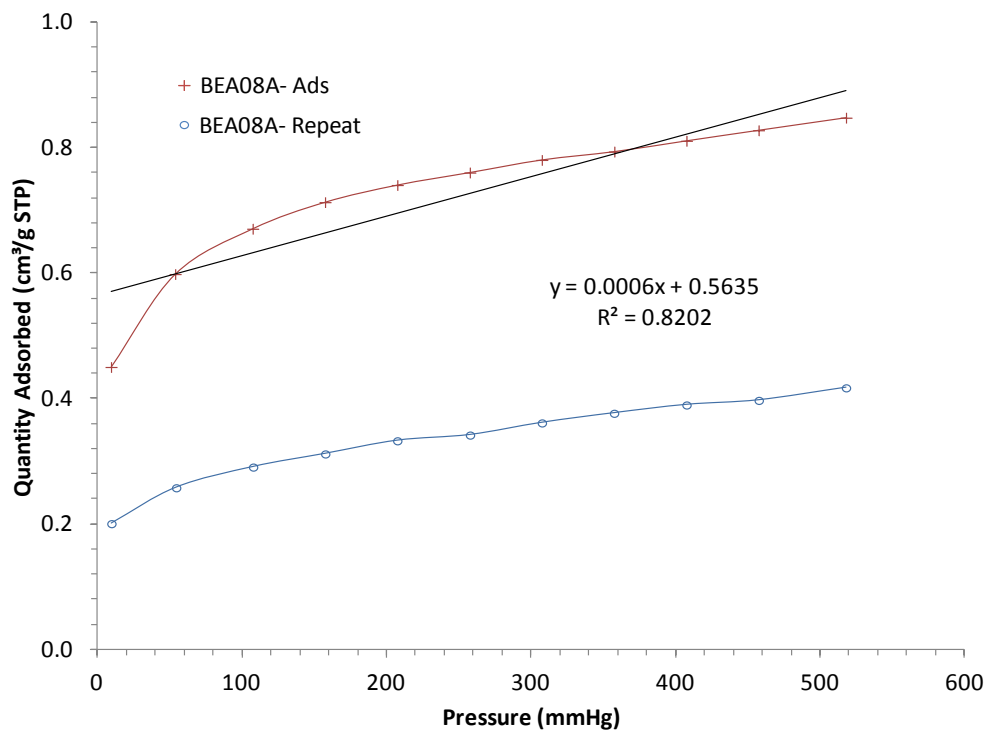




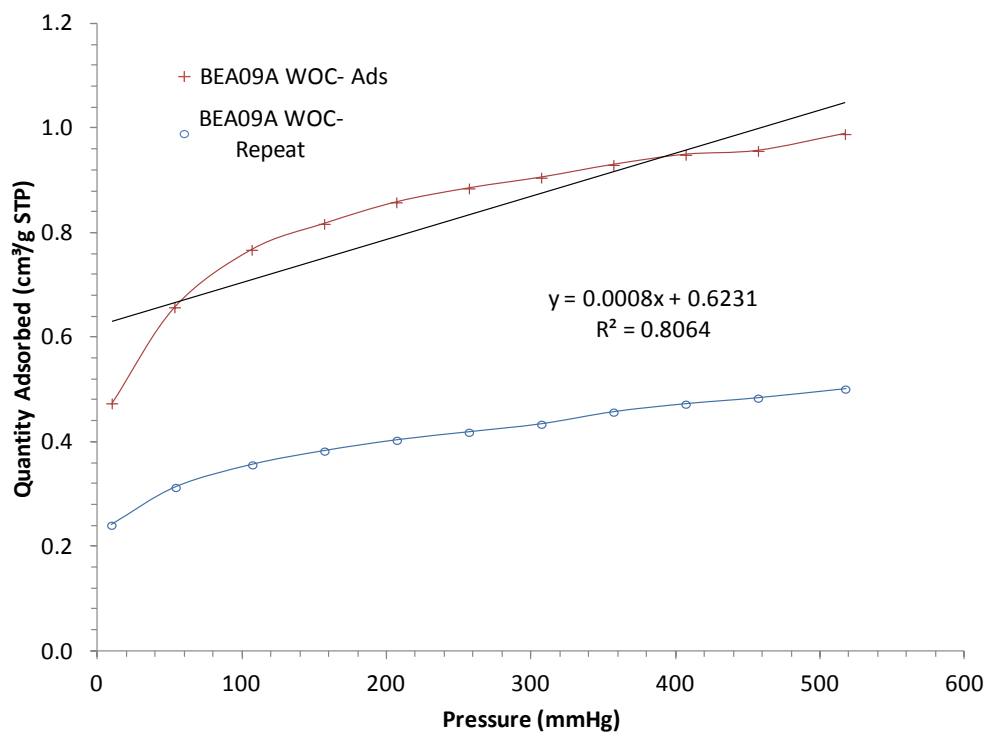
Hydrogen adsorption isotherms for BEA-06AUT



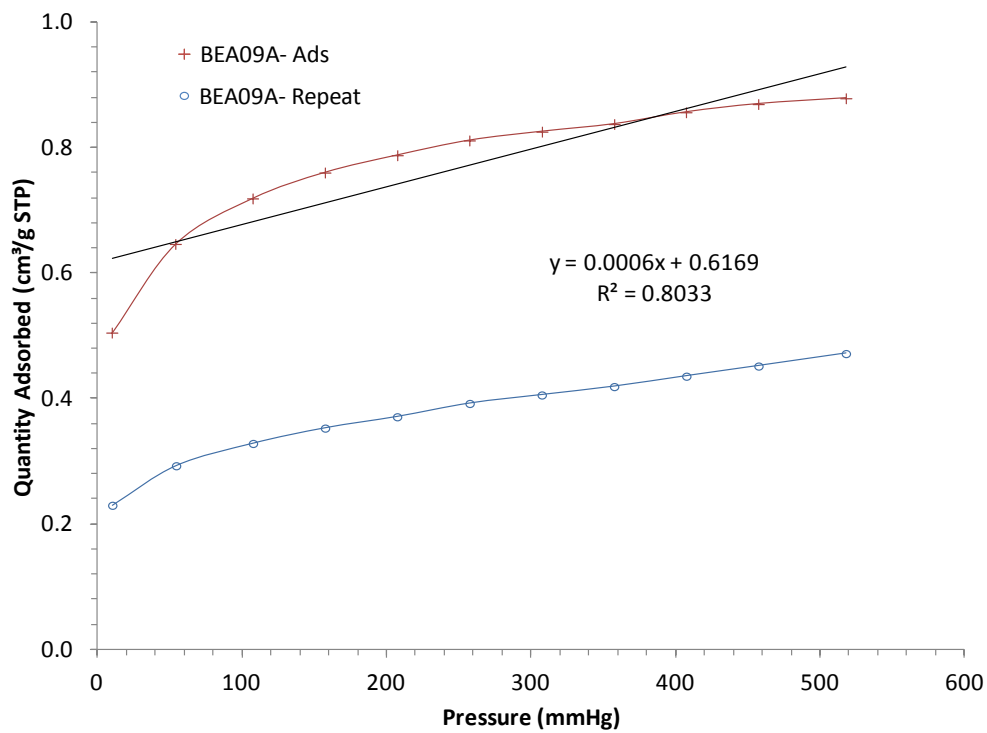
Hydrogen adsorption isotherms for BEA-07AUT



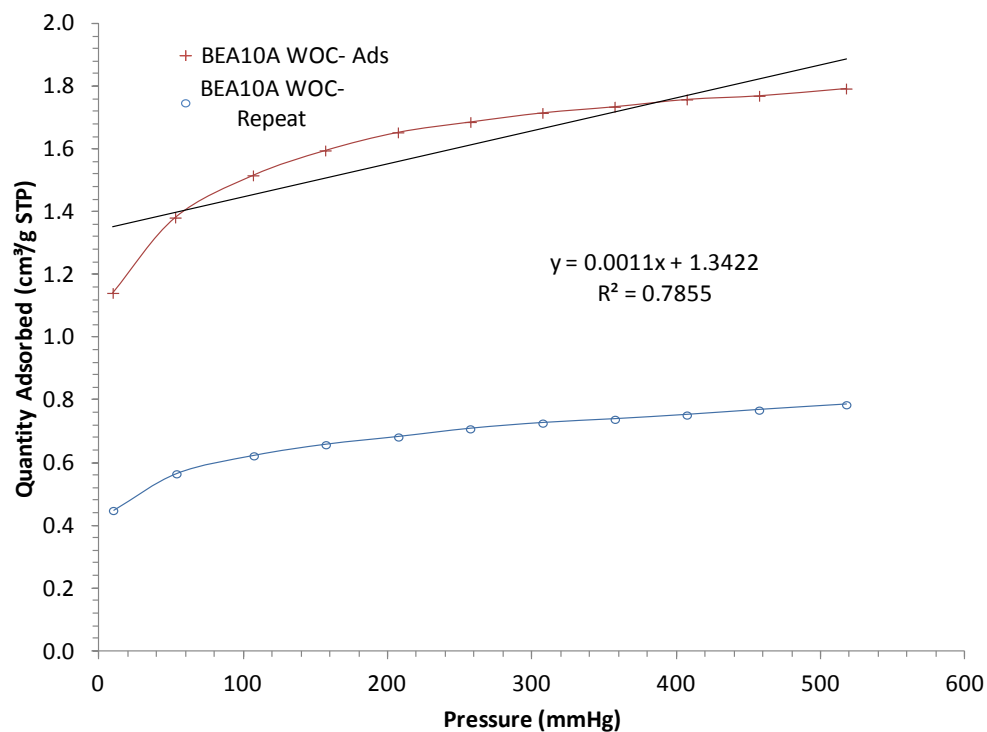
Hydrogen adsorption isotherms for BEA-08AUT



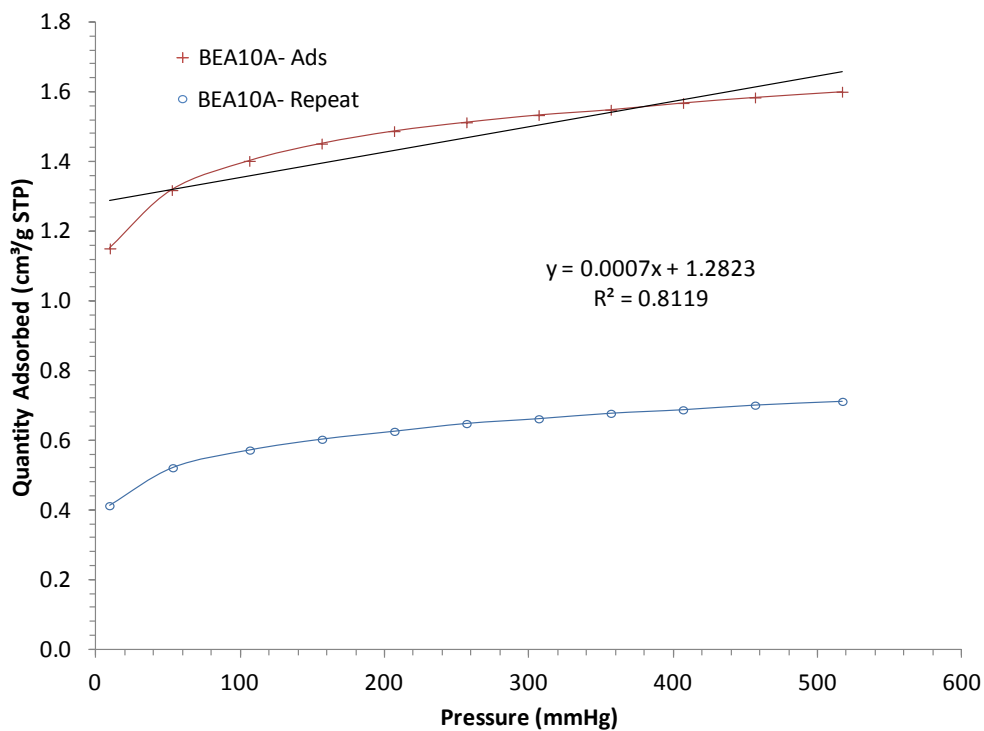
Hydrogen adsorption isotherms for BEA-09AUT WOC



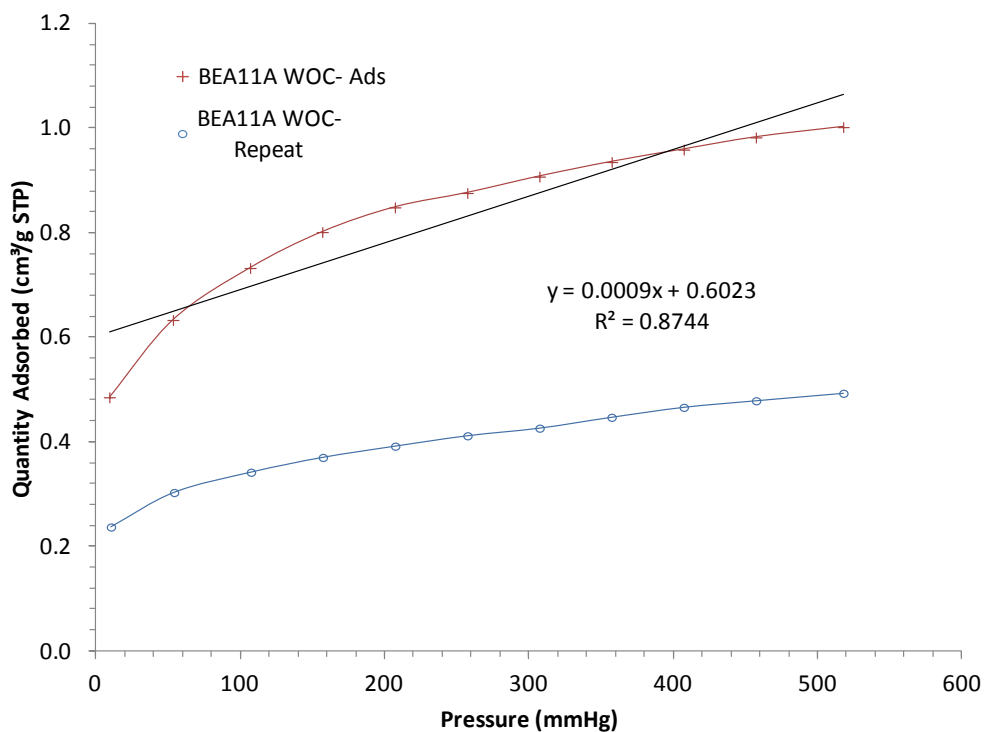
Hydrogen adsorption isotherms for BEA-09AUT



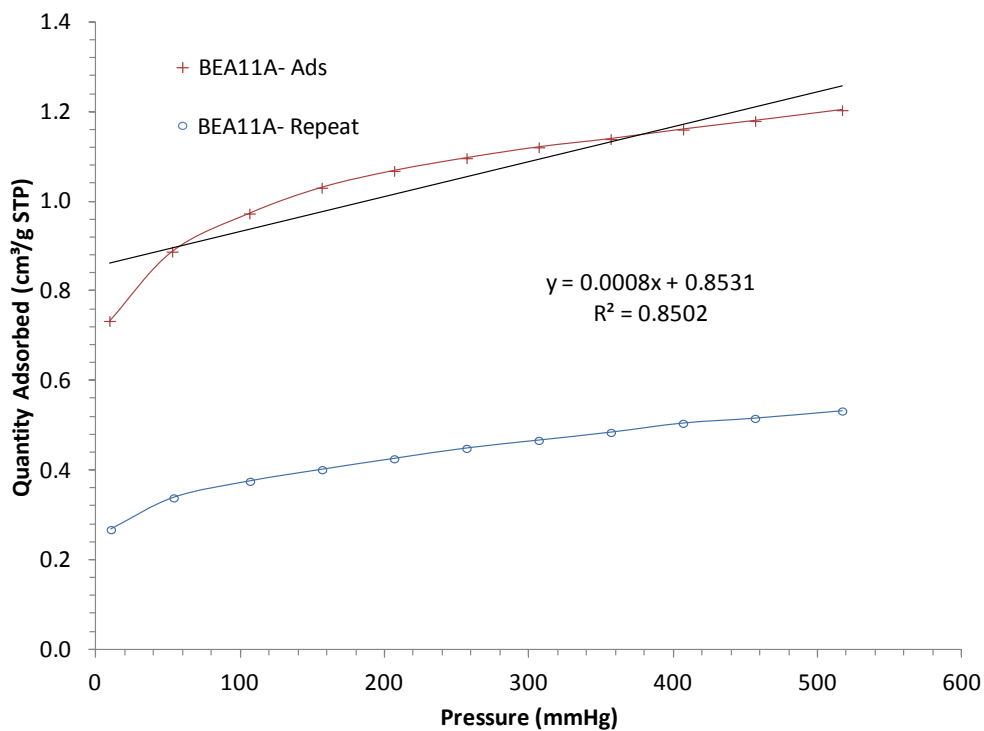
Hydrogen adsorption isotherms for BEA-10AUT WOC



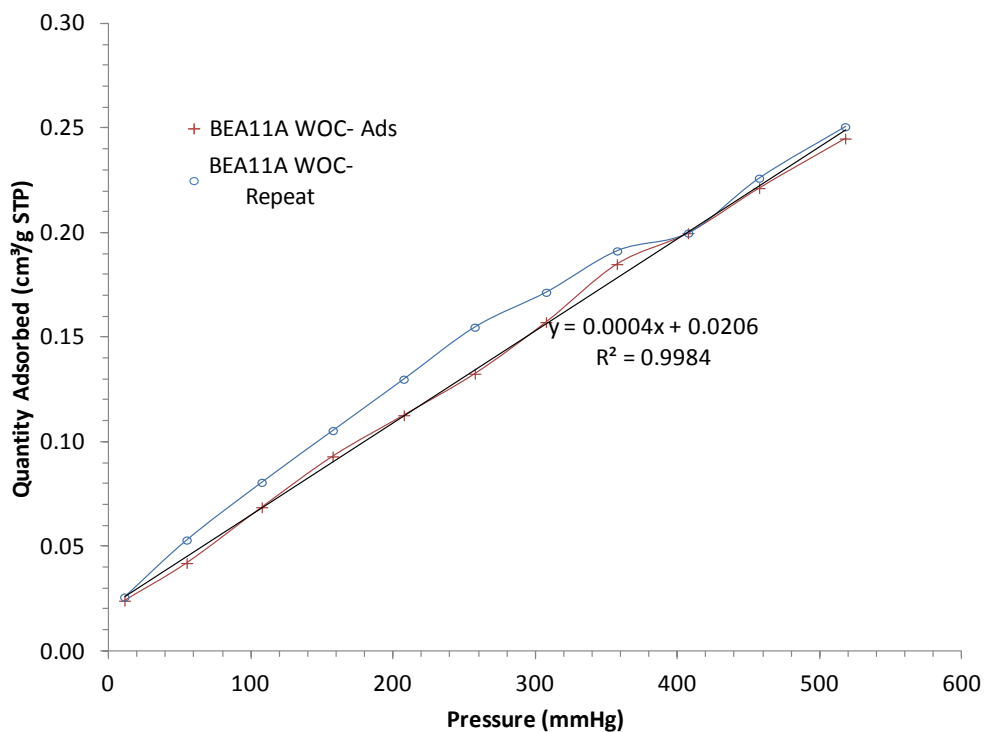
Hydrogen adsorption isotherms for BEA-10AUT



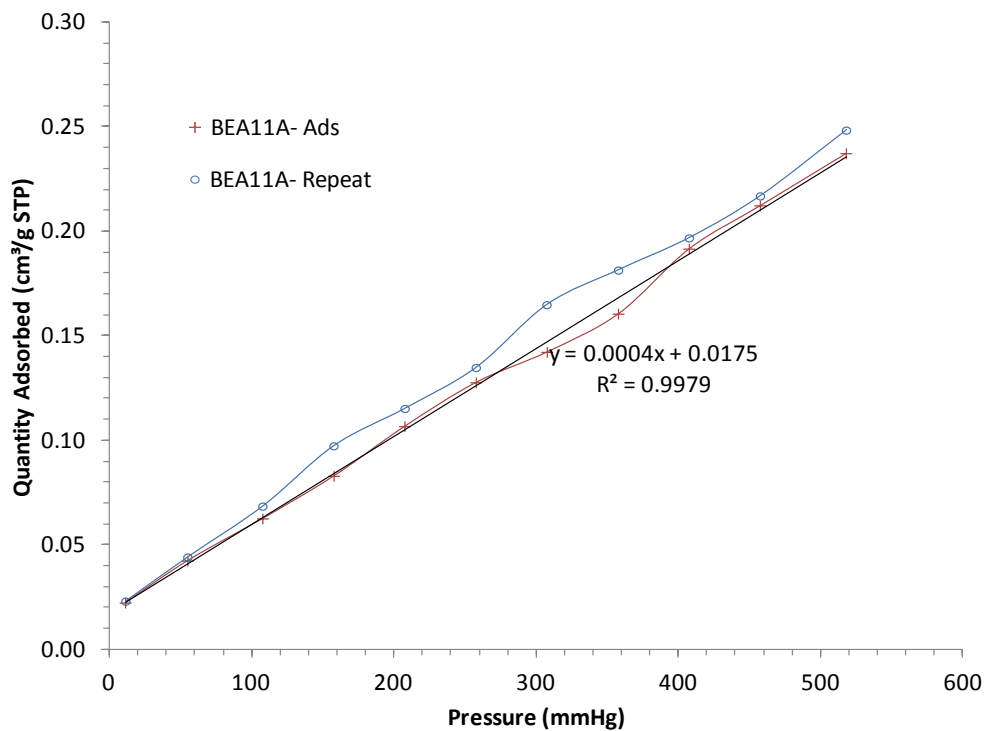
Hydrogen adsorption isotherms for BEA-11AUT BLACK WOC



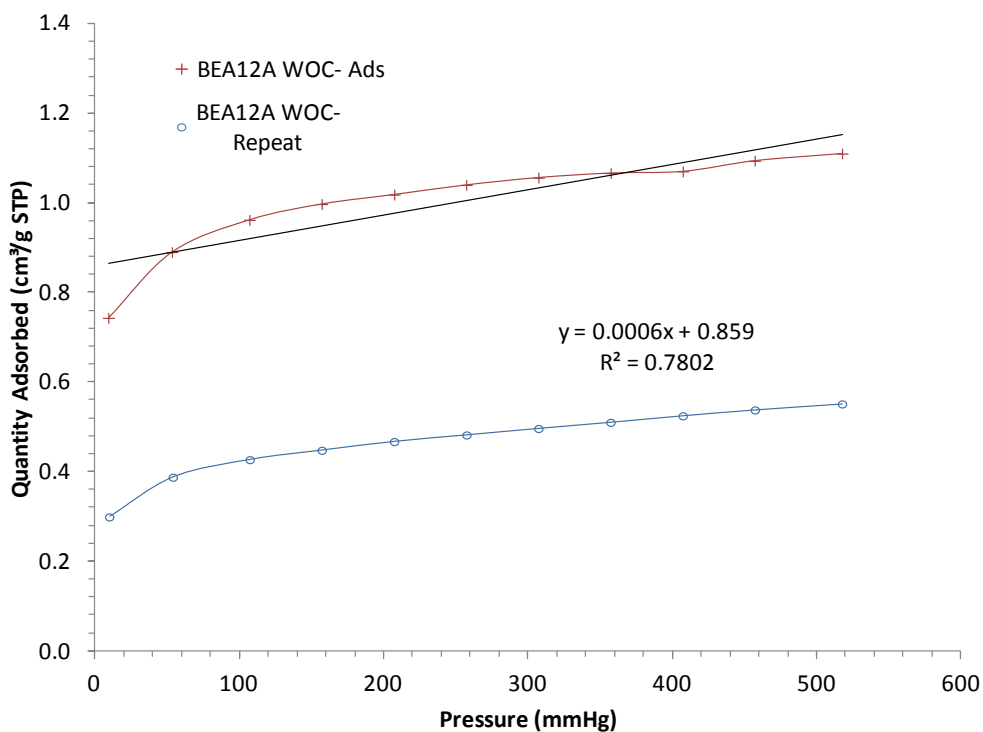
Hydrogen adsorption isotherms for BEA-11AUT BLACK



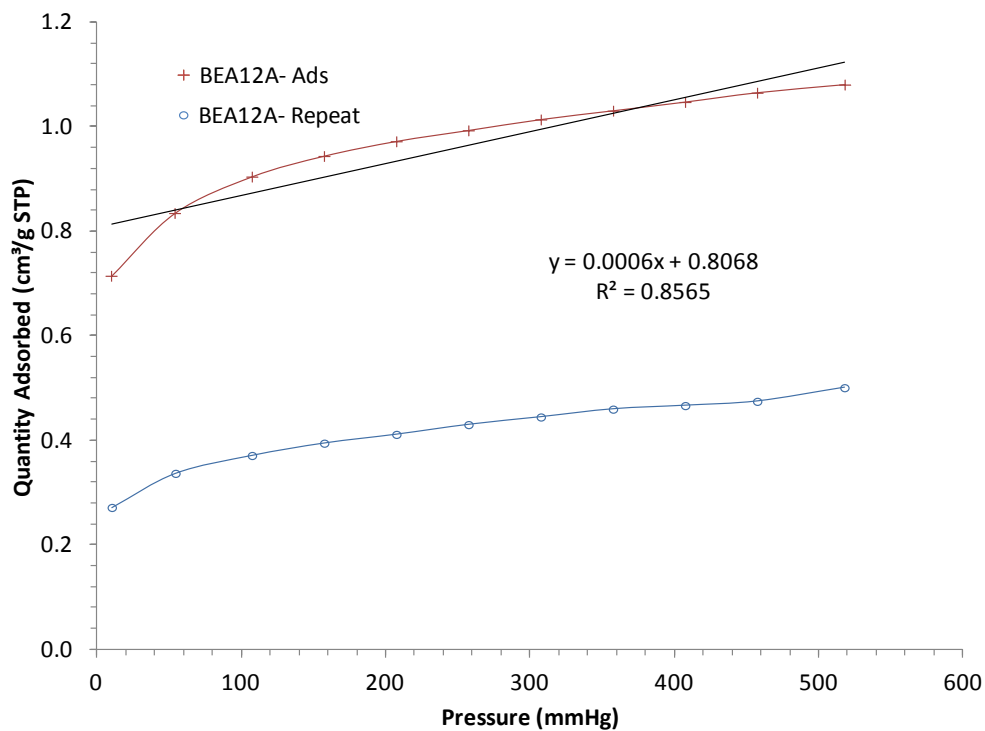
Hydrogen adsorption isotherms for BEA-11AUT WHITE WOC



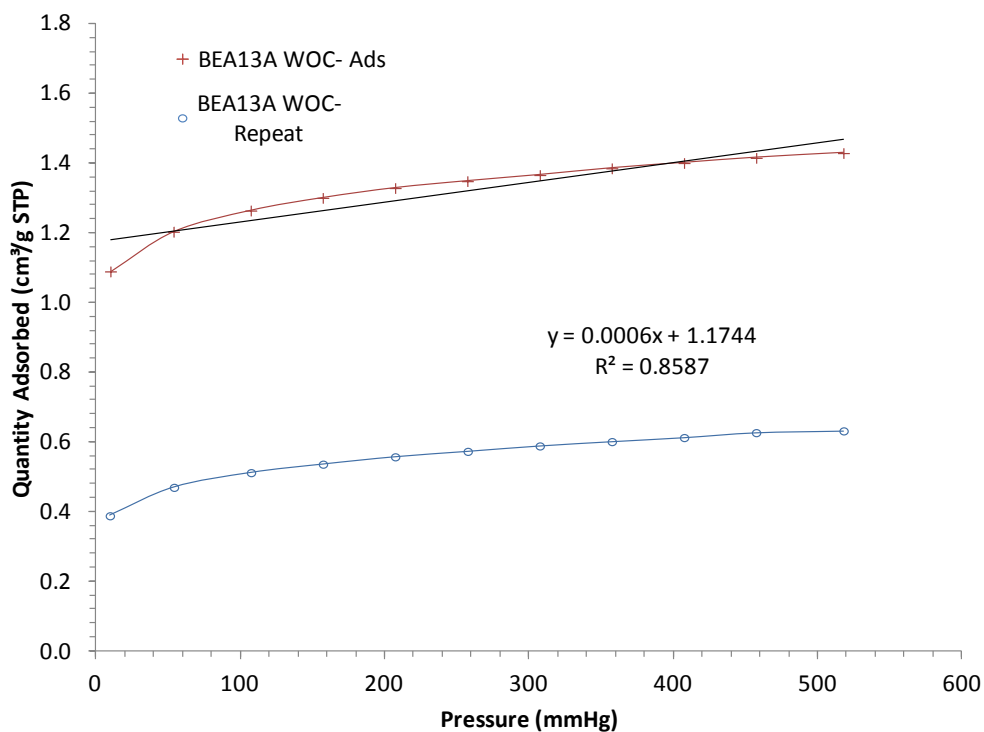
Hydrogen adsorption isotherms for BEA-11AUT WHITE



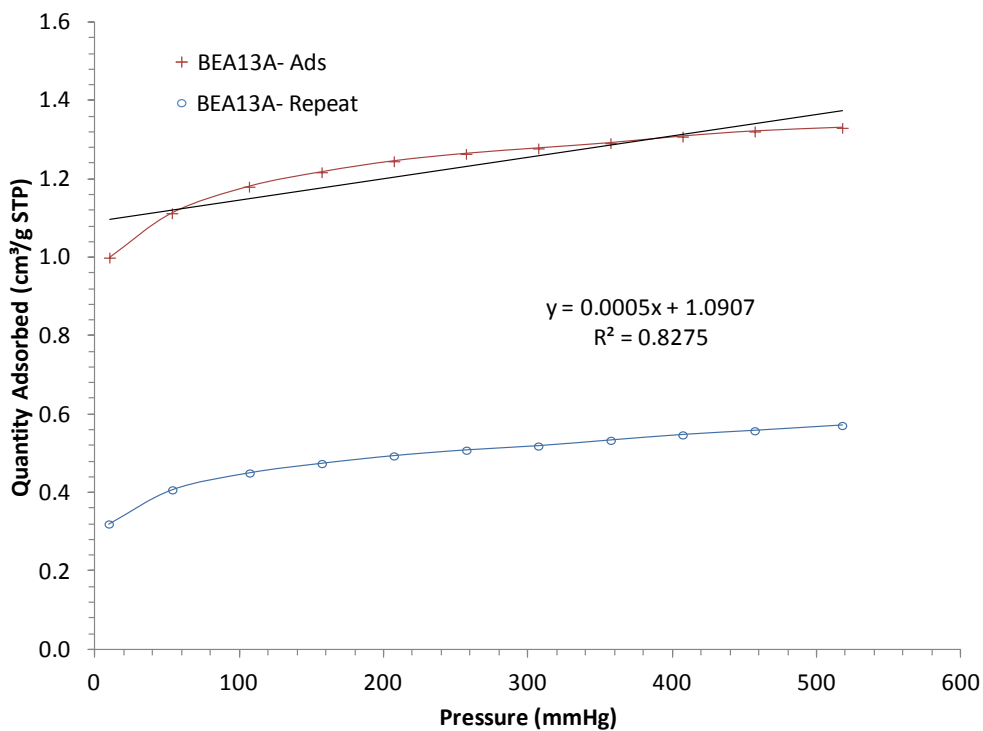
Hydrogen adsorption isotherms for BEA-12AUT WOC



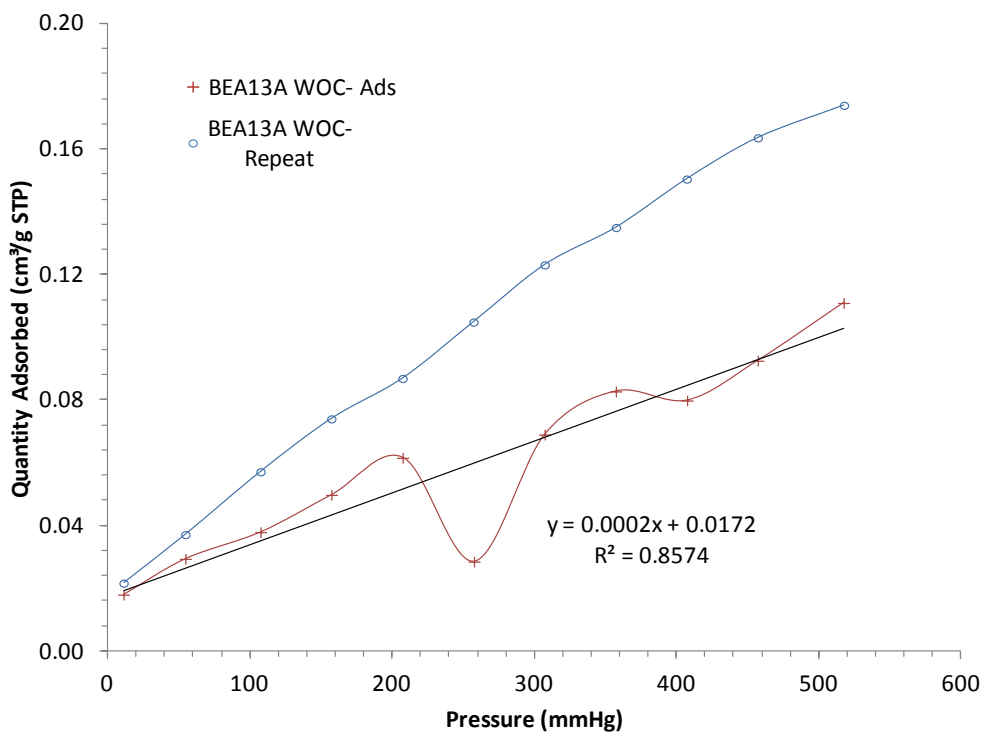
Hydrogen adsorption isotherms for BEA-12AUT



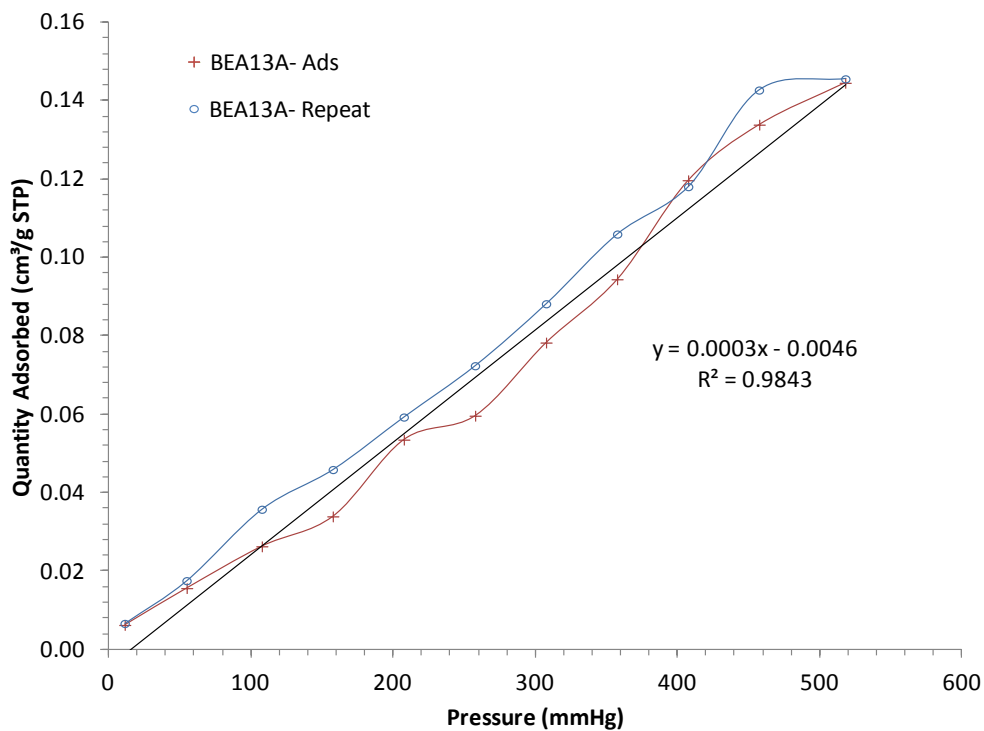
Hydrogen adsorption isotherms for BEA-13AUT BLACK WOC



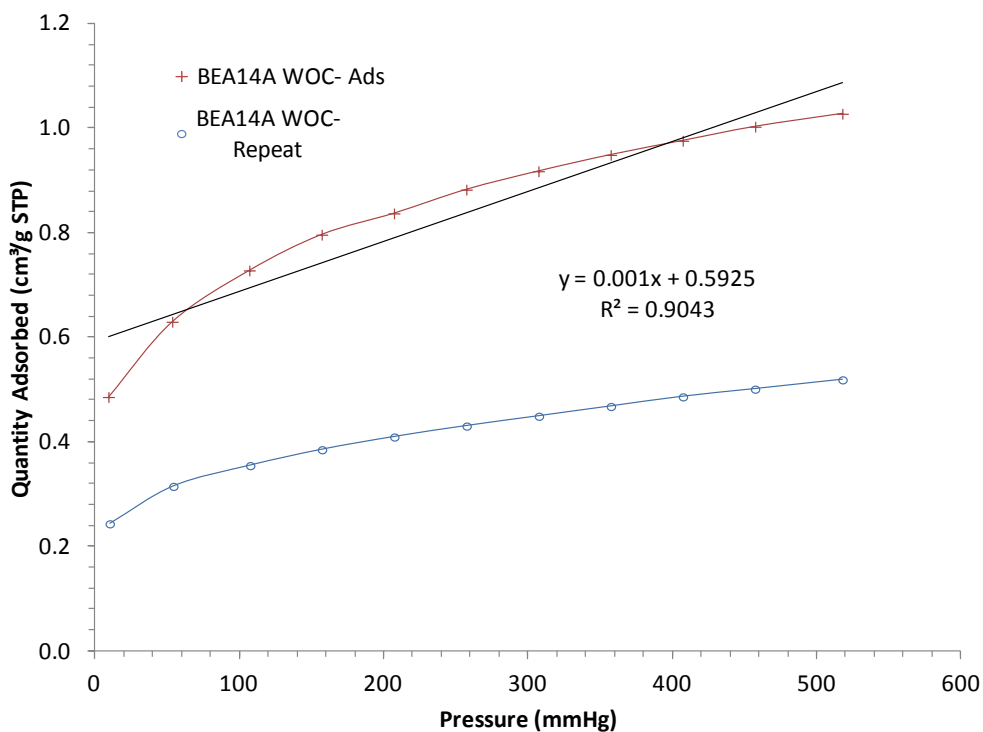
Hydrogen adsorption isotherms for BEA-13AUT BLACK



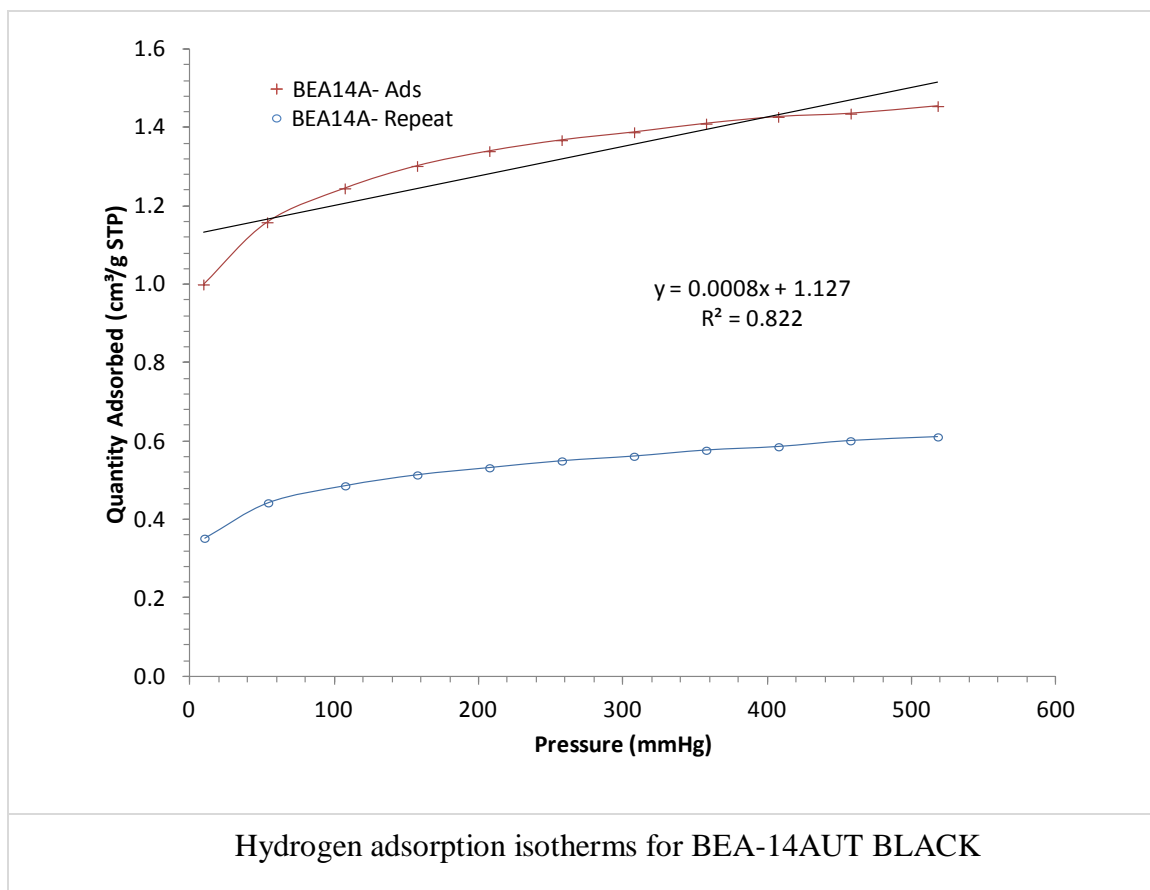
Hydrogen adsorption isotherms for BEA-13AUT WHITE WOC



Hydrogen adsorption isotherms for BEA-13AUT WHITE



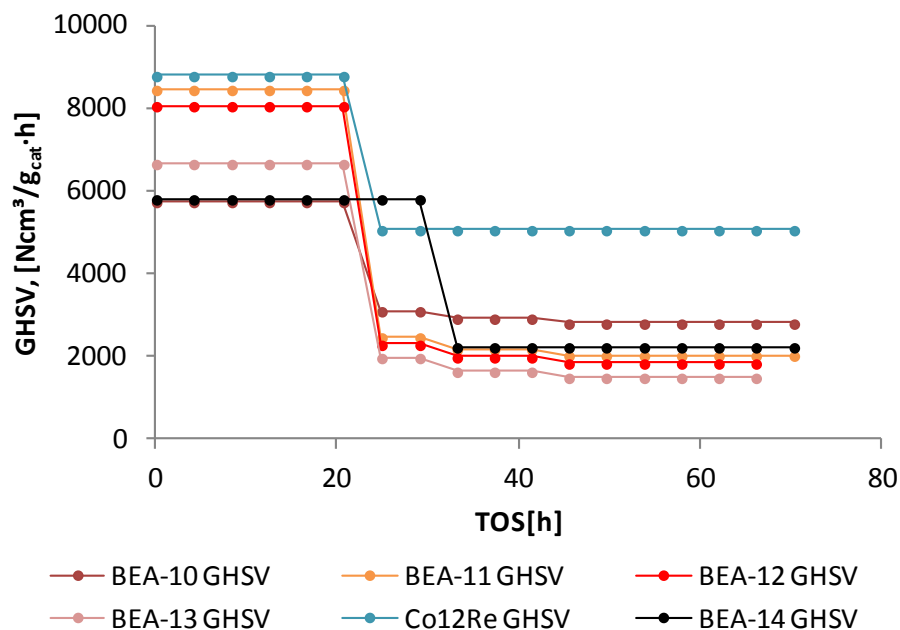
Hydrogen adsorption isotherms for BEA-14AUT BLACK WOC



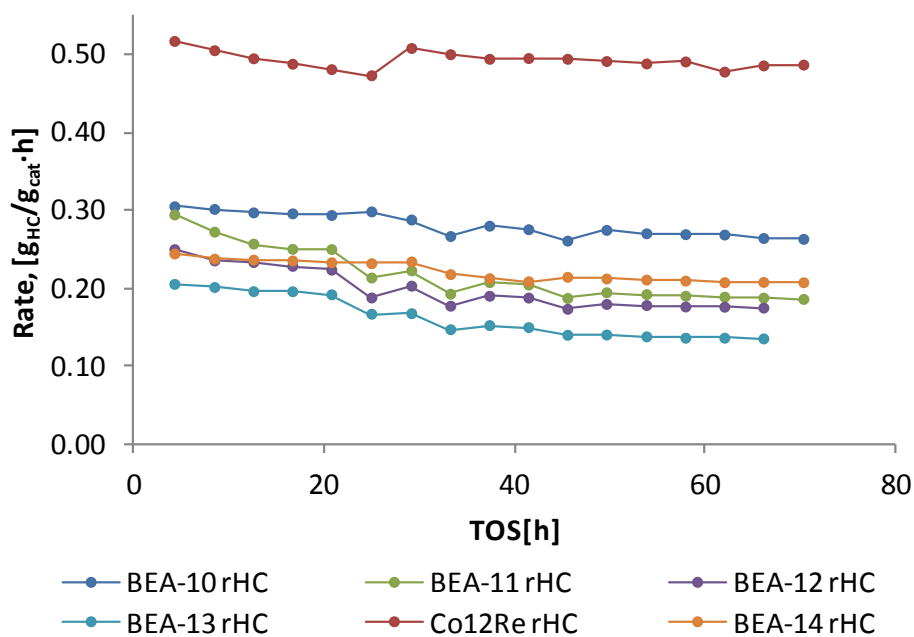
Appendix G

Fischer Tropsch synthesis test

All the names in the legends included in the plot of the tested β -zeolite/FT catalyst in this appendix were simplify, it means instead of BEA-10 AUT to BEA-14 AUT were used BEA10 to BEA14.

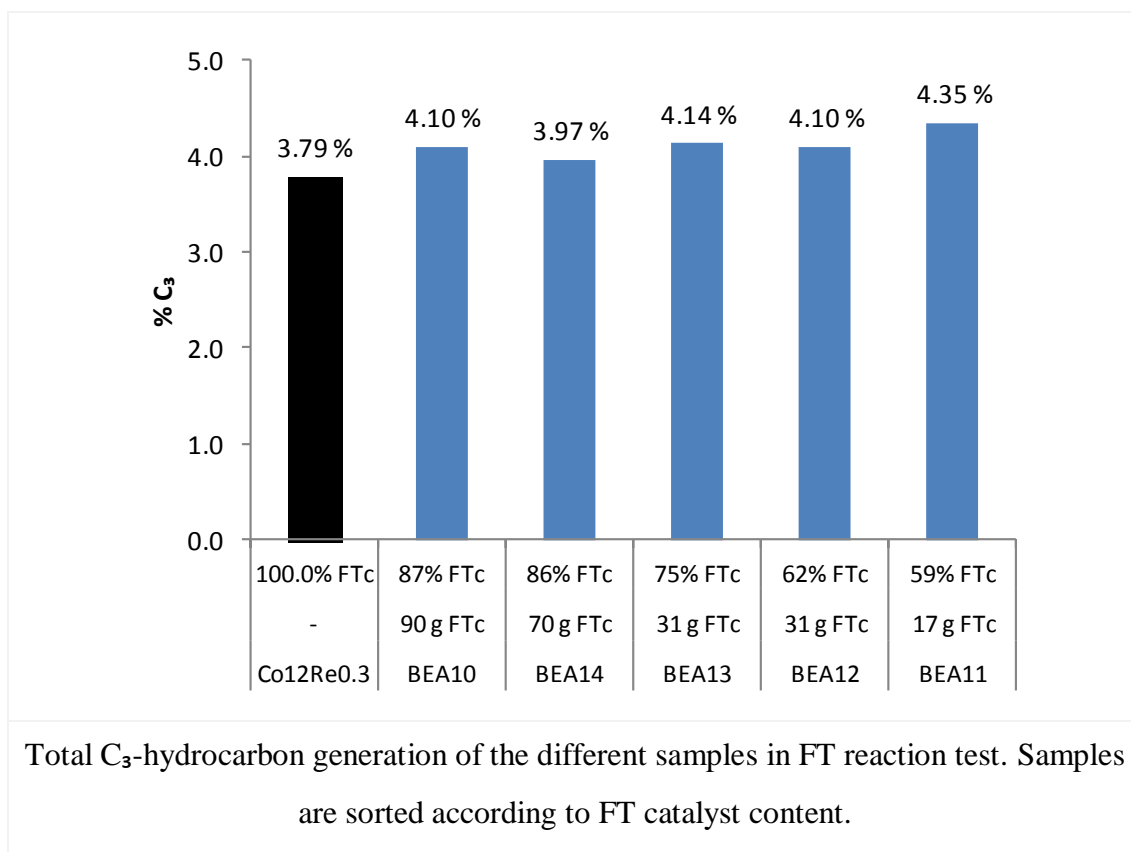
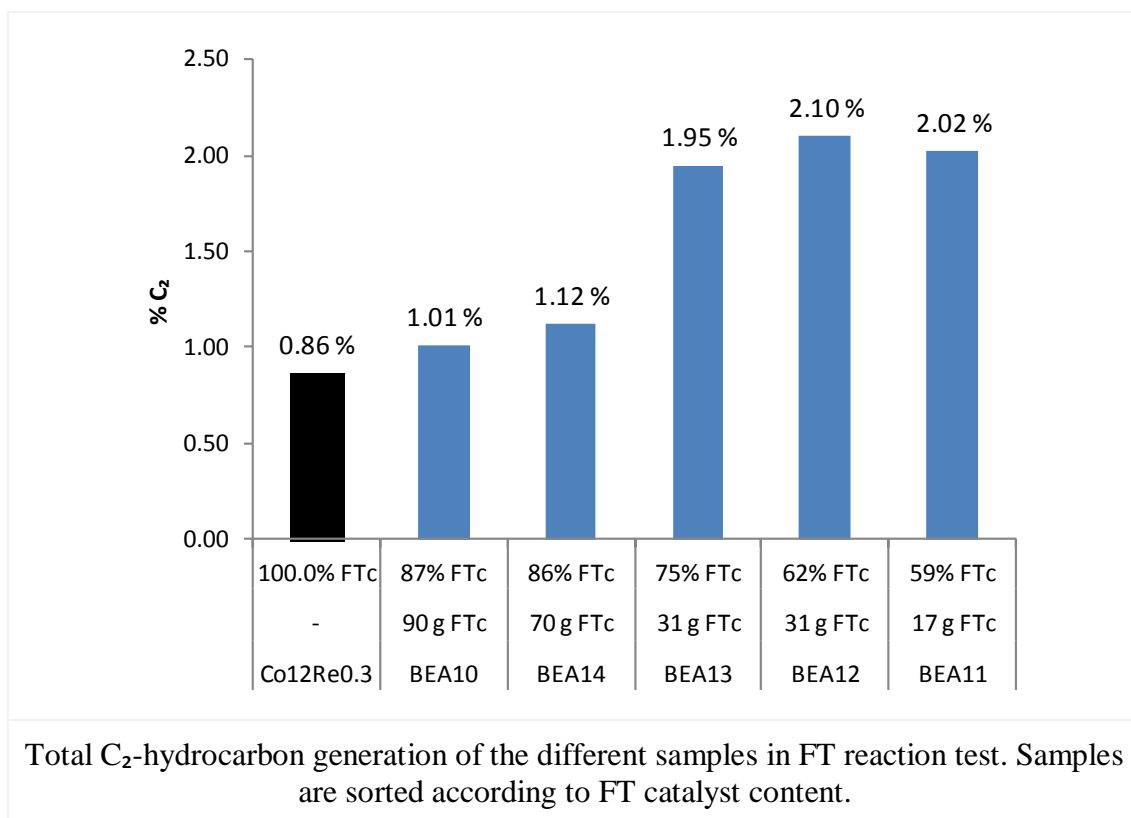


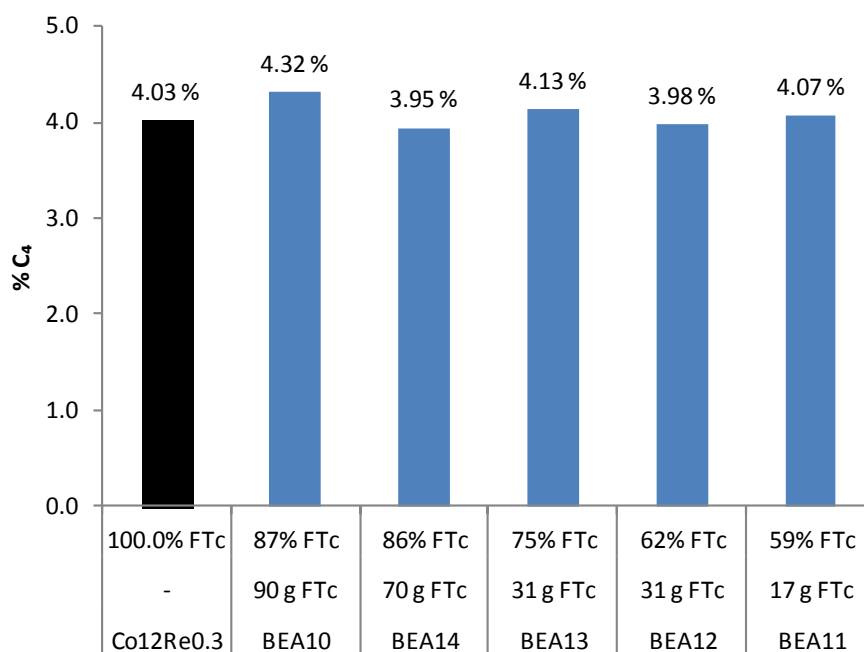
GHSV per gram of estimated β -zeolite/FT catalyst diluted in silicon carbide



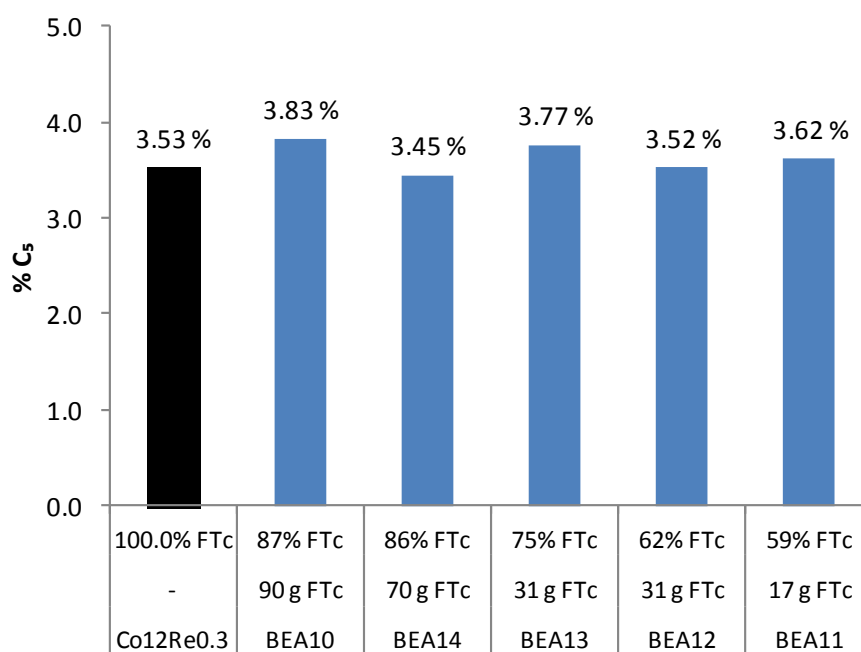
Rate of total mass of hydrocarbons per mass of estimated β -zeolite/FT catalyst diluted in silicon carbide

All the data included in the bar plots in this appendix were based in the average of the last adjustment of gas flow to obtain approximately 50% CO conversion.

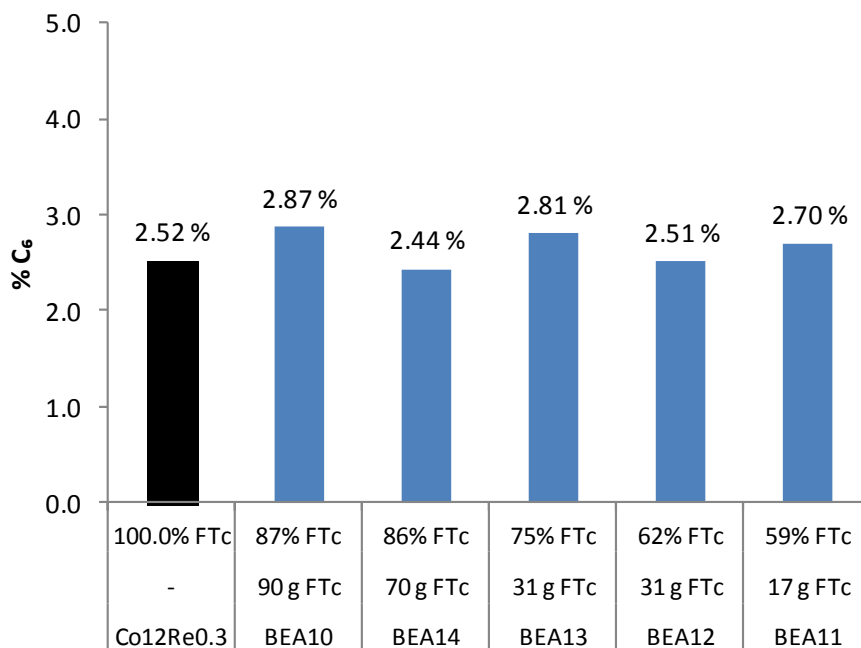




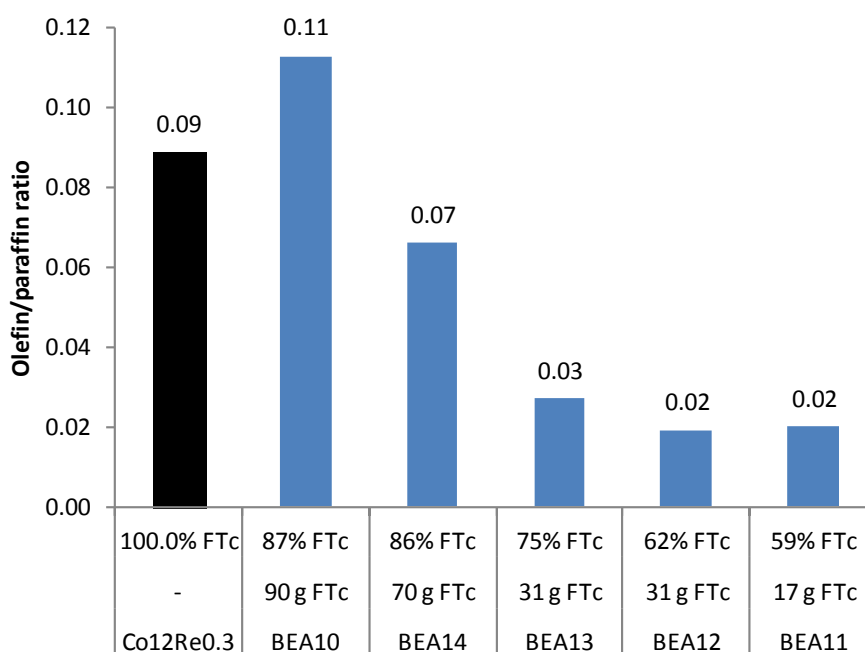
Total C₄-hydrocarbon generation of the different samples in FT reaction test. Samples are sorted according to FT catalyst content.



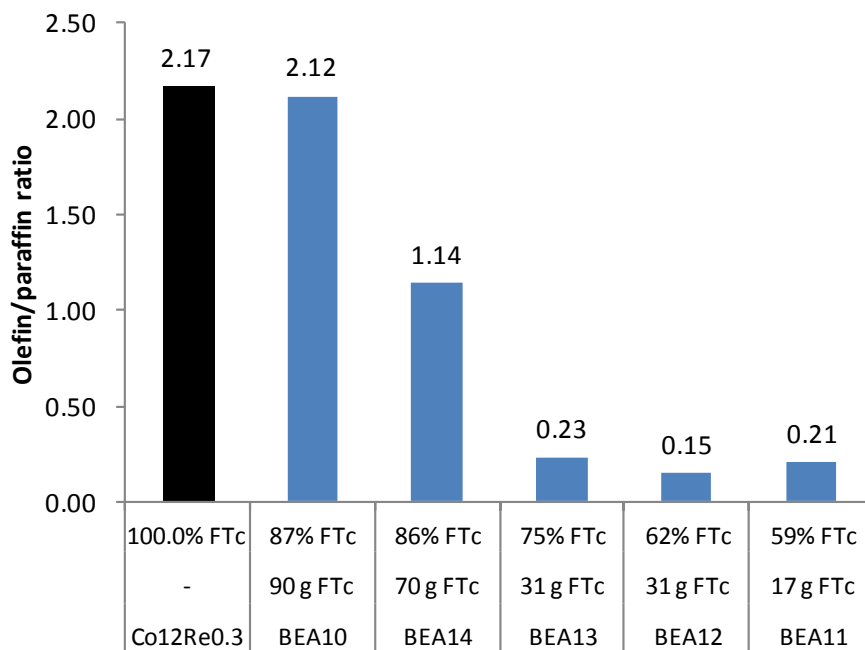
Total C₅-hydrocarbon generation of the different samples in FT reaction test. Samples are sorted according to FT catalyst content.



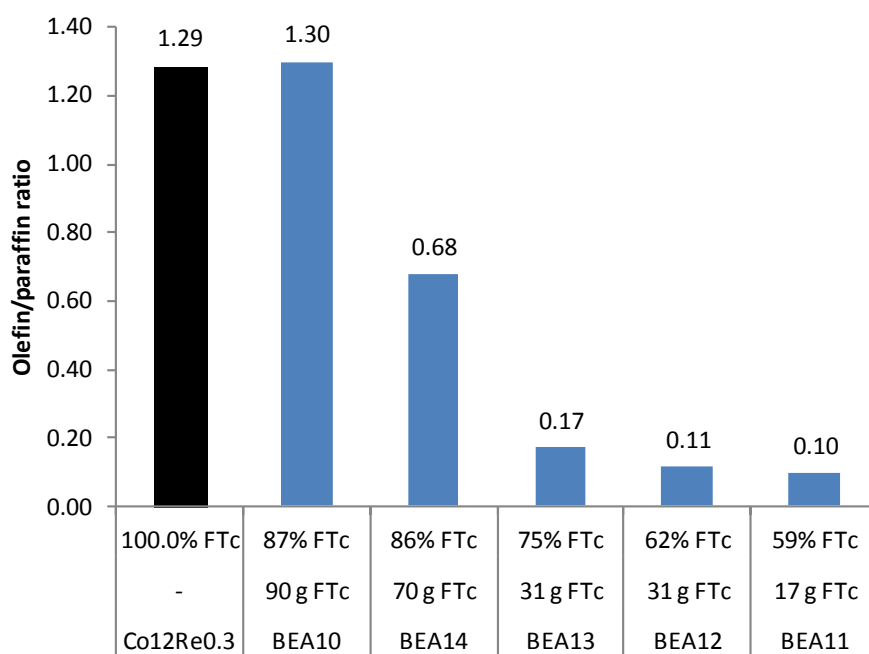
Total C₆-hydrocarbon generation of the different samples in FT reaction test. Samples are sorted according to FT catalyst content.



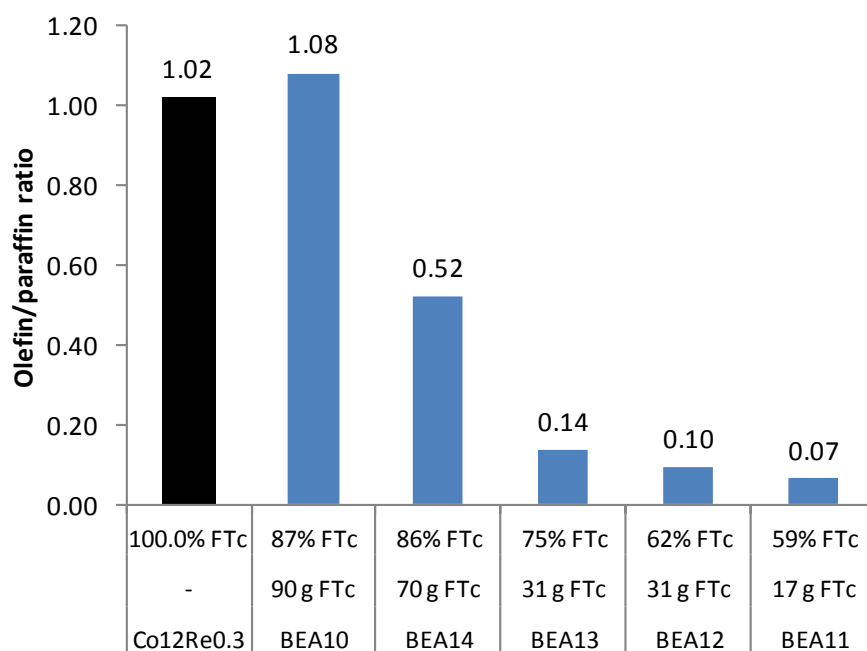
Ethene/Ethane generation of the different samples in FT reaction test. Samples are sorted according to FT catalyst content.



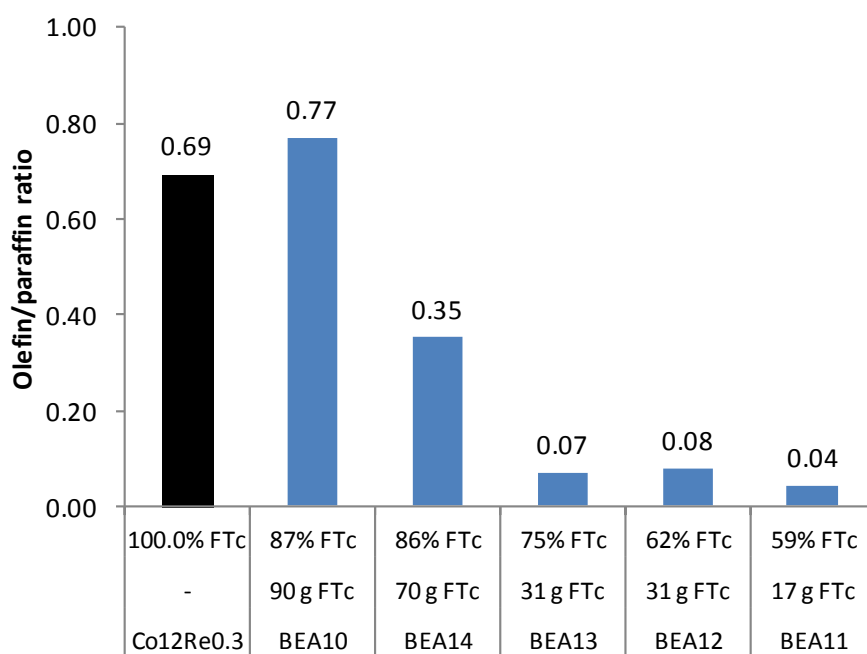
Propene/Propane generation of the different samples in FT reaction test. Samples are sorted according to FT catalyst content.



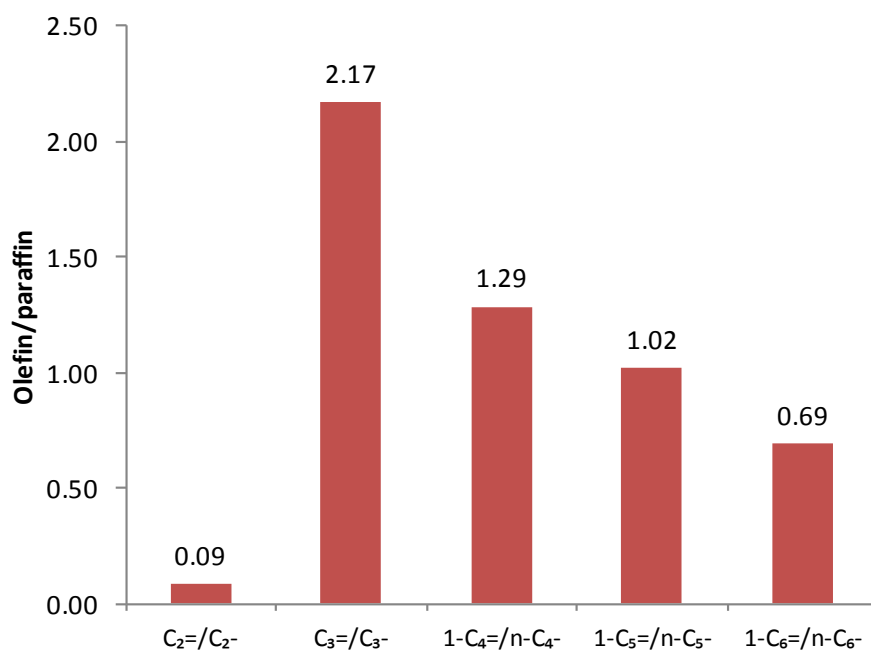
Butene/Butane generation of the different samples in FT reaction test. Samples are sorted according to FT catalyst content.



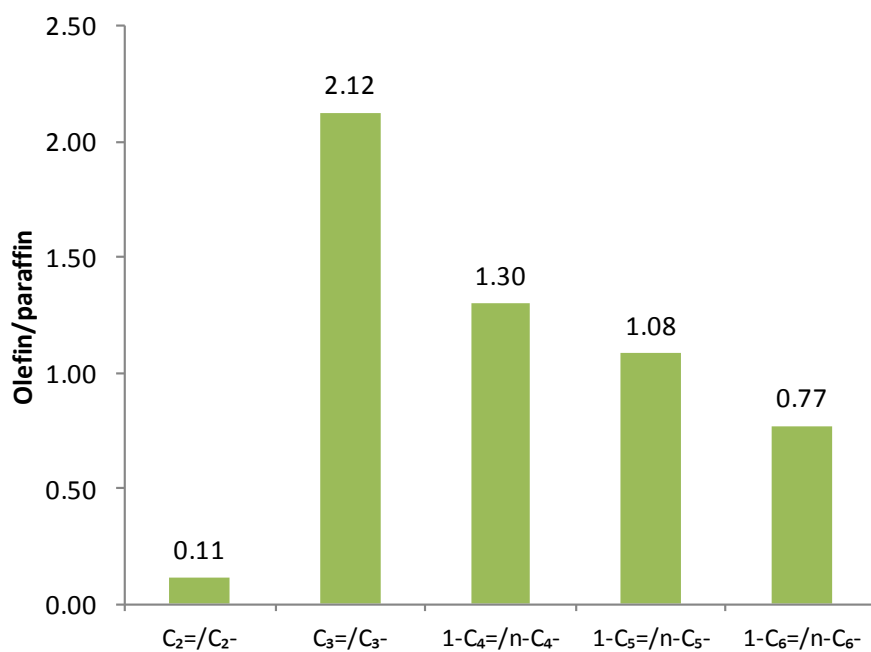
Pentene/Pentane generation of the different samples in FT reaction test. Samples are sorted according to FT catalyst content.



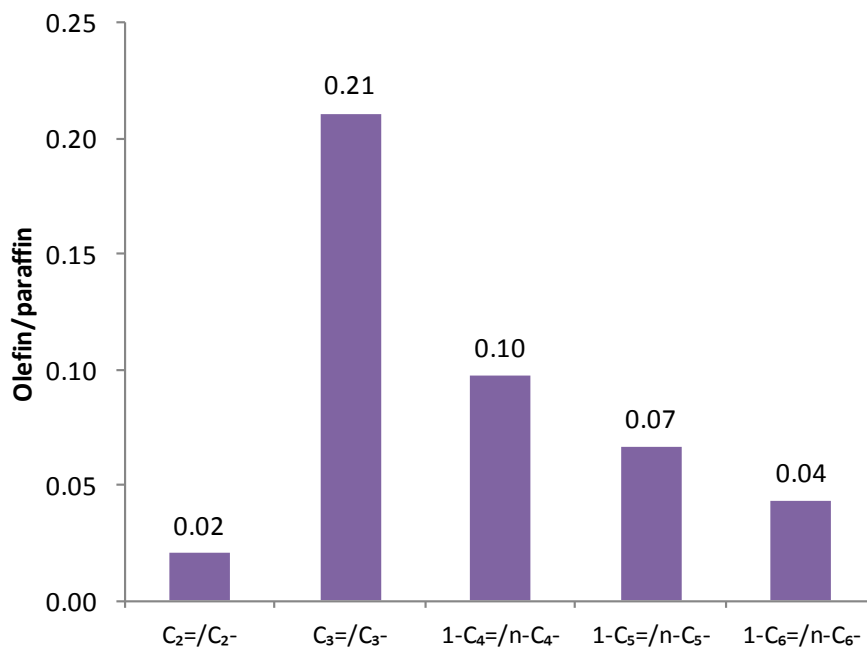
Hexene/Hexane generation of the different samples in FT reaction test. Samples are sorted according to FT catalyst content.



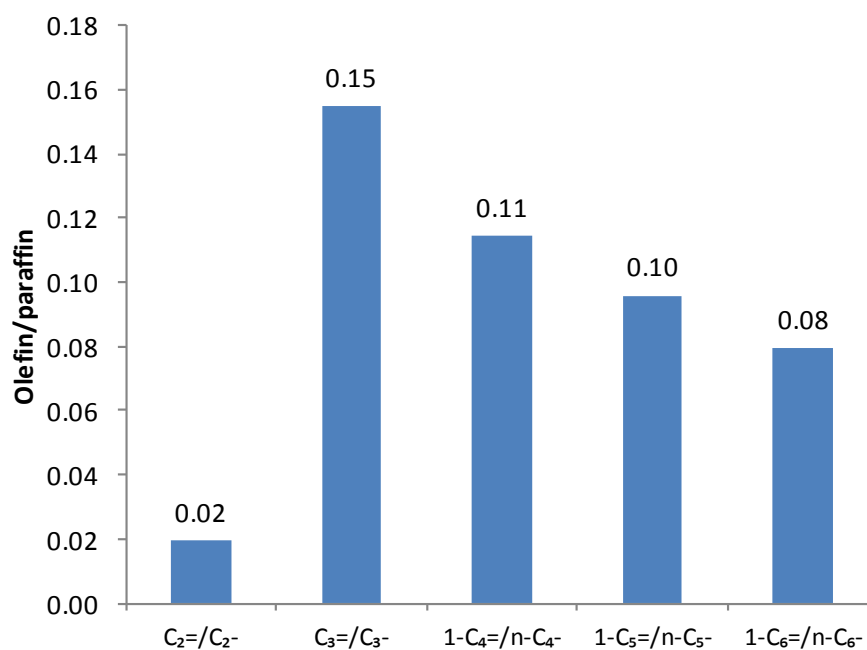
Olefin/paraffin ratio of pure FT cobalt-based catalyst, 0 wt% of β -zeolite, tested in FT reaction reactor



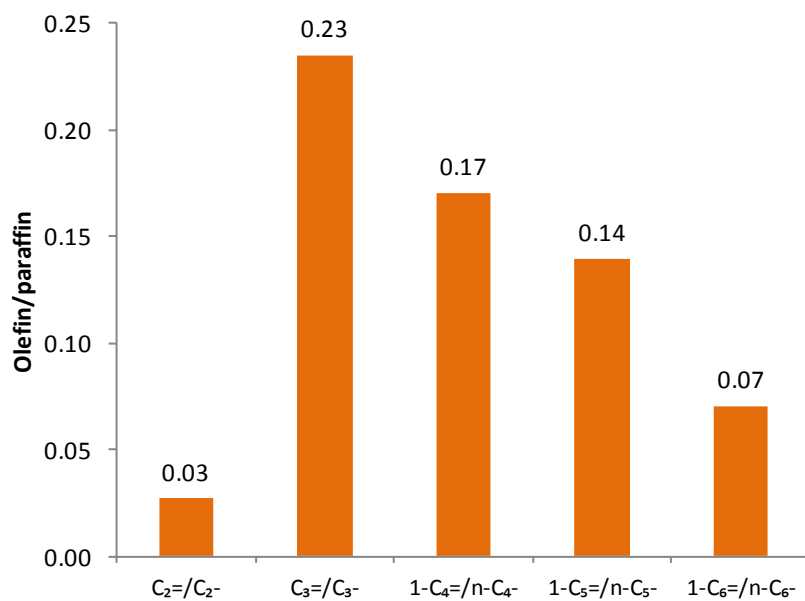
Olefin/paraffin ratio of BEA-10 AUT, 13 wt% of β -zeolite, tested in FT reaction reactor



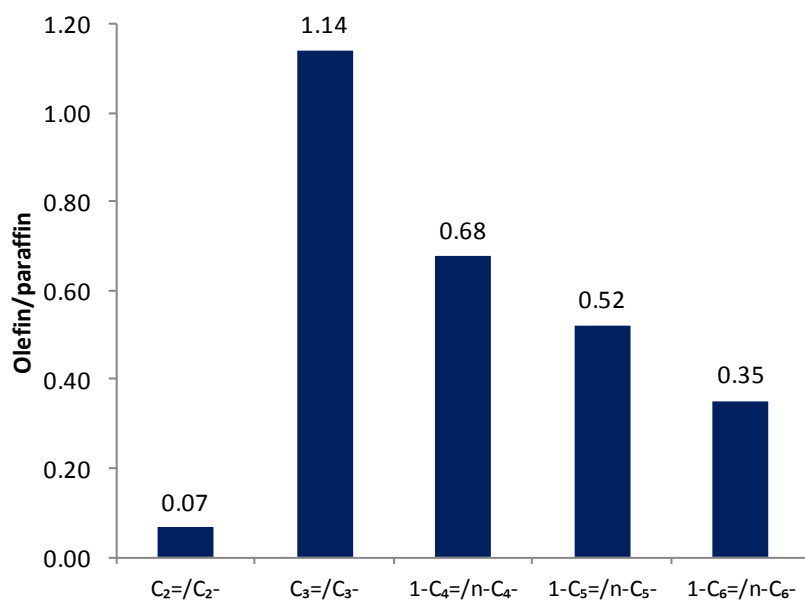
Olefin/paraffin ratio of BEA-11 AUT, 41 wt% of β -zeolite, tested in FT reaction reactor



Olefin/paraffin ratio of BEA-12 AUT, 38 wt% of β -zeolite, tested in FT reaction reactor



Olefin/paraffin ratio of BEA-13 AUT, 25 wt% of β -zeolite, tested in FT reaction reactor



Olefin/paraffin ratio of BEA-14 AUT, 14 wt% of β -zeolite, tested in FT reaction reactor

Appendix H

Zeolite characterization techniques

Compilation of characterization techniques [22].

Technique	Synonym	Structure	Pore size	Chemical composition	Functional groups
Electron microscopy	HRTEM SEM EDX	•	•	•	
Nuclear magnetic resonance (Magic angle spinning)	MAS-NMR		•	•	•
Sorption of probe molecules			•		•
Model reactions			•	•	•
Thermogravimetry, Differential scanning calorimetry	TGA/DSC		•	•	•
Temperature programmed desorption	TPD			•	•
Vibrational spectroscopy		•	•	•	•
X-ray absorption spectroscopy	XAS	•		•	
X-Ray diffraction	XRD	•		•	
X-ray fluorescence spectroscopy	XRF			•	
X-ray photoelectron spectroscopy	XPS			•	•

Appendix I

Synthesis nomenclature

Table I-1 Hydrothermal synthesis products name and general composition

Name	General Composition
BEA-01AUT	Pure β -zeolite
BEA-02AUT *	-
BEA-03AUT	Pure β -zeolite
BEA-04AUT	Pure β -zeolite
BEA-05AUT	Pure β -zeolite
BEA-06AUT	β -zeolite/FT catalyst
BEA-07AUT	β -zeolite/FT catalyst
BEA-08AUT	β -zeolite/FT catalyst
BEA-09AUT	β -zeolite/FT catalyst
BEA-10AUT	β -zeolite/FT catalyst
BEA-11AUT	β -zeolite/FT catalyst
BEA-12AUT	β -zeolite/FT catalyst
BEA-12AUT	β -zeolite/FT catalyst
BEA-13AUT	β -zeolite/FT catalyst
BEA-14AUT	β -zeolite/FT catalyst
Co12Re0.3	FT cobalt-based catalyst

* This product is not successful due to reactor failures

Table I-2 Hydrothermal synthesis products name not calcined products

Name	General Composition
BEA-09AUT WOC	β -zeolite/FT catalyst
BEA-10AUT WOC	β -zeolite/FT catalyst
BEA-11AUT WOC	β -zeolite/FT catalyst
BEA-12AUT WOC	β -zeolite/FT catalyst
BEA-12AUT WOC	β -zeolite/FT catalyst
BEA-13AUT WOC	β -zeolite/FT catalyst
BEA-14AUT WOC	β -zeolite/FT catalyst

Table I-3 Hydrothermal synthesis products name not calcined products

Name	General Composition
BEA-11AUT BLACK	β -zeolite/FT catalyst
BEA-11AUT WHITE	β -zeolite*
BEA-13AUT BLACK	β -zeolite/FT catalyst
BEA-13AUT WHITE	β -zeolite*
BEA-14AUT BLACK	β -zeolite/FT catalyst
BEA-14AUT WHITE	β -zeolite*

* This products contain very low amount of FT catalyst, that it is almost negligible

Appendix J

Synthesis detail

	Silicon Source	TEA-OH *1	Seed-Assisted	FTc *2 g	FTcatalyst as reactant		FT catalyst in the final product	
					β -Zeolite wt%	FTc wt %	β -Zeolite wt %	FTc wt %
BEA-01AUT	LUDOX 40HS	No	No	0.0	100.0	0.0	100.0	0.0
BEA-02AUT	LUDOX 40HS	No	No	0.0	100.0	0.0	-	-
BEA-03AUT	LUDOX 40HS	No	No	0.0	100.0	0.0	100.0	0.0
BEA-04AUT	LUDOX 40HS	No	No	0.0	100.0	0.0	100.0	0.0
BEA-05AUT	Fumed Silica	No	No	0.0	100.0	0.0	100.0	0.0
BEA-06AUT	TEOS 99.0%	No	No	16.5	91.8	8.2	51.0	49.0
BEA-07AUT	Fumed Silica	No	Yes	16.5	92.6	7.4	64.5	35.5
BEA-08AUT	Fumed Silica	No	Yes	16.5	91.7	8.3	47.1	52.9
BEA-09AUT	Fumed Silica	Yes	Yes	16.5	91.8	8.2	50.2	49.8
BEA-10AUT	Fumed Silica	Yes	No	90.0	55.0	45.0	12.6	87.4
BEA-11AUT	Fumed Silica	Yes	No	16.5	91.8	8.2	40.9	59.1
BEA-12AUT	TEOS 99.999%	Yes	No	31.0	84.5	15.5	38.3	61.7
BEA-13AUT	TEOS 99.999%	Yes	Yes	31.0	84.5	15.5	25.1	74.9
BEA-14AUT	Fumed Silica	Yes	No	70.0	65.0	35.0	13.6	86.4

*1 Pretreated sample with Tetraethylammonium hydroxide – TEA-OH

*2 Fischer Tropsch cobalt-based catalyst – FTc